



Vysoké učení technické v Brně  
Fakulta strojního inženýrství  
Ústav konstruování

Brno University of Technology  
Faculty of Mechanical Engineering  
Institute of Machine and Industrial Design

# **ELASTOHYDRODYNAMIC FILM STUDY UNDER IMPACT LOADING AND LATERAL VIBRATIONS**

**Ing. Josef Frýza**

Autor práce  
Author

**prof. Ing. Ivan Křupka, Ph.D.**

Vedoucí práce  
Supervisor

Disertační práce  
Dissertation Thesis

Brno 2017



To an incredibly strong and patient person who has encouraged,  
supported, and loved me throughout all theses and trials of my life;  
to my beloved Klara

—

To a little man who welcomes me home every day with a joyous whoop  
and makes me smile even when I come home tired and later than  
I promised; I promise we'll have more time on ourselves now

—

To my family



---

## STATEMENT

I hereby declare that I have written the PhD thesis *Elastohydrodynamic Film Study under Impact Loading and Lateral Vibrations* on my own according to advice of my supervisor prof. Ing. Ivan Křupka, Ph.D., and using the sources listed in references.

Brno, \_\_\_\_\_

.....

Josef Frýza

## BIBLIOGRAPHICAL REFERENCE

FRYZA, J. *Elastohydrodynamic Film Study under Impact Loading and Lateral Vibrations*. Brno, 2017, 155 p. PhD thesis. Brno University of Technology, Faculty of Mechanical Engineering, Institute of Machine and Industrial Design. Supervisor: Ivan Krupka.

---

## **ACKNOWLEDGEMENT**

I would like to express my thanks to all the people who have inspired, supported, and guided me throughout my life and career; to my grandparents, mum and dad, my teachers from kindergarten up to Brno University of Technology, colleagues, and friends. My sincere thanks must go to my supervisor, the head of Tribology research group, prof. Ing. Ivan Křupka, Ph.D. as well as the director of Institute of Machine and Industrial Design prof. Ing. Martin Hartl, Ph.D. for their support and advice during my doctoral study. Special thank also goes to Ing. Petr Šperka, Ph.D. for his help, motivation, enthusiasm, and immense knowledge in the field of tribology. I particularly want to thank my great friends and colleagues David Nečas and Radovan Galas for an amazing atmosphere in our shared office, even though I sometimes really needed to work. Finally, this thesis would hardly have been written without the support of my family.

---

## **ABSTRACT**

The dissertation thesis deals with the behaviour and frictional response of elastohydrodynamic lubricating (EHL) film under non-steady state operating conditions. The introductory part of the thesis summarizes the knowledge about EHL; ranging from its history, through basic lubrication mechanisms and experimental methods, up to recently published studies focused on transient conditions. The main goal of the doctoral thesis was to experimentally determine the effects of operating parameters and lubricant rheology on the behaviour of EHL films in a point contact during its impact loading and exposure to lateral vibrations. For this purpose, laboratory test rigs have been developed for measurement of EHL film thickness distribution and friction under controlled non-steady state conditions. The experiments revealed a crucial role of an approaching and loading speed on a formation of squeezed films under impact loading. The results were confronted with a recent theoretical solution. Its shortcomings were pointed out and subsequently eliminated by an implementation of empirical relationships taking into account the lubricant rheology. In the case of the lateral vibrations, the thresholds of film breakdowns were found and relationships were established describing the effect of lateral vibrations on the central film thickness and its deviations uniformly for all lubricants. The final part of the thesis provides a new insight into lubricant rheology through an innovative approach in which frictional responses of a lubricant are measured simultaneously in two directions of the EHL contact under lateral vibrations. These original results deepen the understanding of EHL mechanisms and can be used to enhance the design of machines improving their efficiency, reliability, and service life.

## **KEYWORDS**

Tribology, elastohydrodynamic lubrication, EHL, lubricant rheology, film thickness, friction, non-steady state conditions, optical interferometry

---

## ABSTRAKT

Disertační práce se zabývá chováním a odezvou elastohydrodynamického (EHD) mazacího filmu za neustálených provozních podmínek. V úvodní části práce jsou shrnuty poznatky z oblasti EHD mazání; od jeho historie, přes základní mechanismy mazání a používané experimentální metody, až po nedávno publikované studie zaměřené na transienční podmínky. Hlavním cílem práce bylo experimentálně objasnit vliv provozních parametrů a reologických vlastností maziv na chování mazacího filmu v bodovém kontaktu při jeho nárazovém zatěžování a vystavení příčným vibracím. Za tímto účelem byla vyvinuta laboratorní zařízení umožňující měření rozložení mazacího filmu a tření za kontrolovaných nestacionárních podmínek. Experimenty odhalili zásadní roli přibližovacích a zatěžovacích rychlostí na formování stlačených mazacích filmů při nárazovém zatěžování. Výsledky byly srovnávány s nedávným teoretickým řešením. Bylo ukázáno na jeho nedostatky, jež byly následně odstraněny implementací empirických vztahů zohledňujících reologii maziv. V případě příčných vibrací byly nalezeny hranice selhání mazacího filmu a určeny vztahy popisující vliv příčných vibrací na centrální tloušťku filmu a její fluktuace jednotně pro všechny maziva. Závěrečná část práce poskytuje nový pohled na reologii maziv pomocí inovativního přístupu měření třecích reakcí maziva současně ve dvou směrech kontaktu za podmínek příčných vibrací. Tyto původní výsledky rozšiřují pochopení mechanismů EHD mazání a mohou být použity k dokonalejším návrhům strojů, a vylepšit tak jejich účinnost, spolehlivost a životnost.

---

## KLÍČOVÁ SLOVA

Tribologie, elastohydrodynamické mazání, EHD, reologie maziv, tloušťka mazacího filmu, tření, neustálené podmínky, optická interferometrie

## CONTENTS

---

<b>1</b>	<b>Introduction.....</b>	<b>11</b>
<b>2</b>	<b>State of the art.....</b>	<b>14</b>
2.1	Background.....	14
2.1.1	History.....	14
2.1.2	Steady state EHL.....	15
2.2	Non-steady state EHL.....	21
2.3	Impact load.....	22
2.4	Impact/variable load at rolling/sliding.....	36
2.5	Transient unidirectional motion.....	40
2.5.1	Harmonic and accelerated/decelerated motion.....	40
2.5.2	Start/stop motion.....	48
2.6	Reciprocating motion.....	55
2.7	Lateral vibrations.....	65
<b>3</b>	<b>Analysis and conclusion of literature review.....</b>	<b>69</b>
<b>4</b>	<b>Aims of the thesis.....</b>	<b>73</b>
4.1	Scientific question.....	74
4.2	Hypotheses.....	74
4.3	Thesis layout.....	75
<b>5</b>	<b>Materials and methods.....</b>	<b>76</b>
5.1	Experimental apparatus.....	76
5.1.1	Optical tribometer for measurement of film thickness under impact loading.....	77
5.1.2	Optical tribometer for measurement of film thickness under lateral vibrations.....	78
5.1.3	Optical tribometer for measurement of friction under lateral vibrations.....	79
5.2	Measurement method.....	80
5.3	Test samples, experimental conditions, and experimental design.....	82
5.3.1	Paper A – EHL film thickness at pure squeeze action.....	82
5.3.2	Paper B – EHL film thickness under lateral vibrations.....	85
5.3.3	Paper C – frictional response of EHL film under lateral vibrations.....	87
<b>6</b>	<b>Results and discussion.....</b>	<b>90</b>
<b>7</b>	<b>Conclusions.....</b>	<b>134</b>

<b>List of author's publications .....</b>	<b>138</b>
<b>References.....</b>	<b>139</b>
<b>List of figures and tables .....</b>	<b>151</b>
<b>List of symbols, physical constants and abbreviations.....</b>	<b>155</b>

## 1 INTRODUCTION

---

**1**

The research and improvement of machines and their components are nowadays a necessity due to demands from legislation, industrial partners, and concurrent market development. Requirements are particularly a subject of increasing the efficiency, service life, and reliability, together with the reduction in prices, operating costs, and environmental impacts. These parameters of machines determine not only their competitiveness, but also reveal the ability to effectively deal with energy. A large part of the total energy losses (dissipation) arises during transmissions or transformations of mechanical energy due to resisting forces (friction). For example, in the case of combustion engines, frictional forces typically reduce about 5 up to 60% of the motor power depending on its load. Energy dissipation, transmission of traction/friction forces, wear, and fatigue of the contact surfaces are conditioned by mechanisms taking place at the interface of machine components. Unfortunately, the occurrence and overall significance of these mechanisms are considerably affected by contact conditions, and this interdependence then creates relatively complex issues. Understanding the physical origins of the mechanisms is essential for a reliable prediction of the behaviour of these often-lubricated contacts, and consequently for a suitable design of machines. The field of science that attempts to describe and clarify these interactions of mechanisms on the interfaces of contact surfaces together with the interrelated processes of friction, lubrication, and wear has been called tribology since 1966. As this issue is complex, there are subdivisions dealing with traction/friction, thermal phenomena, surface topography, wear, non-steady state conditions, lubricant rheology and other factors affecting lubricated contacts in machines. It is appropriate to address these challenges separately to distinguish the individual effects of various factors, although it is not always possible.

Most of the lubricated contacts working under severe conditions belong to the so-called elastohydrodynamic lubrication (EHL) regime. This type of fluid-film lubrication is associated with counterformal (non-conformal) surfaces in relative motion when these surfaces are separated by a continuous film of lubricant (mineral oils, synthetic esters, greases, and others). The film thickness is usually of the same order of magnitude as the elastic deformations of lubricated surfaces occurring due to a small size of the contact, and subsequently a high contact pressure. The pressure generated in lubrication film carries the applied load wherein the film itself prevents wear and significantly reduces the friction resistance to motion in contact. Friction results exclusively from shearing of the lubricant, but the relationship between friction and film thickness is rather complicated. EHL provides the smallest friction compared to other lubrication regimes (see [Fig. 1](#)); therefore, there is an attempt to design machines so that their contacts can work in this regime. The approximation of stress values in lubricated contacts is essential for design of machines with long service life and it is also important to ensure a full separation of surface asperities by an adequately thick lubricating film to prevent a high shear stress owing to the contact of these asperities. From the above, it follows that the investigation of EHL contacts focuses mainly on film thickness and friction, or phenomena associated with them.

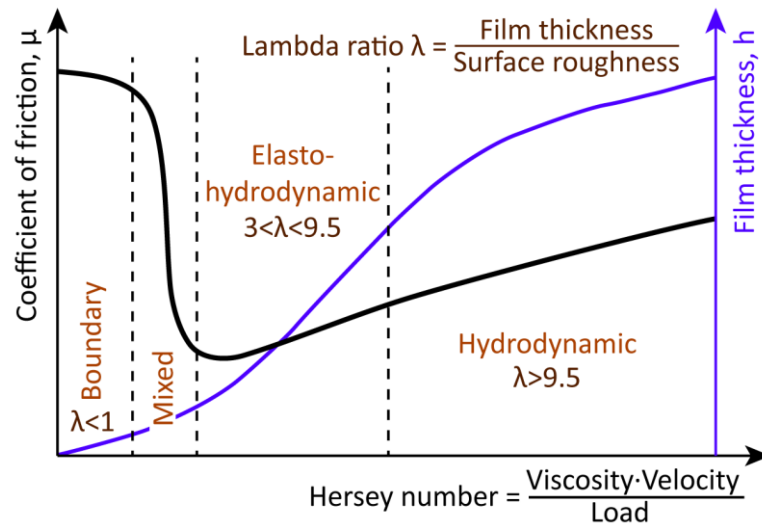


Fig. 1. Stribeck-Hersey (Gümbel) curve, film thickness, and lubrication regimes (the values of lambda ratio are only roughly indicative).

Thanks to developments in tribology, the physical origins of EHL for steady operating conditions are nowadays well described. Both experimental and numerical studies coincide in this area of research and provide satisfactory predictions of film thickness and friction. However, there are no ideal steady operating conditions in actual engineering applications. Many machines employ reciprocating mechanisms where periodic variations in velocity and load of lubricated surfaces usually occur. Similarly, every contact inside the machine must sometimes interrupt its movement, either because of the working nature of machine or due to a failure and machine downtime. Moreover, even the machines with only basic mechanical movements such as shaft rotation, which operate at seemingly constant speeds and torques, include bearings whose rolling elements are subjected to dynamic movements (vibrations) and shocks arising, for example, in transmissions.

Rolling bearings are applied in almost every machine and they are a typical example of machine element exposed to unsteady conditions and vibrations. As shown in a number of studies, if the bearings failed, then from 40 to 50% of these cases were caused by a breakdown in the lubrication film. The vibrations introduced by the operation of the bearing itself are assumed to be given by its internal clearance and a rolling element frequency (over 200 Hz for most of applications). These short sliding motions act in arbitrary directions of EHL contact and are accompanied by vibrations at different frequencies from other sources. The length of motion due to vibrations is almost always shorter than the size of the contact area. This limitation is also given by the internal clearance, which is additionally reduced by preloading of the locating bearing whereas it remains similar for the floating bearing. A prevention or limitation of vibratory motions in the tangential directions relative to the contact surface leads to transient loading, i.e. the tendency to move in the normal direction of contact in response to the vibrations. Nevertheless, in order to ensure a minimum friction torque and low heating, a

certain internal clearance is retained in most applications of rolling bearings. Hereupon, the film of lubricant is transiently shear loaded and affected by the non-steady state entrainment of the lubricant into the contact due to rolling/sliding motions and, at the same time, by squeezing/damping actions resulting from the unsteady loads. On the other hand, the consequences of these concurrent effects are less pronounced due to the decomposition of forces than if only one of these effects takes place. Therefore, it is suitable to study them separately to provide the insights into the mechanisms and nature of these phenomena.

Correspondingly, other EHL contacts are affected, not only those in rolling bearings, but also those in applications of stepper motors, gears, cams and followers, ball screws, constant velocity joints, traction drives, continuously variable transmissions, etc. All these unsteady operating conditions and vibrations affect the essential mechanisms of EHL and could be one of the reasons for EHL film failure that causes an excessive wear leading to a shorter service life of machines. Additionally, the machine designed via often-used unmodified predictions for steady conditions may not achieve the desired efficiency, since the estimated film thickness and friction can be very different from the reality.

The current thesis aims at the study of behaviour and frictional response of EHL films within the concentrated contacts under transient rolling/sliding motions and impact loads. An emphasis is put mainly on the experimental investigations of film thickness under such conditions. This work, due to its limited scope, does not include investigations of the transient effects resulting from changes in the contact curvature or simultaneous variations in load and tangential speeds (such as in cam mechanisms and some gears), or due to surface asperities; and it is primarily focused on point EHL contacts that are a special case of more general elliptic contacts.

## 2 STATE OF THE ART

### 2.1 Background

#### 2.1.1 History

The dawn of tribology and the use of this knowledge can be found in ancient civilizations, much earlier than this science has been called a tribology. Already at that time, lubricants were used to reduce resistance to movement, followed by an application of low-friction materials, and across the centuries, primitive bearings gradually began to emerge. The earliest systematic study of tribology dates back to 1493, when Leonardo da Vinci, a pioneer in tribology, stated the basic laws of sliding friction [1]. Another important milestone was the Hertz theory of elastic contacts in 1881 [2]. However, this theory assumes that there is no lubricant in the contact, and so has been widely used in other engineering disciplines of contact mechanics such as the wheel-rail contact in the issue of rail transportation. With regard to the fluid-film lubrication, the experimental indications that the contact surfaces are separated by a film of lubricant were given by findings of pressure generation in a journal bearing by Tower [3] and by measurement of low friction torques by Petrov [4], both in 1883. These findings came at the right time to help develop the first differential equation of hydrodynamically lubricated contacts explaining the mechanism of lubrication via a generation of lubricant viscous flow in 1886, the Reynolds equation [5].

However, based on the results of Martin [6] and Gumbel [7] investigating the lubrication of gears, this famous theory focused on the lubrication of conformal contacts was not able to explain all mechanisms occurring in the counterformal ones. A predicted minimum film thickness using the Reynolds equation alone was much smaller (about only 1 to 10 nm) than the surface roughness of gears (usually more than 0.4  $\mu\text{m}$ ) which was against a common experience referring to a very low wear of such contacts. After almost 20-year gap, Pepller [8] followed by Meldahl [9] obtained a substantially thicker film by considering the effect of elastic deformation of contact into analyses, but it still was too thin to clarify a full-film lubrication in the counterformal contacts. Independently of these solutions, the increase in film thickness was achieved also by taking into account the enhancement of lubricant viscosity under high pressures, as was reported by Gatcombe [10]. Regardless of the examination of these two effects separately in later years, the most celebrated analytical solution for EHL film thickness in line contacts was given by including the both effects simultaneously by Ertel [11]. The elasto-hydrodynamic lubrication was finally established at the end of World War II, although Grubin [12] had been wrongly recognized as the original author of this theory instead of Ertel for the next 40 years (see [13]).

Since mainly disc machines were employed for investigation of both the film thickness and friction in experimental studies during the early stages of EHL, and the computing power was rather limited at that time, EHL line contacts were experiencing a rapid development, while point and elliptical contacts lagged behind.

Similarly, the measurements of frictional response were relatively straightforward, but the film thickness detection with the accuracy sufficient for improvement of theoretical solutions was a more important challenge. At first, the voltage discharge [14] and the electrical resistance methods [15] were used for film thickness measurements, but without a significant contribution to understanding of EHL. Then, fruitful results confirming the basic trends in EHL were obtained via the capacitance method [16] for measurement of average (central) film thickness. This method was occasionally supplemented by means of the X-ray transmission technique [17] for approximation of minimum film thickness. However, the above experimental techniques were unable to provide a punctual information on the film shape and film thickness behaviour in the contact. The birth of method, which is capable of this, began by an accident with the first measurement of point contact formed between two crossed transparent cylinders employing the capacitive method [18]. The interference fringes altering with speed were observed during an optical verification of contact size. In consequence, the most widely applied method for measuring of EHL film thickness, the optical interferometry, was developed together with the ball-on-disc simulator of point contact by Gohar and Cameron [19-21]. This in-situ approach caused a tremendous progress in understanding EHL mechanisms. Ten years later, in 1976, Hamrock and Dowson presented full numerical solutions and curve-fitting formulas for predictions of the minimum and central film thickness in the general elliptic (point) contacts [22-24]. Here, film thickness is calculated from the dimensionless parameters of material, speed, load, and ellipticity of contact. These analytical approximations are still frequently used, notwithstanding the fact that they are isothermal and particularly suitable for only Newtonian fluids, smooth surfaces, and steady state conditions.

### 2.1.2 Steady state EHL

### 2.1.2

---

Although the reader might have an impression that EHL issues were solved very quickly and straightforwardly 50 years ago, the opposite is true. The evolution of EHL ceased to be straightforward and began to branch out by scientific interests due to its complexity. In view of this complexity, the behaviour of lubricant film as well as the frictional response are given by the interaction of contact conditions (speeds, loads, temperatures, materials, roughness of surfaces, geometries of contact, etc.), used lubricant (mainly molecular composition and structure influencing rheological properties and lubricant flow within the contact), thermal effects (close and within the contact), and other phenomena. Prior to experimental studies dealing with non-steady state conditions that are the main topic of this work, it is first appropriate to mention at least some of the underlying parameters and mechanisms having an impact on the film thickness and friction under steady conditions. Right from the outset, it should be noted that there is a very weak interaction between the film thickness and friction in EHL contacts.

Film thickness is formed and mainly determined with the pressure build-up at the contact inlet, as is illustrated in Fig. 2. Due to the shape of the deformed contact bodies at the inlet (physical wedge effect), a large pressure gradient occurs

generating the Poiseuille flow, wherein the viscosity of the lubricant is relatively low (about ten times higher than at atmospheric pressure) as the increase in viscosity with pressure is almost exponential. The rate of increase in viscosity with the pressure is influenced by a pressure-viscosity coefficient of the lubricant. Based on the Reynolds equation, the Poiseuille flow is balanced particularly by the Couette flow representing the entraining flow rates and resulting from the mean speed of the contact surfaces. It means that the geometry, the entrainment speed drawing the lubricant into the contact (i.e. part of the hydrodynamic effect; the entraining action), and the lubricant properties (especially viscosity) under conditions at the inlet have the greatest influence on the film thickness in EHL contact. On the other hand, load and contact materials have a slight impact on the film thickness. A low sensitivity to load is one of the great advantages of EHL contacts that highlights a high load-carrying capacity of these contacts. Likewise, the changes in shapes of contact bodies due to their deformation are similar for a wide range of commonly used materials in engineering applications (with respect to the viscous-elastic lubrication, i.e. EHL contacts, and not in the case of the isoviscous-elastic one, i.e. “soft” EHL, as flexible seals, tires, contact lenses, human synovial joints, and others). Since the volume of lubricant that can be entrained into the contact is limited, a reverse flow and recirculation of lubricant may take place in front of the contact depending on the contact conditions. Then, the lubricant is sheared by counterflows and its viscosity is reduced as a result of the inlet shear heating, which leads to the reduction in film thickness [25]. Additional drop in the viscosity/thickness can also occur for non-Newtonian lubricants whose molecular structure is affected by a relatively low shear stress about 1 MPa. This effect of shear thinning is more pronounced by increasing molecular weight and polymer chain concentrations of lubricants [26].

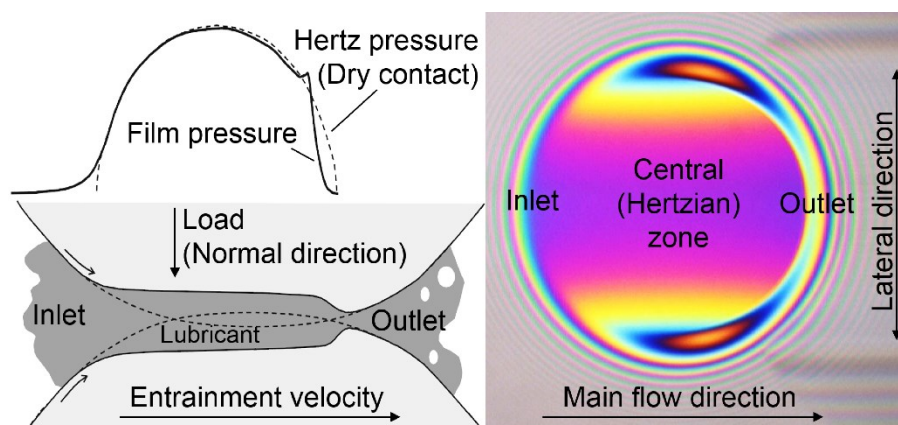


Fig. 2. Left: pressure distribution and film thickness profile in mid-plane of EHL contact (modified from [27]); right: interferogram of point contact with indication of movements/flows directions in tangential plane of contact.

If there are no additional specific phenomena, the film of nearly uniform thickness passes through the central area of contact at the mean speed of contact surfaces. Continuity of lubricant flow is maintained by a horseshoe-shaped

constriction bordering the central plateau region. This shape of constriction is typical for point EHL contacts. The minimum film thickness about 60% of the central thickness is located in two lateral lobes of the constriction reducing significantly a leakage of lubricant in these directions. The pressure distribution is close to the Hertzian distribution of dry contact, when the maximum pressure reaches from 1 to 3 GPa. The Poiseuille flow is negligible because of an extremely high viscosity of lubricant and a low pressure gradients. The dominant flow is the Couette flow accompanied by transient flows due to the squeeze action and thermal expansion of lubricant. The former is based on the damping ability of lubricant which resists to the normal mutual approach of the contact surfaces under load. The latter is a locally transient mechanism resulting from heating of lubricant in the central area of contact and it is necessary to consider this flow at high sliding speeds (sliding speed is defined as the difference in surface velocities). The temperature of lubricant can increase by more than 50 °C within the contact as a result of viscous dissipation under these severe conditions, when the shear strain rate achieves the values from  $10^6$  to  $10^8$  s<sup>-1</sup>. It is important to note that the flow velocity of individual layers of lubricant is assumed to be linearly distributed throughout the overall film thickness in the Reynolds equation and many subsequent applications. Hence, the shear strain rate (the shear rate in short) is subsequently defined as the proportion of the sliding speed to the central film thickness. Unfortunately, numerous recent works have pointed out that the actual velocity profile may differ significantly from this theoretical linear profile, especially at high sliding speeds and contact pressures.

Due to high pressure, shear rate, and resulting shearing of highly-viscous lubricant, the overwhelming part of EHL sliding friction (for full-film lubrication sometimes called traction) originates from the central area of contact. This is also the reason why the film thickness and friction are in principle almost independent, since their only interconnection is via the definition of shear rate and they are determined under completely different conditions. Unlike the film thickness predictions, the Newtonian behaviour of lubricant may not be considered in the predictions of friction. Furthermore, the lubricant passing through the high-pressure area can cease to behave as a purely viscous fluid. Its viscosity increases to the values from  $10^7$  to  $10^{12}$  Pa·s and thus approaches the glass transition state, when the characteristic properties of solids begin to appear [28] (i.e. exhibiting viscoelastic behaviour). Such glassy state or solid-like state of lubricant is often referred to as solidified in the literature, although it is not a case of full solidification because of short times for lubricant passage through the contact (approximately  $10^{-4}$  s), during which the crystals of substance cannot be formed [29] (another method is rapid cooling of viscous liquid to obtain a supercooled liquid). There are three main obstacles to full understanding and a reliable prediction of EHL friction. The first one is a detection of lubricant parameters (especially viscosity) and its characteristics that are not affected by multiple transient variables simultaneously under severe conditions of EHL conjunctions. The second one is the application of this knowledge to improve or establish appropriate relationships and rheological models, whose suitability is still

a topic to be discussed [30-32]. And thirdly, there is a lack of adequate description of lubricant behaviour at the molecular level where the friction in lubricants originates. Therefore, an attempt is offered to solve this issue in particular by molecular dynamics simulations [33]; however, they are still not so advanced to encompass the conditions in EHL contacts. A frictional response of EHL contacts according to the contact conditions is described below.

At the outlet of contact, both the contact pressure and the lubricant viscosity drop rapidly and the Poiseuille flow begins to be substantial again. To compensate this sudden decrease in viscosity the flow speed has to be increased to maintain the continuity of flow. This is achieved by formation of constriction, which in turn, generates a sharp pressure spike on the upstream side of constriction (see Fig. 2). This “Petrusevich spike”, as it takes after the first author who numerically demonstrated it for the line contact [34], further enhance the pressure gradient resulting in a lower pressure than the Hertzian one in the rest of contact outlet. The outlet pressure spike can overcome the maximum Hertzian pressure depending on the entrainment and sliding speeds and the pressure-viscosity coefficient of lubricant. When the contact surfaces begin to separate due to their shape at the contact outlet, the volume of lubricant leaving the contact is not sufficient to fill this space. A growing space is then balanced by the volume of air streamers and bubbles interspersed in lubricant. Although this region behind the contact is referred to as a “cavitation” zone, there is no evaporation or mass transfer by diffusion. A length of cavitation zone may be in multiples of the contact size with respect to lubricant properties and entrainment speed [35]. It is important in view of multiple contacts running in succession as in the case of rolling bearings, when the presence of air at the contact inlet leads to the reduction of lubricant supply and the EHL starvation (reduction in film thickness and load-carrying capacity).

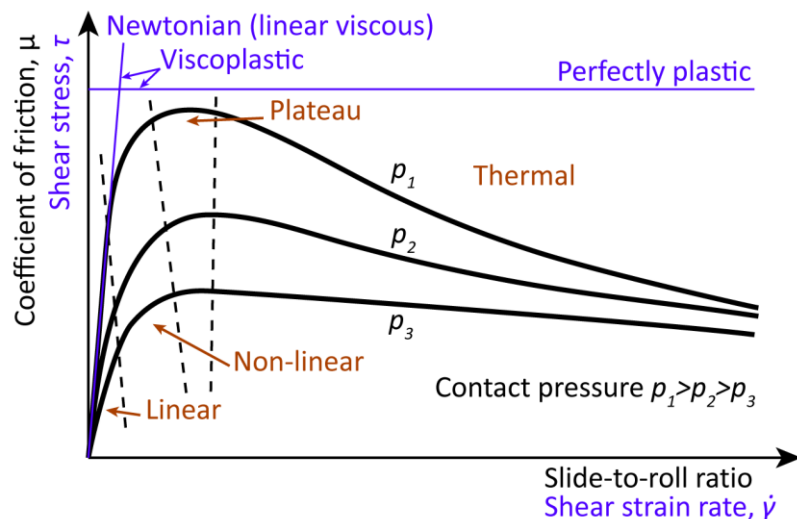


Fig. 3. Traction curve at various contact pressures (black) and asymptotes of some rheological models of viscoelastic fluids (blue).

The frictional response of EHL contacts may be compartmentalized into four regimes considering the contact conditions [36], as is demonstrated on the traction curve in Fig. 3. The slide-to-roll ratio (SRR) on the horizontal axis of diagram is the ratio of sliding to rolling (entrainment) speed. In general, friction decreases with the increase in rolling speed because the thicker film reduces the shear rate of lubricant at the same sliding speed. However, this trend cannot be found from the presented traction curve since it is obtained at the constant rolling speed and different sliding speeds to demonstrate the effect of lubricant shearing. It is evident that a higher contact pressure at the same SRR leads to a higher friction due to a higher viscosity of lubricant, but the viscosity is also markedly conditioned by temperature. Therefore, the lubricant rheology is the most important aspect of EHL friction. The linear (Newtonian) viscous behaviour of lubricant, which is common for hydrodynamic lubrication, can also be observed for EHL, but only at low pressure and SRR. The Newtonian fluid model thus predicts an unrealistically high friction for most of EHL applications (see a nearly vertical blue line in Fig. 3). Shear thinning is the primary mechanism affecting the friction in the non-linear viscous regime. However, less pronounced consequences of thermal dissipation or limiting shear stress (LSS) on behaviour of lubricant can be included. The concept of LSS, as a lubricant property, was first discussed by Smith [37] and subsequently confirmed experimentally by Plint [38] in 1960s. Fundamental of LSS is that both the friction and shear stress in lubricant increase with the sliding speed to the limit value (LSS), then the shear stress no longer depends on the increase in shear rate (see a blue line representing a perfectly plastic fluid in Fig. 3). It is assumed that a slip occurs between the layers of lubricant localised in the middle of film thickness [39], or close to one [40] or both [41] surfaces when LSS is reached. Unfortunately, then also the linear velocity profile of lubricant flow (determination of shear rate), together with the speed-based boundary conditions of Reynolds equation, are no longer valid. The plateau regime of friction is therefore controlled mainly by LSS, when the asymptotic value of friction is achieved. This regime is often merged with the non-linear regime, or it is seen only as a transition to the thermal regime. A typical feature of the thermal regime is a decrease in friction with an increase in SRR. Heat dissipation and shear thinning effects, due to a high sliding speed, play a major role and outweigh the impact of LSS in this regime. These findings are the basis of many models for the description of EHL friction and its prediction. Most of these predictions include combinations of viscoelastic models (Maxwell, Kelvin-Voigt) to approximate the responses of real lubricants. For this reason, the blue lines in Fig. 3 are only the asymptotes of such rheological models, since viscoelastic fluids lack a yield stress unlike the depicted theoretical viscoplastic fluid. EHL rheology models are beyond the scope of this thesis.

A combination of contact conditions and film-reducing effects may cause that the film thickness will not be sufficient (film failure), and interactions of surface asperities may occur. These interactions then lead to undesirable resisting forces, mechanical energy is dissipated into heat and deformations of the asperities. Subsequently, the viscosity of lubricant along with the thickness of the remaining film decrease due to a temperature rise. This encourages further interactions of

asperities, increase in friction, wear, noise, vibrations, and dynamic phenomena, which can deteriorate this process of transition from EHL lubrication to boundary regime (see [Fig. 1](#)). In the extreme case, the whole process may lead to a full seizure of the contact. However, as outlined in the introduction, all EHL machine contacts work under transient conditions and in the presence of vibrations that act in arbitrary directions and cannot be completely suppressed [\[42\]](#).

## 2.2 Non-steady state EHL

EHL contacts exposed to non-steady state conditions are often substantially affected by transient flows due to the squeeze and entraining action. The first studies dealing with a pure squeeze action (impact loading) took place during 1960s. The impulse for these investigations were the findings that the metal surface could be damaged by the impact of steel body, albeit the surfaces are separated by a thick film of lubricant during the impact [43]. Therefore, the following part of this chapter is devoted to the issue of lubricant squeezing under normal approach of the contact surfaces, where the surfaces do not move along their tangential directions. Nevertheless, most of EHL conjunctions move tangentially during their operation, when the influence of lubricant entrainment is essential. The further part of the state of the art is focused on the quasi-steady rolling/sliding conjunctions subjected to impact or variable load.

A squeeze phenomenon is also important when tangential velocities of the contact surfaces, and thus the film thickness, vary over time. However, the experimental and computational options were initially technically very limited to investigations of transient phenomena. Hence, the greatest expansion of studies involving non-steady state conditions occurred almost at the turn of the millennium, thanks to the development of computer technology and the affordability of high-speed cameras. In particular, periodic variations in speeds and accelerations are used in experimental studies as many machines operate under conditions that are repeated in cycles. Some of these non-steady state motions are illustrated in Fig. 4. The remaining parts of this chapter deal with the behaviour of EHL contacts under the conditions of transient unidirectional motions (Fig. 4a-c), reciprocating motions (Fig. 4d-f), and lateral vibrations, respectively.

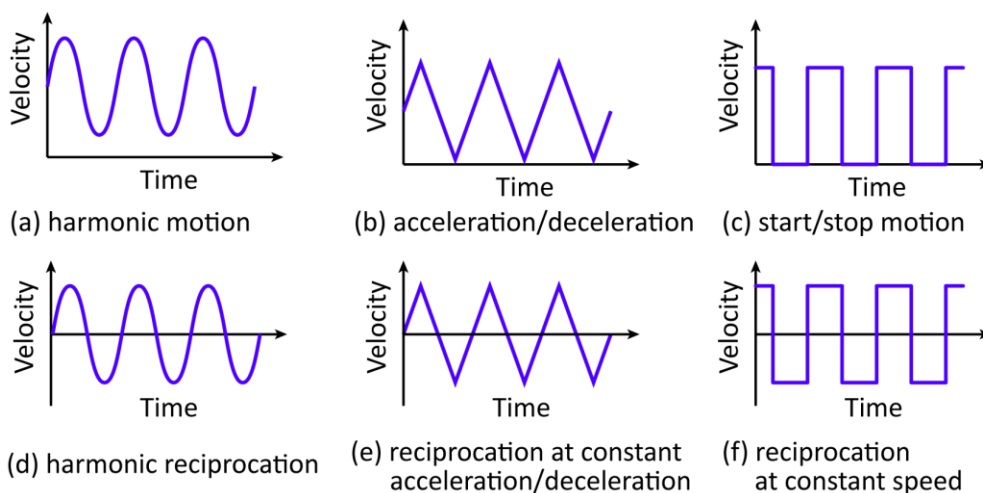


Fig. 4. Non-steady state motions (modified from [44]).

## 2.3 Impact load

Christensen's pioneering work investigating the normal approach of contact bodies separated by a lubricant was published in 1962 [45]. First, the pressure distribution and film shape were solved numerically for four cases of boundary conditions including rigid or elastic bodies and constant (isoviscous) or variable (piezoviscous) viscosity of lubricant. However, the only practical case in relation to EHL was a combination of elastic bodies and piezoviscous lubricant. It was predicted that the minimum load of contact occurs at specific conditions of central film thickness and pressure in film with respect to the pressure-viscosity coefficient  $\alpha$  of the lubricant. The pressure distribution was very sharp at this minimum load producing a dimple film shape in the centre of contact. This elastic deformation was considered as the analogy to the outlet constriction in the rolling contacts. The dimple expanded with the reduction in film thickness. Moreover, it was recalculated that the piezoviscous lubricant causes a higher maximum pressure than the predicted one by the Hertz theory in dry contacts. This was also indirectly confirmed by experiments. A steel ball was dropped onto the polished surface of metal specimen. The resulting plastic deformation of this surface was deeper and more concentrated for lubricated contact than that for dry contact. These results are summarized in Fig. 5. A deformation was smaller for the metal specimen with smaller Young's modulus  $E$ , since the generated pressure is dependent on the value of  $\alpha E$ .

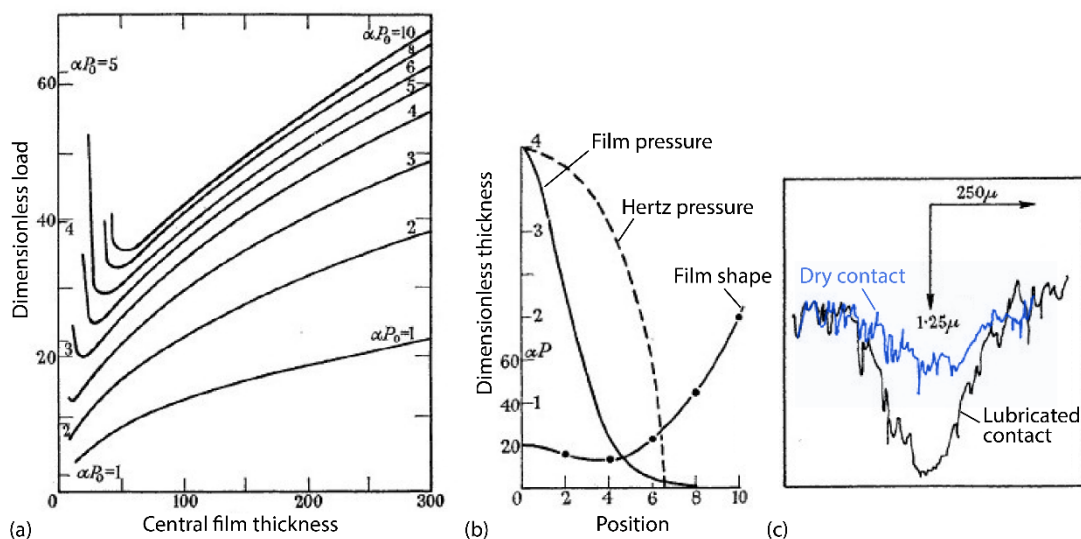


Fig. 5. (a) Load as function of film thickness at various pressures; (b) Pressure distribution and film shape; (c) Deformation of flat surface [45].

The entrapment of lubricant in the central area of contact together with the dimple development over time were subsequently proved by a direct observation via the optical interferometry by Dowson and Jones, whose results were published in the Nature journal [46]. It was also noted that the entrapment persisted for many hours after the impact with pressurized lubricant leaking across the periphery of contact.

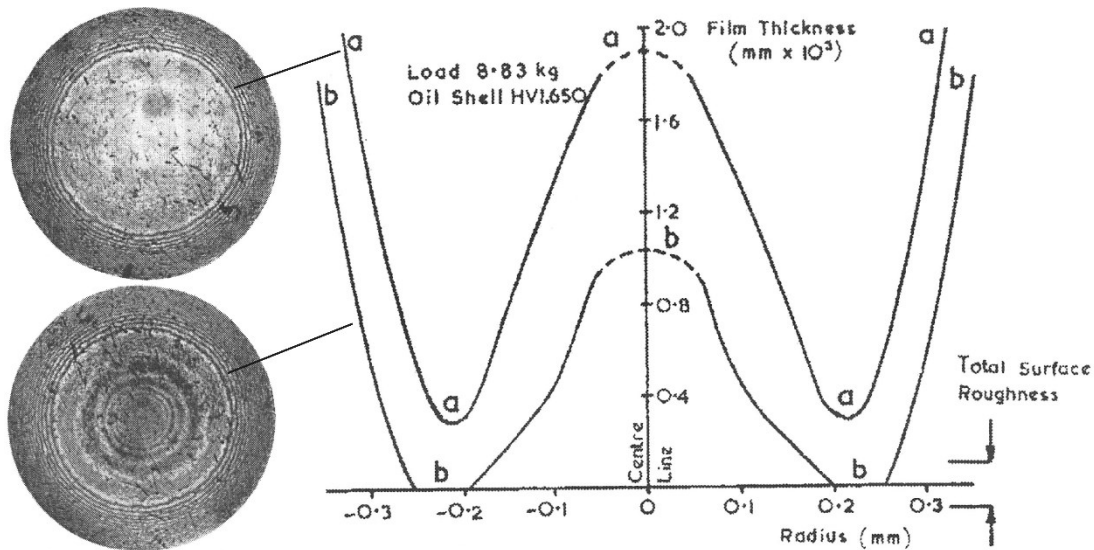


Fig. 6. The interferograms and film thickness distribution of entrapped lubricant 1.6 s and 60 s after the impact loading [46].

Subsequently, Conway discussed the issue of dynamic simulations for normal approach action where the constant rate of film thickness variation regardless of the instantaneous value of film thickness was often assumed at the time [47]. It was pointed out that the rapid changes in film thickness and pressure during the impact can significantly affect the numerical results due to this assumption, especially for high velocities of approach and thin films of lubricant. Then, Conway inspected the pressure distribution as the function of impact time [48]. Based on the findings of Christensen [45], both solutions employing an isoviscous or piezoviscous behaviour of lubricant were compared. The conclusions of this study suggest that the lubricant entrapment and formation of dimple film shape observed by Dowson originate from the pressure development in the course of impact reflected in the increase of lubricant viscosity. A highly pressurized and viscous lubricant then cannot leak out of the contact.

Kuwano and Ohno [49] experimentally studied the influence of rheological properties of lubricants on their entrapment. Four mineral oils and their mixtures were analysed via the high pressure viscometer and the film thickness was measured by means of optical interferometry. It was shown that the depth of dimple and the amount of entrapped oil enlarge with the increasing viscosity and molecular weight of oils. The oil was entrapped for a long time (hours) after the impact and its leakage was determined by viscosity, as is shown in Fig. 7. The film pressure derived from film thickness supports the theoretical findings of previous authors that the EHL pressure exceeds several times the pressure in dry contact at squeeze action. Moreover, the pressure needed for glass transition was found to be higher under the dynamic impact conditions than under quasi-steady conditions in the high pressure viscometer. Accordingly, it was more difficult to cause the glass transition for oils of higher viscosity in the impact test.

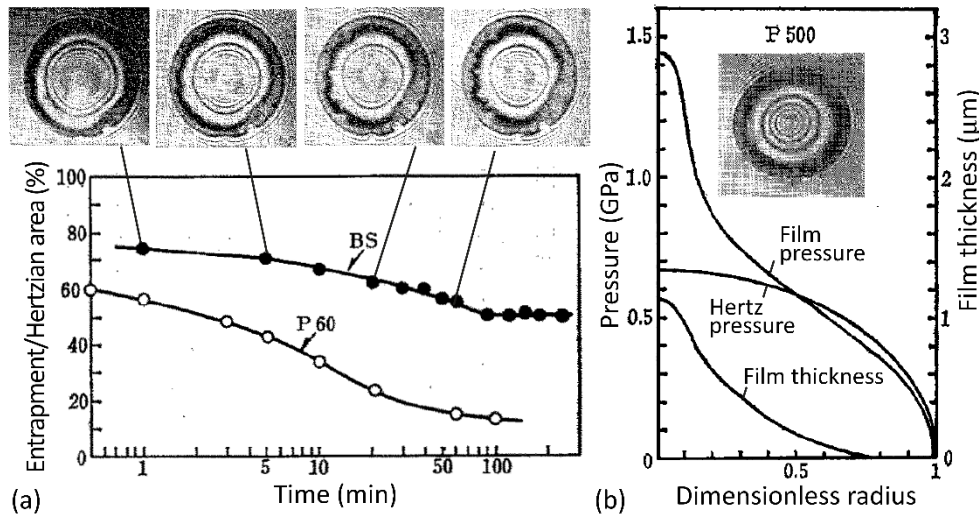


Fig. 7. (a) Changes in entrapment of low-viscosity P 60 and high-viscosity bright stock (BS) oil over time; (b) Film shape and pressure distribution of P 500 oil [49].

The development of pressure was measured with a very thin manganin pressure transducer placed in the centre of impacting EHL contact [50]. The two successive pressure peaks were discovered using this unusual experimental approach. The first gradual pressure peak was generated at the moment of maximum impact load. The second sharp peak in the central area corresponded to the end of impact stage when the steel ball nearly rebound from the lubricated glass plate. The time sequence of pressure development including the two peaks was similar to the pressure distribution in the mid-plane of steady rolling EHL contact (see Fig. 8). Both effects of increasing the drop height and the ball weight cause generally a higher pressure due to the increased impact force. Again, the effects correspond to the effect of load in the rolling EHL contact. These results were analysed in order to advance the numerical procedure for the normal bouncing of the ball on the oily plate by Dowson [51]. The resulting numerical solution predicted the second pressure peak and the entrapped lubricant with the minimum film thickness at the periphery of contact when the ball was decelerated by viscous damping of lubricant.

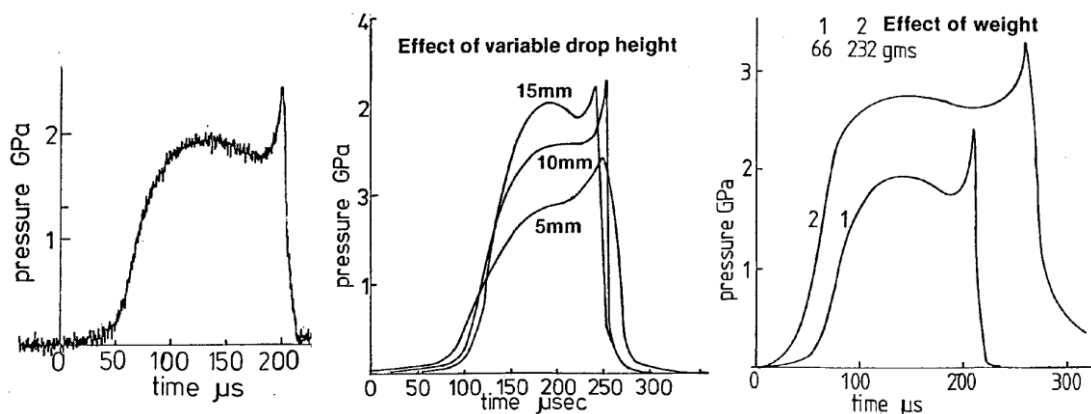


Fig. 8. The pressure-time trace and effects of drop height and ball weight [50].

In the same year as the previous paper, broad theoretical descriptions of the impact and rebound were presented by Larsson, et al. [52, 53] where the effects of initial impact velocity, ball mass, and lubricant properties were considered. In principle, the identical pressure course over time was shown as in [50]. Furthermore, the EHL cavitation occurred at the beginning of the ball rebounding and another pressure spike was computed along the periphery of the central area of contact [53]. A phase shift between the minimum film thickness at the contact periphery and the maximum impact force took place due to lubricant damping and the elasticity of materials. The phase shift increased with the reduction in the initial impact velocity and the ball mass, whereas the minimum film thickness became thicker when the impact velocity was increased. The central dimple decreased during a rebound when also the absolute minimum film thickness emerged. The affection of minimum film thickness was explained by the continuity of lubricant flow under squeezing. When the pressure in lubricant and its viscosity, and thus also the shear flow resistance, are increased as a result of a higher impact speed, the clearance represented by the minimum film thickness has to be increased to allow for the lubricant escape from the high-pressure area of contact. A similar effect as the impact speed was found in the pressure-viscosity coefficient  $\alpha$ . Additionally, the higher the viscosity of lubricant due to these parameters, the more lubricant was entrapped; the film in the central area was thicker.

These theoretical studies were followed by experimental work [54] focused on the influence of viscosity and impact velocity on the depth and diameter of dimple. An impact of ball on glass disc was attained via a freely falling pendulum with a ball mounted at its end. Tests were performed for 25 combinations of five synthetic poly- $\alpha$ -olefin (PAO) oils of different viscosity and five impact speeds. The results are illustrated in Fig. 9. The maximum dimple depth over the impact time was achieved almost immediately at the beginning of the impact for the low-viscosity oils (VG15, VG46), while the dimple depth for high-viscosity oils (VG150, VG320, VG1000) gradually increased up to its maximum, which took some time. It was also shown, that the dimple becomes deeper with the increase in viscosity and the

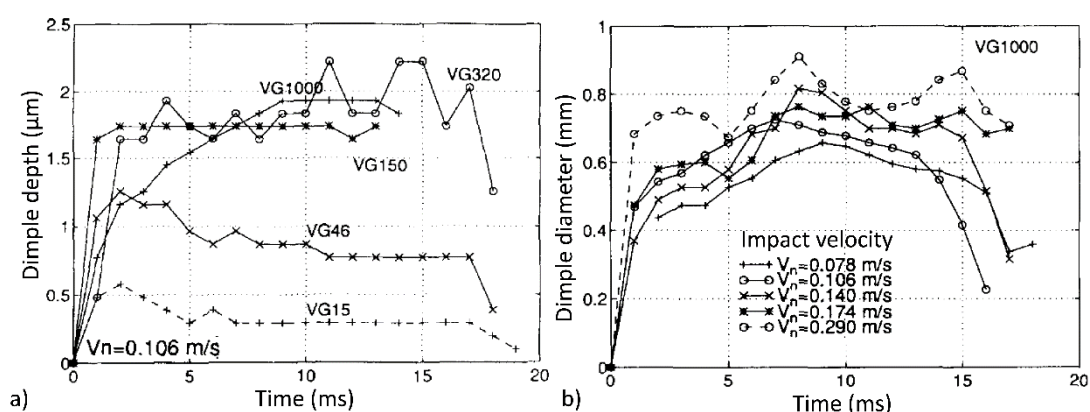


Fig. 9. The influence of lubricant viscosity on dimple depth (a) and the influence of impact velocity on dimple diameter (b) [54].

reduction of impact time, particularly for low-viscosity lubricants. This confirms the previous theoretical suggestions [52, 53] and experimental conclusions [49]. The influence of impact speed was later confirmed by Chu [55]. In contrary to the results of Kuwano and Ohno [49], a diameter of dimple was not affected by viscosity; however, it was enlarged by the impact velocity. The EHL cavitation was observed under all test conditions at the end of the impact and it was localised on the outside of the dimple boundaries. Unfortunately, the results [54] were affected by the vibrations of the experimental device, as is evident from the large fluctuations in the measured data.

A cam mechanism was used to introduce a pure cyclic squeeze motion representing normal vibrations in the point EHL contact [56]. A variation of film shape was roughly reverse during loading and unloading processes when the central film thickness remained constant over the entire cycle. The observed phenomenon was attributed to the viscoelastic and elastic-plastic (glassy state) behaviour of oil under given pressure. Under conditions of small amplitudes ( $9\ \mu\text{m}$ ) and high frequencies (40 Hz), the air bubbles produced during the unloading process remained in the course of loading, especially for lubricants out of solid-like state, and the air prevented the pressure generation. Due to suppression of pressure generation, the oil entrapment may fail or the asymmetric entrapment can be formed instead of the stable concentric one. A similar cyclic squeeze motion was afterwards analysed numerically in [57]. A general agreement with the experimental results [56] was achieved regarding to the film shape during the approach-separation cycle. The differences were ascribed to a neglect of thermal effects. The dimple film thickness at the end of loading exhibited a linear relation with the frequency in a log-log scale, as the squeeze effect was enhanced by the increase in frequency. However, the occurrence of air bubbles was not considered.

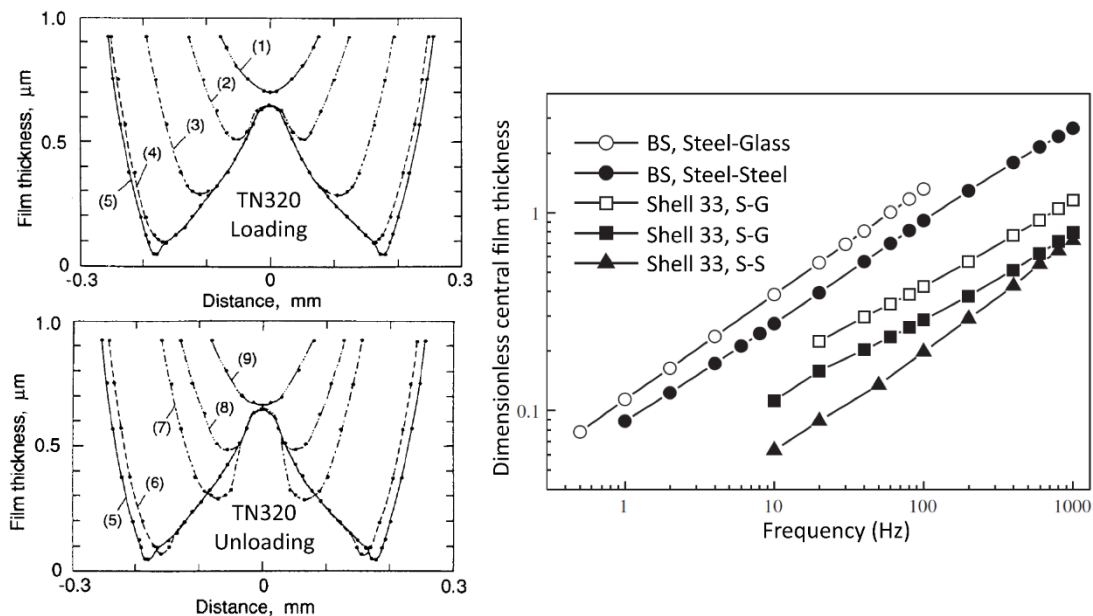
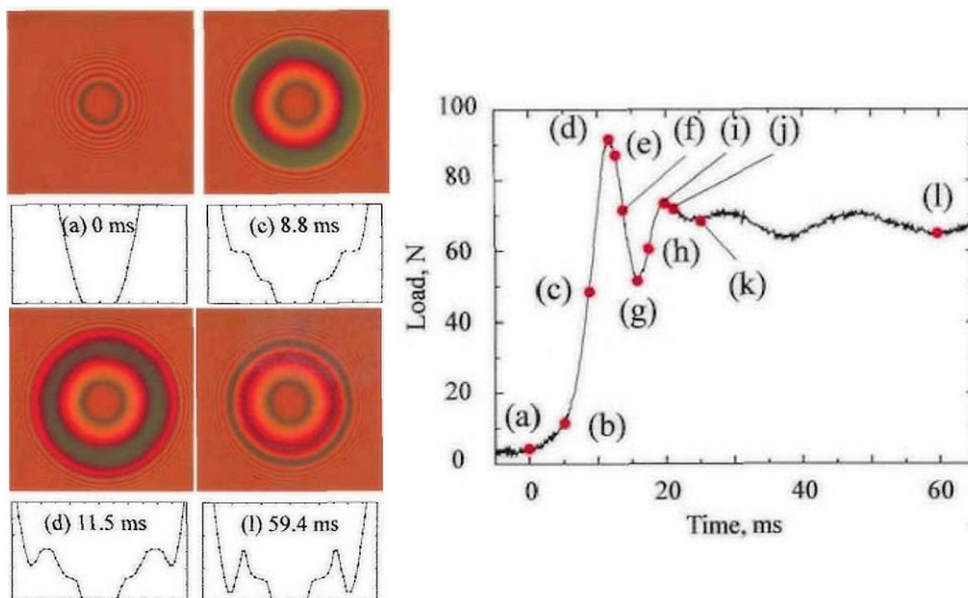


Fig. 10. A dimple film shape during cyclic loading and unloading (left; [56]) and relation between the dimple film thickness and the frequency of squeeze cycles (right; [57]).

After 1995, the attention of non-steady state EHL research was turned mainly to the integration of both the effects of squeeze and entraining action resulting from transient tangential speeds, the consequences of which are listed in the relevant subchapters. The studies dealing with the pure squeeze action began to appear again almost 10 years later. Sakamoto et al. [58] introduced the impact load via a direct-current solenoid to a preloaded contact or to a contact with the initial gap where a thick layer of oil separated the contact surfaces of a steel ball and a glass disc. They used mineral bright stock oil (BS), PAO-based traction oil (ST100), and tar-hydrogenerated oil (TN320); all these oils have a relatively high viscosity and pressure-viscosity coefficient. An interesting phenomenon was observed when the contact was initially loaded before a sudden load was applied. The BS oil was entrapped at the periphery of the contact, whereas the inner portion of initial film distribution remained unchanged. This periphery entrapment brings an increase in the contact region. The final shape of the film was affected by oscillations of load immediately after the impact. The higher the initial load was used, the thinner the film of entrapped oil in the periphery was obtained. The effect of initial load on the entrapped film thickness was negligible at long impact times. Comparing different lubricants, thickness and the amount of oil at the periphery increased with the increase in viscosity of oil. However, this trend was not true for the condition of the initial gap between the surfaces. Under such condition, the lubricant was entrapped in the central area of contact, as was published by previous authors. It is suggested that the entrapment is dependent mainly on loading speed, applied load, and ambient viscosity (viscosity at atmospheric pressure) and pressure-viscosity coefficient of lubricant.



**Fig. 11.** Interferograms and mid-plane film profiles demonstrating the film entrapment at the contact periphery and the corresponding load curve [58].

Kaneta, Nishikawa, Guo, and other co-authors further investigated the phenomenon of periphery entrapment (noncentral dimple) in a greater detail. They solved this problem numerically assuming the Newtonian lubricant and ignoring thermal effects [59]. A viscosity-pressure relationship was adopted according to Roelands [60]. It should be noted that this numerical simulation did not directly correspond to the preceding experimental study [58]. The steel ball approached the lubricated glass plate at different initial impact gaps, initial impact speeds, and thicknesses of oil layer. The initial gap and speed were revealed as substantial parameters for the formation of periphery dimple when the thickness of oil layer was less pronounced, but also important. The resistance of lubricant to Poiseuille flow rate  $(\rho h^3/\eta)(\partial p/\partial x)$  was considered as the purpose of dimple formation. At large initial gaps (i.e. high local film thickness  $h$ ), the flow resistance is first magnified in the central area of contact due to high viscosity  $\eta$  caused by a central pressure  $p$ , whereas the flow resistance is low in the periphery region. Consequently, the lubricant will escape from the closing surface gap at the periphery, and a certain volume of lubricant is entrapped in the central area of the contact – the central dimple with the minimum thickness at the periphery is formed as in the case of free dropping ball. However, when the initial gap is sufficiently

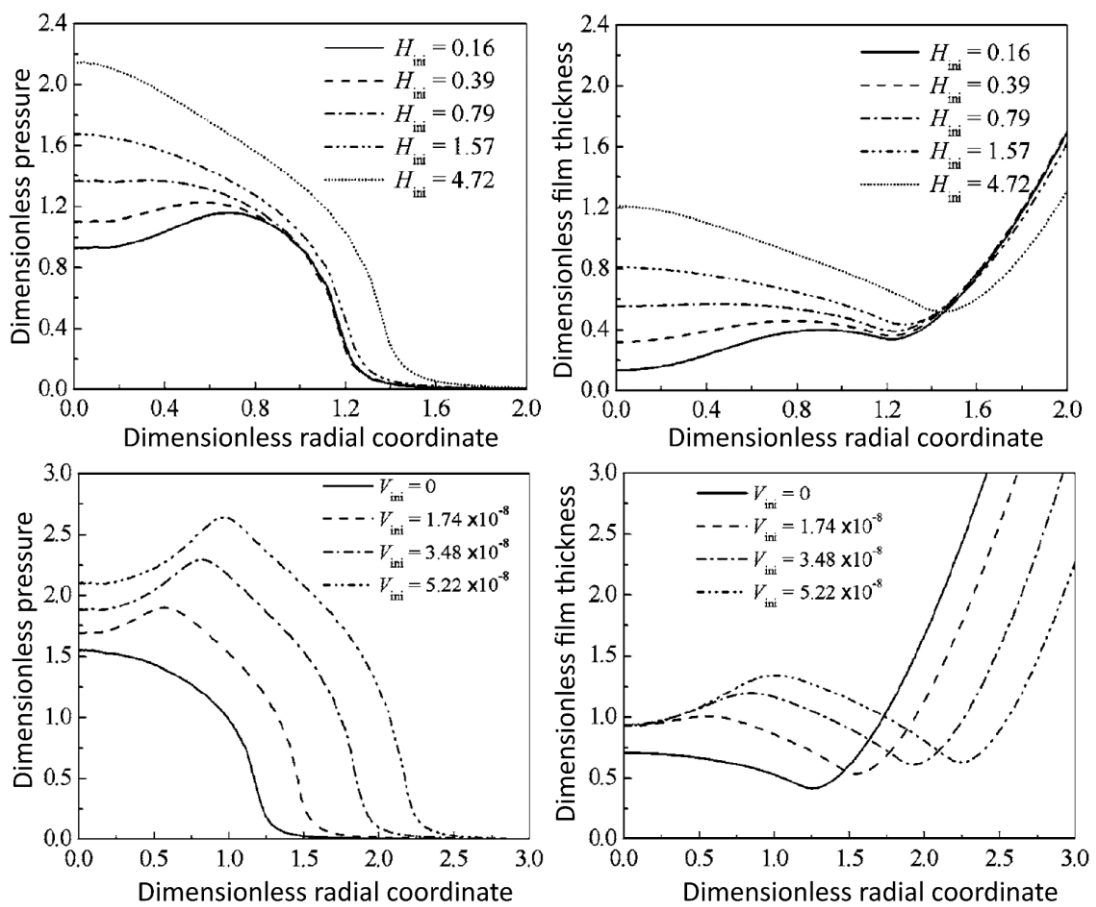


Fig. 12. The effect of initial impact gap (top) and initial impact speed (bottom) on the pressure (left) and film thickness (right) distributions [59].

small, the thin central film is difficult to squeeze; thus, it remains almost unchanged (no significant central dimple is formed), and the pressure peak changes its location from the central to the periphery area during the impact. Here, the squeeze action takes place, the local flow resistance becomes strong, and the gap between the surfaces is reduced at a larger distance from the contact centre. The thickness of lubricant layer has to be sufficiently thick to fill the whole gap, generate the local pressure, and create the periphery dimple with minimum film thickness in the central area of contact. It also means that the reduction of initial gap suppresses the second pressure spike in the central area demonstrated by Safa and Gohar [50]. Moreover, the squeeze action was markedly determined by the initial impact speed. A higher speed enhanced the generation of pressure at the contact periphery and led to the formation of noncentral dimple. Additionally, the stepwise load was simulated. After the application of the first low load step of 4 N, the squeeze force rebounds the ball and the following impact causes the central dimple. After the second step load of 60 N, the periphery dimple appeared around the central dimple.

The predicted effect of initial impact gap [59] was examined via the optical interferometry for BS oil in [61]. The ball was pushed against the glass disc by a piezo-actuator where the linear load rate of 12 N/ms was assumed. It was identified that both the maximum thickness of entrapped film and the central thickness were identically reduced together with the reduction in the initial gap up to the point where the dimple moves away from the central area to the periphery. A shape of dimple top was gradually changed from convex (central dimple), through flat (still central dimple) to concave (periphery dimple). The results were supported via the numerical scheme, which was used in [59]. The same conclusions were deduced based on the flow resistance represented by  $\eta/h^3$  as the response to Poiseuille flow. Nevertheless, in the results of experiments, the central thickness was fixed over the whole process of the closing surface gap at the periphery, although the numerical results indicated a decrease in this thickness in the course of the process.

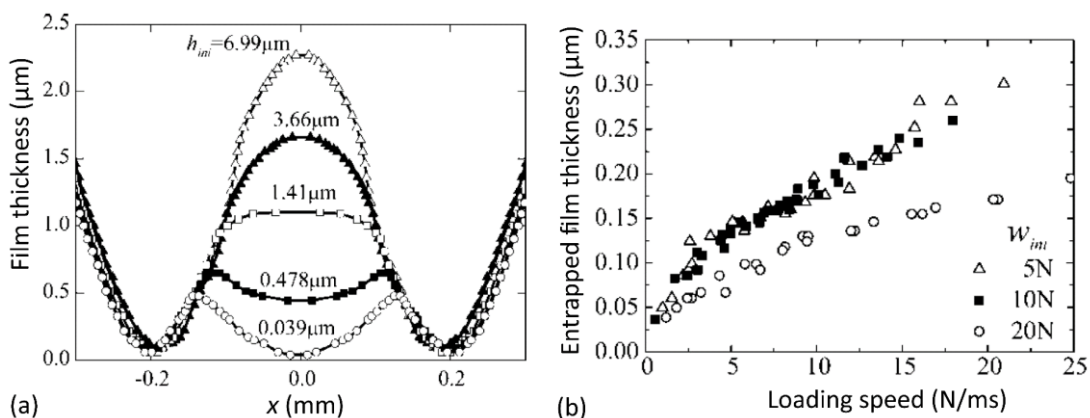
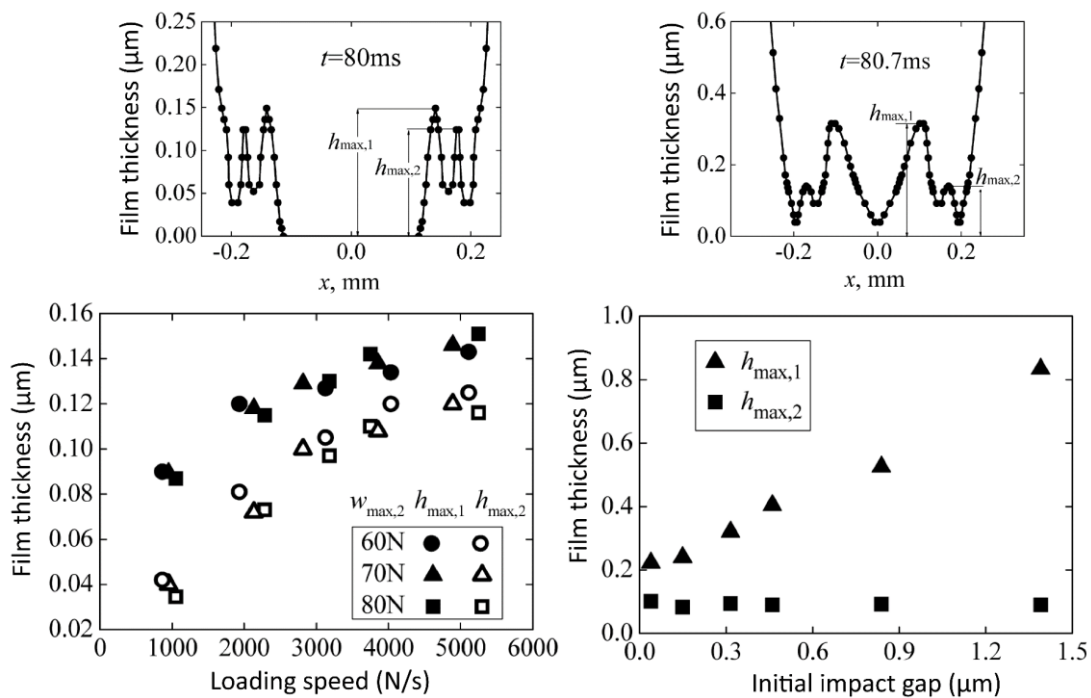


Fig. 13. The experimental results of the influence of initial impact gap (a) and average loading speed (b) on the film thickness [61].

Furthermore, a markedly higher loading speed in simulations (about ten times) was necessary to achieve similar dimple. This contradiction probably results from the assumption of Newtonian fluid in the simulation, while the BS oil under pressure in experimental conditions can get close to the glass transition state, as was shown by Ohno [62] for this lubricant. Therefore, the Newtonian model may not be suitable for impact or sudden load conditions.

Moreover, the impact on the EHL contact preloaded by different initial forces was examined experimentally in the same paper [61] and the effect of loading speed was included. For the preloaded contact (zero initial gap), the periphery dimple was formed confirming the findings of Sakamoto [58]. The increase in loading speed reduced the time needed for the lubricant to flow out of the contact, and thus a larger amount of oil was entrapped and a thicker film was formed in the dimple. Consequently, the entrapped film thickness decreased with the increase in the initial load due to the increase of boundary area through which the lubricant was leaking. It also implies that the entrapment is influenced by a rate of change in Hertzian contact radius during the impact.

Next experimental study [63] was focused on the factors affecting the entrapped film thickness at the periphery under two-stage impact load. The very same experimental device and the lubricant were employed. When the two impacts were sequentially applied to the preloaded contact, the equivalent number of periphery dimples was formed outside the previous Hertzian contact radius. The maximum entrapped thicknesses of dimples remained constant during tests, but they were influenced by loading speed. The thickness of succeeding dimple was



**Fig. 14.** The two-stage impact results: the impact at preloaded contact (left) or including initial gap (right) and corresponding effects of average loading speed and initial impact gap on the film thickness [63].

smaller than the thickness in the previous one since the rate of the increase in contact radius was reduced. In the case of the impact with an initial gap, only a small amount of lubricant was entrapped at the second impact, but the initial gap influenced substantially the first dimple. A glassy state was discussed because the entrapped lubricant was frozen-like after the first-stage impact. A comparison of the one-stage and two-stage impacts revealed that the final film shape of the two-stage impact is given by a superposition of the individual corresponding one-stage impacts.

Due to the divergence in numerical and experimental results [59, 61], the effects of important parameters for lubricant entrapment were further investigated, mainly numerically in [64]. This time, a viscosity-pressure relationship proposed by Bair [65] was employed instead of previous Roelands one. The Bair's relationship predicted a higher viscosity and the rate of viscosity increase with the pressure than the Roelands' relationship. Consequently, a comparison of numerical and experimental results showed a good agreement according to the effect of initial gap. Unfortunately, no further direct comparison with experimental data is included in this study, and the remaining conclusions were based only on the analysis of numerical simulations. Film thickness and pressure distribution were significantly

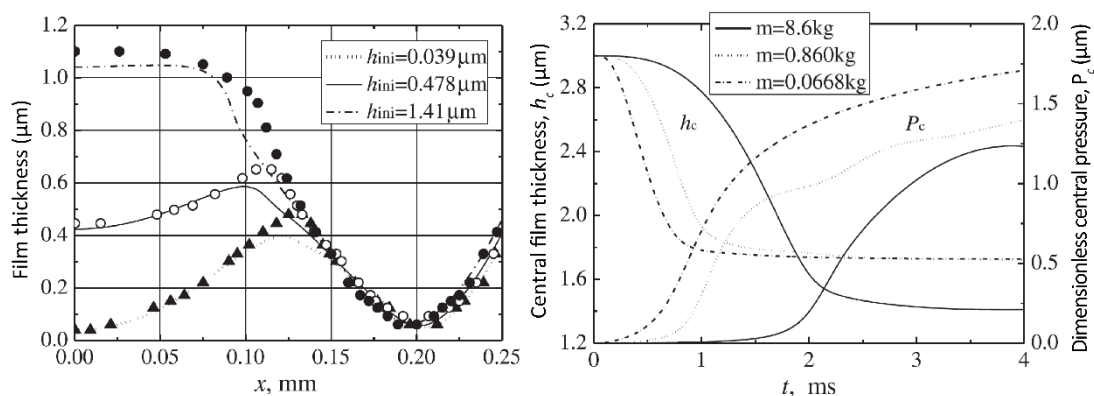


**Fig. 15.** Left: Comparison of experimental (symbols) and numerical (lines) results for various initial gaps; Right: Time trace of central film thickness and pressure representing the effect of impact body mass [64].

affected by the mass of the moving body, which determined the initial approaching (squeeze) speed. Its influence was described as remarkable since the central film pressure was, in particular, built up at the beginning of impact when the central dimple was formed almost immediately along with the impact. Besides that, the thickness and film shape in the central area of contact were accordingly given by the viscosity at the very beginning of impact, and also due to the initial stage of loading. The periphery region was determined in the late stage of loading before the load reached its maximum. Therefore, the maximum applied load increasing the Hertzian contact radius led to the entrapment of more lubricant. Also, the higher the loading or the approaching speed, the shorter the time enabling the lubricant to escape; and thus, more lubricant was entrapped. The central film thickness can reach a limiting value with the increase in loading speed because the pressure peak,

likewise the entrapped film shape, was shifted from the centre to the periphery during the increase in loading speed. Moreover, it seems that the film thickness and pressure distribution were not significantly affected by the viscosity-pressure coefficient. In addition, the formation of multiple dimples was predicted under two-stage impact loading, as was proved in foregoing experimental study [63].

Martini and Bair [66] focused on the mechanism of lubricant entrapment and its persistence in the dimple from the rheological point of view, with respect to a glass transition and fragility. The term fragility related to glass-forming liquids represents their characteristic that a degree of viscosity dependences on temperature and pressure increases when the viscosity proceeds towards a glassy state. The numerical analysis [66] included a realistic viscosity-pressure dependence of lubricants based on measurements with high pressure viscometers. Rheological characteristics of used oils only vary significantly under high pressure. Only the squeeze and Poiseuille terms of Reynolds equation were used in the numerical solution, as is common for simulations of the pure squeeze action. The analysis was

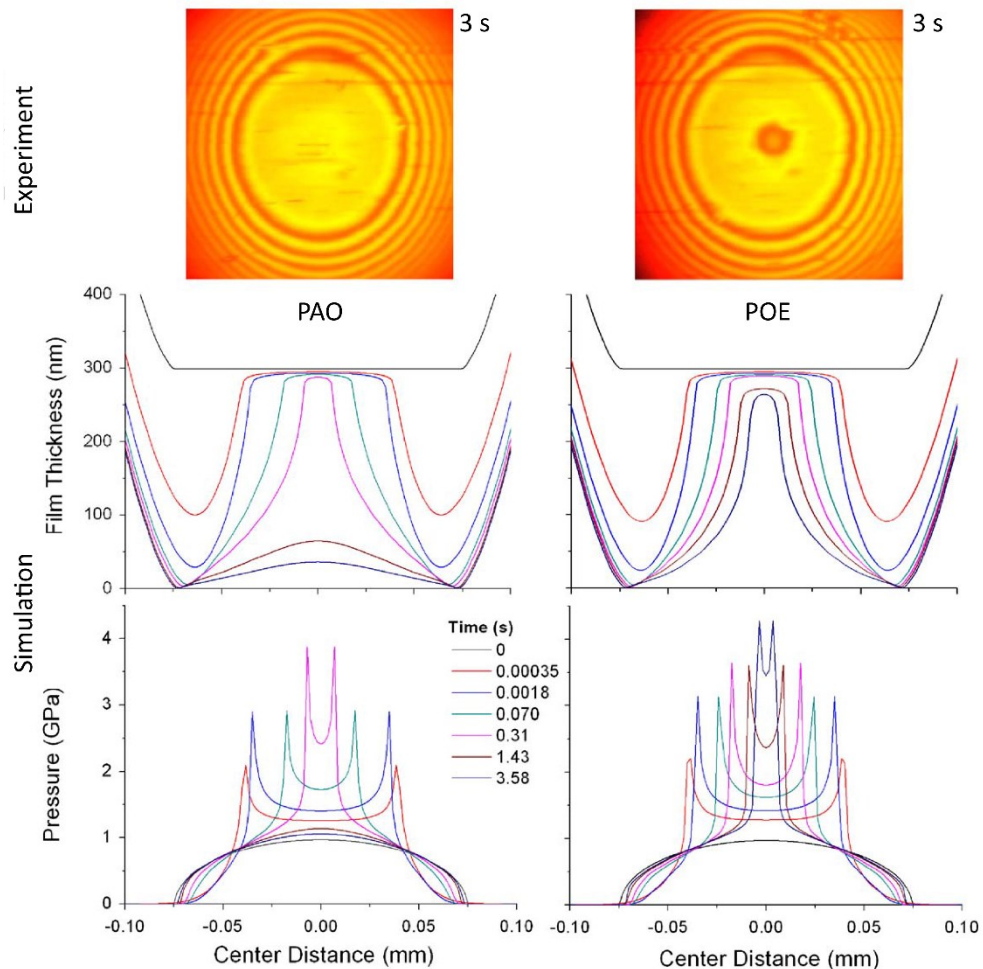


Fig. 16. The interferograms of PAO and POE entrapment and predicted film thickness and pressure distributions [66].

followed by experimental validation. It was experimentally shown and predicted by the simulation that the POE (polyol-ester) oil sustained the entrapment of 3 seconds after the impact, while the entrapment of PAO was much smaller for the same time. This is in contradiction to the previous findings since both the ambient viscosity and the pressure-viscosity coefficient of PAO are higher than in the case of POE. The cause of this opposite behaviour was attributed to the rheology of oils at high pressure (fragility) where the rate of viscosity increase of POE was more pronounced than that of PAO; POE also has a lower glass pressure transition. In addition, oils should be affected by shear thinning because the shear stress was high (about 5 MPa) close to a pressure spike. In conclusion, the study clearly demonstrated that assuming only the low-pressure characteristics of lubricants, such as ambient viscosity and pressure-viscosity coefficient, may result in predictions contradicting the actual behaviour of entrapment, in particular for the after-impact phase when the lubricant leaks out of the contact. Unfortunately, it is often difficult to gain such high-pressure characteristics of lubricants.

In recent years, a pure squeeze action has been investigated primarily theoretically. A comparison of linear, progressive, and degressive loading with respect to the loading speed confirmed the importance of the initial stage of impact [67]. With progressive loading, only a small amount of lubricant was entrapped, especially for a small initial gap, due to a low initial loading speed resulting in a low rate of pressure build up and viscosity increase. The inverse case

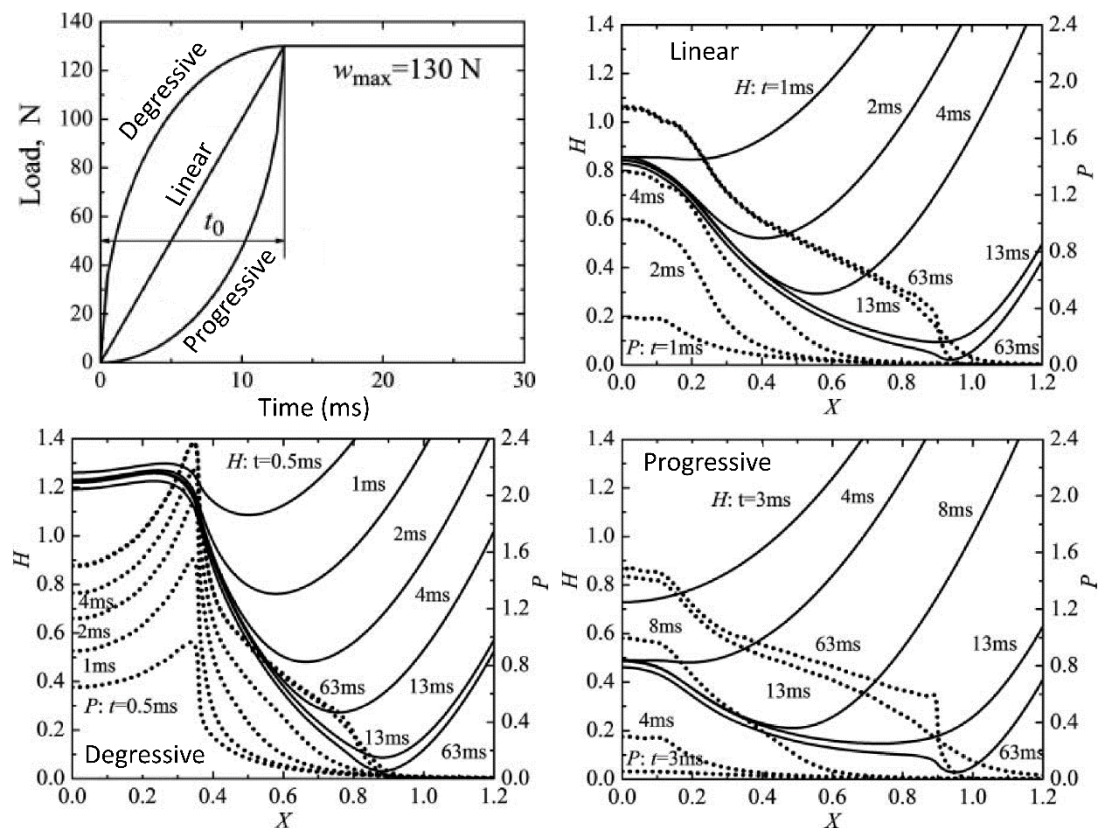


Fig. 17. Linear, progressive, and degressive loading curves and corresponding distributions of film thickness (solid line) and pressure (dotted line) [67].

was degressive loading. The extremely high rate of speed at the beginning of the impact caused a nearly flat central thickness distribution surrounded by the periphery dimple. Linear loading led to the film shape and pressure distribution corresponding to approximately their mean values from the previous loading processes. The rest of the article was devoted to the influence of surface asperities. The effect of asperities on EHL behaviour is beyond the scope of this thesis, as mentioned in the introduction; however, the interested reader is referred to the papers by Kaneta [68-71] where this issue is theoretically solved for pure impact.

The thermal effect was considered in [72] for Newtonian fluid exposed to the impact-rebound motion. The pressure distribution was reflected in the distribution of temperature. The thermal effect reduced the pressure, and central and minimum film thickness. During the impact stage, dissipation to heat took place mainly in the central area of contact due to the compressive work. Then, as the oil was leaking out of the contact and the rebound time was approached, the pressure was increased and shifted from the centre to the periphery area to balance this flow. Consequently, a much higher flash temperature occurred during the beginning of rebound process. A quantity of heat produced was affected by the initial impact gap. The larger the initial gap, the higher the initial impact speed, pressure, and temperature.

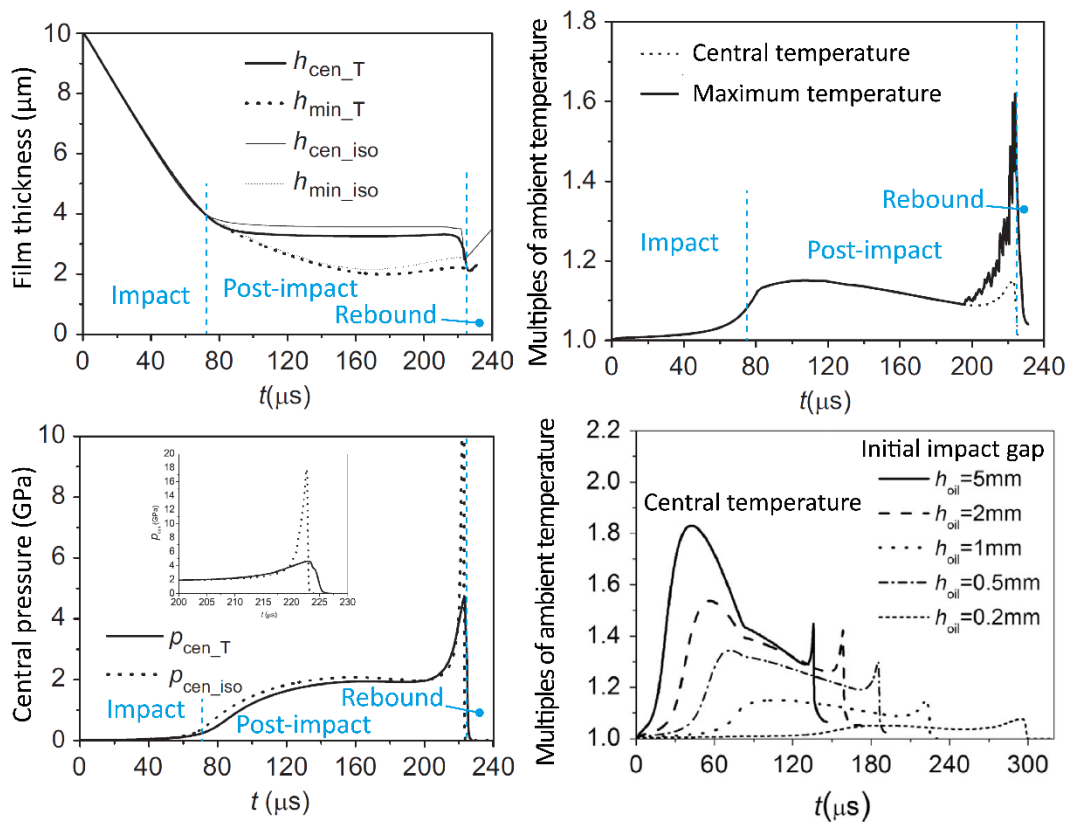


Fig. 18. Comparison of thermal and isothermal solutions (left), corresponding temperature rise (top-right), and the effect of initial impact gap on temperature rise (bottom-right) [72].

Chu studied residual films caused by a continuous leakage of lubricant from the contact long after the impact. The simulations [73, 74] showed that the pressure and film thickness may be affected by surface forces (the van der Waals and solvation forces were assumed), when the film thickness fell under approximately 5 nm. Small oscillations in pressure and film thickness mainly due to molecular interaction (solvation forces) were presented at the contact periphery with the minimum film thickness. The effect of the van der Waals forces was negligible in relation to these oscillations. Furthermore, Chu assumed an adsorption of lubricant on the contact surfaces in the case of thin films [75]. This approach of three layers of lubricant predicted a very slightly thicker film by 2 nm in comparison with the usual EHL solution. However, these findings are not very important from the EHL point of view because such thin films belong rather to the boundary lubrication regime.

An analytical prediction of central film thickness for EHL line contacts was derived by means of a curve fitting the numerical results in 2013 [76]. A squeeze action was simulated by a cylinder falling onto a lubricated plate. The Roelands' equation for viscosity-pressure relationship and a modification of impact analysis for dry contact by Johnson [77] were implemented. The final predictive equation  $H_c = 2.3M^{0.2}L^{0.55}$  was based on the Moes dimensionless parameters of material  $M$  and load  $L$  (the smallest set of dimensionless parameters used for numerical solution of EHL; the parameters do not have a direct physical significance regardless of their designation). Very recently (in 2016), the prediction of entrapped central film thickness was also published for the point contact (impacting ball) by Venner, Wang and Lubrecht [78]. The same approach and assumptions including the impact time were used as those in the case of line contact. The curve fitted equation of central film thickness was provided as follows  $H_c = 0.73M^{1/6}L^{0.55}$ .

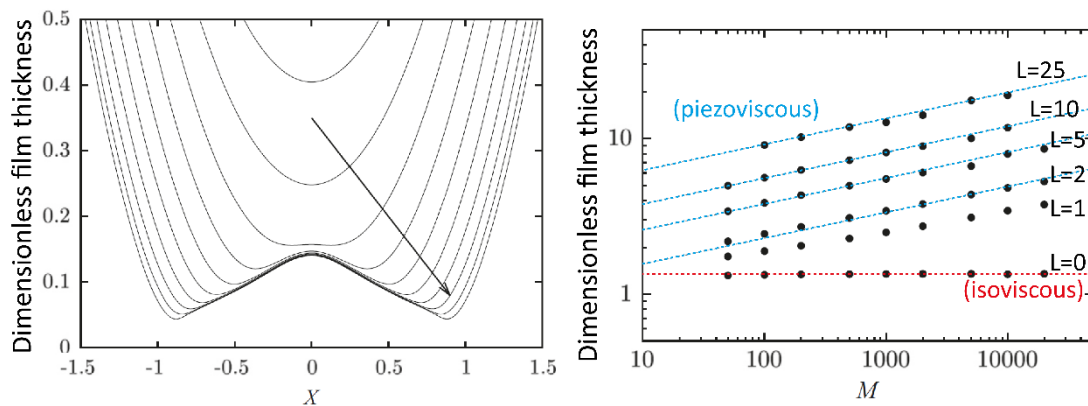


Fig. 19. Simulation of film thickness at different times during impact (left) and estimated central film thickness (Moes) as a function of  $M$  and  $L$  parameters (right) [78].

## 2.4 Impact/variable load at rolling/sliding

In the early work of Vichard [79], in 1971, the effect of load variations on the rolling EHL contact was investigated both theoretically and experimentally. The theoretical calculation of film thickness was simplified using the Grubin's approximation and the average film thickness was measured via the capacitance method. Both approaches pointed out the importance of squeeze action, which contributed to resistance to changes in film thickness resulting from transient operating conditions. It was established that the squeeze action corresponds to viscous damping of lubricant.

Ren et al. [80] performed experimental analyses of rolling point and line contacts under sinusoidal dynamic load. A new apparatus employing an optical interference method was presented. In the case of point contact, the shape of film thickness was significantly different from that predicted by the EHL theory. A dimple film shape appeared in the contact near the contact outlet with the increase in load. This was not observed for the line contact. This contrary was attributed to its higher contact stiffness. A similar increase in film thickness with a lubricant entrapped in the central area of contact was simulated and demonstrated by Scales et al. [81] when the contact was subjected to a sudden increase in load.

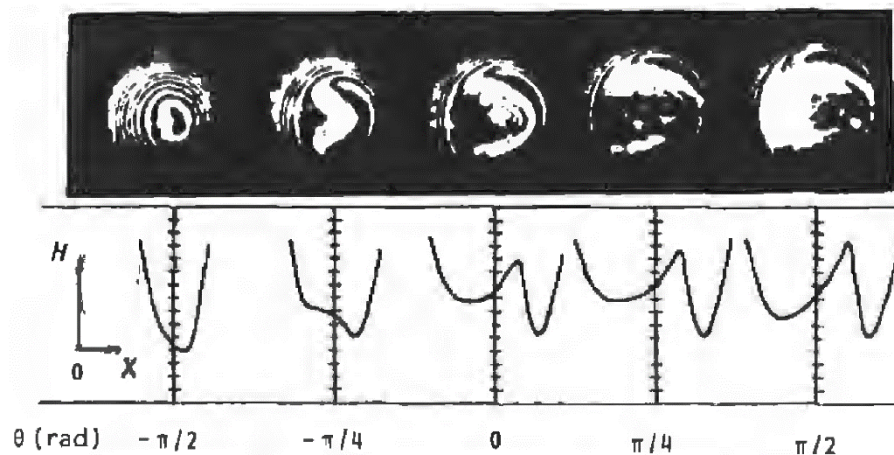


Fig. 20. Film shape variations under sinusoidal load [80].

Later, a sudden load of rolling contact was also introduced by Wijnant et al. [82]. The load increase was immediately followed by the enlargement of Hertzian contact area, whereas the film thickness was initially affected by load outside of the contact. Consequently, a thicker film of lubricant due to the squeeze motion passed through the contact from its inlet side at the average speed of the contact surfaces. This behaviour was previously observed by other authors [83, 84] for contacts with artificial surface asperities. After a sudden load, the oscillations of contact bodies (ball and disc), i.e. structural vibrations, took place and were reflected in film thickness fluctuations. This film thickness pattern propagated through the central area of contact at a specific wavelength when the fluctuations were gradually

suppressed due to viscous damping of lubricant. A dynamic model of EHL contact was tailored to these conditions showing the similar results of film thickness variations. Simultaneous effects of squeeze and entrainment were highlighted for analyses of rolling bearings. Wijnant and Venner [85] further improved the numerical model of structural vibrations with regard to EHL starvation, when the load oscillated sinusoidally. Film thickness fluctuations due to vibrations were induced at the time of starvation. The wavelength of fluctuations was dependent on the excitation frequency.

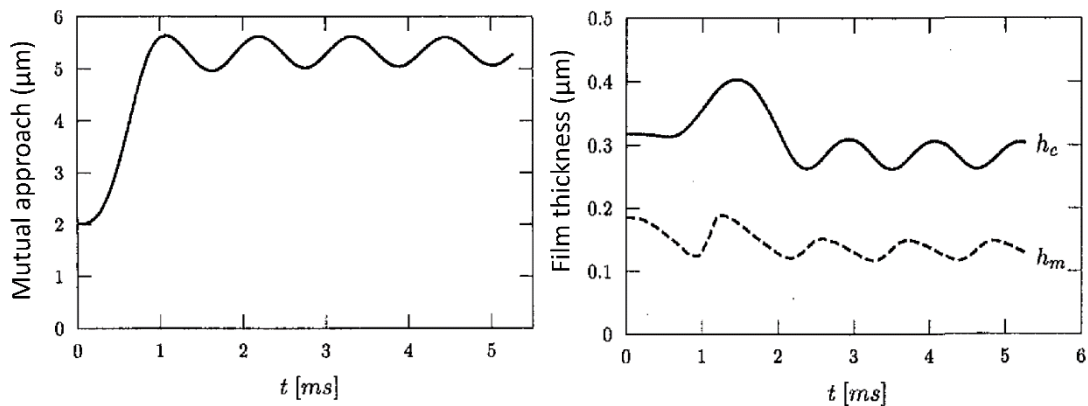


Fig. 21. Mutual approach, and corresponding central and minimum film thickness under structural vibrations [82].

Besides the first experimental evidence of periphery dimple for pure impact loading, Sakamoto et al. [58] examined the film entrainment under pulsating load in rolling and rolling/sliding contacts. It was shown that the crescent-shaped thick and thin films were induced at the contact inlet and they moved through the contact without a change in their shape and thickness at approximately entrainment speed. Likewise, as in the case of periphery dimple, a sudden increase in load led to the entrapment of thick film just outside the initial Hertzian contact; subsequently, the thick film was entrained into the contact. A thin film was caused by starvation due to the presence of air bubbles at the inlet; these were brought about by sudden unloading. The effect of pulsating load on film thickness was diminished with the increase of entrainment speed (film fluctuations approached steady state thicknesses), since the squeeze action was reduced by high overall thickness. On the other hand, the thickness of crescent-shaped dimples increased along with the impact speed. Moreover, the film behaviour was hardly affected by a slide-to-roll ratio (different speeds of the contact surfaces). A similar behaviour, effects of impact speed, and formation of crescent-shaped dimple were later observed under impact load of rolling contact [61]. Additionally, a two-stage impact load produces two, mutually independent, crescent-shaped dimples at the inlet periphery of rolling/sliding contacts [63]. It is emphasised that the initial phase of film entrapment never occurs inside the rolling/sliding contact and the film within the contact is not directly influenced by the impact, because the central area of EHL contact is only slightly sensitive to the change in load due to a flat shape of film and

high viscosity of lubricant in this area, and thus the viscous damping reduces the local approach of surfaces. These findings refute the conclusions of early studies where a dimple film shape was seemingly formed within the contact near the contact outlet [80, 81].

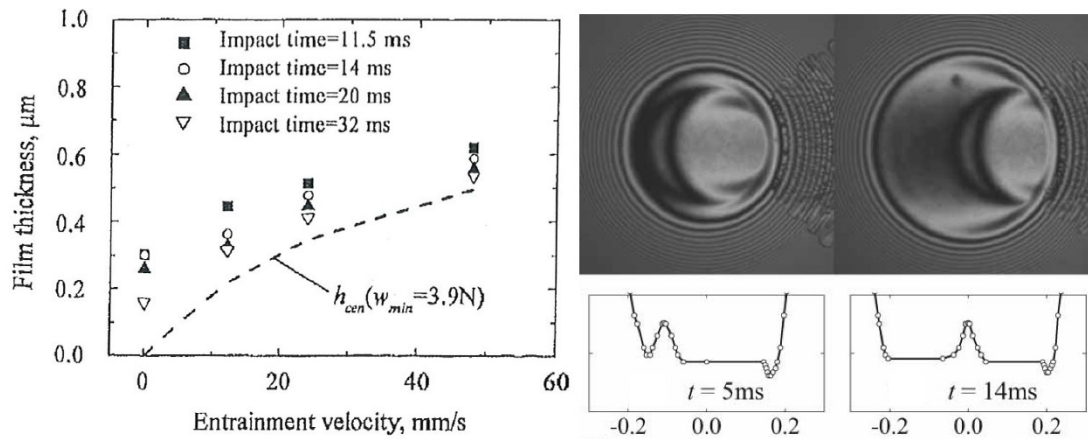


Fig. 22. Effect of entrainment and impact speed on film entrainment (left; [58]) and the passage of crescent-shaped entrapped lubricant through a point contact (right; [61]).

Yang et al. [86] studied numerically a response of point contact exposed to normal harmonic vibrations, wherein the thermal and shear thinning effects were considered. A transient analysis reveals the cyclic variation of load-carrying capacity, pressure, temperature as well as film thickness, and coefficient of friction. These parameters differed from those obtained via the steady state solution. The difference was pronounced mainly at very high frequencies (around 1 000 Hz), and when the amplitude exceeded the initial clearance between the contact surfaces. A comparison of isothermal and thermal, and Newtonian and non-Newtonian approaches pointed out only small differences in pressures and film thickness, but substantial changes in temperature and friction (see Fig. 23). Furthermore, the time-spike of central pressure can be generated during vibrations when the contact surfaces move away from each other, similarly as was simulated and confirmed experimentally previously for rebound phase after the impact.

The EHL film response of PAO to harmonic vibrations was investigated experimentally by Kalogiannis, Mares, and Glovnea [87]. The load varied in sinusoidal fashion between 20 and 30 N at frequencies of 10, 50, and 100 Hz. Film fluctuations were confirmed only for the highest frequency when these fluctuations reached about 10% of overall film thickness and no crescent-shaped entrainment was clearly visible. The absence of significant fluctuations was attributed to small changes in load and insufficient accelerations for this purpose.

An overwhelming majority of articles dealing with smooth EHL contacts under impact/variable load, which were published later, were solved theoretically and were focused, in particular, on line contacts. For example, Morales-Espejel [88] performed an inlet analysis of EHL contact, introducing a time-varying normal approach. The analytical and semi-analytical solutions for approximation of central

film thickness and inlet pressure were derived from the transient Reynolds equation for the inlet shape of contact. The predictions showed a good agreement with full numerical solution of line contact, but the results for point contacts were underestimated.

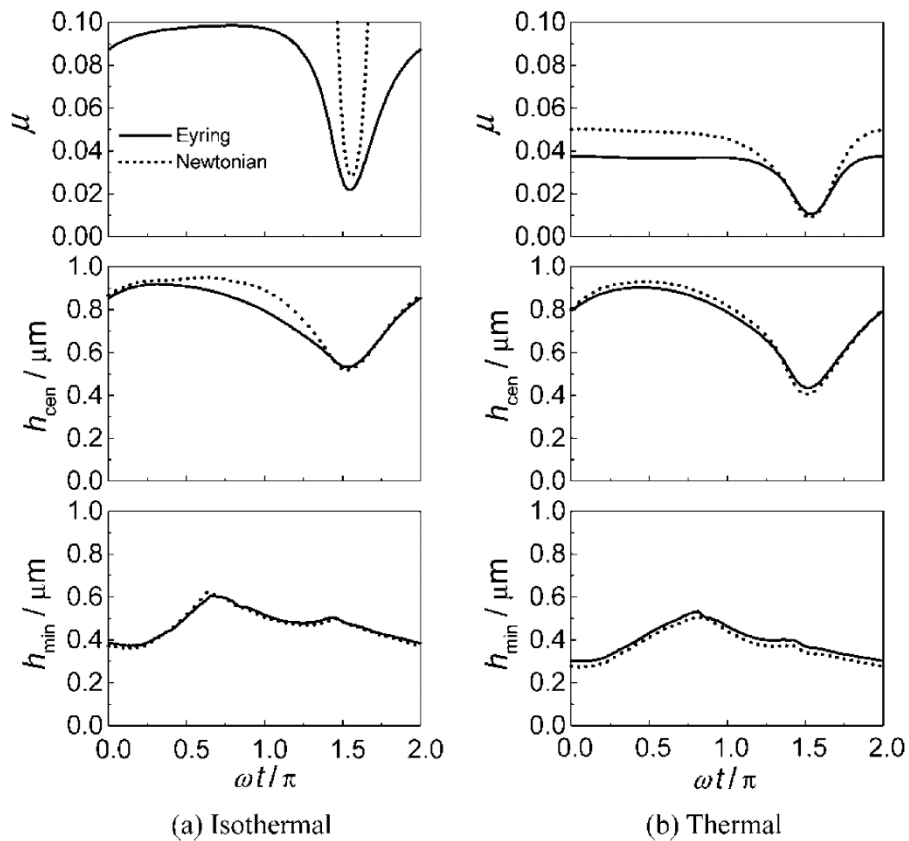


**Fig. 23.** Cyclic variation in coefficient of friction, central and minimum film thickness (top to bottom) predicted by isothermal or thermal and Newtonian (dotted lines) or non-Newtonian (solid lines) solutions [86].

## 2.5 Transient unidirectional motion

### 2.5.1 Harmonic and accelerated/decelerated motion

Most of studies, which considered the influence of transient entrainment motion not only on film thickness but also on EHL friction, did not appear before 1990s. Then, Hess and Soom [89] employed a disc machine to investigate friction in mixed, elastohydrodynamic and hydrodynamic lubrication regimes. A disc formed a line contact with a flat fixed rider. Pure sliding speed oscillations followed a triangular wave pattern at constant acceleration and deceleration and frequencies up to 5 Hz. Four mineral oils of different viscosities were used as lubricants. The coefficient of friction (CoF) was different for acceleration and deceleration, especially at low sliding speeds, creating friction loops around the steady state values. A friction force increased during deceleration, and vice versa for acceleration. The size of loops increased with both the frequency of oscillations and the viscosity of oil. However, at higher speeds, where EHL regime occurs, no significant divergences of friction were observed. Moreover, a time delay between the minimum speed and the maximum friction force was observed; it increased with viscosity of oil and normal load. The time delay was nearly independent of speed or constant distance between the inlet and the central area of the contact (transport delay). Constant time delays from measurements were consequently used for approximation of friction via simulations by a simple friction model when a good agreement with measured data was obtained. This delay was attributed to a combination of entrainment and squeeze action resulting in squeezed films in EHL regime and to deformation of surface asperities in mixed lubrication regime. These results, together with simple model of friction, were a starting point for further theoretical studies (for example [90-93]) simulating mainly the line contacts in mixed or boundary lubrication regime.

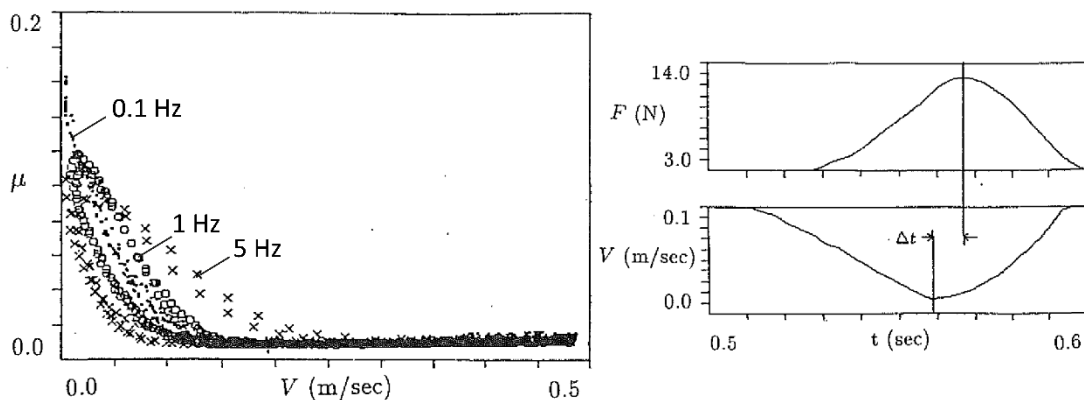


Fig. 24. Effect of frequency on friction loops and time delay between the points of the minimum sliding speed and the maximum friction force [89].

Glovnea, Diaconescu, and Flamand [94] derived a relationship for approximation of film thickness in the line contact under transient speed conditions including the effect of inertia forces on the oil flow. A numerical solution indicated

that the influence of inertia forces results in the increase of maximum pressure and decrease of load carrying capacity for motion with positive acceleration, and vice versa, for negative acceleration (deceleration). The derived analytical solution predicts that the positive acceleration causes a reduction in film thickness and deceleration leads to the increase in thickness. This predicted effect for line contacts was not very strong, since the very high accelerations about  $10 \text{ m/s}^2$  and rolling speeds of  $1 \text{ m/s}$  were needed for a change in film thickness by 12%. The effect of acceleration/deceleration on film thickness was also assessed experimentally for the point contact via the optical interferometry method. A similar trend was found at harmonic variation of speed and acceleration, but the measured deviations of film thickness for acceleration/deceleration were higher than those calculated. The measurements were carried out only at low accelerations up to  $0.25 \text{ m/s}^2$  and rolling speeds up to  $0.2 \text{ m/s}$ , because of vibrations of a test rig.

Sugimura et al. [95, 96] measured the variations of central film thickness in the point contact undergoing an acceleration/deceleration motion. The results confirmed that the film thickness at transient speed differs from thickness at constant rolling speed. A higher value of acceleration or deceleration (and thus frequency of oscillations) caused more pronounced negative or positive deviations of film thickness, respectively. These deviations were suppressed by the increase in rolling speed and enhanced by using a lubricant forming a thicker film for the same steady conditions. In the case of the highest value of acceleration of  $0.74 \text{ m/s}^2$  (frequency of 2 Hz), the lubricant was probably entrapped in the contact at the end of deceleration phase causing a slower rate of film thickness change. In general, the effect of acceleration on film thickness seems to be linear with respect to the rolling speed.

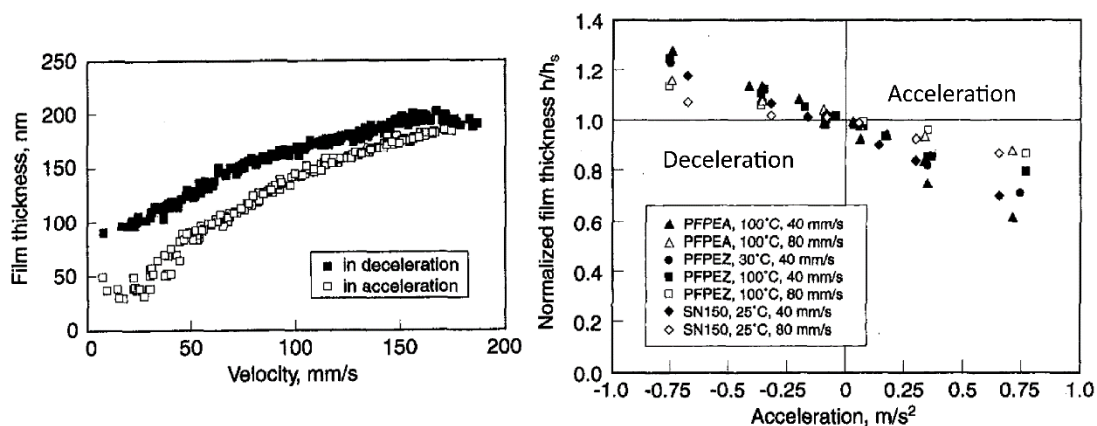


Fig. 25. Changes in central film thickness with speed at frequency of 2 Hz (left) and dependence of normalized film thickness on acceleration [95].

The results were subsequently analysed analytically in [97] where the empiric relationship  $h = h_s(1 - 0.67a\xi b/u^2)$  was suggested for prediction of film thickness  $h$  affected by acceleration  $a$ . This prediction is based on the continuity of

the flow and the film thickness under corresponding steady state conditions  $h_s$  with respect to the entrainment speed  $u$ . It is assumed that the film thickness is determined somewhere upstream of the contact inlet at the immediate flow speed and then it passes unchanged through the contact at mean speed of surfaces. Therefore, the delay in the film thickness response to the speed variation occurs and the predicted film thickness is determined by location of film formation from the centre of contact. This distance is given by the parameter  $\xi$  whose values range from 4 to 9 times the Hertzian contact radii  $b$ . If the value of parameter  $\xi$  is selected correctly, the predicted thickness agrees with the measured data. However, there is no rule how to correctly choose the parameter  $\xi$ .

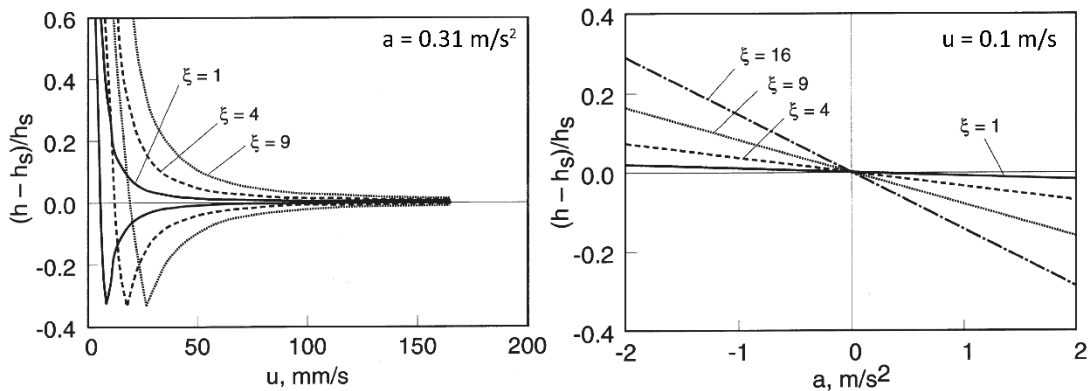


Fig. 26. Variation of normalised film thickness deviation with speed and acceleration [97].

Furthermore, Al-Samieh and Rahnejat [98] provided the full numerical solution leading to similar results as those demonstrated by Sugimura et al. in [95]. The solution was unique because it included the effects of viscous, surface and molecular forces in EHL contact under transient conditions. The importance of squeeze action at the very beginning and the end of cyclic change in speed is highlighted. The squeeze action was manifested in a separation effect at the beginning of acceleration and in the squeeze effect (dimple formation) at the end of deceleration. Additionally, when the film thickness drops under 5 nm, the structural solvation forces assumed control of pressure-generation mechanism over the hydrodynamic effect. Then, the molecules of lubricant are ordered into discrete layers, and the effect of squeeze action is negligible.

Tozaki et al. [99] conducted experiments, where the rotation speed of glass disc followed the triangular waveform and a roller was driven through traction forces from the disc. A slip between the disc and the roller occurred at sudden changes in disc speed due to the inertia force. Film thickness and traction force were measured and simulated numerically, involving thermal and non-Newtonian models. As the slip ratio increased, the traction increased only at the beginning of roller slip, and subsequently it decreased because of heating by shear of lubricant film. Similarly, the film thickness increased with the speed of disc, but was reduced by slip. The thermal effect was also proved by numerical simulations, when the isothermal calculations predicted a much thicker film and higher traction, whereas the

calculations considering the thermal effect were close to experimental results. The accuracy of the prediction was about  $\pm 20\%$  and  $\pm 10\%$  for film thickness and traction, respectively.

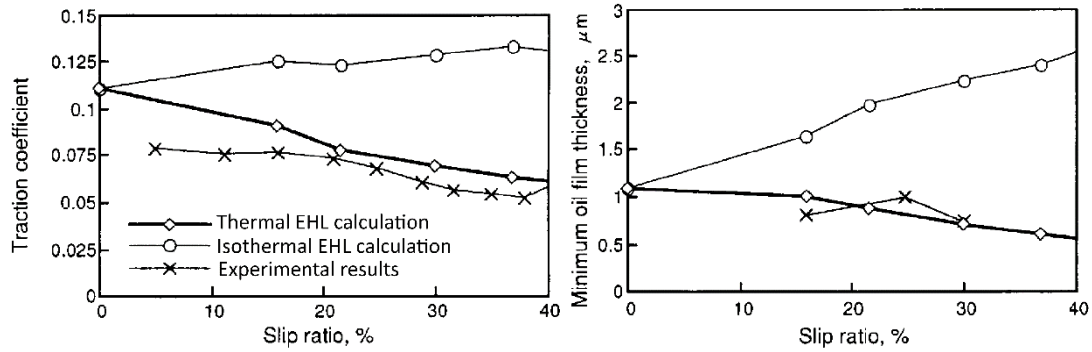


Fig. 27. Traction coefficient and minimum film thickness obtained experimentally and numerically with respect to the slip ratio [99].

The influence of the pressure-viscosity coefficient  $\alpha$  of lubricants on transient film thickness was assessed by Glovnea and Spikes in [100]. The lubricants of the same viscosity of 0.15 Pa·s but with different values of the pressure-viscosity coefficient (PAO with  $\alpha = 21.3 \text{ GPa}^{-1}$  and 5P4E with  $\alpha = 30.3 \text{ GPa}^{-1}$ ) were used. The disk rotated at a constant speed, whereas the speed of ball varied sinusoidally (unidirectional motion) with frequency of 5 (acceleration of  $1 \text{ m/s}^2$ ) and 50 Hz ( $10 \text{ m/s}^2$ ), so SRR changed from 0 to 1 during the cycle. The measured thicknesses were compared with the prediction of Hamrock and Dowson [22-24] for steady state EHL contacts considering Newtonian fluid and pure rolling conditions.

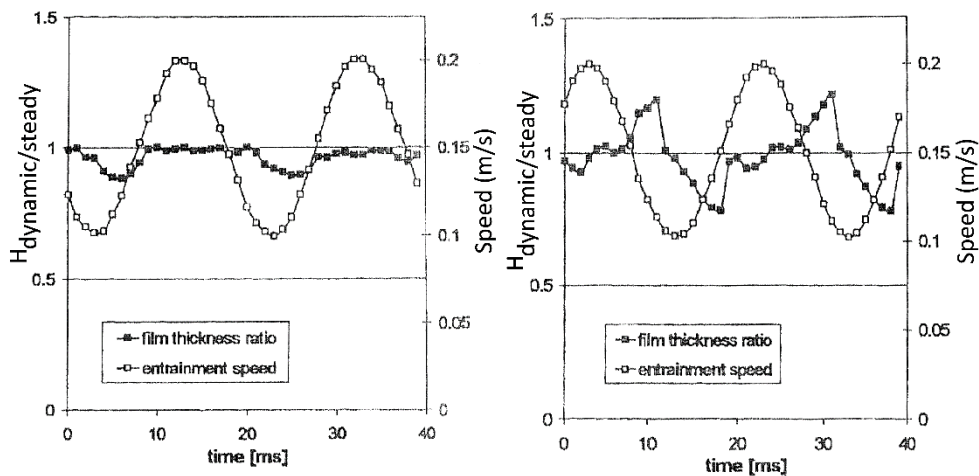


Fig. 28. Film thickness ratio for PAO (left) and 5P4E (right) at 50 Hz and 1 GPa [100].

Since the film thickness was measured at the contact centre, the time delay between the speed and film thickness was noticeable due to the time needed for a lubricant passage from the inlet of contact to its centre. It was found that the

course of the thickness of 5P4E over the cycle differed from the predicted values even at lower frequency, while the thickness of PAO deviated slightly. These deviations dramatically increased for a higher frequency of motion. The time delay was significant for 5P4E, and both the negative and positive deviation of film thickness appeared regarding to the predicted thickness. The thickness of PAO was equal to or less than the predicted values. The deviations were mainly attributed to the effects of time delay and the squeeze action. The effect of SRR was supposed to be negligible; but, in fact, it could be substantial under such conditions (shear thinning and heating effects).

Afterwards, these experimental results were investigated numerically assuming the Newtonian rheological behaviour [101]. The central film thickness was affected notably by the amplitude and frequency of speed variation, especially for very high frequency of 500 Hz, when the excited wavelength of film was shorter than the size of contact. The predicted film thickness for PAO coincided with the behaviour described in [100], but the predicted thickness of 5P4E was similar to that of PAO, and thus markedly different from the experimental findings. This clearly indicates that the consideration of non-Newtonian responses and advanced rheological models is essential for predictions of transient EHL film thickness.

Bassani and Ciulli et al. carried out several experiments on the ball-on-disc simulator, where the entrainment speed varied according to the sinusoidal law. Since both the disc and the ball were driven separately, different values of SRR were employed and the effect of SRR on friction and film thickness was studied. After the development of evaluation methodology, combinations of three low frequencies of speed variation (0.01, 0.1, and 1 Hz) and three values of SRR (0.25, 0.5, and 1) were used [102]. Friction loops were reported, where friction was larger at acceleration than at deceleration, as was found by Hess and Soom [89] mainly for mixed lubrication regime. Similarly, higher frequencies led to larger loops due to the squeeze effect. The negative squeeze effect reduced the rate of the increase in film thickness during acceleration compared to the increase in thickness according to speed under stationary conditions. Subsequently, a thinner film for the same speed gave a higher shear rate and thus a higher frictional response. The contrary squeeze effect took place during deceleration. The increase in SRR or speed diminished

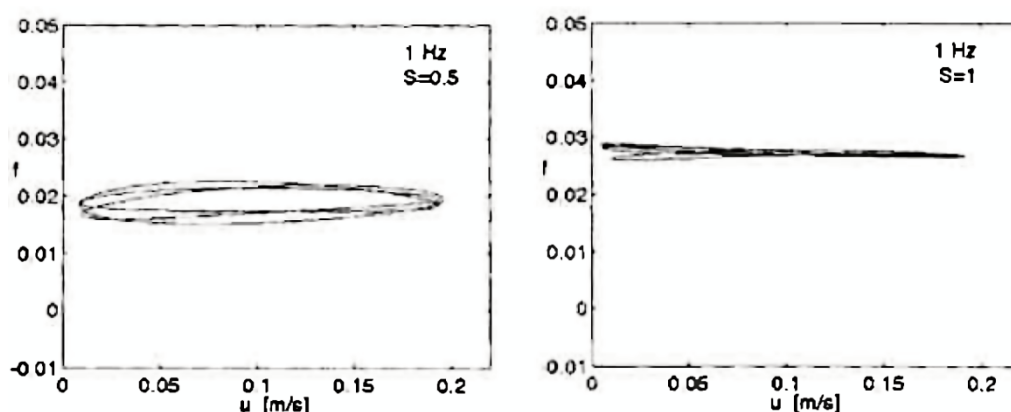


Fig. 29. Effect of SRR on friction loops [102].

these differences in friction (especially for a line contact with higher surface roughness), which indicated the thermal effects. These thermal effects are also probably the reason, why the friction loops were not observed for high sliding speeds in [89].

Hereafter, besides a glass disc (glass-on-steel contact), a steel disc was used (steel-to-steel contact) to demonstrate the effect of different thermal properties of contacting materials [103]. Friction loops were very similar for positive SRR (the ball faster than the disc) and negative SRR (the faster disc) in the case of steel-on-steel contact, but they differed for a glass-on-steel contact. This response of friction was reflected in film thickness when friction increased with a decrease in film thickness. The thicker film was formed during deceleration while the thinner one during acceleration at the same speed. Behaviours of film thickness and friction were determined by squeeze effects, as described above, and by thermal effects due to different thermal properties of contacting materials. More specifically, the so-called temperature-viscosity wedge effect was considered to be the cause of this behaviour and could amplify the squeeze effect.

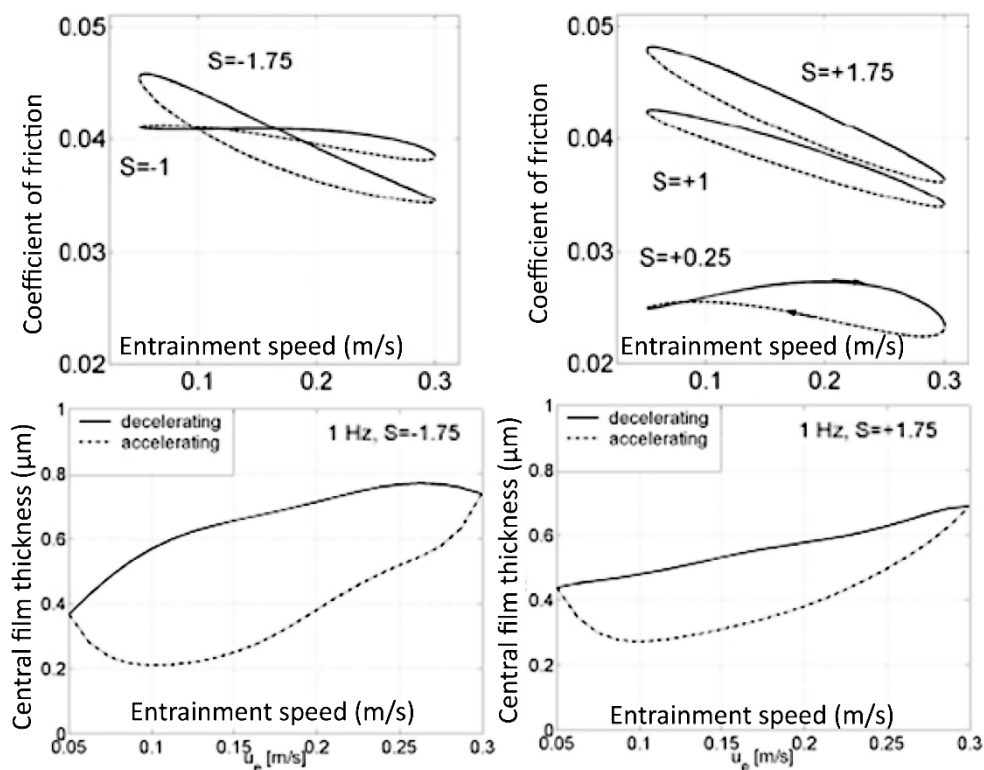


Fig. 30. Effect of thermal properties and SRR on friction and central film thickness [103].

The temperature-viscosity wedge effect was previously predicted and experimentally confirmed, especially for high values of SRR, by Yang, Kaneta, Guo, and others under steady state conditions [104-107]. In short, the temperature-viscosity wedge effect may cause a formation of dimple in the central area of contact close to the inlet under rolling/sliding conditions and thus an

increase in the central film thickness to reduce friction. The mechanism of the inlet dimple formation is based on variations of temperature and viscosity across the film thickness. Viscosity is lower close to the surface of material of low thermal conductivity (glass disc) due to the accumulation of heat compared to the case of surface of steel ball (high thermal conductivity). When the glass disc moves faster (negative SRR), a flow of low-viscosity fluid is resisted by a high-viscosity fluid acting like a wedge and the inlet dimple is formed.

A smaller steel ball was used and the film thickness was mainly analysed in [108] under similar tests conditions to those in [103]. It was pointed out that the reduction of film thickness loops is not necessary proportional to the reduction in friction loops, which should be caused by combinations of squeeze, thermal, and geometrical effects. Mutual influences of these effects on friction and film thickness were not directly determined due to their complexity. In addition, the thermal effects, especially bulk heating, can be more important for specimens of smaller radius at high speeds. It is due to the proportionally higher rotational speeds required for the same surface speed as compared to larger specimens and hence less heat is transferred from the contact through the specimen.

Ernesto et al. [109] performed experiments at transient kinematics including consecutive phases of pure rolling, acceleration, pure sliding, and deceleration. The film thickness and friction were simultaneously measured. Transitions from pure rolling to pure sliding conditions caused changes in lubrication regimes from full-film (film of 80 nm) to boundary (film of 3 nm) lubrication, respectively. The contact was emptied or filled with lubricant during acceleration or deceleration phases by means of squeeze and entraining actions, thereby several sub-contact areas of different sizes and thicknesses of film separated the contact. An additive friction model was based on this observation of time-dependent film thickness distribution where the total friction was given by the contributions of the individual sub-areas. Friction was assumed to be caused by viscous shearing of non-Newtonian fluid for the EHL regime and by plastic interfacial shear stress for the boundary regime of lubrication. Thermal effects were neglected. A very good

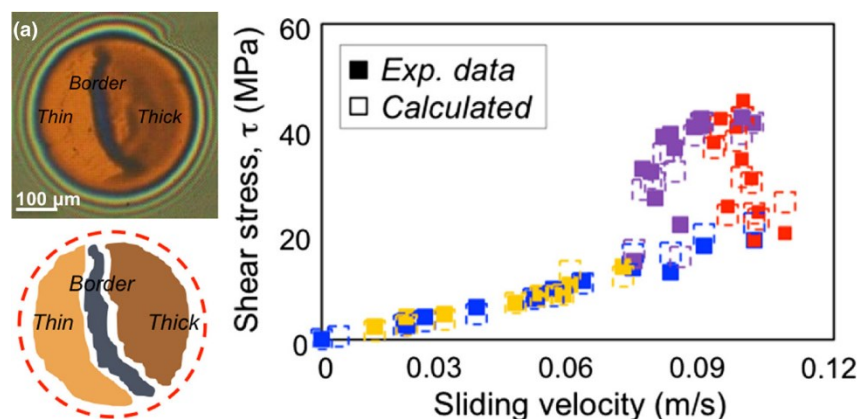


Fig. 31. Typical contact sub-areas during transition of lubrication regimes (left) and comparison of experimental and theoretical shear stresses (right) [109].

agreement was obtained between the measured and calculated shear stress explaining the origins of local friction distribution under such transient conditions of multiple lubrication regimes. A friction hysteresis (loops) occurring during acceleration/deceleration was attributed to the changes in the flow rate of lubricant.

## 2.5.2 Start/stop motion

In 1990, Kaneta, Nishikawa and Kameishi [40] excited a start/stop motion of ball or disc via a stepping motor. A set of crescent-shaped entrapped films was produced within an EHL contact by rapid speed fluctuations due to the intermittent motion of the contact surfaces. Similar crescent-shaped films were reported later by Sakamoto et al. [58] and others for pulsating load in rolling/sliding contact, as described above. A film was formed in the contact inlet at sudden start of motion and was entrapped at sudden stop of motion. The entrapped film was thicker at its entry side and decreased towards its exit with respect to the direction of motion. At low rotational speeds of stepping motor, when the amplitude of speed fluctuations was high, the entrapped thickness was higher than that obtained under steady speed conditions and some lubricants exhibited a solid-like behaviour. Since this occurred only for pure rolling conditions, not for pure sliding ones, it was suggested that the entrapped solid-like film may be collapsed by shear stress. Moreover, the moved distance of the crescent-shaped films was approximately half the moved distance of the disc under sliding conditions. The only explanation for this phenomenon is that the lubricant slippage occurred at or very close to the surface (wall-slip).

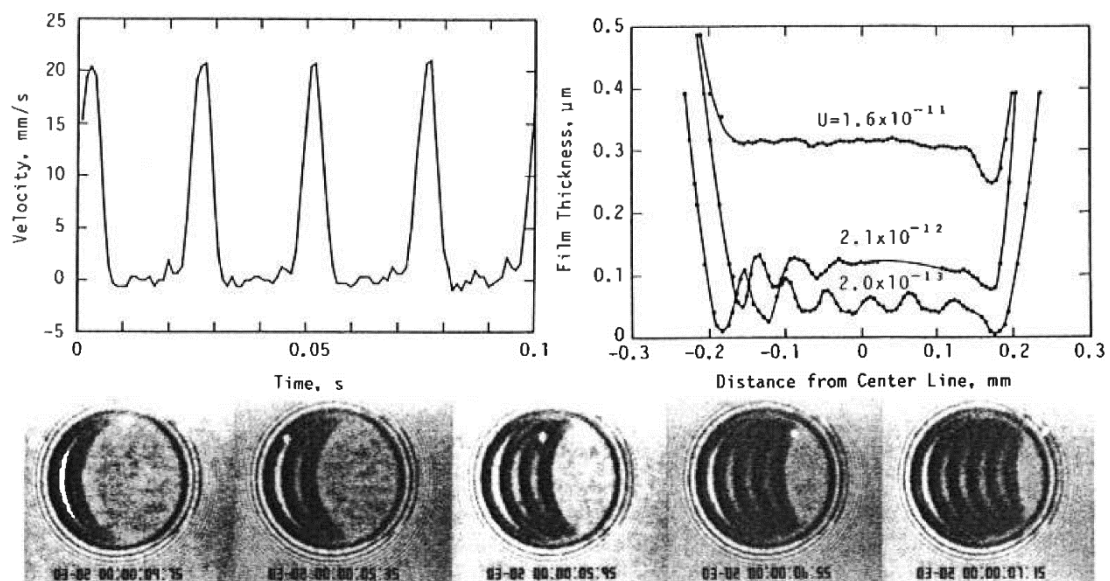


Fig. 32. Speed variation of glass disc (top-left), mid-plane film profile at different sliding speeds (top-right), and interferograms of crescent-shaped film at start/stop sliding motion (bottom) [40].

Sugimura et al. [95, 96] demonstrated the lubricant entrapment in a shape of the central dimple at halting of motion for low frequency of 1 Hz of start/stop motion. The entrapment mechanism was assumed to be analogous to a pure squeeze action. The rate of film reduction was dependent on the used lubricant. No detailed insight into the transient behaviour of EHL films was provided since the contact was recorded by a camera with a low frame rate of 50 Hz. Subsequently, Glovnea and Spikes [110] used a high-speed camera with sampling frequency of

1 000 Hz to examine the film behaviour during sudden halting of sliding motion at initial speeds from 0.1 to 1 m/s. Two distinct stages of EHL films collapse were described for different oils. The overall film thickness was reduced nearly without a change in film shape during the first stage when a rapid deceleration took place before a complete halt of motion. Duration of this stage (3 to 6 ms) was dependent on the initial speed reflected in the initial film thickness, and thus a high initial speed (thickness) was balanced by low deceleration due to inertia and lubricant damping. Correspondingly, the effect of initial speed on film thickness at the end of the first stage was negligible, while the effect of lubricant properties was substantial. Therefore, the first stage was driven by a combination of entraining and squeeze action. Interestingly, the ratio of initial thickness and the thickness at the end of the first stage was almost constant regardless of the lubricant viscosity. The first stage of film collapse was not detected if the initial speed/thickness was below a certain critical value. Then, the second phase of film collapse immediately occurred when only a pure squeeze action affected the film thickness by formation of central dimple film shape, since the motion was completely stopped. The thickness and shape of entrapped film were strongly determined by both the viscosity and pressure-viscosity coefficient of lubricant. Dimples with a flattened top were formed for oils with high pressure-viscosity coefficient.

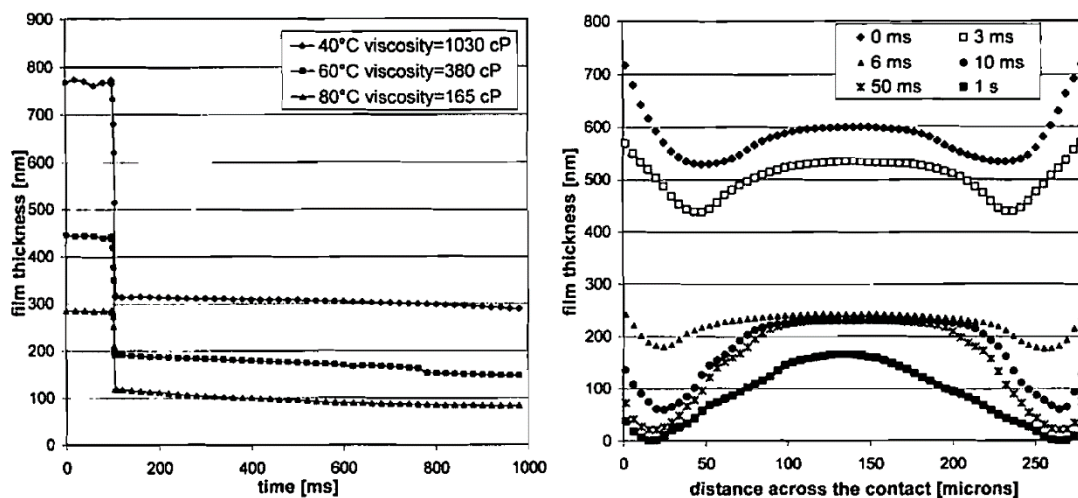


Fig. 33. The effect of viscosity on central film thickness during sudden halting (left) and film profiles at different time intervals after halting (right) [110].

The follow-up paper [111] was aimed at clarification of film collapse during controlled halting of rolling and sliding motion by a given value of deceleration from 0.5 up to  $75 \text{ m/s}^2$ . An attention was paid mainly to the first stage of film collapse, which conditions the initial thickness for the second stage driven by pure squeeze effect. As in the previous paper [110], it was shown that the overall film thickness distribution with a classical EHL horseshoe-shaped constriction is reduced during deceleration (first stage) without a change in shape. This indicated that the pressure distribution was broadly constant during deceleration. Moreover, the film was thicker during deceleration than the film predicted from the steady-state

theory [22-24], which confirmed the early findings [94-96] obtained at lower decelerations. The film shape began to change if the entrainment speed dropped below approximately 2 mm/s, then the film thickness at the inlet decreases rapidly and the dimple starts to be formed (the effect of entraining was then unimportant). The film thickness at the end of the first stage was substantially affected by the value of deceleration, whereas the initial speed had only a little effect on film thickness. The effect of deceleration for pure rolling and pure sliding was similar although a reduction in the initial thickness was slightly higher for sliding, which indicated the influence of heat dissipation on viscosity. The results were subsequently compared with the empirical relationship considering acceleration  $h = h_s(1 - 0.67a\xi b/u^2)$  [97], but a reasonable agreement was achieved only at the lowest deceleration of 0.5 m/s<sup>2</sup>. In response to this mismatch, Glovnea and Spikes [112] developed a new semi-analytical model of film thickness affected by deceleration based on Grubin's analytical solution of EHL. Film thickness is assumed to be given by a sum of the steady state thickness depending on the contact coordinates and the transient thickness depending on the time. A good agreement with experimental data was reached only at the initial part of the first stage of film collapse. The predicted thickness overestimates the measured thickness at the final part of the first stage. This was very probably caused by neglecting the influence of squeeze action, as noted in [113], where another theoretical model was published. The model [113] takes into account a combined behaviour due to the entrainment and squeeze motion. Unfortunately, any comparison of this model with the experimental data of halting motion was presented.

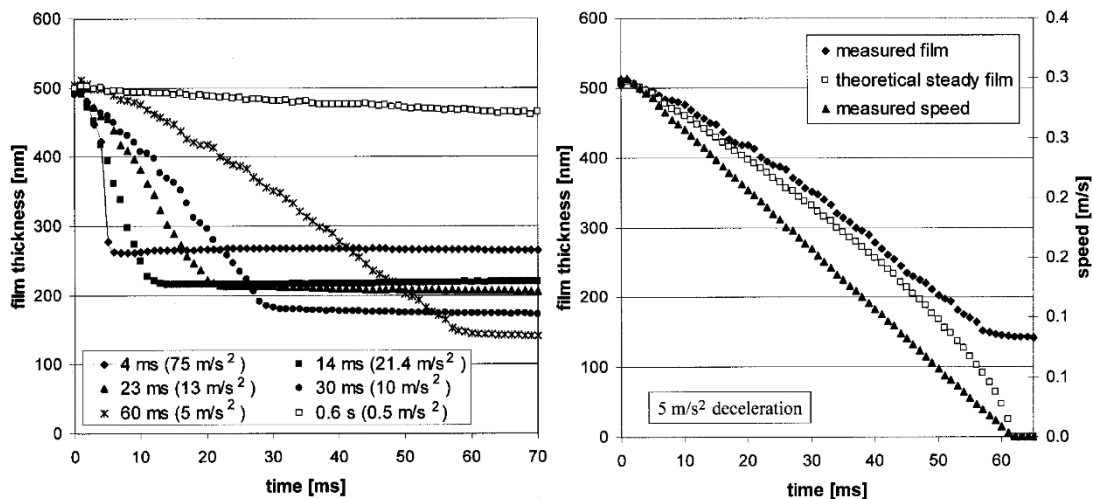


Fig. 34. The effect of deceleration on film thickness during rapid halting of motion (left) and comparison of experimental data with predicted steady state thickness [111].

Glovnea and Spikes [114] also investigated the EHL film formation at the start-up of rolling and sliding motion for accelerations from 2.5 up to 50 m/s<sup>2</sup>. The film formation was greatly influenced by acceleration. It was observed that the formation of the lubricating film took place in the individual fronts of the entrained lubricant. At first, the first front of the lubricant, without a significant change in

thickness, began to pass through the contact separating the contact surfaces. The front edge of the advancing lubricant had a circular shape across the contact with the centre towards the contact outlet. The shape of the front edge through the film thickness differed from the predicted wedge shape by conventional models and varied with acceleration. After some time, depending on acceleration, the second front and gradually the next fronts of thicker lubricant were formed at the contact inlet. Subsequently, a stepped film profile emerged as the individual fronts progressed through the contact. Furthermore, the film was thicker than that from the steady state predictions when the acceleration increased above  $5 \text{ m/s}^2$ . This was associated with the fact that the next fronts of lubricant entered the contact before it was completely separated by the first front of lubricant. For accelerations over  $20 \text{ m/s}^2$ , it was no longer possible to distinguish the individual stepped increments of overall film thickness due to a limited sampling rate of camera. Moreover, oscillations of film thickness occurred at the highest acceleration. Popovici et al. [115] simulated the effects of loading system on a dynamic response of the contact to explain these oscillations. The model predicted film thickness oscillations with the amplitude of order of several nanometers, but experimental results showed oscillations in the tens of nanometers. It means that the origin of observed oscillations was of a different nature.

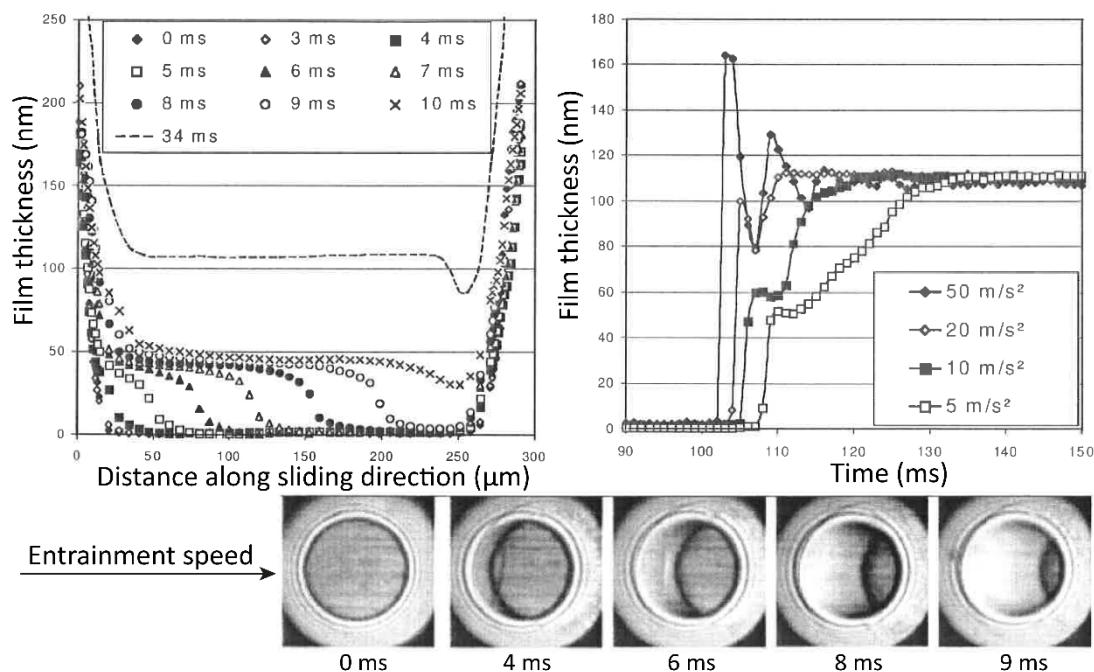


Fig. 35. Film thickness profiles (left) with interferograms (bottom) at acceleration of  $5 \text{ m/s}^2$  and central film thickness at different accelerations (right) [114].

On top of that, some differences in film behaviour were found for pure rolling and pure sliding conditions. Under rolling conditions, the first front of lubricant passed through the contact at a lower speed than the entrainment speed in the first half of the contact and a higher speed in the second half. However, in the case of

sliding, the speed of the first lubricant front was equal to the entrainment speed only close to the contact inlet, but higher in the remaining part of the contact. An analysis of film formation with regard to lubricants properties indicated that high-viscosity lubricants are able to form the stepped film shape only at high accelerations. Besides that, a transient film behaviour can be more affected by the value of pressure-viscosity coefficient than by viscosity itself. A similar study to that by Glovnea and Spikes [114] was carried out earlier by Kaneta [116], but considerably lower accelerations and lubricants forming thicker films were used, so the shape of the lubricant profile appeared to be wedge-like. Additionally, the study [116] was focused mainly on the lubricant entrapment and a subsequent wall-slip rather than the film formation after the beginning of the motion.

Holmes et al. [117] compared numerical simulations with start-up experiments at pure sliding [114]. A non-Newtonian rheological model was used and thermal effects were neglected. The numerical result showed a similar pattern of film thickness evolution, but a detailed comparison revealed considerable differences in film profiles, especially at high values of accelerations. The speeds of lubricant passage through the contact was kept at entrainment speed due to the Couette flow described by Reynolds' equation, while the front of lubricant moved in advance of this speed in experiments. Furthermore, the shape of the front edge was not stepped (S-shaped), but rounded, and the predicted thickness was thinner than the experimental values. Additionally, no film oscillations were detected. It was suggested that a substantially larger amount of oil was entrained into the contact in experiments than was considered in the calculations based on Reynolds' equation. Two possible reasons for this larger amount were discussed: a dynamic response of measuring rig caused a rapid reduction in load at the start-up followed by load oscillations and lubricant squeeze action, or the initial sticking of dry contact caused speed oscillations.

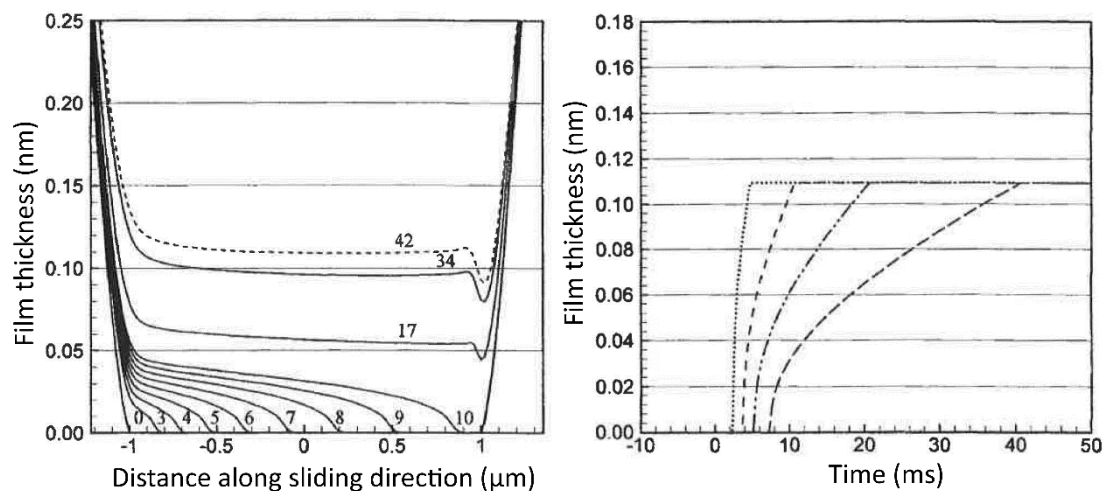
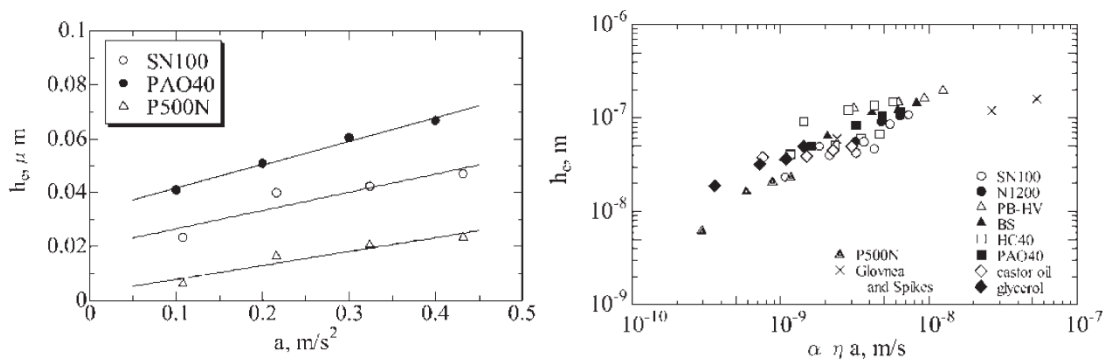


Fig. 36. Results of numerical analysis [117] to describe experimental start-up results in [114].

Later, a mathematical model of rolling line contact during the start-up was presented by Usov [118]. The model assumed a viscoelastic lubricant and three zones of contact: the zone of direct contact of surfaces (dry contact), the transient zone where the lubricant is formed by a rigid body, and the zone where the surfaces are separated by lubricant. A similar character of front speeds of lubricant was obtained as that in the experimental study by Glovnea and Spikes [114] when the front speed was determined by width of transient zone and thus, basically, by viscoelastic properties of lubricant. The lubricant properties likewise influenced the thickness of front, which was thick at the start-up of motion, when the speed of front is low, and thin at high speeds of front.

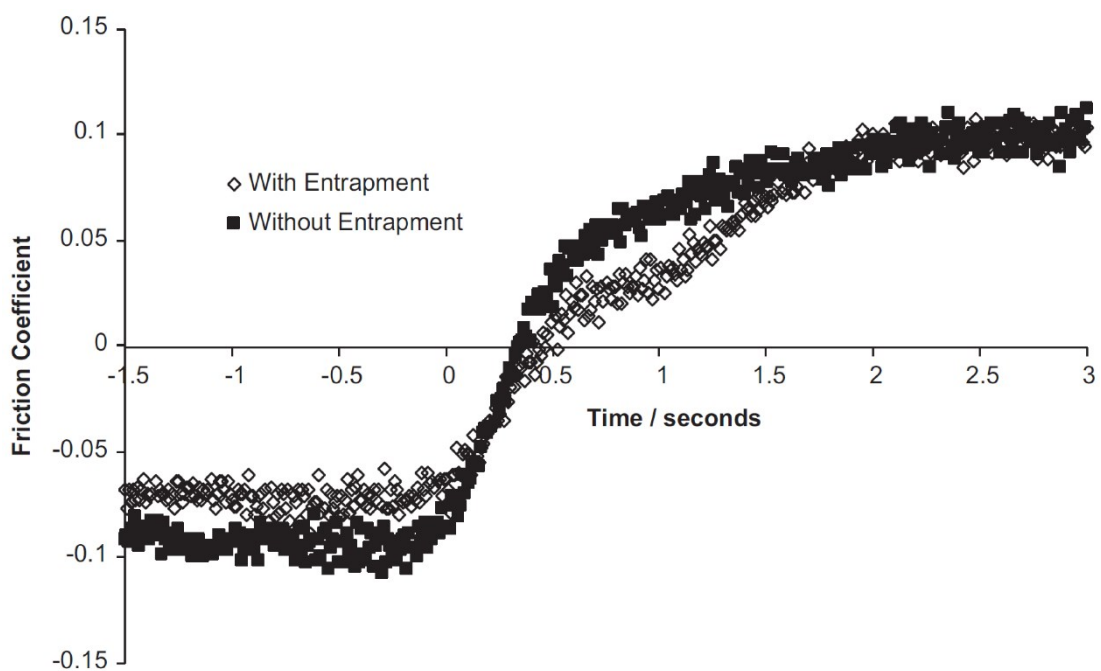
Ohno and Yamada [119] performed experiments at halting of rolling motion for deceleration from 0.1 up to 0.5 m/s<sup>2</sup>. The entrapped film thickness  $h_e$  was measured at the end of deceleration (the first stage of film collapse) together with the time required for the entrapped lubricant leakage out of the contact. First, the effects of value of acceleration and lubricant properties (pressure-viscosity coefficient  $\alpha$  and viscosity  $\eta$ ) on thickness of entrapped films were investigated. For individual lubricants, it was shown that the entrapped film linearly increases with deceleration. Moreover, when the entrapped thickness was arranged by the product of deceleration  $a$  and lubricant parameter  $\alpha\eta$ , a clear collation was found where  $h_e = (\alpha\eta a)^{0.74}$ . Next, the results demonstrated that the time of lubricant leakage out of the contact is affected by high-viscosity rheology. Nearly no leakage occurred until the viscoelastic solid transition temperature was higher than the oil temperature due to a solid-like behaviour of entrapped lubricant.



**Fig. 37.** Effect of deceleration on entrapped film thickness (left) and relation between film thickness and product of deceleration and lubricant parameter [119].

Martini and Bair [66] highlighted that the presence of entrapped lubricant eased the start-up of lubricated contacts. The entrapped film results in a lower sliding friction than the contact without entrapped film for a short period after the start-up of motion. Then, the entrapped film was displaced out of the contact due to the entraining action, and the friction was comparable with that in the contact without the entrapped film. Martini and Bair used PAO and mineral oil of high viscosity to evaluate the lubricant entrapment after a sudden halting of motion. Duration of lubricant entrapment of PAO was shorter than that of mineral oil. This

result is in contradiction with the results of Ohno and Yamada [119], since the lubricant parameter  $\alpha\eta$  of PAO was higher than in the case of mineral oil. The explanation for this disagreement is a role of fragility (high-pressure rheology) and a lower glass transition pressure of PAO compared with the mineral oil, similarly as was discussed in the subsection dealing with the impact load. In addition, Kumar and Kalita [120] simulated an isothermal line contact after halting of motion where they studied the effects of shear-thinning behaviour and oils exhibiting linear piezoviscous response at low pressures (for example water/glycol solutions or low viscosity oils). These oils show a fast leakage of the entrapped lubricant and thus short time of entrapment. The shear-thinning effect was unimportant after stopping the motion because of the absence of Couette flow and thus a low shear stress.



## 2.6 Reciprocating motion

The early work of Petrousevitch [121] concerning a sliding reciprocation of steel ball on a glass/sapphire plate was published in 1971. The optical interferometry was used to measure the film thickness and the point contact was recorded at a frequency of 800 frames per second. It showed that the shape of film thickness changed during reciprocation with the direction of motion and with the speed. The film thickness was reduced at the contact inlet when the speed slowed down, and a low thickness took place at both the contact inlet and outlet after the interruption of motion. At the reversal of motion, a zone of minimum film thickness gradually disappeared from the contact. Unfortunately, the information on the frequency of reciprocation or sliding speeds was not listed.

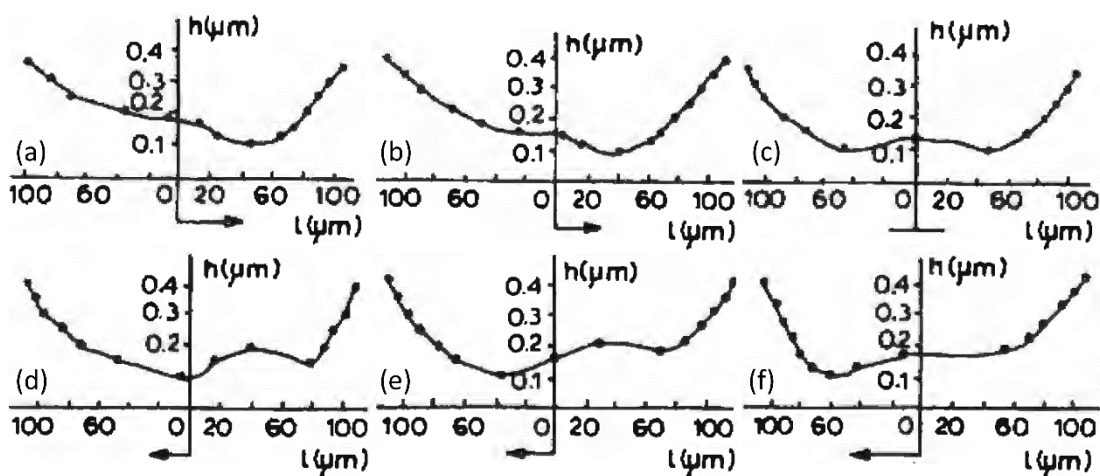


Fig. 39. Film profiles of cylinder oil at (a-b) left to right motion, (c) interruption of motion, (d-f) right to left motion [121].

Nishikawa, Handa and Kaneta [122] provided a detailed description of behaviour of TN 320 and BS oils at sinusoidal reciprocating rolling and sliding motions. The maximum dimensionless velocity was kept fixed, while the frequency was changed with respect to the stroke length of 10, 5, 2, and 1 mm. Both oils were entrapped between the contact surfaces at the end of the stroke. This entrapment was also confirmed and simulated by Scales et al. [81]. Additionally, Sugimura et al. [95, 96] performed the experiments with the reciprocation at constant speed (see Fig. 4f). However, the results of Sugimura were not verifiable due to numerous limitations of the measuring device and techniques.

The entrapped film was thicker at the outlet side of contact than at its inlet side considering the previous direction of motion. This was caused by a more pronounced leakage of lubricant at the inlet of originally higher thickness. When the motion was restored in the opposite direction, the entrapped oil in the same shape moved towards the outlet at the average speed of surfaces and a new film was formed at the inlet. It means that the film thickness was changed cyclically as the entraining and squeeze action were out of phase (this phenomenon is called the

film breathing). Since the entrapped film of TN 320 was thinner under sliding than under rolling, it was concluded that the oil in glassy state might collapse or become be fluid under shear loading. The film thickness in the middle of the stroke for all stroke lengths (frequencies) was comparable with the thickness under steady state conditions, except for the shortest stroke length of 1 mm and a high frequency. For stroke lengths over 1 mm, the overall film thickness increased with a decrease in stroke length because of more frequent formation of the entrapment and a reduction of time for lubricant leakage. At high frequency and short stroke length of 1 mm, the EHL cavitation zone, which was formed at the contact outlet in the course of the preceding stroke, reached inlet boundary at the moment of reverse. Consequently, the build-up of hydrodynamic pressure at the inlet was inhibited by the air interspersed in lubricant, which led to a reduction of film formation and EHL starvation. The EHL contact may thus collapse under conditions of short stroke length and high frequency of reciprocation.

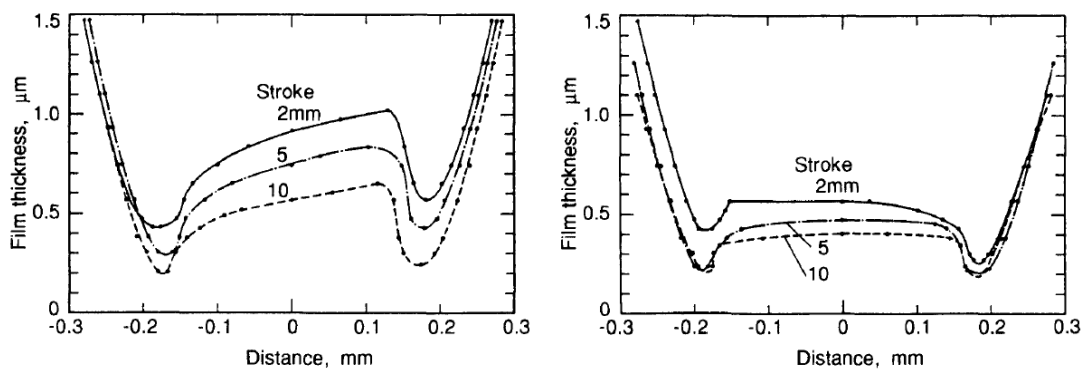


Fig. 40. Effect of stroke length on film profile at the end of stroke for rolling (left) and sliding (right) reciprocation [122].

The previous article was immediately followed by the study [123] investigating friction under pure sliding reciprocation. The maximum friction occurred at the end of stroke where a characteristic bump-shape of friction curve took place, presumably in relation to the film entrapment. The minimum friction was associated with the maximum speed in the middle of stroke due to frictional heating. This minimum value was similar to the friction under steady state conditions, as well as the film thickness. Only small variations of friction were found over wide ranges of sliding speeds and film thicknesses indicating a viscoelastic response of oils in glassy state. At low speed and stroke length of 5 mm, friction increased with a decrease in sliding speed during the reciprocation cycle, and the EHL film collapsed in some area of contact. The mean shear stress (the traction force divided by the contact area) increased nearly linearly with the parameter  $\alpha p_m$ , where  $\alpha$  is the pressure-viscosity coefficient and  $p_m$  is the mean Hertzian pressure. Moreover, the effect of cyclic impact loads on friction in the course of reciprocation cycles was examined. First, it was demonstrated that the presence of entrapped thick film produced by single impact load reduces friction. Then, friction was declined with the increase in the frequency of impact loads

during reciprocation. This effect was further enhanced for the stroke lengths shorter than the contact area when a discharge of entrapped film hardly occurred. In contrary, the EHL film collapsed, friction significantly increased, and contact surfaces were damaged for reciprocation without the cyclic impact loads at short stroke lengths. These findings show that starvation due to the conditions of short-stroke reciprocation can be suppressed by the presence of entrapped thick film within the contact and, as consequence, friction is substantially reduced.

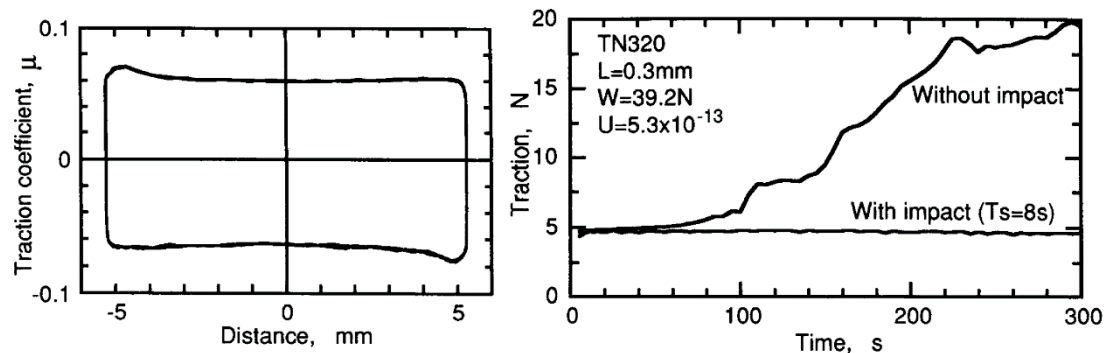


Fig. 41. Variation of friction over the reciprocation cycle (left) and comparison of frictional response at short-stroke reciprocation with and without cyclic impact loads (right) [123].

In the next paper, Kaneta and Nishikawa [124] studied the effect of slide-to-roll ratio at reciprocation on film thickness. The traveling distance and the amount of entrapped oil varied with the values of SRR of 1, 0, and -1, since the amplitude of disc was changed with respect to SRR, whereas the amplitude of ball was fixed at the value close to the diameter of Hertzian contact area. The overall film thickness was thicker when the disc was faster than the ball due to a longer traveling distance of disc, and thus a larger amount of lubricant entrained into the contact. This study also included the effect of transversely oriented bump on both the film thickness and friction. Interestingly, friction was lower for the ball with bump than for the smooth ball under conditions of short disc reciprocations (SRR = -1). A clear explanation of this phenomenon was not given but probably the bump introduced some lubricant into the contact inlet. The effect of surface asperities at reciprocating motion was likewise investigated in [125], where a local collapse of film was observed under short stroke and high frequency similarly as in the case of smooth contact.

Later, a numerical algorithm for solution of film thickness in EHL point contacts employing the entraining and squeeze action was presented by Jalali-Vahid et al. [126]. The Newtonian fluid was assumed while thermal effects and inertia forces were neglected. Numerical simulations adopted the conditions of experimental study of Nishikawa et al. [122] for the case of pure rolling reciprocation and a stroke length of 5 mm. A comparison of numerical results with experimental findings showed a generally similar behaviour of film shape during one cycle of reciprocation; in particular, in the middle and the ends of stroke. Unfortunately, the authors of [126] have not admitted that the film shapes distinctly differed at

moments of acceleration and deceleration of motion when the entrapped film was formed or pushed out of the contact. Additionally, film thicknesses were not the same over the entire cycle. These differences are attributed by the author of this thesis mainly to a complex rheology of BS oil, which was not taken into account in the simulations.

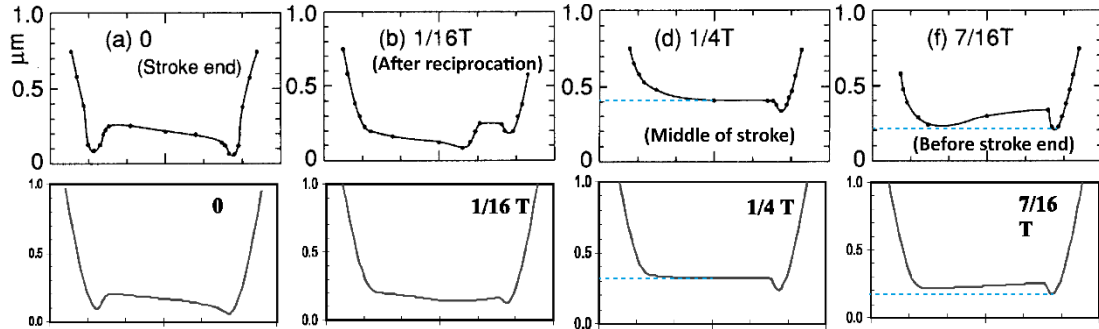


Fig. 42. Comparison of experimental results [122] (top) with the results of numerical simulation [126] (bottom).

Glovnea and Spikes [127] carried out experiments where sliding or rolling/sliding speed of reciprocation motion varied cyclically at constant acceleration/deceleration (see Fig. 4e). Unlike the studies of Nishikawa and Kaneta employing high-viscosity oils, the PAO oil of low viscosity of 0.053 Pa·s was used. The frequency from 2 up to 50 Hz corresponding to the accelerations of 2 to 50 m/s<sup>2</sup> were applied when the entrainment speed varied between ±0.125 m/s. Similarly as in the case of accelerated/decelerated motion [95], the central dimple film shape was formed under deceleration, and the thickness of dimple increased with the increase of frequency/acceleration of reciprocation motion. The thickness of entrapped film was asymmetrical as in [122], but another explanation was provided: a thicker film was localised at the outlet side of the contact due to the previously higher speed at the contact inlet during deceleration and the time

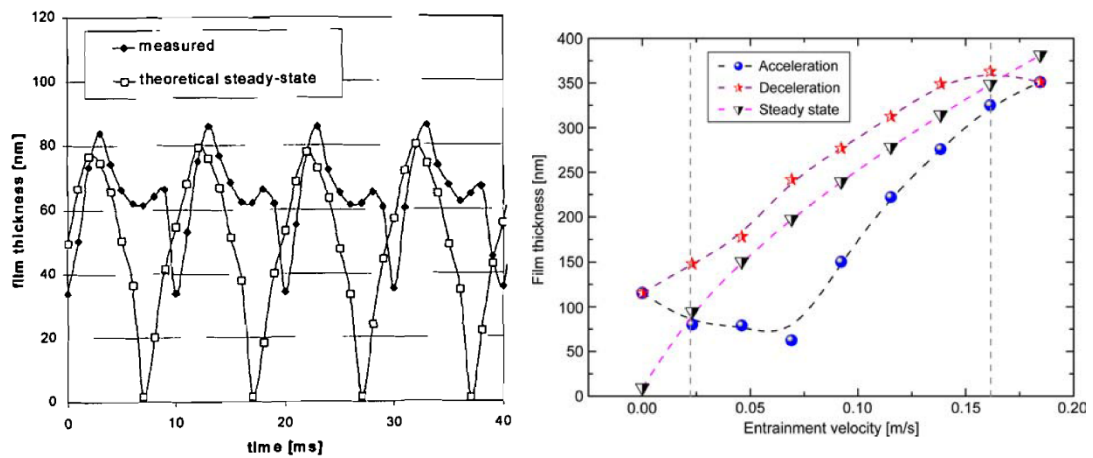


Fig. 43. Central film thickness of PAO for reciprocation frequency of 50 Hz under pure sliding conditions (left; [127]) and central film thickness of lithium grease over the reciprocation cycle for frequency of 2 Hz under pure rolling conditions (right; [128]).

needed for passage of this thick film from the inlet to the outlet of contact. A time lag between the moments of zero entrainment speed and the minimum of central film thickness was detected since the periphery constriction of dimple reached the contact centre after a reversal of entrainment. Moreover, the contact surfaces alternately moved in the same or opposite directions with the entrainment speed reversal under rolling/sliding conditions. The central film thickness variation over the stroke was comparable for both conditions of pure sliding and rolling/sliding. The main difference was that the thickness of periphery constriction was thinner with decreasing sliding speed and thicker with increasing sliding speed, which was attributed to the effect of shear heating.

The same type of reciprocation motion as in [127] was applied later by Li et al. [128]. Kinematic conditions were pure rolling with frequency of 2 Hz and acceleration/deceleration of  $1.38 \text{ m/s}^2$ . Instead of liquid oil, a lithium grease was used, as greases lubricate an increasing number of EHL contacts under transient conditions. The sampling rate of camera was only 60 fps. The grease behaviour was basically the same as in the case of oils, and the previous findings were supported also for this type of lubricant.

Wang et al. [129] simulated a line contact under reciprocation motion considering the thermal effects and non-Newtonian behaviour of BS oil for various operating conditions. It was pointed out that the results of steady-state solution and transient solution are considerably different. The effects of frequency and stroke length on film thickness and traction and their evolution over the reciprocation cycle were in general accordance with the previous experimental findings. Friction decreased with the increase in frequency or decrease of stroke length due to the increase in overall film thickness and the temperature rise. The influence of EHL cavitation zone was not considered in simulations. The temperature rise was caused mainly by shear heating, whereas the compressive heating played an insignificant role. It was highlighted that a large drop in friction may occur (considering the specific condition) despite only a slight rise of temperature.

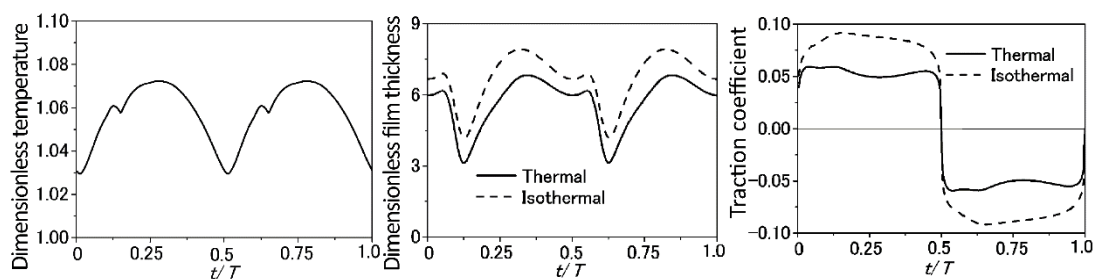


Fig. 44. Temperature rise (left), and comparison of isothermal and thermal results of film thickness (middle) and friction (right) over the reciprocation cycle [129].

Consequently, Wang et al. [130] examined a point contact lubricated by BS oil under pure rolling reciprocating motion with a short stroke length of 1 mm by means of optical interferometry and theoretical analysis. Surprisingly, a very good

agreement between the numerical solution and the experimental results was achieved in spite of the assumption of Newtonian fluid and neglecting the thermal effects and inertia forces, whereas the simulations by Jalali-Vahid et al. [126] were far from such agreement for very similar solution. Only small deviations of the results for frequency of 7.78 Hz occurred due to a minor effect of starvation initiated by occurrence of cavitation zone at the contact inlet after a reverse of motion. When the frequency of 14.4 Hz was employed, the starvation brought about a significant reduction of film thickness and the film thickness predicted by the fully flooded model was thus markedly thicker than the real one. It was noted that it is not clear, what practically happens in the starved area; however, to improve the analysis, a simplified algorithm of starvation was involved. The starvation algorithm presumed a formation of an oil-air meniscus in front of the contact (inlet area) when the film thickness was attributed by the ratio of thickness of oil layer and total gap at the position of meniscus. It was necessary to take the thickness of oil layer from experiments; therefore, the usage of this solution is probably limited only to a few experimental conditions. Starved and fully flooded oil films coexisted in the contact as the meniscus changed its position during the stroke. A good coincide was obtained between the starved model and the experimental data. Starvation was serious only on a limited interval of stroke and it reduced mainly the central film thickness rather than the minimum film thickness, so the general performance of EHL contact was not affected.

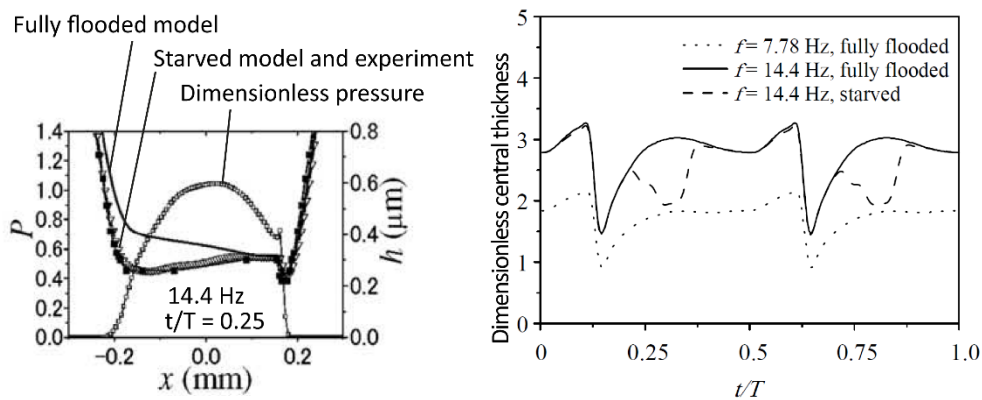


Fig. 45. Comparison of experimental and theoretical results (left) and variation of predicted central film thickness with frequency over reciprocation cycle (right) [130].

As the EHL contact under reciprocation can suffer from oil starvation, Stadler et al. [131] proposed the equation for estimation of cavity length of rolling point contact applicable for transient simulations. The cavity zone was determined by the cavity pressure about a vacuum pressure of  $-0.1$  MPa (this value was obtained by a simple test; the exact value of cavity pressure for a thin film of oil is unknown and very difficult to measure), but only when the cavity was fully surrounded with oil. It means that the solution is limited only to the cavity of air produced in lubricant and not included the air at ambient pressure breaking through the oil layer. Additionally, the calculations were carried out for steady state conditions with the inlet fully

flooded with oil having the properties similar to the BS oil. The simulated cavity length, defined as the distance from the centre of contact to the end of cavity zone, increased with an increase in speed, viscosity, and the reduced radius of curvature, and with a decrease in cavity pressure and contact area. The estimated cavity length was compared with the experimental results under fully flooded conditions for different oils, steady loads, and rolling speeds of trapezoid pattern (reciprocation). A good agreement was reached. It was revealed that the pressure-viscosity coefficient, and thus piezoviscosity, has a minor influence on the cavity length since the pressure close to the cavity is low. This influence may increase for thick films where a more diverse film thickness distribution may occur under transient conditions. Moreover, the central film thickness affects the shape/geometry of contact, and subsequently the cavity length. The higher the thickness, the longer the cavity zone. The estimated cavity length may indicate a degree of starvation.

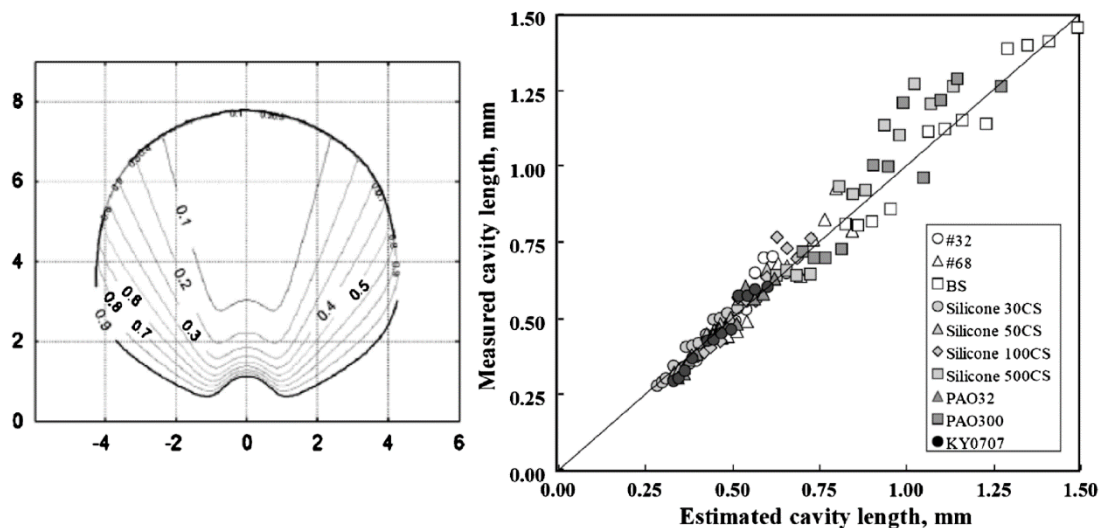


Fig. 46. Numerical simulation of cavity zone (left) and comparison of measured and predicted cavity length (right) [131].

Maruyama and Saitoh [132] found a critical degree of vibrations for sliding point contacts when the oil film separates the contact surfaces over the entire reciprocation cycle. A degree of vibrations (referred to as the amplitude ratio; however, in the opinion of the author of this thesis, the stroke ratio,  $S/D$ , designation is more appropriate) was expressed by the ratio between the moving distance of the contact area (stroke length) and the diameter of Hertzian contact area. The experimental conditions included two PAO oils of different viscosity, maximum sliding speeds of harmonic motion from 2 up to 30 mm/s, and contact pressures from 0.29 to 0.54 GPa. The minimum film thickness was defined from a mid-plane of contact area parallel to the direction of motion over one cycle. It was revealed that the minimum thickness remains zero up to the critical  $S/D$  ratio of 1.6. Above this value, the contact began to be separated by the oil film also at the end of the stroke when the minimum film thickness occurred. The formation of this film was attributed to the squeeze action since entraining acting was none or negligible.

The critical value of  $S/D$  ratio was unaffected by the used oil, contact pressure, and maximum speed of motion, except for the lowest speed of 2 mm/s where the film failed to be formed. The speed likewise not influenced the saturation value of minimum film thickness, unlike effect of oil and contact pressure, when the effect of the  $S/D$  ratio was irrelevant. In addition, the critical ratio of  $\pi/2$  was calculated assuming the average contact length with respect to the location of point contact.

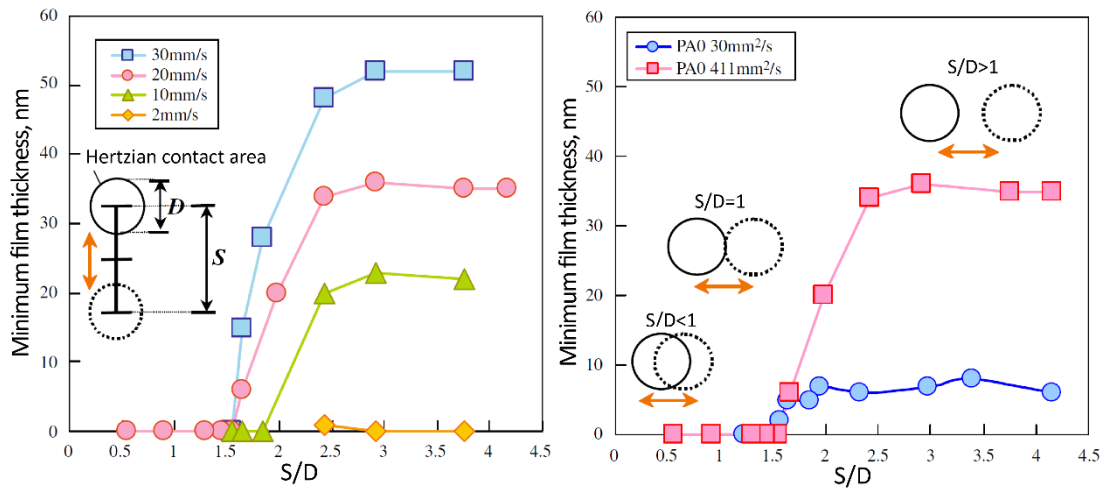
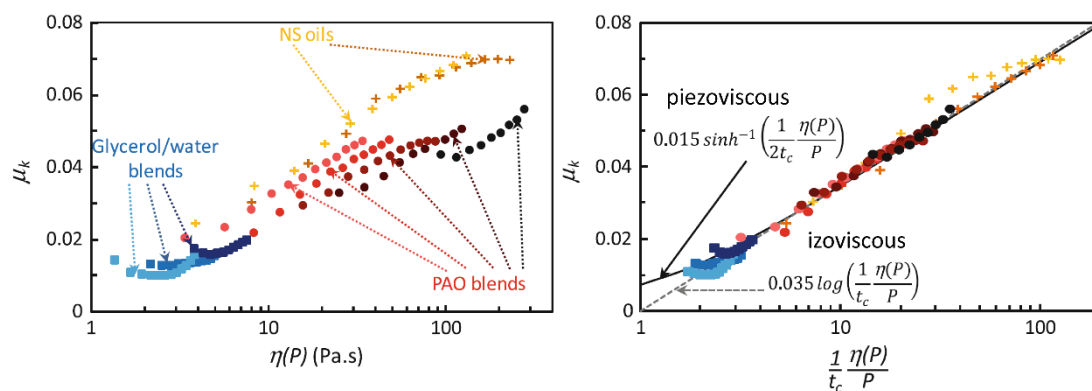


Fig. 47. Effect of maximum sliding speeds (left) and used oil (right) on minimum film thickness over reciprocation cycle [132].

Li et al. [133] exposed a lithium grease to reciprocating rolling and sliding microoscillations, where the stroke length was shorter than the Hertzian contact area. Before the microoscillations, the central dimple of entrapped film was established by impact load. In case of rolling conditions, the entrapped film moved at entrainment speed to the outlet and a new crescent-shaped film was formed at the inlet. The dimple film shape and crescent-shaped film remain unchanged before they reached the outlet. A similar behaviour occurs also for sliding conditions. However, the glass disc moved faster than the entrapped film when the ball was fixed. It was deduced that the lubricant was in glassy state, and the slip occurred at or close to both interfaces of the grease/disc and the grease/ball. The thickness of entrapped film was lessened with the increase in repetition of microoscillation cycles due to starvation when the grease was pushed out of the track and the replenishment effect was not fast enough to ensure a sufficient supply of lubricant at the contact inlet.

Rigaud et al. [134] employed a dynamic oscillating tribometer for the establishment of friction law of point contact under free sliding oscillating motion. The oscillations were initiated when a hemispherical pin located at the free end of a flexible bi-blade was released from the initial position (maximum amplitude of the motion). The steel pin then slid on a steel flat surface covered with lubricant until the given kinetic energy was dissipated. Different contact loads/pressures up to 550 MPa, initial positions/sliding speeds up to 0.1 m/s, and lubricants (isoviscous glycerol/water blends, piezoviscous PAO blends, and neutral solvent base oils) were

used. A frictional response was not evaluated from the measurement of frictional forces, but deduced from the energy decay in the course of oscillation motion. The instantaneous sliding speed dependent and independent contributions to energy decay were discriminated. The part of energy dissipation dependent on the sliding speed was associated with viscous damping of lubricant surrounding the contact as the pin passed through the lubricant layer on the flat surface during reciprocation. Since this viscous damping was affected by volume of applied lubricant (thickness of the layer) and it did not change with the load of contact, the remaining part of dissipated energy independent of the sliding speed was addressed to friction within the contact. Friction increased with viscosity of lubricants, but it was significantly dependent on load only for piezoviscous PAO blends, whereas the impact of a change in load was very weak in the case of isoviscous glycerol/water blends. The results revealed that friction logarithmically increases with oil viscosity at given pressure (see Fig. 48), which explained the responses of isoviscous and piezoviscous lubricants. A parameter, referred to as the characteristic time  $t_c$ , was employed to shift all experimental data to the master curve. The characteristic time  $t_c$  involves empirical constants, operating conditions and rheological properties (ambient viscosity and pressure-viscosity coefficient). Since  $t_c$  includes also the sliding speed, it is related to the shear rate, and thus also to the rheological response of lubricant. The master curve with the corresponding friction laws for isoviscous and piezoviscous fluid is shown in Fig. 48. Moreover, the viscoelastic behaviour of piezoviscous lubricants was confirmed via the calculation of Deborah number. This study clearly showed that the oscillatory approach is very appropriate for investigation of frictional responses of EHL contacts when the obtained friction law predicts the sliding friction as a function of operating conditions considering the lubricant rheology.



**Fig. 48.** Frictional response versus viscosity at contact pressure (left) and friction versus dimensionless parameter involving the characteristic time [134].

In the paper of Majdoub et al. [135] related to the previous one [134], the dynamic responses of the oscillating tribometer were analysed both numerically and experimentally. Linear and quadratic friction models were compared. Based on numerical simulations, the linear model was not appropriate for such dynamic system. The experiments confirmed that the quadratic-based model is more

convenient for the system. Besides that, the next benefits of the oscillatory approach measurements were emphasised: Stribeck-type friction curve can be obtained very quickly (within a few seconds) and it allows for measuring extremely low values of friction (CoF under 0.01) with an “unsurpassed” accuracy (CoF  $\pm 0.0002$ ).

As it was not possible to evaluate a distribution of film thickness on the dynamic oscillating tribometer employed in [134, 135] (only electrical contact resistance method was used), a new tribometer has been very recently developed involving a combination of forced oscillations and the optical interferometry method [136]. For demonstration of the tribometer, the film thickness and friction of PAO oil were simultaneously measured. The fixed stroke length was a substantially higher than the contact diameter when the reciprocation frequency was linearly reduced from 50 to 5 Hz at rate of 0.25 Hz/s (corresponding to maximum sliding speed 157 to 15.7 mm/s). The friction coefficient was out of phase with both the displacement and the sliding velocity. Nevertheless, the average values of speed and friction suggested a purely viscous origin of friction. The amplitude of friction (size of friction loops) and the dependence of friction with the speed decreased with the reduction of the sliding speed (frequency). In parallel, the friction curves were less waved with the decrease in speed and they led to a more elliptic form at low speeds. This was associated with the differences of the film thickness distribution at acceleration/deceleration and the film breathing. A typical drop in the central film thickness occurred during acceleration with a time lag between this drop and the minimum speed moments, as was reported previously by other scientists.

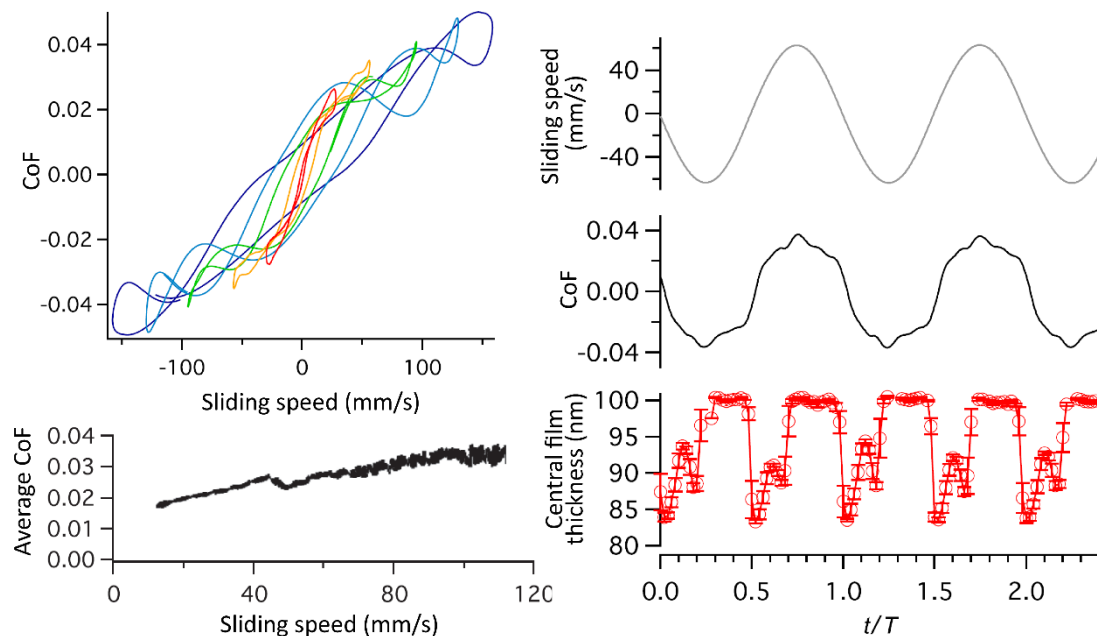


**Fig. 49.** Friction loops from 48 Hz (purple-blue) to 7 Hz (red) and average friction values (left); sliding speed, friction, and central film thickness over the reciprocation cycles (right) [136].

## 2.7 Lateral vibrations

Besides the main characteristic motion due to the operation of machine, whether a quasi-steady or transient one (intermittent, reciprocation, harmonic, and other types of motion), all EHL rolling/sliding contacts are subjected to generally undesirable vibrational motions. Although the vibrations determined by their source and by a response of the entire system act in seemingly arbitrary directions of the contact, the normal and tangential directions relative to the contact surface are solely considered for investigation of vibration consequences. The publications dealing with motion in the normal direction, when this mutual approach or depart of the contact surfaces is reflected in sudden/transient loads, are listed above in the relevant subchapters. The same applies to tangential vibrations acting directly in the direction of main motion and causing a variation of its speed. Therefore, this last subchapter of the state of the art is focused on the effects of additional/secondary transient motions, vibrations, which take place simultaneously with the main motion in the tangential plane of contact and their direction is perpendicular (lateral) to the direction of main motion.

As scientists started to address this issue only a few years ago, only a very limited number of publications are available. This may be due to greater demands on the measuring apparatus, equipment, and technique in the case of experimental approach, and due to the lack of experimental data and the excessive complexity in the case of numerical solutions. The first mentions of the development of experimental device involving lateral vibrations in point EHL contact were very probably presented by Glovnea and Spikes [137] at the World Tribology Congress in 2005, and subsequently by Kalogiannis, Glovnea and Ioannides [138] in 2009. It can be found from the abstracts of their conference contributions that lateral vibrations may introduce some oscillations of film thickness in the dependence on conditions. These film oscillations travelled through the contact at an angle given by a ratio of main and lateral motion. It was concluded that the lateral oscillations influence a film thickness only if both motions have a similar magnitude of entrainment velocity. Furthermore, it was added in the article [139] that the crescent-shaped fluctuations of film thickness were observed. These fluctuations were caused by the squeeze effect at the contact inlet as a result of rapid variation of film thickness. Since the fluctuations were obtained only at the contact pressure of 0.75 GPa, whereas at higher pressure of 1.78 GPa, they were not revealed, it was deduced that the fluctuations depend on the contact pressure.

Later, Nagata, Kalogiannis and Glovnea [140] employed lateral vibrations for track replenishment of rolling grease-lubricated point contact. The ball-on-disc simulator was used and film thickness was measured by means of optical interferometry. Before the lateral vibrations were exerted, the grease was spread over the disc surface and the contact was run under pure rolling conditions at speed of 0.5 m/s for 5 minutes to ensure starvation. Thereafter, the ball began to perform the additional harmonic motion of frequency of 10 Hz and the stroke length of 355  $\mu\text{m}$  (maximum speed of 12 mm/s) in the transverse direction to the main rolling direction. Immediately after the exposure of the contact to vibrations, the film

thickness in the starved contact was completely recovered to the value of fully flooded contact. This was due to a change in the initial circular track, where the lubricant supply was depleted, to the wavy-like track with a new or previously pushed-out-of-track grease. The initial degree of starvation was not observed until the end of the test lasting for 15 minutes, although the film thickness varied during the stroke. The minimum of film thickness took place periodically in the middle of stroke where the original track depleted of grease was located. The results indicated that the lateral vibrations could be one of the mechanisms of grease replenishment in the rolling element bearings. Unfortunately, it should be noted that the results of this study are not directly applicable for rolling bearings, since the stroke length was about 1.5 times higher than the diameter of the contact area. The interested reader is referred to Nagata's PhD thesis [141].

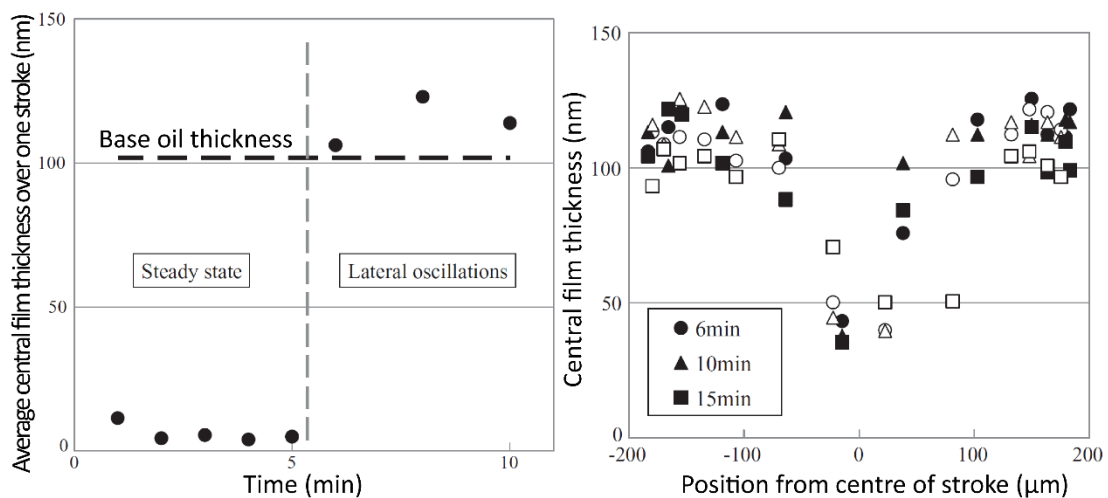


Fig. 50. Average central film thickness in the course of experiment (left) and the central film thickness with respect to lateral position and time of experiment [140].

The above results have also been included in the dissertation thesis by Kalogiannis [142] where the effect of  $S/D$  ratios of 0.185 and 1.3 on the replenishment was additionally investigated. Moreover, the frequencies of 10, 50, and 100 Hz and rolling speeds of 0.05, 0.1, and 0.5 m/s were utilized. It was demonstrated that the  $S/D$  ratio plays a substantial role in the track replenishment mechanism. For low value of  $S/D$  ratio, the film thickness was lower than the steady state thickness of base oil at all frequencies and rolling speeds (starvation). On the other hand, a degree of starvation was reduced, especially at high rolling speeds, when the film thickness exceeded the thickness of grease under steady state conditions. In the case of high  $S/R$  ratio, the film thickness was recovered at the level of base oil similarly as in [140] where the increase in rolling/lateral speed ratio diminished the effect of lateral vibrations on track replenishment.

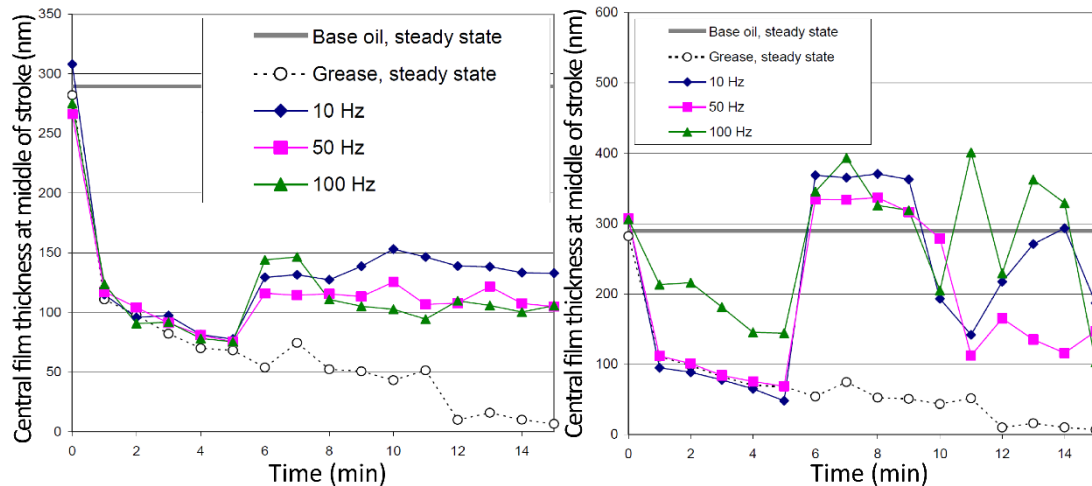


Fig. 51. Central film thickness in the middle of stroke for rolling speed of 0.5 m/s and S/D ratio of 0.185 (left) and 1.3 (right) [142].

Besides the replenishment issue, the Kalogiannis' PhD thesis [142] was mainly devoted to the film thickness behaviour of PAO oil under vibrations. The work involved the rolling speeds from 0.05 up to 1 m/s, frequencies of lateral oscillations of 10, 50, and 100 Hz, two material configurations giving the contact pressures of 0.67 GPa (steel-glass contact) and 1.78 GPa (tungsten carbide-sapphire contact), and PAO was pure or mixed with a 10.7wt% viscosity index improver additive. The S/D ratio was close to unity for the steel-glass contact and nearly three for the tungsten carbide-sapphire contact. For PAO without the additive, no fluctuations of film thickness were detected at all frequencies and material configurations when the rolling speed was higher than 0.05 m/s. The film thickness fluctuation was reported only for the combination of the minimum rolling speed of 0.05 m/s and the maximum frequency of 100 Hz (lateral sliding speed of 0.13 m/s). A crescent-shaped thinner film by 13 nm was formed during deceleration at the end of stroke due to a lower entrainment speed. This film subsequently passed through the contact with respect to the instantaneous entrainment velocity. The results were comparable for both material configurations, and thus the effect of contact pressure was considered as insignificant. However, this is in contradiction with the previous results of Kalogiannis et al. published in [139] where the same apparatus and very similar conditions were used, but the contact pressure affected the fluctuations.

Moreover, the film thicknesses obtained in the experiments with pure PAO were compared with the predicted values. A simple theoretical analysis calculated the film thickness from the predictions of Hamrock and Dowson [22-24] for steady state conditions assuming a variation of entrainment speed and the time of lubricant passage through the contact. It was deduced that the ratio between the main rolling speed and the lateral oscillating speed is an important parameter determining a degree of vibrations and possible film fluctuations. The calculated fluctuations of film thickness due to a variation of entrainment speed roughly correlated with those measured in the experiments for low rolling speeds. However,

the observed values were higher than those predicted for higher rolling speeds. This was attributed to viscous heating at the inlet, but this claim is obviously wrong since the thermal effects are not included in the prediction and thus heating may reduce only the observed film thickness and not the calculated one.

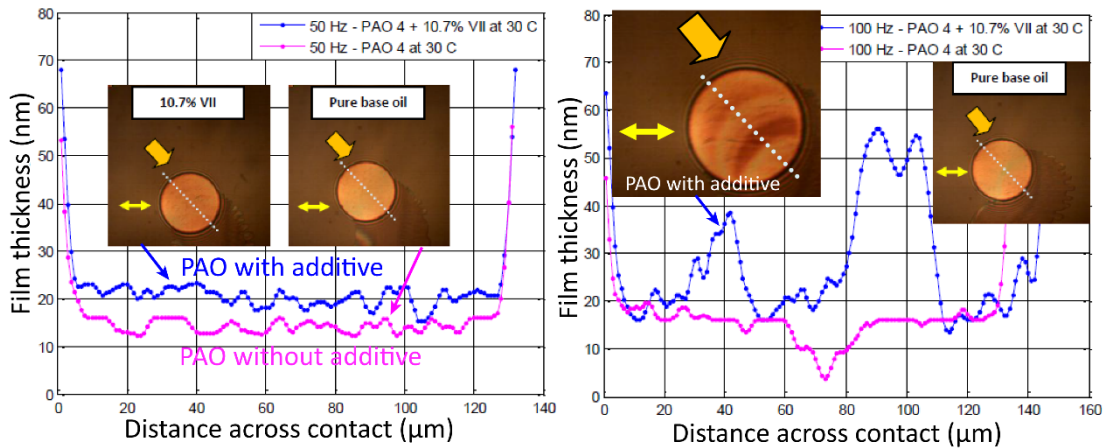


Fig. 52. Comparison of film thickness of PAO with and without additive for rolling speed of 0.05 m/s and frequency of 50 Hz (left) and 100 Hz (right) [142].

Temperatures of 30 and 80 °C were used in the experiments with PAO containing the additive when the rolling speed ranged from 0.05 up to 0.3 m/s. The behaviour of PAO with additive was significantly different from the behaviour of pure PAO at 30 °C and frequency of 100 Hz. A series of waves of a thick film and different wavelengths were formed at the ends of stroke. High fluctuations from 30 to 50 nm occurred even for higher rolling speeds. This was ascribed to the viscosity instability due to repeated shearing of polymer additive. The fluctuations of PAO with and without the additive were similar for lower frequencies as well as for the temperature increase to 80 °C. This was explained by the reduction in squeeze action for thin films caused by a lower viscosity of oil at higher temperature.

### 3 ANALYSIS AND CONCLUSION OF LITERATURE REVIEW

From the previous chapter of the state of the art, it is apparent that transient operating conditions can positively or negatively influence the behaviour and frictional response of EHL film depending on the specific conditions. However, there is currently no universally applicable theoretical model that predicts these behaviours and responses, and the models for steady state conditions [22-24] often fail in these cases. Many studies in this area end with hypotheses that need to be proven or refuted, and likewise many scientists demand more experimental results for a variety of operating parameters. These facts confirm the topicality of issue.

The early studies involved a free-falling body onto a flat lubricated surface to introduce a pure squeeze action. It was predicted [45, 47, 48, 51] that a higher pressure occurs in the lubricated contact compared to the dry contact, and a dimple film shape can be formed in the centre of contact due to a high viscosity of lubricant in this area. Both the long-lasting entrapment of highly pressurized lubricant in the central dimple with the minimum film thickness at the periphery of contact [46, 49] and the generation of high pressures [50] during the impact load were proved experimentally. The increase in ambient viscosity [49, 52-54], pressure-viscosity coefficient [52, 53], and impact speed [52-55] cause a generally thicker entrapped film in the central dimple. In addition, a variation of film shape is roughly in the reverse order under a driven cyclic approach-separation motion [56, 57]. This points out to a viscoelastic behaviour and a possible glassy state of entrapped lubricant. Moreover, the dimple formation is weakened by produced air bubbles during unloading process for high frequencies and small amplitudes, as was demonstrated experimentally [56], whereas the numerical approach [57] predicted the increase of film thickness as a power function of frequency.

Besides that, the film entrapped in the periphery area of contact (periphery dimple) with the minimum film thickness in the central area was revealed [58] for the preloaded contact and forced impact load. The related theoretical [59, 64] and experimental [61, 63] studies identified that the initial impact gap between the approaching surfaces and the loading speed are substantial parameters for formation of periphery dimple when the dimple shifts away from the central area to the periphery with a reduction in the initial gap or an increase in the initial speed. Moreover, a local resistance of lubricant to the Poiseuille flow was suggested to be the purpose of dimples formation (both the central and periphery one) [59, 61]. The results of experimental study [61] also indicated that the entrapped film is affected by the rate of change in the Hertzian contact radius during the impact load. When the two-stage impact is employed [63, 64], the consequential shape of two concentric dimples is given by the superposition of individual dimples from one-stage impacts. Furthermore, a numerical analysis [64] showed a remarkable effect of mass of moving body, which determined the approaching (squeezing) speed, on film entrapment. The simulations [64, 67] pointed out the importance of the initial stage of impact when the central dimple is formed almost immediately with a build-up of pressure and viscosity with respect to the initial loading speed. A high-pressure rheology including the lubricant fragility and glass transition should

be considered in the analyses of entrapped films, especially in the late stage of impact, when the lubricant leaks out of the contact [66, 119]. Otherwise, the analyses can lead to the predictions contradicting the actual behaviour of entrainment [66]. A distribution of temperature during the impact follows the pressure distribution within the contact [72] where the dissipation to heat results from the compressive work and shear heating. Based on the references [73-75, 98], the effect of surface forces is negligible for films over 5 nm, as well as the effect of lubricant adsorption on film thickness regarding the EHL regime. Recently, the analytical predictions of central entrapped film thickness for line [76] and point [78] contact have been derived from numerical results.

When the impact or variable of loads are applied on the rolling/sliding contact, the squeeze action corresponding to viscous damping enhances the resistance of film to its variations originating from transient conditions [79, 82, 85]. Film thickness is affected mainly at the contact periphery and not directly within the contact during sudden loading of the rolling/sliding contact. Then, a thick, often crescent-shaped, squeezed film passing through the contact from the inlet without a change in its shape at the entrainment speed, as was demonstrated by many authors [58, 61, 63, 82-85, 87]. The effect of slide-to-roll ratio on the entrapped film is unimportant [58]. A comparison of numerical solutions pointed out that the assumption of Newtonian fluid and isothermal conditions may substantially devalue the predictions of temperature and friction [86, 99]. Additionally, the approximations of transient film thickness applicable for line contacts may underestimated the thickness in point contacts [88].

Other conclusions can also be drawn from the works investigating the influence of transient unidirectional motions at steady load. It was proved experimentally and numerically that a hysteresis occurs for accelerated or decelerated motions when different values of both the central film thickness [94-101, 103, 108, 127, 128, 136] and friction [89, 99, 102, 103, 108, 136] can be obtained at the same entrainment or sliding speed. Hysteresis loops for dynamic motions are created around steady state values [89, 95, 96, 100-103, 127, 128, 136] when the central film thickness and friction are higher at deceleration and lower at acceleration of motion than in the case of steady conditions. This effect is nearly linear for low accelerations (under  $0.5 \text{ m/s}^2$ ) [95-98]. The differences in central film thickness, and consequently in friction, are attributed to the squeeze effect (viscous damping) and to the distortion due to the time (transport) delay of lubricant [95, 96, 98, 100-102, 127, 136]. Besides that, a temperature-viscosity wedge effect, caused by different thermal properties of contacting materials and high sliding speeds, can amplify the squeeze effect [103]. This squeeze effect was unimportant for films under 5 nm [98]. Moreover, the size of hysteresis loops grew with the increase in frequency of motion [89, 95, 96, 102, 103, 127] and viscosity of lubricant [89, 95, 96], while the increase in entrainment and sliding speeds diminished these differences from steady state values. The changes in size of friction loops are not necessarily proportional to those of film thickness [108, 109]. It was elucidated that the total friction is given by contributions of individual contact sub-areas of different sizes and film thicknesses [109].

In the case of unidirectional intermittent motion, a set of crescent-shaped entrapped films can be gradually formed during a sudden stop of motion at the contact inlet [40]. Moreover, the film collapse consists of two stages [110, 111, 119] during a sudden stop: reduction of overall film thickness without a change in film shape during deceleration and formation of central dimple (pure squeeze action) after the stop. Film thickness before the pure squeeze action is influenced substantially by lubricant properties [110, 119] and by a value of deceleration [111, 119], albeit the effect of initial speed (thickness) of stopped motion is negligible [110, 111]. This thickness linearly increased with deceleration and correlated with the product of deceleration and the low-pressure lubricant parameter  $\alpha\eta$  [119]. Simulations of film behaviour during halting of motion were only partially successful [112, 113, 120]. Friction can be reduced in the course of motion start-up if the entrapped lubricant is present between the contact surfaces [66]. A film formation at the start-up of motion takes place in individual fronts of entrained lubricant establishing a stepped (S-shaped) film profile; it is also significantly affected by acceleration and the lubricant rheology [114]. In addition, the speed of fronts alters within a passage of oil through the contact and differs from the mean speed of surfaces. Again, only a partial agreement of numerical simulations [117, 118] with the observed behaviour [114] was achieved.

For reciprocating motions, film thickness varies cyclically (film breathing) with respect to the lubricant rheology and acceleration/deceleration of motion [121-130, 136] since the entraining and squeeze action are out of phase. A central film dimple is formed at the end of stroke separating the contact surfaces and avoiding wear [123] at zero entrainment speed. A critical case occurs for high frequencies and short stroke lengths when the EHL cavitation zone reaches contact inlet at reverse of motion causing starvation, film failure [122, 123, 125, 130], and a substantial increase in friction [123]. Starvation is also significant for the grease-lubricated contacts [133]; under such conditions, a replenishment of oil is not fast enough. The failure of film can be suppressed by cyclic impact loading (thick film entrapment) during reciprocation [123]. On the other hand, it was pointed out that the entrapped solid-like film may collapse under shear stress [40, 122]. However, it is unclear what happens in the starved (cavitation) zone at the contact inlet [130] and the behaviour of this zone is very difficult to predict [131]. Furthermore, S/D ratio of 1.6 (ratio of stroke length and diameter of contact area) is needed at least to separate the contact surfaces by EHL film over the whole pure sliding reciprocation cycle [132]. A frictional response follows the course of sliding speed according to the rheological state of lubricant (viscous, viscoelastic, glassy state) and the distribution of film thickness; the higher the sliding speed, the lower the EHL friction due to thermal phenomena [123, 129, 136]. Theoretical studies [126, 129, 130, 135] showed a general agreement with experimental findings, but some deviations of results can be found due to simplifying assumptions (omitted cavitation zone and neglected inertia forces, complex rheology, and/or thermal effects). Moreover, investigation of EHL friction via the oscillatory (reciprocation) approach is very beneficial in terms of operating conditions, low values of friction and accuracy of measurements [134-136].

Some initial investigations have been conducted to understand the influence of lateral vibrations on film thickness by one of scientific groups [137-142] during the years 2005-2013; however, it seems that this attempt was terminated. Lateral vibrations can be one of the mechanisms causing a track replenishment in grease-lubricated rolling element bearings [140, 141] when S/D ratio is an important parameter for track replenishment and thus for a reduction of EHL starvation [142]. Crescent-shaped fluctuations of film thickness can take place under specific conditions of lateral vibrations [139, 142]. These fluctuations caused by the squeeze action pass through the contact according to the instantaneous entrainment velocity [138, 139, 142] and are significantly influenced by lubricant rheology [142] and a ratio between the main rolling speed and the lateral speed from vibrations [138, 139, 142].

In the final summary, the foregoing works revealed that a distribution of EHL film under impact load, i.e. a pure squeeze action, is mainly determined in the initial stage of impact. The essential parameters for film entrapment are the initial impact gap, loading speed/rate of change in Hertzian contact radius, impact/approaching speed, and rheological properties of lubricants (viscosity, pressure-viscosity coefficient, molecular weight, complex viscosity-pressure-temperature characteristics, etc.). It should be pointed out that the effect of approaching speed was analysed only theoretically; thus, an experimental evidence of the impact of this parameter is still missing. Similarly, the recently published prediction of entrapped film thickness [78] is based on the approaching speed and numerical results, while the validity of the prediction has not been experimentally verified yet. On the other hand, the loading speed parameter has been employed exclusively in experimental studies, and so an exact role of simultaneous action of approaching and loading speed on the formation of entrapped film is not clear. Moreover, the previous investigations frequently used/analysed a limited number of very specific lubricants and unrealistically large initial gaps in contrast to the EHL contacts of actual machines.

In the case of transient conditions including tangential motions of the contact surfaces, film thickness is driven by the entraining and squeeze action while friction is the result of lubricant film shearing. The effects of lubricant parameters and rheology, acceleration, frequency, stroke length, S/D ratio, ratio of main rolling speed and lateral speed were emphasised for their major impact on film thickness and friction. Nevertheless, no quantitative description of most of these effects, except for the effect of acceleration on film thickness, has been derived from experimental findings. Furthermore, numerical simulations, even though they were directly designed to evaluate EHL contacts under non-steady state conditions, have not agreed to the results of measurements in certain details. Although the presence of vibrations in EHL contacts is indisputable, there is a very limited knowledge about the influence of lateral vibrations on film thickness; excessive values of S/D ratio were particularly applied. Besides that, a frictional response under lateral vibrations has been completely omitted. The aim of the present thesis is defined on the basis of these facts in the next chapter.

## 4 AIMS OF THE THESIS

The aim of the dissertation is to experimentally determine the effects of operating parameters on the EHL film behaviour in the point contact under impact load and lateral vibrations with an emphasis on the film thickness. For this purpose, the film thickness distribution during impact loading will be examined via the optical interferometry method. In the case of lateral vibrations, the same method will be employed for the measurement of film thickness and a frictional response will be investigated in two perpendicular directions by means of force sensors.

Achieving the main goal of the dissertation is conditional upon the fulfilment of the following partial objectives:

### **Preparatory stage of work:**

- Modifications of the measuring devices required to excite the impact loading and lateral vibrations enabling the measurement of film thickness and friction.
- Creation and debugging of systems for controlling the test conditions enabling their repeatability.
- Selection of the spectrum of lubricants with respect to their rheological properties.
- Execution of introductory measurements to verify the applicable range of operating parameters and the accuracy of their control together with the accuracy of friction force measurements.

### **Main stage of work:**

- Implementation of a systematic series of experiments considering various operating parameters and/or lubricants.
- Analysis of measured data and description of EHL film behaviour under specific conditions.
- Comparison of the results with theoretical predictions (film thickness after impact load).
- Comparison of the results obtained under transient and steady state conditions at corresponding instantaneous values of operating parameters (film thickness and friction under lateral vibrations).
- Deduction or derivation of new empirical rules, laws, or knowledge.
- Discussion and publication of research results.

---

## 4.1 Scientific question

What is the effect of individual parameters of impact load and lateral vibrations on the behaviour of EHL film thickness and its frictional response in the point contact regarding to lubricant rheology?

---

## 4.2 Hypotheses

In the light of the previous findings of other authors, it is expected for the conditions of impact load that:

- **H1** the effect of approaching and loading speed on the formation of dimple film shape and resulting film thickness is the same
- **H2** the influence of pressure-viscosity coefficient on the thickness of entrapped film is more significant than the effect of ambient viscosity since the pressure-viscosity coefficient determines the rate of the increase in the lubricant viscosity with respect to pressure build-up during impact

Similarly, it is suggested for the conditions of lateral vibrations that:

- **H3** the passage of lubricant through the contact is driven by the entrainment velocity despite the sliding velocity
- **H4** the fluctuations of central film thickness originate only in the film formed at the contact inlet
- **H5** the thermal and other effect on friction are equally pronounced in both the main and lateral direction of the point contact as friction is given by viscous shearing of lubricant; i.e. the effective viscosity and thus frictional response are isotropic
- **H6** the frictional responses in the individual directions of the point contact interact with each other

### 4.3 Thesis layout

The dissertation is composed of the two papers published in a journal with an impact factor [A, B] and one paper [C] published in a peer-reviewed journal:

**Paper [A]** [143] FRYZA, J., P. SPERKA, M. KANETA, I. KRUPKA and M. HARTL. Effects of lubricant rheology and impact speed on EHL film thickness at pure squeeze action. *Tribology International*. 2017, vol. 106, p. 1-9. DOI: 10.1016/j.triboint.2016.10.023.

(Author's contribution 60%)

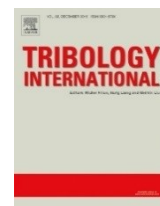
(Journal impact factor = 2.903, CiteScore = 3.16)



**Paper [B]** [144] FRYZA, J., P. SPERKA, I. KRUPKA and M. HARTL. Effects of lateral harmonic vibrations on film thickness in EHL point contacts. *Tribology International*. 2018, vol. 117, p. 236-249. DOI: 10.1016/j.triboint.2017.08.022.

(Author's contribution 75%)

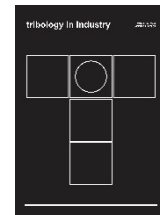
(Journal impact factor = 2.903, CiteScore = 3.16)



**Paper [C]** [145] FRYZA, J., P. SPERKA, I. KRUPKA and M. HARTL. Frictional response of lubricant in EHL contact under transient bi-directional shear loading. *Tribology in Industry*. 2017, vol. 39, no. 4, p. 506-518. DOI: 10.24874/ti.2017.39.04.10.

(Author's contribution 70%)

(CiteScore = 1.32)



Once the preparatory stage of work was completed, the experiments focused on film thickness behaviour under transient conditions of impact load were conducted. The results of these experiments together with their discussion and deduction of conclusions are reported in paper [A]. The findings included in article [A] established new rules of dimple film shape formation and film entrapment considering both operating conditions and lubricant rheology. Consequently, the EHL point contact was exposed to various conditions of lateral vibrations. The film thickness is investigated in publication [B] providing the quantitative description of the effects of lateral vibrations on EHL film thickness and stating relevant empirical relationships. The last part of the thesis, which is reflected by the related study [C], reveals simultaneous frictional responses of lubricant in the main and lateral direction of the contact and their interactions with respect to operating conditions of lateral vibrations.

## 5 MATERIALS AND METHODS

### 5.1 Experimental apparatus

The original measuring apparatus, referred to as the optical tribometer, was designed in a tribological laboratory at the Institute of Machine and Industrial Design during the 1990s. Since then, this apparatus has undergone a gradual development. The optical tribometer, shown in Fig. 53, consists of the following main parts: a microscope imaging system with a light source and camera, a test rig, and a control and evaluation computer-aided system. With respect to the purpose of this thesis, the design of the test rig and some components of the control and evaluation system differs through the papers [A-C].

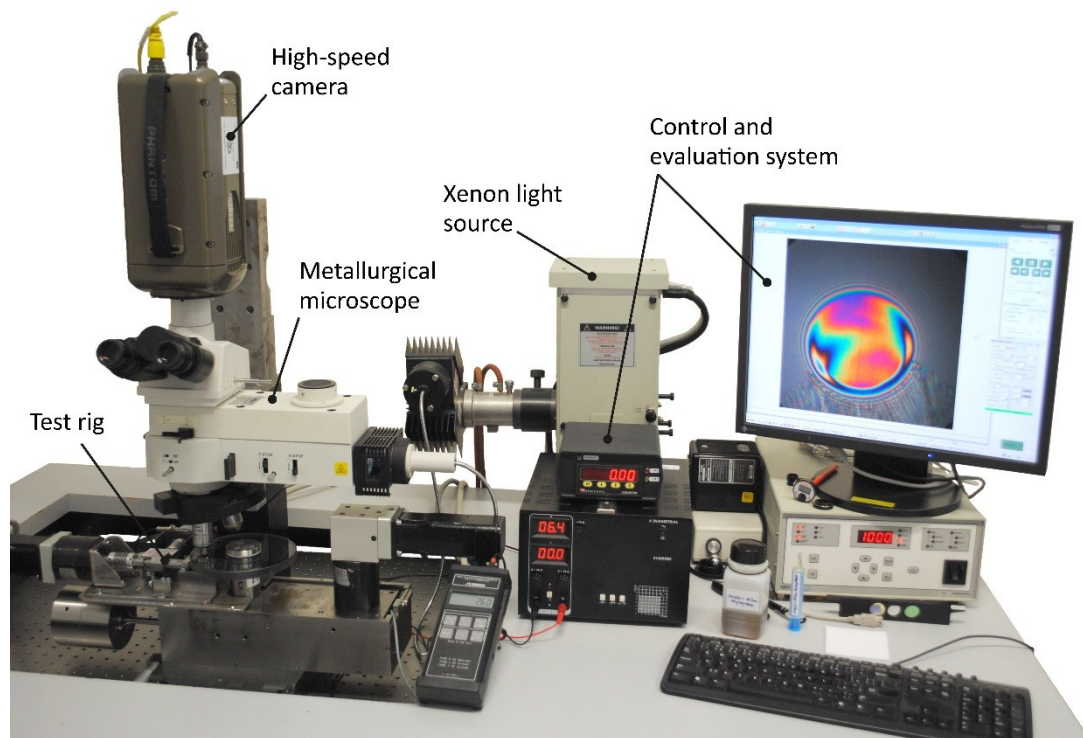


Fig. 53. Optical tribometer.

A point EHL contact is realized in the test rig described below according to its individual modifications. The contact area is illuminated and observed through an optical train of the industrial/metallurgical microscope (Nikon Optiphot 150) employing Köhler illumination technique. The stabilized white light is provided by a continuous 1 kW xenon lamp (LOT-Oriel Group Europe) where an optical fibre transmits the light from the lamp to the microscope. The microscope is equipped with Nikon long-working-distance chromatic aberration-free objectives (20x and 10x magnification) to produce a parallel (collimated) beam of light and form an interference pattern without optical aberrations. The contact area is recorded by a colour high-speed CMOS camera (Vision research Phantom v710) mounted on the

eyepiece port of the microscope. Interferometric images were captured with a resolution of 800 x 800 pixels, where one pixel corresponds to 1 and 2  $\mu\text{m}$  for the objective with 20x and 10x magnification, respectively. At this resolution, the sampling rate of the camera was maintained at 10 000 frames-per-second with camera timing resolution better than 20 ns. The high-power xenon lamp allows to use a short exposure time of camera of 40  $\mu\text{s}$ , while keeping an appropriate brightness of images. With this setting, it is possible to capture short-term transient phenomena in the EHL contact with a negligible motion blur with regard to applied speeds of contact surfaces.

### 5.1.1 Optical tribometer for measurement of film thickness under impact loading

5.1.1

A scheme of the test rig employed for impact loading of the EHL point contact is illustrated in Fig. 54. To introduce a pure squeeze action of lubricant, a ball is pushed against a fixed lubricated plate by a preloaded piezoelectric linear drive (Physik Instrumente 841.3). The highly-polished ball is 25.4 mm in diameter and is made of bearing steel 100Cr6 (AISI 52100). The plate, made of homogenous optical crown glass (BK7), is 13 mm in thickness. As the optical interferometry method is used, the glass plate is coated with a semi-reflective layer of chromium on its underside (contact surface) and an anti-reflective layer on its upper surface.

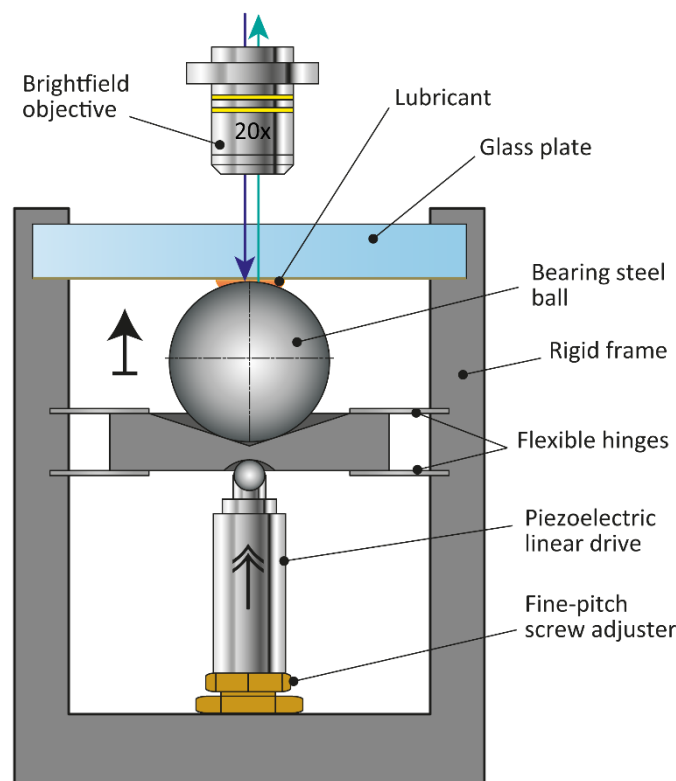


Fig. 54. Scheme of the test rig for impact loading [A].

The lower part of the piezoelectric actuator is attached to the rigid frame by means of a fine-pitch screw adjuster. This simple design makes it possible to manually set the initial gap between the surfaces of the ball and the plate with an accuracy about 10 nm. The ball is fixed on the rig movable part joined to the frame by flexible hinges. The total moving body mass is 0.2675 kg. The piezoelectric actuator has a travel range of 45  $\mu\text{m}$  and the maximum push force of 1 kN. A motion of the piezoelectric actuator can be driven by a microprocessor controller (Physik Instrumente E-517) in an open-loop or close-loop operation regime. In the open-loop regime, the piezoelectric actuator moves according to the used voltage. The advantage of the close-loop regime is that the target position (absolute distance) and speed of the motion can be set. On the other hand, an achievable speed and acceleration of motion are lower than in the case of open-loop regime. Moreover, the set position and speed was found to be affected by a stiffness of the flexible hinges and EHL contact. Regarding the required precision of the control of experimental conditions to ensure their repeatability, the close-loop regime is not suitable for this purpose. Consequently, sets of instructions (scripts), based on the empirical data, are applied in the open-loop regime to control the motion of the piezoelectric actuator while the controller is commanded via a computer. The lubricant temperature is measured by a small thermocouple (accuracy 0.5 °C; repeatability 0.2 °C) near to the contact.

---

### 5.1.2 Optical tribometer for measurement of film thickness under lateral vibrations

In this configuration, the optical tribometer utilizes a modified version of the ball-on-disc simulator, the principle of which was introduced by Gohar [21], as the test rig. The EHL contact is formed between the ball (the same as described above) and a glass disc with a diameter of 150 mm and thickness of 13 mm, see Fig. 55. The load of contact is applied through the disc by putting a deadweight on a lever arm fixed in a tilting frame. The rotational speed of the disc (made of the same material and with the same coated layers as the glass plate described above) is driven by an AC servomotor through a toothed belt. Another AC servomotor is used to drive the rotation of the ball about its horizontal axis. Since both servomotors are driven separately by close-loop servo drivers (programmable electronic amplifiers), various combinations of entrainment and sliding speeds can be achieved in the main (rolling) direction of the contact. Besides the rotatory motion of the ball and the disc, the ball can perform a harmonic reciprocating motion in the direction perpendicular to the main rolling direction. This reciprocating motion, simulating lateral vibrations, is excited by means of a simple cam mechanism, which is driven by a DC motor. A frequency of the ball reciprocation (speed of the motor) can be adjusted continuously up to 300 Hz via a laboratory power supply. The amplitude of the lateral motion (from 20 to 1 000  $\mu\text{m}$ ) is given by an exchangeable eccentric part of the cam mechanism. A capacitive displacement transducer (Micro-epsilon CSH1FL-CRm1.4) with a dynamic resolution under 20 nm is utilized to record the lateral motion of the ball at a sampling rate of 10 kHz determining precisely the

applied frequency and stroke length. The lubricant in an oil reservoir is heated by two cartridge heaters (100 W each). The temperature of the lubricant is measured near the contact inlet by the thermocouple and is maintained by a three-term (PID) temperature controller.

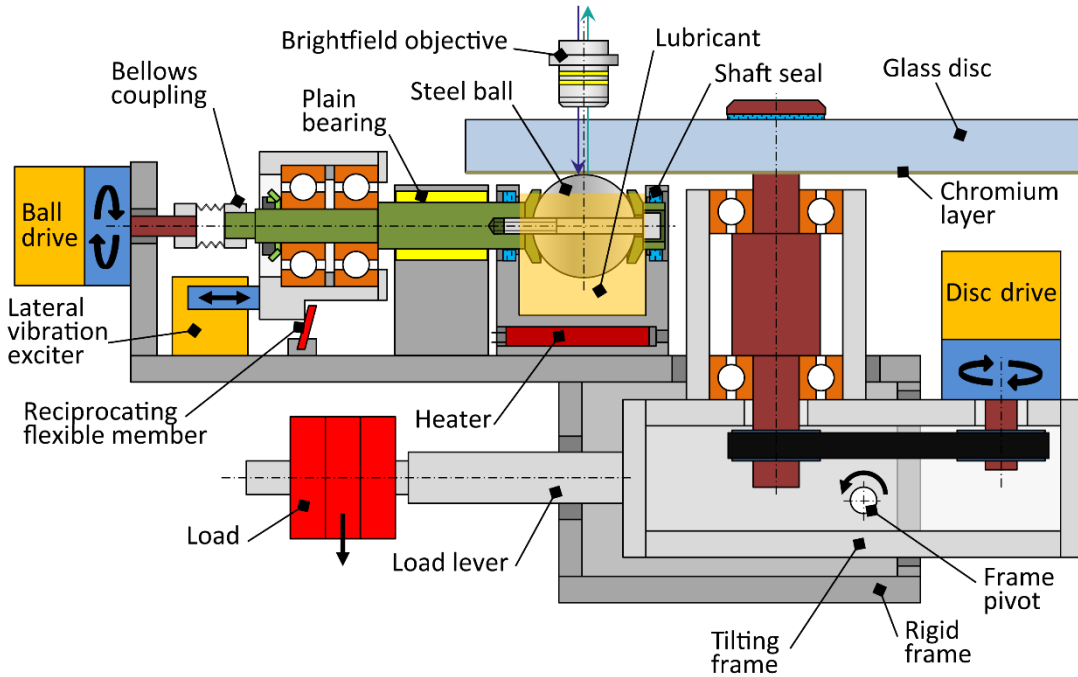


Fig. 55. Scheme of the modified ball-on-disc simulator for excitation of lateral vibrations [B].

### 5.1.3 Optical tribometer for measurement of friction under lateral vibrations

A very similar test rig as the previous one is used to measure friction forces simultaneously in the main direction and the lateral direction of the contact. The disc is replaced by a transparent window fixed in a compliant mechanism with flexure hinges when a rigid part of this mechanism is mounted on the tilting frame.

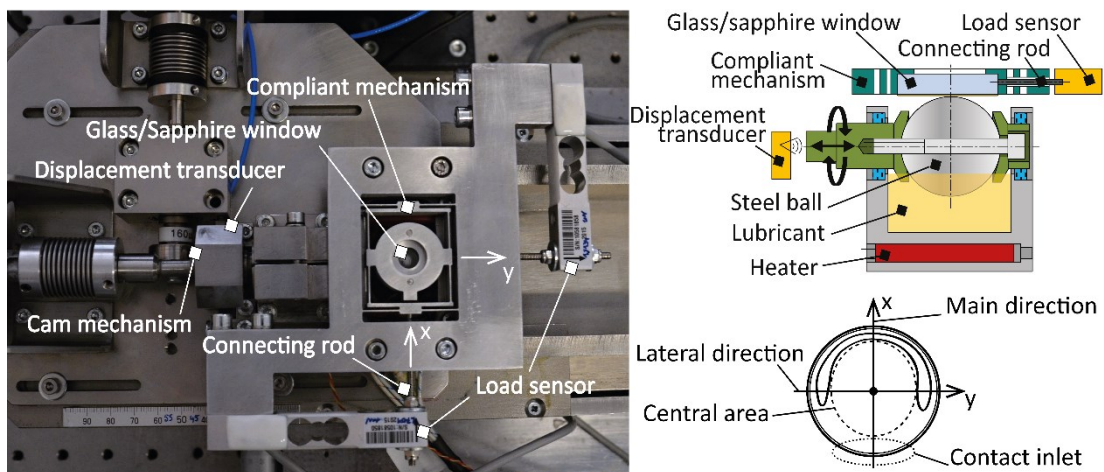


Fig. 56. Photo and scheme of the test rig enabling friction measurement under lateral vibrations [C].

The chromium-coated window, made of BK7 glass or sapphire, is 3 mm in thickness and 12.5 mm in diameter. It is evident that this design is well suited for measurement of film thickness. However, the film thickness measurement plays only a supporting role in paper [C] where this apparatus is used, whereas the main emphasis is put on the frictional response of the lubricant. Since the window does not rotate, only a pure sliding motion can be applied in both directions of the contact. The friction forces, due to a bi-directional shear loading of the lubricant, are transferred from the contact through the compliant mechanism and connecting rods to load sensors (double bending beam load cells; HBM DF2S-3 10 N  $\pm$ 0.03%). An overall stiffness of this system (sensors, connecting rods, compliant mechanism) in the lateral and main direction of the contact is 0.165 N/ $\mu$ m. This system is capable to measure a coefficient of friction with an uncertainty under 0.0005 in the range from 0.005 to 0.2. The friction forces, coefficients of friction, lateral position of the ball, and frequency and stroke length of lateral motion are evaluated and recorded synchronously in real time at a sampling frequency of 10 kHz.

---

## 5.2 Measurement method

To study the behaviour and thickness of EHL film, the Thin Film Colorimetric Interferometry (TFCI) method is employed in this thesis. TFCI was developed at the author's workplace by Hartl and Krupka et al. [146-149]. The method makes it possible to precisely determine the thickness of lubricating film sandwiched between the contact surfaces (one transparent and other with reflective surface) for each pixel of the contact image (interferogram) and thus to reconstruct the EHL film shape. TFCI is a combination of chromatic (white light) interferometry with digital image processing. The principle of optical interference along with the film thickness calibration and evaluation is illustrated in Fig. 57.

When the interference system (both-sides-coated transparent plate, lubricating film, reflective ball) is illuminated by a beam of white light, the Fizeau fringes (Newton's rings) of different intensity (and colour) are produced. This interference phenomenon is due to the rays of light reflected at different interfaces of the system and their subsequent coherent superposition (constructive or destructive interference). The creation of a Fizeau fringe can be explained as follows: the beam of light transmits through the transparent (glass, sapphire) plate and is divided into two by the semi-reflective layer of chromium. One part of the beam reflects from the layer, while the other part passes through the film of lubricant and reflects from the polished surface of the ball. Since these reflected parts travelled different lengths of their paths, a phase shift between the rays occurs, resulting in constructive (bright fringe) or destructive (dark fringe) interference.

With respect to TFCI, the interference images can be evaluated in real time using the "Automatic Chromatic Interferogram Laboratory Evaluation System" (ACHLES) software. At first, a calibration is needed for given lubricant, lighting conditions and camera setting, all must be retained for the rest of the measurement at this calibration. The calibration is carried out for a static lightly loaded contact,

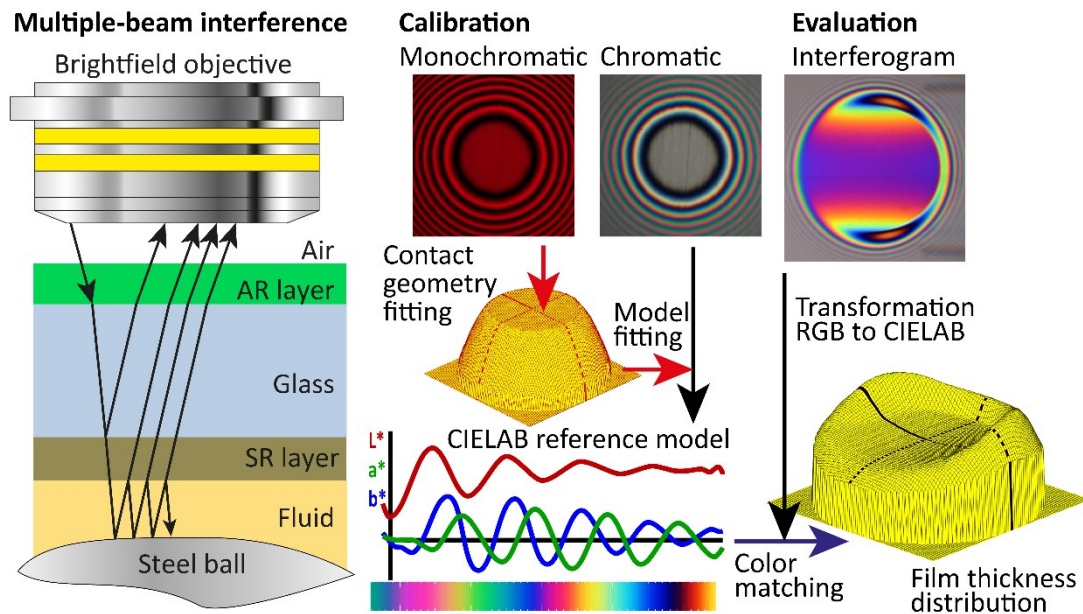


Fig. 57. Optical interference by reflection (left) and TFCI method (right).

when the interferograms of this contact are captured under a monochromatic (single light wavelength, i.e. single colour) and chromatic (white) light. The geometry of the space between the surfaces (lubricant film thickness) is approximated from the monochromatic interferogram by a polynomial fitting of Fizeau fringes. Similarly, the fitting is applied on the chromatic interferogram, a fringes' centre of which is aligned with the centre in the monochromatic interferogram, to obtain colour-coordinate profile expressed in CIELAB colour model. A reference CIELAB model (colour scale) establishing the calibration is determined by interconnection between the colour-coordinates and film thickness data. During the film evaluation, the captured interferogram (chromatic) is transformed into CIELAB colour space and a film thickness distribution is reconstructed by a colour-matching algorithm comparing the reference CIELAB model with CIELAB values of individual pixels in the interferogram. The thickness range of the reference model is limited by a used spatial (optical) resolution (1 to 900 nm). This range is sufficient to cover a coherence length of white light (corresponding to the film thickness of 60 up to 800 nm), where the resolution of TFCI is better than 1 nm. When the film thickness (equal to the half of the difference in rays path lengths) is beyond this interval, the interference weakens. To overcome the lower limit down to 1 nm, the chromium layer can be overlaid by a transparent spacing layer (usually made of silicon dioxide) of convenient thickness.

### 5.3 Test samples, experimental conditions, and experimental design

The experiments were conducted for two material configurations of contact bodies. The configuration steel ball - glass disc/plate was applied in papers [A, B], where the film thickness behaviour was investigated. Both configurations steel ball - glass window and steel ball - sapphire window were used in paper [C] devoted to a frictional response of lubricant under vibrations. The sapphire has a much higher Young's modulus than glass which results in a smaller contact area and a higher contact pressure under the same load. Moreover, the thermal conductivity of sapphire is similar to that of steel. The effect of different material configurations is analysed only with respect to frictional response, since the impacts of contact area size, contact pressure, and thermal properties are more pronounced for friction than for film thickness. The properties of the contact bodies are listed in Table 1, while their dimensions can be found above for the relevant experimental apparatus.

**Table 1** Mechanical and physical properties of contact bodies.

Material:	Steel (100Cr6)	Glass (BK7)	Sapphire (Al <sub>2</sub> O <sub>3</sub> )
Young's modulus, GPa	207	81	400
Poisson's ratio	0.3	0.208	0.27
Specific heat capacity, J·kg <sup>-1</sup> ·K <sup>-1</sup>	490	858	761
Thermal conductivity, W·m <sup>-1</sup> ·K <sup>-1</sup>	43	1.114	30

The surface of the steel ball was polished with a diamond paste before each series of measurements. The average roughness of the ball surface, analysed via a using a 3D optical microscope (Bruker ContourGT-X), was kept under Ra 0.007 µm. The contact surface of the chromium layer is considered to be optically smooth. The contact bodies and some parts of the test rig, which come into contact with the lubricant, were cleaned with acetone before measurements. Small objects (ball, oil reservoir, and others) were cleaned in an ultrasonic acetone bath.

In the view of the fact that the test rigs or studied parameters, and thereby experimental conditions differed considerably from article [A] to article [C], the remainder of this chapter is divided in accordance with the individual papers [A] to [C].

#### 5.3.1 Paper A – EHL film thickness at pure squeeze action

In the first experimental study, the entrapment of the lubricant in the EHL point contact was investigated during the introductory part of the linear impact loading as the film distribution is mainly determined during this short interval. Before the impact load was carried out, an initial gap of 0.5 or 0.8 µm was established by positioning of the ball through the fine-pitch screw adjuster (see Fig. 54). These initial gaps, measured by TFCI, were chosen considering film thicknesses in EHL contacts of actual machines.

The introductory part of the impact is divided in paper [A] into the approach stage of the contact bodies and the loading stage of the contact. The approach stage is characterized by the time of approach and the rate of decrease in the gap between the contact surfaces (approaching speed). Let us recall that the effect of the approaching speed on EHL film was investigated by previous authors only theoretically. The loading stage is represented by the time of loading (impact time) and the rate of change in the Hertzian contact radius (loading speed), when the instantaneous load is calculated from the Hertz theory. Five loading curves (LC1 to LC5) were used in the experiments for two initial gaps. The loading and approaching speeds and corresponding times were determined for contact without lubricant (dry contact). In order to distinguish whether the film was affected by the approaching speed or by the loading speed, the approaching speeds were different for individual combinations of initial gaps and loading curves, whereas the loading speeds were almost equal for both initial gaps. Although the maximum contact load during the impact was 125 N, the film distribution was examined only to the instantaneous value of a load of 110 N (contact pressure of 0.8 GPa) to avoid distortive effects that could affect the results. The first undesirable effect is that the rate of loading ceases to be linear at the end of the impact (near to the maximum load) due to inertia forces. The second effect is that the dimple film shape is gradually affected by lubricant leakage in the peripheral area as time passes, especially when the rate of loading is reduced at the end of the impact. The used impact loadings are illustrated in Fig. 58 and corresponding numerical data are summarized in Table 2.

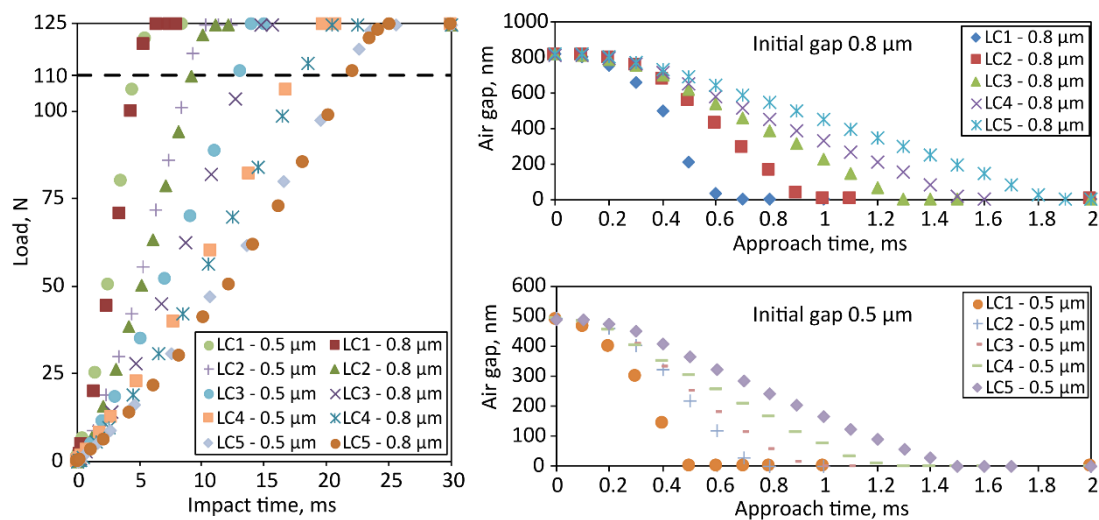


Fig. 58. Impact load curves (left) and initial approach of contact surfaces (right) for dry contact [A].

When the kinematic conditions were established for a dry contact, the gap between the top of the ball and the glass plate was filled by a lubricant. To encompass the influence of lubricants rheology, eleven lubricants were employed in this study. Their rheological properties can be seen in Table 3. The properties of the lubricants were obtained either from scientific articles, or were measured if the required data were not available. The dynamic viscosity was measured on a

rotational rheometer (HAAKE RotoVisco 1). For a known viscosity under different temperatures, the pressure-viscosity coefficient (PVC) was extracted by means of the Hamrock-Dowson predictions [22-24] from the film thickness measurements on a ball-on-disc optical tribometer. The molecular weight was estimated with respect to the lubricant viscosity. The experiments were performed for all combinations of load curves, initial gaps, and used lubricants at ambient temperature  $25 \pm 2$  °C. Subsequently, the results were analysed and film profiles compared with each other to determine the role of approaching and loading speed during the formation of entrapped film. The influence of lubricant rheology on film distribution was evaluated in a similar way. Finally, the empirical relationships, describing the dependence of dimple film shape and its central film thickness on the operating parameters, were established, when the experimental results were confronted with the theoretical prediction recently published by Venner, Wang, and Lubrecht [78].

**Table 2** Summary of experimental conditions for impact loading [A].

Load curve	Initial gap ( $\mu\text{m}$ )	Approaching speed ( $\mu\text{m}/\text{ms}$ )	Loading speed ( $\text{N}/\text{ms}$ )	Approach time (ms)	Impact time (ms)	Time at 110 N (ms)
LC1	0.5	1.358	24.6	0.5	4.7	5.2
	0.8	2.170	22.9	0.6	4.8	5.4
LC2	0.5	0.948	14.0	0.7	8.9	9.6
	0.8	1.144	12.1	0.9	9.1	10.0
LC3	0.5	0.737	9.2	0.9	13.0	13.9
	0.8	0.783	8.3	1.3	13.3	14.6
LC4	0.5	0.489	6.5	1.2	17.4	18.6
	0.8	0.579	6.1	1.5	18.0	19.5
LC5	0.5	0.409	5.1	1.4	21.5	22.9
	0.8	0.473	5.0	1.8	22.0	23.8

**Table 3** Viscosity at ambient pressure, pressure-viscosity coefficient (PVC) and molecular weight of lubricants at 25 °C used in paper [A].

Lubricant	Viscosity ( $\text{Pa}\cdot\text{s}$ )	PVC ( $\text{GPa}^{-1}$ )	Mol. wt. ( $\text{g}/\text{mol}$ )	Reference
GC	1.01	5.4	92	[150, 151]
SQ	0.025	22.3	423	[26]
PAO 4	0.023	11.9	437	[26, 152]
PAO 6	0.046	11.1	529	[150]
BS	0.903	22.67	$\approx 600$	*1
CAS	0.75	14	927	[153, 154]
DMPS	1	15.2	$\approx 32\,000$	[155, 156]
KTF-1	0.062	34.8	$\approx 250$	[157, 158]
SR 90	0.032	21.9	$\approx 410$	
SR 150	0.056	22.8	$\approx 430$	
SR 600	0.245	24	$\approx 450$	

\*1 values provided by Kaneta and Sakamoto

### 5.3.2 Paper B – EHL film thickness under lateral vibrations

In the next paper [B], an EHL contact was exposed to harmonic lateral-sliding vibrations to study the impact of these vibrations on film thickness behaviour via TFCI. First, the kinematics within the contact was analysed describing instantaneous magnitudes (speeds) and vectors of surface entrainment and sliding velocities (see Fig. 59). The kinematic analysis is based on time-independent angular speeds of the ball and the disc, taking into account their radii in the point of the contact, together with the time-dependent motion of the ball in the lateral direction (perpendicular to the main rolling direction) of the contact. A stroke length, frequency, and time of the lateral motion of the ball are used to determine the ball position, speed, and acceleration in this direction via harmonic functions. The time-dependence causes non-steady state operating conditions. The instantaneous value of SRR is defined as a ratio between the sliding speed and the entrainment speed, where the sliding velocity is projected in the vector of entrainment velocity. Furthermore, an elementary estimation of lubricant passage through the contact was introduced involving the entrainment velocity and ignoring the sliding velocity. This theoretical estimation was compared with experimentally observed passage of lubricant to clarify a control mechanism of the lubricant passage, which affects film thickness distribution under transient conditions.

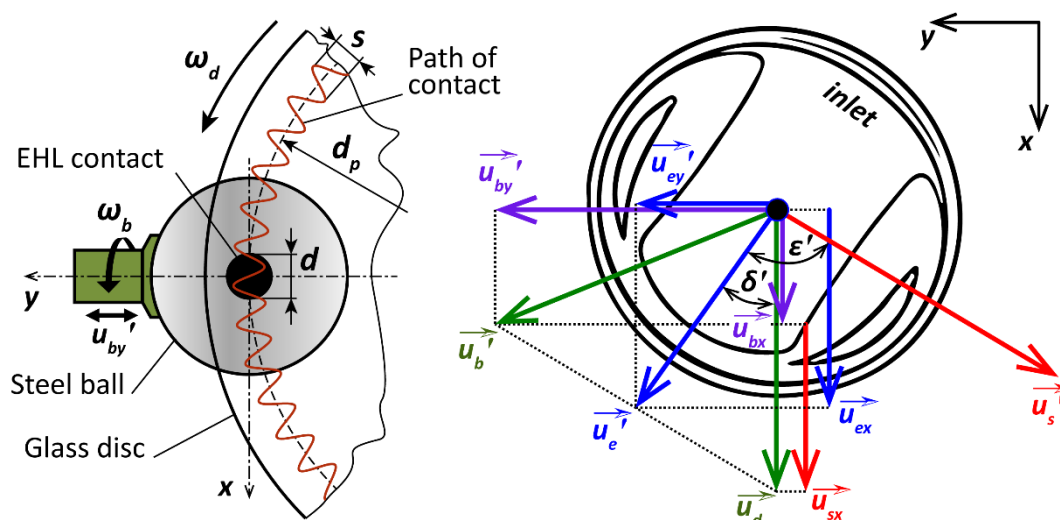


Fig. 59. Movement of EHL contact (left) and velocities within rolling/sliding EHL contact (right) under lateral vibrations [B].

On the subject of the conditions set for the experiments, pure rolling was applied in the main direction of the contact, while pure sliding took place in the lateral direction of the contact. Different main rolling speeds, lateral-sliding harmonic motions, contact loads, and lubricants were combined (over two hundred combinations used). The frequency of lateral vibrations was up to 300 Hz and the stroke length was always smaller than the Hertzian diameter of the contact respecting vibrations in actual EHL contacts, especially those in rolling bearings. The ranges of the instantaneous values of individual operating parameters are listed in

**Table 4.** Five liquid solutions (lubricants or its mixtures), whose rheological properties can be found in [Table 5](#), were employed in the experiments representing different types of lubricants (Newtonian, mixtures and blends, non-Newtonian). The values of the rheological parameters were acquired in the same way as in the case of paper [\[A\]](#). The experiments were conducted at temperatures 30 and  $40 \pm 0.5$  °C. For the individual conditions, the contact was subjected to vibrations only for approximately 5 seconds to minimize shear heating of lubricant. To detect such undesirable effect on film thickness, the records of film thickness behaviour were inspected and tests were repeated if the changes in film thickness during ten consecutive strokes exceeded 15 nm. The interferograms from the end of the stroke were mainly evaluated, when the investigated film profiles were oriented with respect to the median of entrainment velocity vector obtained over a half-stroke.

**Table 4** Ranges of operating parameters used in paper [\[B\]](#).

Operating parameter	Minimum value of parameter	Maximum value of parameter
Entrainment speed (m/s)	0.006	0.55
SRR (1)	0	-1.99
Frequency (Hz)	0	300
Stroke length ( $\mu\text{m}$ )	80	400
Lateral entrainment acceleration ( $\text{m/s}^2$ )	0	335
Entrainment acceleration ( $\text{m/s}^2$ )	0	250
$S/D$ ratio (1)	0.1	0.9
Contact pressure (GPa)	0.45	0.88

**Table 5** Viscosity at ambient pressure, pressure-viscosity coefficient (PVC) and molecular weight of lubricants at given temperature used in paper [\[B\]](#).

Lubricant	Temperature (°C)	Viscosity (Pa·s)	PVC ( $\text{GPa}^{-1}$ )	Mol. wt. (g/mol)	Reference
SN650+PIP	30	1.007	$\approx 12$	$\approx 450/40\ 000$	
CAS	40	0.239	12.4	927	<a href="#">[153, 154]</a>
R560/88	40	0.406	$\approx 30$	$\approx 500$	
SQ+PIP	40	0.071	20.9	423/40 000	<a href="#">[159]</a>
PGLY	40	16.3	13.2	12 000	<a href="#">[159]</a>

In order to quantitatively evaluate the effect of lateral vibrations on film thickness, the central film thickness of the lubricants was first measured under steady state conditions. The same contact loads/pressures and temperatures were applied as those used in the transient conditions, but both the entrainment speed and SRR slightly exceeded the ranges in [Table 4](#). Subsequently, the empirical relationships between the film thicknesses and operating parameters were

determined by fitting these data via polynomial models (see Appendix in [B]). The central film thickness estimated from these relationships for equivalent instantaneous values of operating parameters is referred to as the reference film thickness. The reference film thicknesses were compared with film thickness distribution in the contact under lateral vibrations considering the time of lubricant passage through the contact. This enable to elucidate the origin of film thickness distribution and its predictability by means of usual film thickness predictions for steady state conditions. Thereafter, film profiles were compared for conditions, where one operating parameter was changed (lubricant, main entrainment speed, lateral entrainment speed), while other parameters were kept fixed, to determine the effect of this parameter on film thickness under lateral vibrations. The effects of operating parameters on film thickness were evaluated using the dimensionless numbers (ratios). The “local” numbers, originating only from the central area of given film profile, are defined as the relative deviations of film thickness (positive, negative, and overall) related to the mean value of film thickness in this area. The “global scale” (the relative mean value of film thickness) is represented by a ratio of this mean film thickness and the reference film thickness resulting from steady state conditions. Based on the effects of lateral and main entrainment speed on film thickness, their ratio was assumed as the rate of lateral vibrations (more detailed specification can be found in [B]). The effect of lateral vibrations on film thickness was subsequently identified by a systematic comparison of film profiles for various conditions considering the dimensionless numbers and the rate of lateral vibrations.

### 5.3.3 Paper C – frictional response of EHL film under lateral vibrations

5.3.3

---

Similar kinematic conditions as in article [B] were also employed in paper [C], where the frictional response of lubricant was examined simultaneously in the main and the lateral direction of the contact. Due to the design of the test rig, only pure sliding motions were used in both directions of the contact. In view of this, relatively low speeds were applied to reduce thermal effects resulting from high sliding speeds, when a lubricant temperature was regulated at  $40 \pm 0.5$  °C. The utilized lubricant was bright stock mineral oil with ambient viscosity of 0.329 Pa·s and the pressure-viscosity coefficient of 19.03 GPa<sup>-1</sup> at test temperature. Measurements were carried out for steady state and non-steady state conditions. Under steady state conditions, the steel ball rotated at its surface sliding speed ranging from 0.01 to 0.5 m/s. Under non-steady state conditions the sliding speed in the main direction was maintained at 0.1 m/s and, at the same time, the ball performed reciprocating motion in the lateral direction of the contact. The frequency of the lateral harmonic motion differed from 30 up to 100 Hz in 10 Hz increments. The stroke length of this motion ranged from 30 to 220 μm and was always smaller than the Hertzian contact diameter. Consequently, S/D ratio was from 0.06 to 0.62 considering the contact diameter. Since two loads and two material configurations (glass or sapphire window) were employed, three contact pressures and two diverse diameters of the contact were combined with the kinematic conditions. This led to nearly a hundred combinations involved in the

measurements under lateral vibrations. The experimental conditions are summarized in Table 6. These conditions were chosen with respect to findings in paper [B] to ensure an almost stable central film thickness for given main sliding speed. Accordingly, the impact of film thickness variations on measured friction is negligible.

**Table 6** Experimental conditions of measurements under lateral vibrations employed in paper [C].

Window material	Contact load (N)	Contact pressure (GPa)	Contact diameter ( $\mu\text{m}$ )	Main sliding speed (m/s)	Lateral sliding speed (m/s)	SRR
Glass (BK7)	35	0.53	357			
Glass (BK7)	89	0.72	487	0.1	0 to 0.07	-2
Sapphire ( $\text{Al}_2\text{O}_3$ )	89	1.32	358			

The coefficients of friction in the main and the lateral direction of the contact were calculated in real time (LabVIEW software by National Instruments) by dividing the individual friction forces by the normal load of the contact. Before the measurements, the normal load was determined for a static contact, when the deformed shape of the contact bodies obtained via TFCI was fitted by the deformed shape calculated from the Hertz theory. The load uncertainty for such an approach is lower than 0.5 N. Since the contact window is attached to the rigid part of the compliant mechanism by means of the flexure hinges, the friction forces cause the windows movement to allow their measurement. The window movement was included in calculations through the stiffness of this system to quantify a relative displacement and sliding speed between the surface of the ball and the surface of the window. Similarly, the normal load of the contact affects the complaint mechanism, and accordingly signals (then converted to forces) from the load sensors. To compensate such errors, the friction forces are corrected via a balance of zero signal. In practice, this means that the friction forces are balanced to obtain the same coefficient of friction, when the direction of the sliding motion is reversed. The matrix-based MATLAB language developed by MathWorks was used for post-processing and evaluation of the measured data.

First, the frictional response of lubricant was measured under steady state conditions (unidirectional shear loading of lubricant) to assess the regime of friction and related phenomena according to the similarities with a general traction curve (see Fig. 3). Once the frictional response was known for the given range of steady conditions, the lubricant was exposed to transient bi-directional shear loading due to lateral vibrations. The influences of operating conditions on the frictional response in the lateral direction of the contact were analysed using the Lissajous curves. Moreover, the viscoelastic response was investigated, because such friction behaviour is expected at high pressures and oscillation shear loading of lubricant. To clarify an interdependence of the frictional responses in the lateral and the main direction of the contact, the responses were compared for different transient conditions considering thermal and other effects, and a total friction. The total

friction was calculated as a vector sum of the friction components in the direction of sliding velocity vector. Furthermore, the frictional responses of uni- and bi-directional shear loaded films were compared to deduce their origins. These origins explain the reasons for the differences and compliances of the frictional responses with respect to various phenomena. Besides of this, the direct comparison was used to assess the impact of the rate of lateral vibrations on the total friction.

## 6 RESULTS AND DISCUSSION

In the first experimental study [A], the role of approaching and loading speed on dimple film shape formation and resulting film thickness was examined under conditions of pure squeeze action using the optical tribometer. Along with that, also the effect of lubricant rheology on film thickness distribution during this impact loading was considered. For these purposes, two realistic initial gaps were combined with five loading curves of differently graded loading and approaching speeds calculated for dry conditions.

First, a single mineral oil was employed and the temporal evolutions of its film profiles were analysed with respect to individual conditions (load curves and initial gaps). Due to a pressure build-up and growth in lubricant viscosity particularly in the central area of contact during the impact process, the amount of entrapped lubricant within the central dimple and accordingly the central film thickness (dimple depth) increased with the increase in the approaching speed, loading speed, and initial gap. These results followed the previous theoretical and experimental findings. Nevertheless, a crucial feature of the central dimple formation was revealed. It was observed that the apex of the dimple began to be visible at a time, which was close to the approach time of a dry contact. It means that the beginning of the dimple formation took place at the end of the initial approach stage of the impact process. The central film thickness was then directly given by the apex of dimple, because this thickness (or the position of apex) was not significantly changed in the course of the impact process and even persisted for a long time afterwards. Moreover, the time of the apex occurrence was not affected by the different initial gaps and was driven by the used loading curve. The central film thickness can therefore be attributed to approaching speed or loading speed. The former determines the approach time, close to which the apex was observed. The higher approaching speed, the shorter approach time, and hence the top of the dimple is formed at a thicker residual film during the proceeding of the contact surfaces towards each other. On the other hand, if the latter was changed, the central film thickness did would not necessarily follow these changes, as found via a comparison of the film profiles for different loading curves. This is clear evidence that the approaching speed is one of the key factors determining the central film thickness, whereas the loading speed is irrelevant in this respect. Unfortunately, this also indicates that the claims in many of previous experimental studies of other authors, that the central film thickness is given by the loading speed, are not correct. Another key factor is the initial gap. Although the initial gap had no effect on the beginning time of the dimple formation, it predetermines the residual film thickness at which the dimple is formed. This is the reason why a large initial gap results in a deeper dimple.

Once the initial approach stage was over, the dimple film shape started to be formed during the loading stage of the impact process. The shape of the dimple was analysed with respect to the slope of its sides. Together with the central thickness, the dimple side shape influenced the amount of entrapped lubricant within the EHL contact. Since a linear loading progress was applied, a major part of dimple sides

was straight, where the film thickness diminished at a gradually increasing radius from the contact centre. The remaining part at the contact periphery (lower thickness) was more flattened due to lubricant leakage out of the dimple. The analysis proved that the slope of dimple sides is linearly dependent on the loading speed and is influenced by the initial approach stage of the impact. At a high loading speed, the rate of increase in viscosity was high as well; the lubricant could not leak out and a steeper shape of the dimple was formed. Correspondingly, the flattened shape was formed with a small amount of entrapped lubricant at low loading speeds. These results support the theoretical findings in [67], where non-linear progresses of loading speed were simulated.

After that, the tests were repeated with the same loading curves and initial gaps for the next ten various lubricants to assess the effect of lubricant rheology. These experiments also confirmed the general validity of the above results obtained for a mineral oil. It was demonstrated that ambient viscosity is another key factor affecting overall film thickness of the dimple, while PVC plays only a minor role. The effect of ambient viscosity took place mainly during the initial approach stage, when it determined (together with the approaching speed of dry contact) the rate of the reduction in the central film thickness and the time required for its stabilization. The low viscosity lubricants quickly escaped from the closing gap at the contact periphery (minimum thickness) due to their low flow resistance. Hence, the apex of the dimple was produced at low residual film thickness at a time close to the approach time of dry contact and the lubricant was almost immediately entrapped within the dimple resulting in stable central film thickness. This is in accordance with the numerical results presented in [120]. The higher flow resistance caused the low rate of reduction in the central and minimum film thickness of high viscosity lubricants. Consequently, a deep dimple was formed, but the stabilization of the central film thickness took more time, because the slow decrease in the central thickness during the impact process as the lubricant leaked out of the dimple. Furthermore, it was shown that the slope of dimple sides can be affected by PVC, since it determines the rate of viscosity build-up during the loading stage of the impact. However, the influence of PVC, the increase of which led to a steeper shape of the dimple, was proved only for the loading curve with high approaching speed as well as loading speed giving a high rate of the increase in the contact pressure. For low speeds, the effect of PVC was inconclusive. Some very high viscosity lubricants were out of these general trends due to their specific rheology (extremely low or high molecular weight, strongly non-Newtonian behaviour, viscoelastic behaviour). For instance, the bright stock mineral oil formed a non-central (periphery) dimple when the combination of high approaching speed and small initial gap was utilized; as was described by other authors. Except for the non-central dimple, the initial gap had no effect on the minimum film thickness at contact periphery at the end of the impact process. It was also pointed out that both the central and maximum film thicknesses of the central and periphery dimple follow power-law dependences on the approaching speed.

The central thicknesses of entrapped films obtained in the experimental study [A] were subsequently compared with their predicted values by means of the

analytical solution recently published by Venner et al. [78]. This direct comparison revealed that the theoretical prediction underestimates the central film thickness by 32% on average. The discrepancy was attributed to the employed viscosity-pressure relationship and the omission of the initial gap parameter in the prediction. Moreover, the predicted data differed from the measured ones in their trend according to the impact times/speeds on which this prediction is based. This trend is stated in the theoretical solution by a fixed value of the index of the power-law dependence resulting from the impact analysis for dry contact by Johnson [77]. Nevertheless, the impact times/speeds are also affected by the used lubricant, because its rheological properties influence the rate of the reduction in the central film thickness; as it was described above. The effect of impact time, loading and approaching speed on the central film thickness, as well as the index of the power-law dependence, was found to be given by the product of ambient viscosity and PVC of lubricant. Optionally, only the ambient viscosity can be considered when PVC is unknown, because the effect of PVC is less pronounced. In view of this, the empirical relationships were established and, if implemented in the prediction [78] instead of the fixed value of index, lead to satisfactory estimates of the central film thickness of entrapped lubricant in the central dimple despite different initial gaps.

The previous theoretical and experimental studies of other authors showed that the squeeze action is also important when the tangential speed of contact surfaces vary over time, especially in the course of deceleration of this speed (typically during a sudden stop of motions, close to the end of strokes for reciprocating motions, or during vibrations). Although vibrations are inseparably linked to the operation of every machine, their impact on EHL film thickness was examined only sporadically lacking any quantitative description and exceeding realistic values of  $S/D$  ratio. To correct this unjustified overlook, study [B] including a variety of conditions of harmonic lateral vibrations was performed, when  $S/D$  ratio was kept under one.

In the first part of study [B], the lubricant passage through the contact and the origin of film thickness distribution was investigated at fixed conditions of lateral vibrations. The actual passage of a small section of lubricant was directly compared with the estimated position of this section via a sequence of interferograms captured at different times. The theoretical estimation was based on the kinematic conditions when it involved entrainment velocity but neglected sliding velocity. The passage of film thickness distribution in the central area of the contact followed a sine wave pattern without a change in the film thickness or its shape. This scenario was periodically repeated each cycle of lateral vibrations when the very same film distribution was achieved for a given period of lateral motion. A very good agreement was obtained between the estimated and actual passage of the section of lubricant. This result emphasized that the effect of sliding vector is negligible in this respect and the passage of lubricant can be simply predicted considering only entrainment speed. After that, the individual film thicknesses in the contact were assigned to the times at which the thicknesses were entrained into the contact inlet under lateral vibrations. In this way it made possible to determine the immediate

values of entrainment speed and SRR responsible for the formation of the film at the contact inlet at given times. The design of this experiment was straightforward, if film thicknesses acquired under lateral vibrations are comparable with the thicknesses formed under corresponding steady state conditions in terms of entrainment speed and SRR, then the overall film thickness distribution can be estimated from the thickness under steady state conditions or from Hamrock-Dowson predictions [22-24] in the case of low SRR. The film thicknesses were identical for the film formed at the end of the stroke when the lateral sliding speed was equal to zero and at half of the stroke when the maximum lateral speed was achieved. In these circumstances, the effect of lateral vibrations on the film thickness was unimportant. However, when the entrainment speed and SRR began to increase after the end of the stroke and appropriately thicker film was measured under steady state conditions, the film thickness in the contact affected by vibrations was dramatically reduced. This reduction was due to the presence of EHL horseshoe-shaped constriction. The constriction was entrained into the central area of the contact when it approached the contact inlet, the position of which varied according to the immediate vector of the entrainment velocity. Another significant disagreement in the thicknesses was noted during the deceleration of the entrainment speed when a substantially thicker film was entrained into the contact in the shape of a crescent. With respect to the previous finding in paper [A], this increase in the film thickness was attributed to the squeeze action at the contact periphery resulting from the reduction in the entrainment of lubricant at the contact inlet. It was elucidated that the thickness of squeezed/entrapped film was controlled by the immediate value of deceleration. Then the crescent shape was a consequence of gradual entrainment of the entrapped lubricant into the contact inlet oriented in accordance with the vector of entrainment velocity. Moreover, these film fluctuations were beyond thicknesses formed at extreme steady entrainment speeds and SRRs exceeding speeds and SRRs applied under vibrations. Consequently, this demonstration revealed that fluctuations of central film thickness due to lateral vibrations cannot be directly estimated via a common film thickness predictions or by means of thickness formed under steady state conditions.

When the origin of film distribution under vibrations was clarified, the influence of the main entrainment speed, lateral entrainment speed, and lubricant rheology on the central film thickness was studied using the dimensionless numbers (ratios), which were designed by the author of this thesis to describe the effects of vibrations. More detailed information on these dimensionless numbers (relative positive, negative, and overall film deviation and relative mean film thickness) and experimental conditions can be found in paper [B] (preferably) or in subchapter 5.3.2. The impact of lateral entrainment speed was represented by the frequency of vibrations, because these parameters are linked via a fixed relationship. For other given operating parameters, the effect of vibrations was small, when frequency was under 100 Hz, causing a reduction in mean thickness by 5% and overall deviations about 15%. As the frequency increased up to 300 Hz, the overall film deviation grew exponentially to almost 100% of the mean value of central thickness due to the

entrainment of thin and thick films in the central area of the contact and more pronounced squeeze action. Simultaneously the relative mean film thickness exponentially declined to 70%. The effect of the main entrainment speed was found to be opposite to the effect of the lateral entrainment speed. It was observed that the squeeze action is reduced and EHL constriction ceased to encroach upon the central area of the contact when the main entrainment speed was increased. Consequently, the exponential growth in the relative mean thickness and exponential decline in relative overall deviation was revealed for the increase in the main entrainment speed. Very high values of the coefficients of determination (above 0.998) were achieved by fitting the experimental data with general exponential functions, thus highlighting the reliability of these trends. Thereafter, the film thickness distributions of four lubricants were compared under the same non-steady state conditions of lateral vibrations. The influence of lubricant rheology was substantial. It was pointed out that the squeeze/entrapment effect was more significant for lubricants forming a thicker film. This finding is in accordance with the results in study [A] where the thickness of entrapped film increased with the increase in the initial gap between the contact surfaces. Besides this, another source of the film thickness deviations was unexpectedly found. The film of non-Newtonian polyglycol (PGLY) was disrupted by low-thickness sharp stripes in the central area of the contact, which may affect contact fatigue. Surprisingly, the stripes were not produced at the contact inlet but directly in the central area of the contact at the moment of maximum sliding speed and they disappeared before reaching the contact outlet. The production of the stripes was attributed to transient bi-directional shearing of PGLY in combination with its high molecular weight. Regardless of these differences in film distributions due to lubricants rheology, the relative mean thickness was almost the same for all lubricants, since this dimensionless number involves the reference film thickness of particular lubricant suppressing these differences.

Further, a broad spectrum of operating parameters (see [Table 4](#) and [Table 5](#)) was employed to gain a quantitative description of film behaviour under lateral vibrations. Based on the knowledge that the effects of main and lateral entrainment speed are inverse, the parameter referred to as the rate of lateral vibrations (entrainment speeds ratio; for more details see [B]) was stated to summarize the impact of these opposing influences on film thickness. The rate of lateral vibrations represents a transition between the steady state pure rolling conditions (its value near to zero) up to the pure sliding reciprocating motion (its value approaching infinity). Another reason for choosing this parameter was that the  $S/D$  ratio, used by other authors for evaluation of film thickness under non-steady state conditions, is unable to include complex kinematic conditions of this study, and its application to experimental data did not lead to any clear trends describing the effects of lateral vibrations. A simple exponential relationship was established from a large amount of experimental data to estimate the effect of lateral vibrations on the reduction in the mean film thickness uniformly for all lubricants considering the reference film thickness and the rate of lateral vibrations. In addition to this estimation, certain characteristic behaviour of film thickness distribution was observed with respect to

the rate of vibrations. If the lateral entrainment speed was under 60% of the main entrainment speed, the effect of lateral vibration on the mean film thickness was of little importance. Over this value, the central film thickness began to increasingly suffer from vibrations (entrainment of thin and thick films, production of low-thickness stripes). Furthermore, the overall film thickness was gradually reduced due to oil starvation when the entrainment speeds ratio exceeds 1. Under such conditions, the EHL cavitation zone approached the inlet of the contact reducing oil entrainment similarly as found by other authors for short stroke lengths and high frequencies of reciprocating motions. Moreover, the combination of film fluctuations and contact starvation subsequently led to local film breakdown at the ratio of 1.8 even though the mean film thickness was reduced only by 40%. Complete collapse of EHL film then took place for the rate of vibrations over 6. Along with the estimation of reduction in the mean film thickness, the appropriate equations were established also for the positive, negative, and overall film deviations common to all lubricants. All deviations exponentially grew with the increase in the rate of lateral vibrations. The analysis of these deviations revealed that the positive and negative deviations are symmetrical around the mean value of the central film thickness up to the point of local film failure. This symmetry of deviations was likely caused by in-contact mechanisms maintaining a load-carrying capacity of EHL film.

Articles [A, B] were devoted to the effects of operating parameters and lubricant rheology on the behaviour of film thickness under non-steady state conditions. The last article [C] of this dissertation thesis followed mainly paper [B] where the impact of lateral vibrations was studied. This time, the frictional response of lubricant was investigated under lateral vibrations. So far, there was no experimental or numerical study examining the effect of lateral vibrations on EHL friction; especially inspecting the frictional responses simultaneously in both the main direction and the lateral direction of the EHL contact. Due to this lack of knowledge, the focus of paper [C] is not only on the influence of operating conditions but also on the interaction of these responses considering total friction under steady state and non-steady state conditions, and on an evaluation of lubricant rheology via this unusual approach. To achieve these goals in a non-distorted way, experimental conditions were designed to avoid the significant fluctuations of film thickness observed in study [B], i.e. the rate of lateral vibrations was maintained below 0.6.

The starting point in study [C] was the determination of the coefficient of friction (CoF), friction regime and associated phenomena affecting friction under appropriate steady state conditions, which can be subsequently compared with friction under lateral vibrations. The lubricant (BS mineral oil) was shear loaded unidirectionally in the main direction of contact at different sliding speeds, contact pressures, and material configurations (for more details see subchapter 5.3.3). All measured frictions curves belonged to the thermal regime while CoF decreased with the increase in the sliding speed due to a drop in lubricant viscosity resulting from the effects of in-contact shear heating and/or shear thinning. The lower CoFs were more likely to be obtained for the configuration of steel-glass than for the

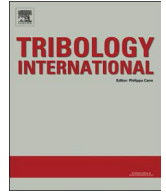
steel-sapphire configuration, because thermal properties of glass led to a greater accumulation of heat in the film (reduction in viscosity) and the contact pressure was a substantially higher in the case of the sapphire window (increase in viscosity). There was a notable observation that CoF was higher at a lower pressure for the steel-glass EHL contact than CoF at a higher pressure for the same material configuration. It must have been due to more pronounced thermal effects on viscosity at a higher pressure.

The frictional response in the lateral direction was examined in the first place when the contact was subjected to lateral vibrations and the lubricant underwent transient bi-directional shearing. The level of viscoelasticity was quantified via an analysis of the phase shift between the lubricant excitation (lateral position representing a strain of lubricant) and its response (CoF representing lubricant shear stress). The mean value of the phase shift about  $\pi/2$  and its low standard deviations indicated a purely viscous behaviour of lubricant for different combinations of kinematic and contact conditions; even at a pressure exceeding 1.3 GPa. This was also confirmed by Lissajous curves (lateral position – CoF) demonstrating concentric ellipses symmetrical around both the horizontal and the vertical axis with dimensions in accordance with applied stroke lengths and frequencies of lateral motion. Moreover, the ellipses did not differ over individual vibration cycles highlighting a stable rheological response of lubricant in the lateral direction of the contact without the influence of thermal effects. Then, the results showed that the only fundamental parameter determining CoF in the lateral direction of the contact is the lateral sliding speed representing the shear rate of lubricant at given film thickness. The frictional response was linearly dependent on this speed pointing to an isothermal Newtonian behaviour of lubricant. It should be emphasized that such response is highly desirable for determination of rheological properties of lubricants, but at the same time it is very difficult to obtain this response unaffected by thermal phenomena under severe conditions of actual EHL contacts involving high pressures and sliding. In addition, it is also remarkable that the contact pressure and material configurations had no impact on CoF in the lateral direction of the contact in contrast to CoF in the main direction of the contact under both steady state and non-steady state conditions. These results led to the important conclusion that the frictional response and thus effective viscosity of lubricant cannot be considered as isotropic, because they are predetermined by a measurement direction in spite of the same shear rate. This conclusion answered the question on the an/isotropy posed by Dowson in [29].

Subsequently, the reason for absence of above-mentioned effects in the lateral direction of the contact was investigated via a comparison of origins of frictional responses under uni- (steady state) and bi- (lateral vibrations) directional shear loadings. It was calculated that the shear stress applied in the experiments to the lubricant was many times higher than the shear stress perturbing or disrupting a molecular structure of lubricant. This influenced the lubricant viscosity by shear-thinning, and simultaneously the viscosity was affected by the other effects of shear-heating and pressure. The consequences of these effects were observed only in the main direction of the contact, because the majority of lubricant shear flow

was maintained in this direction by a fixed rotational speed of the ball. Accordingly, it was deduced that the isothermal Newtonian response in the lateral direction of the contact originated from short-term perturbation of lubricant structural arrangement in the perpendicular direction to its main flow while the lubricant structure was re-arranged after its unloading at the ends of strokes of lateral motion.

Furthermore, it was revealed that the frictional response in the main direction of the contact was influenced by the friction in the lateral direction of the contact, but not vice versa as the majority of shear flow was maintained in the main direction. This was found from the comparison of CoFs in the different directions of the contact with its total friction. Although various stroke lengths and frequencies of vibrations were used and resulted in different lateral sliding speeds, the total CoF remained the same until the pressure was kept fixed. The independence of friction on the sliding speed indicated the achievement of the limiting shear stress phenomenon, when the shear stress transferred through a film of lubricant (CoF) is unable to exceed a certain value. The total friction measured under vibrations therefore corresponded to the total friction measured under steady state conditions. This means that the effect of lateral vibrations on the total friction was negligible in the range of used experimental conditions, similarly as in the case of film thickness when the rate of lateral vibrations was lower than 0.6 (as demonstrated in [B]).



# Effects of lubricant rheology and impact speed on EHL film thickness at pure squeeze action

Josef Fryza\*, Petr Sperka, Motohiro Kaneta, Ivan Krupka, Martin Hartl

Faculty of Mechanical Engineering, Brno University of Technology, Technická 2896/2, 61669 Brno, Czech Republic

## ARTICLE INFO

### Keywords:

Elastohydrodynamic lubrication  
Non-steady state film thickness  
Squeeze action  
Lubricants

## ABSTRACT

A squeeze film action is an essential phenomenon in elastohydrodynamically lubricated conjunctions subjected to impact loading or sudden halting of motion and affects both film thickness and friction. This study presents experimental results of film thickness behaviour of lubricant entrapment under diverse conditions including initial impact gaps, initial approaching speeds, loading speeds and variety of lubricants during introductory part of impact loading. The results are compared with recent theoretical solution. It is shown that the entrapped film shape directly depends on loading speed and the central film thickness is mainly determined by the approaching speed and lubricant viscosity and can be approximated by power law where the influence of impact times/speeds can be estimated from basic rheological properties of lubricants.

## 1. Introduction

Majority of studies concerning elastohydrodynamic lubrication (EHL) have been focused in the past on phenomena occurring under steady state conditions. The steady state EHL is nowadays well understood via both experimental and theoretical investigations and it is possible to reliably predict film thickness and friction of such EHL contacts. However, in many machine elements, such as traction continuously variable transmissions (CVT), gears, cam and followers and even steadily loaded rolling element bearings, neither the speeds nor the loads are time-independent. Also, every machine has to stop sometimes due to an accident or due to the nature of machine operating conditions, as in case of CVTs or rolling bearings of stepper motors. The resulting mutual normal approach of contact surfaces given by impact loading or sudden halting of motion causes a squeeze film action to have a crucial influence on EHL conjunction.

Since the beginning of investigations of non-steady state EHL contacts in 1960s, there has been a particular interest in impact loading issues. Christensen, in his pioneer work [1] dealing with a ball impacting a lubricated layer, found that very high contact pressures arose and deep dents were produced for lubricated contacts in comparison with dry contacts. Subsequently, the occurrence of a dimple with maximum film thickness in central area of contact and an entrapment of very high-pressured lubricant in this area were confirmed experimentally by direct observation [2]. Also, the effects of piezoviscosity of lubricants were considered in the theoretical studies [3,4] and the effects of molecular weight of mineral oils were

investigated experimentally [5]. An interesting attribute of squeezed films – the second sharp pressure peak – was revealed using a thin pressure transducer in the centre of contact; the peak occurs at the end of impact time when the steel ball rebounds from the lubricated surface [6]. Theoretical evidence of this phenomenon was given in papers [7–9] together with broad description of EHL contacts subjected to impact loadings where a time lag between the occurrence of maximum force and minimum film thickness was analysed as a result of damping and elasticity of lubricant film. The study [7] further pointed out that minimum film thickness of entrapped lubricant increases with increase in impact velocity of falling ball on a flat lubricated surface. The related theoretical works [10–12] investigated pressure and film thickness distributions under squeeze motions.

The biggest boom of experimental studies in this research field took place at the end of 1990s, mainly due to the affordability of high speed cameras. Larsson and Lundberg [13] demonstrated via optical interferometry that a depth and a diameter of central dimple are affected by lubricant viscosity, maximum applied load and impact speed of the ball mounted on the pendulum falling onto a lubricated glass disc. Other experimental works [14,15] focused on pure squeeze action shown, as well as previous contributions, that a central dimple film shape with minimum thickness at the periphery region of contact is formed and a pressured lubricant is entrapped between the approaching surfaces for a long time after the impact.

For lubricant entrapment under conditions of sudden halting of rolling/sliding motion, acceleration together with rheological properties of lubricants have been proved both experimentally [16–20] and

\* Corresponding author.

E-mail address: [fryza@fme.vutbr.cz](mailto:fryza@fme.vutbr.cz) (J. Fryza).

### Nomenclature

$a$	deceleration	$n$	power-law index
$a_h$	slope of dimple side curve	$t$	time
$C$	dimensional constants	$t_O$	impact time
$h$	film thickness	$t_{ini}$	approach time
$h_c$	central film thickness	$v_{ini}$	initial approaching speed
$h_{gap}$	air gap between surfaces	$v_F$	loading impact speed
$h_{ini}$	initial central impact gap	$v_{hc}$	initial speed of central film thickness reduction
$h_{max}$	maximum film thickness	$w$	load
$L, M$	dimensionless Moes parameters	$\alpha$	pressure-viscosity coefficient
		$\eta$	dynamic viscosity
		$\eta_O$	dynamic viscosity at ambient pressure

theoretically [21–23] as important parameters for squeezed films phenomena. Furthermore, if the rolling/sliding conjunction was subjected to sudden changes in load, the squeezed film of lubricant was generated at the inlet of contact and was entrained through it without a change in thickness and shape [24,25]. Sakamoto, Nishikawa, Kaneta, Guo and other authors [25–30] revealed formation of non-central dimple occurring under pure squeeze motions. This kind of dimple of entrapped lubricant was produced at the periphery of EHL contact where the maximum film thickness was also located. The periphery dimple was obtained especially for small initial gaps between the approaching surfaces or pre-loaded oiled contacts and also for high loading speeds and lubricants close to glass transition due to their dynamic properties associated with increase in pressure.

In recent years, an EHL squeezed films behaviour has been investigated mainly theoretically. For very thin films under 5 nm, it was shown in theoretical analyses [31,32] that both pressure and film thickness oscillate during squeeze action due to an action of surface forces. Moreover, Kumar and Kalita [33] employed a shear-thinning model pointing out that assuming a Newtonian model may be inappropriate for linear piezoviscous oils which exhibited rapid film entrapment. A substantial effect of lubricant viscosity on entrapped film thickness was studied by another numerical simulation [34] involving a mixture of a Newtonian base oil and couple stress fluid at various volume ratios. Further, a response of the EHD contacts under load variations (normal vibrations) was examined using dynamic models [35,36] with respect to lubricant film stiffness and damping.

Previous studies usually considered squeezed films problems of EHL conjunctions as an action of a free falling body onto flat lubricated surface. Analytical predictions of central entrapped film thicknesses in line [37] and point [38] contacts for this case of squeeze motion were recently published. Unfortunately, unrealistically large initial gaps exceeding 1  $\mu\text{m}$  were often applied/analysed compared to EHL contacts in actual machines, and also a limited number of lubricants or only very specific lubricant(s) were frequently employed in previous studies. There are still many particular parameters of impact loading, such as initial approaching speed of contact surfaces exhibiting a remarkable effect on the film thickness and pressure [29]. The effects of these parameters on lubricant film entrapment have not been fully clarified or experimentally confirmed yet. Hence, in this paper, the entrapment of EHL films is investigated experimentally under diverse conditions including initial impact gaps, initial approaching speeds, loading speeds and a variety of lubricants. The experimental results are compared with the recent theoretical solution [38]. The current study is mainly focused on the introductory part of impact action and thus it does not include rebounding or long-term monitoring of lubricant leaking out of EHL contact.

## 2. Materials and methods

A schematic view of the experimental apparatus used in this study is shown in Fig. 1. A smooth bearing steel ball of 25.4 mm diameter was pushed against a lubricated glass plate of 13 mm thickness with

semi-reflective layer of chromium by precise piezoelectric linear drive. The moving body mass was 0.2675 kg including the ball and associated movable part of apparatus. The behaviour of EHL film was recorded through a microscope by high-speed colour camera with image sampling frequency of 10 000 frames per second. As a light source, a xenon lamp of 1 kW performance was used. This adjustment allows capturing of very short term transient phenomena in EHL contacts. The method of thin film colorimetric interferometry (TFCI) was employed to determine film thickness up to 900 nm and film shape of lubricant. For more details about this method see Refs. [39,40].

The impact load of 125 N was applied after the initial central gap  $h_{ini}$  of 0.5 or 0.8  $\mu\text{m}$  was set. The initial gap was measured by TFCI before each test. However, it should be noted that the actual initial gap was slightly changed for lubricated contacts before starting the test due to poor stability of these contacts. The error of initial gap setup at 0.5 and 0.8  $\mu\text{m}$  was  $\pm 4\%$  and  $+2$  up to  $+11\%$ , respectively. Nevertheless, the differences in initial gaps do not influence the conclusions of the current study.

Fig. 2 shows the progress of loading process for dry contact where the dashed line encloses linear segments of load curves (LC) at load  $w$  of 110 N corresponding to the maximum Hertzian pressure of 0.8 GPa. Since the current paper investigates the effects of lineal loading on film thickness distribution, the final interferograms were captured for lubricated contact at this instantaneous load. The instantaneous load of 110 N was chosen with respect to better stability of overall dimple film shape than that in the case of final impact load of 125 N at which the film shape is more affected by oil leakage, especially in the peripheral area of the contact. For these reasons, the film thicknesses distributions caused by nonlinear sections of load curves above the

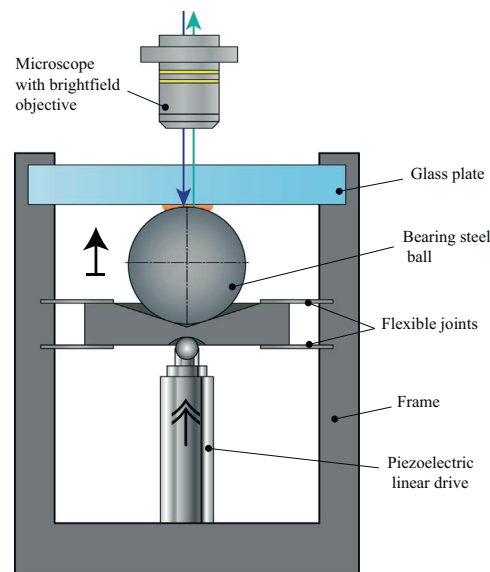


Fig. 1. Schematic representation of experimental apparatus.

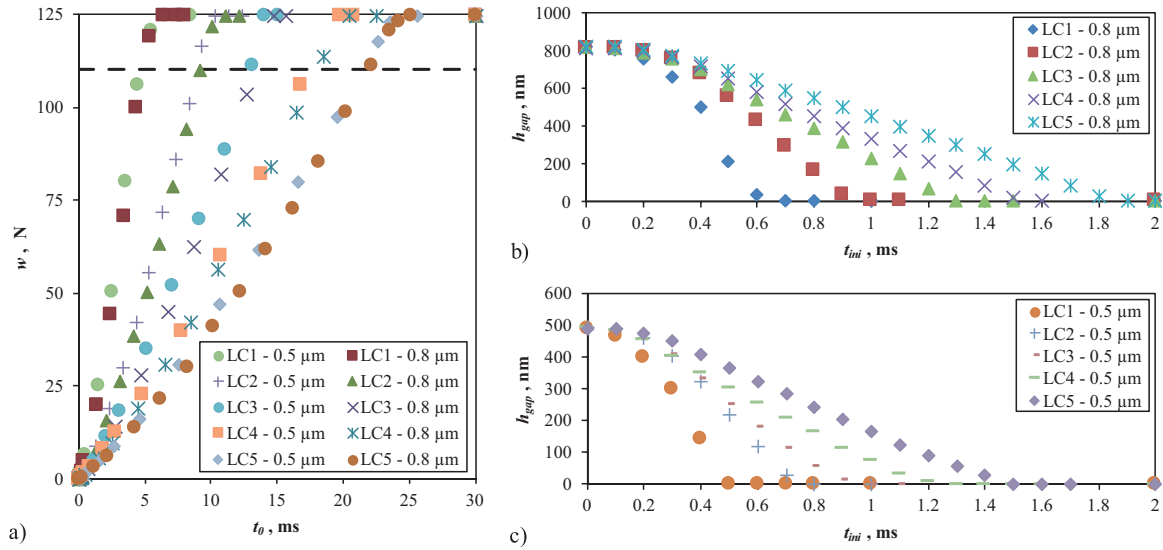


Fig. 2. Scatter charts of (a) impact load curves and of initial approach of contact surfaces for dry contact at (b)  $h_{ini}=0.8 \mu\text{m}$  and (c)  $h_{ini}=0.5 \mu\text{m}$ .

dashed line are not investigated in this study.

The progress of impact loading can be divided into two subsequent stages – the initial approach of contact bodies and the contact loading itself, which corresponds to the approach time  $t_{mi}$  and the impact time  $t_0$ , respectively. The values of instantaneous load were derived from the size of the contact diameter via the Hertz theory. However, the actual load during the initial approach could not be captured in this way. Please note that the progress of contact loading is almost identical for both initial gaps used. The initial approaching speed  $v_{mi}$  was obtained from linear sloped segments of the approach curves as a rate of change of gap between the contact surfaces with respect to time of approach. The loading speed  $v_F$  was determined in a similar manner. Determination of speeds does not take into account curved sections

Table 1  
Numerical details of loading processes.

Load curve	Initial gap ( $\mu\text{m}$ )	Approaching speed ( $\mu\text{m/ms}$ )	Loading speed (N/ms)	Approach time (ms)	Impact time (ms)	Time at 110 N (ms)
LC1	0.5	1.358	24.6	0.5	4.7	5.2
	0.8	2.170	22.9	0.6	4.8	5.4
LC2	0.5	0.948	14.0	0.7	8.9	9.6
	0.8	1.144	12.1	0.9	9.1	10.0
LC3	0.5	0.737	9.2	0.9	13.0	13.9
	0.8	0.783	8.3	1.3	13.3	14.6
LC4	0.5	0.489	6.5	1.2	17.4	18.6
	0.8	0.579	6.1	1.5	18.0	19.5
LC5	0.5	0.409	5.1	1.4	21.5	22.9
	0.8	0.473	5.0	1.8	22.0	23.8

Table 2  
Ambient viscosity, pressure-viscosity coefficient (PVC) and molecular weight of lubricants used at 25 °C.

Lubricant	GC	SQ	PAO 4	PAO 6	BS	CAS	DMPS	KTF-1	SR 90	SR 150	SR 600
Viscosity (Pa s)	1.01	0.025	0.023	0.046	0.903	0.75	1	0.062	0.032	0.056	0.245
PVC ( $\text{GPa}^{-1}$ )	5.4	22.3	11.9	11.1	22.67	14	15.2	34.8	21.9	22.8	24
Mol. wt. (g/mol)	92	423	437	529	$\approx 600$	927	$\approx 32\ 000$	$\approx 250$	$\approx 410$	$\approx 430$	$\approx 450$
Reference	[41,42]	[43]	[43,44]	[41]	<sup>1</sup>	[45,46]	[47,48]	[49,50]			

<sup>1</sup> values given by Kaneta and Sakamoto.

of curves, thus the speeds are higher than average speed values. As the maximum load was the same for all experiments, the loading speed can be adequately represented by the impact time as a part of overall time of the loading process. The overall time is considered as the time at load of 110 N. The above mentioned parameters of loading processes are listed in Table 1 for appropriate load curve and initial gap. It should be noted that the approaching speed becomes high as both the initial gap and the loading speed increase.

Since the squeeze effect and subsequently the oil entrapment introduced by normal approach are also substantially affected by lubricant rheology, the eleven different lubricants were employed in experiments. As the lubricant were used synthetic ester glycerol 99.5% (GC), paraffinic squalane 99% (SQ), two polyalphaolefins spectrasyn 4 (PAO 4) and spectrasyn 6 (PAO 6), mineral bright stock oil (BS), castor oil (CAS), silicone oil dimethylpolysiloxane (DMPS), traction fluid Nissan CVT (KTF-1) and three paraffinic mineral oils (SR 90, SR 150 and SR 600). Properties of lubricants are listed in Table 2. The experiments were conducted at ambient temperature of  $25 \pm 2 \text{ }^\circ\text{C}$ .

### 3. Results and discussion

#### 3.1. Impact film shape behaviour

Fig. 3 compares the mid-plane film profiles of mineral oil SR 600 received for the LC1 with the highest loading speed, and, in contrast with the profiles obtained for the LC5, with the lowest speed used in tests at initial gap of  $0.5 \mu\text{m}$ . The film profiles temporal evolution is shown from the impact beginning when the initial gap was settled until the final load of 110 N was reached. A very small reduction of film thickness occurs at the first illustrated time step of 0.2 ms for both types of LCs. This is given by nearly the same very early parts of LCs

(see Fig. 2) when the piezoelectric linear drive firstly overcomes the inertia of loading system of experimental apparatus and then the surface of ball starts to approach the lubricated surface of glass plate. As the contact surfaces are approaching each other, the viscosity of lubricant increases significantly due to pressure build-up, particularly in the central area of the contact. Here, the lubricant flow is more reduced in comparison with the peripheral contact area and the apex of dimple film shape appears at the end of the initial approach stage.

As the load grows during the loading stage, the contact area expands simultaneously with the formation of dimple film shape until the final load is reached. It can be concluded from Fig. 3 that, besides the above mentioned actual and final load, the amount of lubricant entrapped within the dimple also enlarges with increase in approaching speed and subsequently with loading speed. The mid-plane film profiles obtained for initial gap of 0.8 μm and for almost identical progress of contact loading are illustrated in Fig. 4 showing a similar tendency of impact film shape behaviour and lubricant entrapment as Fig. 3. However, the increase in initial gap results in deeper dimple. It is important to note that the time when the dimple film shape starts to be formed seems to be the same or very similar for identical LCs irrespective of the initial gap.

A direct comparison of film profiles for SR 600 given by three LCs at load of 110 N is shown in Fig. 5. It can be seen that the minimum film thicknesses of final film profiles are exactly the same with respect to LCs. Therefore, the minimum thickness is not affected by the initial gap under equivalent load but it is dependent on the progress of loading over time and its approaching and loading speeds. The position of minimum film thickness is slightly smaller than the Hertzian contact diameter. Fig. 5 also well illustrated the effect of approaching speed on the beginning of dimple formation, and subsequently on the amount of entrapped oil within the dimple. As was noted above, the start time of dimple formation is equal for corresponding LCs and unrelated to the

initial gap. Hence, for the same initial gap, when the initial approaching speed increases from LC5 to LC1, the time required to reach the apex of dimple film shape is reduced and thus the dimple occurs at a thicker residual film when approaching the contact surfaces. Moreover, the residual film is thicker for a larger initial gap.

This mechanism occurring at the end of the initial approach stage leads to the formation of deeper dimple followed by entrapment of larger amount of lubricant during the loading stage; this also naturally leads to higher central film thickness. However, for the conditions applied in the tests, the effect of approaching speed on central film thickness is stronger than the consequences of different initial gaps. This is obvious from Fig. 5 where the variation of central film thickness is the smallest for LC3 in comparison with other LCs because the LC3 has similar approaching speeds for different initial gaps unlike in other LCs where these speeds differ more. It should be noted that this behaviour of central film thickness does not follow the changes in loading speeds of LCs as in the case of approaching speeds. For example, the loading speeds of LC5 are very similar for both initial gaps used but the resulting central film thicknesses are distinctly various.

For lubricants with similar rheology, the shape of dimple is particularly determined by loading progress and loading speed during the loading stage of impact. In this study, nearly linear progress of loading process was used. Accordingly, the largest part of dimple side shape is straight as is highlighted in Fig. 5 by the trend line. It means that the film thickness decreases uniformly at the appropriate distance from the midpoint of circular contact up to the point where the film profile is influenced substantially by lubricant flow out of the contact due to low local viscosity.

The estimation of slope value of dimple side shape  $a_h$  was done for all film profiles at load of 110 N. It comes from approximately 100 middle points of film profile whereby each point corresponds to 1 μm of length dimension of contact. A number of points taken into estimation

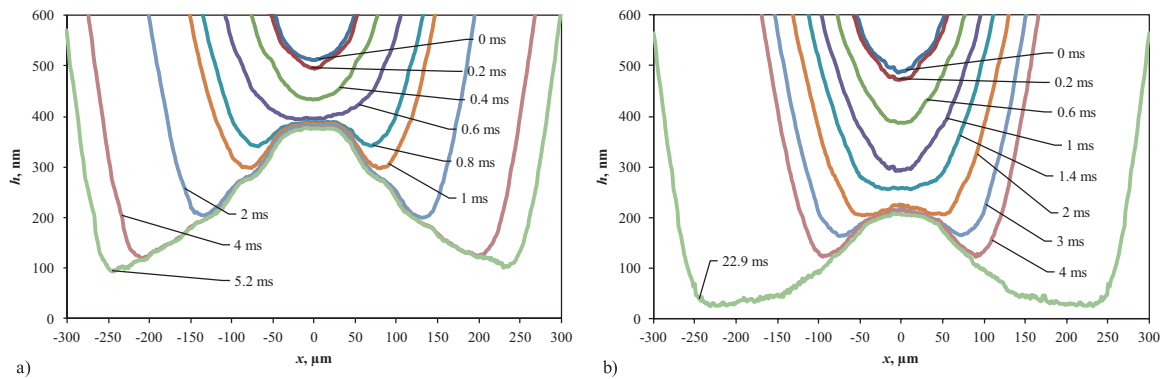


Fig. 3. Temporal evolution of the mid-plane film profiles of SR 600 lubricant at  $h_{0i}=0.5 \mu\text{m}$  for the load curve (a) LC1 and (b) LC5.

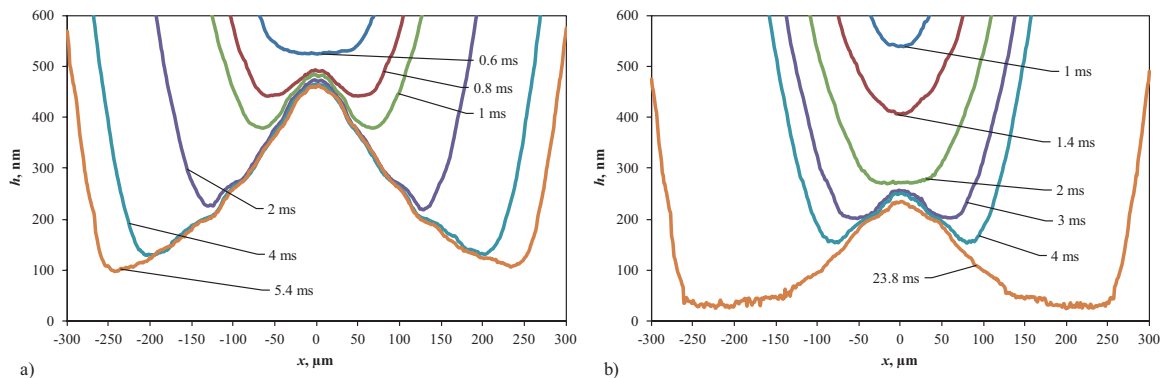


Fig. 4. Temporal evolution of the mid-plane film profiles of SR 600 lubricant at  $h_{0i}=0.8 \mu\text{m}$  for the load curve (a) LC1 and (b) LC5.

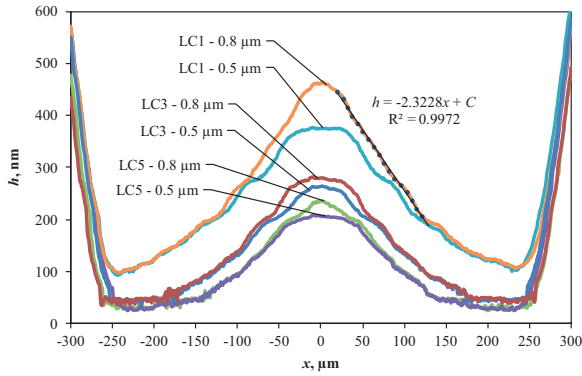


Fig. 5. Effect of initial gaps, approaching speeds and loading speeds of LCs on entrapped oil film thickness profiles for SR 600 lubricant at  $\omega=110$  N.

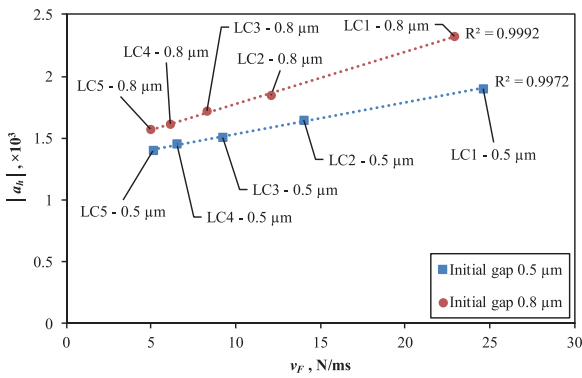


Fig. 6. Influence of loading speed and initial gap on the slope of dimple side shape for SR 600 lubricant at  $\omega=110$  N.

was extended from the middle of side curve of film profile, first in the direction of the top of dimple, then in the direction of the minimum thickness, until the coefficient of determination  $R^2$  for linear trend line got over the value of 0.99. If the value of  $R^2$  got under 0.99, which indicates the end of the straight part of the profile, just added points were excluded and the slope estimation was established.

Fig. 6 illustrates that the value of slope of the straight part of dimple side directly depends on loading speed and it is also predetermined by the initial gap, eventually by the approaching speed, from the introductory stage of impact loading. For low loading speeds, which are associated with low approaching speed, the rate of build-up of lubricant viscosity was likewise low. The lubricant could easily leak out from the contact area. As a result, the shape of dimple is flattened with low value of the slope, which is reflected in a small amount of entrapped lubricant. Conversely, the slope and the amount of entrapped lubricant were high due to a sharp increase in the viscosity of lubricant, which resulted from the LCs with high loading and approaching speed; a steeper shape of dimple was formed.

These findings can be also applied to non-linear progresses of loading where the loading speed is a simple function of time. For example, progressive loading with a low load rate at the beginning and a high load rate at the end of loading correspond to a dimple shape which is flattened near the centre of contact and becomes steep in the peripheral region of contact, and vice versa as for degressive loading. This suggestion is in good agreement with numerical results in [30].

### 3.2. Effect of rheology on film shape and thickness

Figs. 7 and 8 show the mid-plane film profiles of all eleven lubricants used in tests at actual load of 110 N under the LC1 and the LC5, respectively. Please note that the range of the film thickness axis of charts varies because of better clarity of film profiles. Generally,

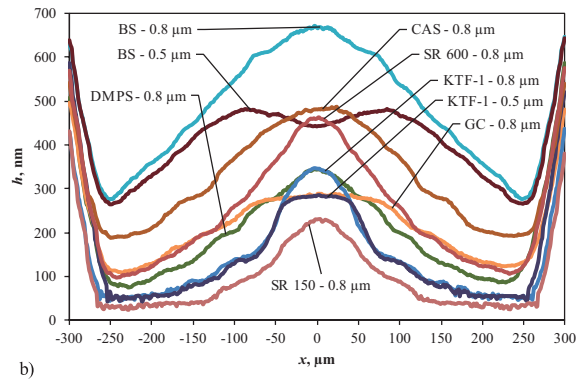
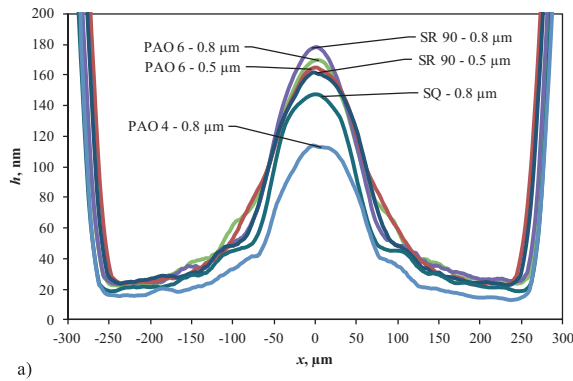


Fig. 7. Mid-plane film profiles of different lubricants with central film thickness (a) under 200 nm, (b) above 200 nm for load curve LC1 at  $\omega=110$  N.

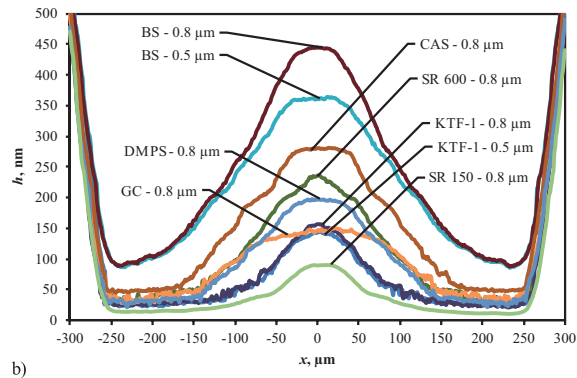
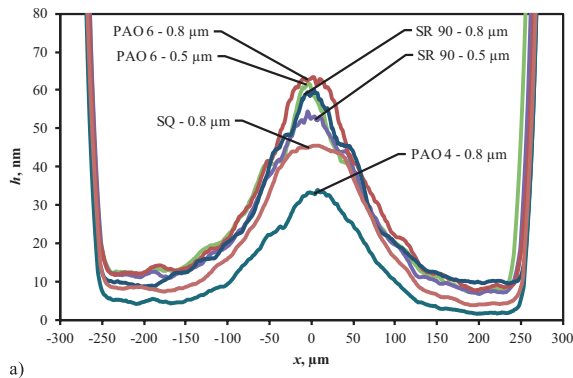


Fig. 8. Mid-plane film profiles of different lubricants with central film thickness (a) under 80 nm, (b) above 80 nm for load curve LC5 at  $\omega=110$  N.

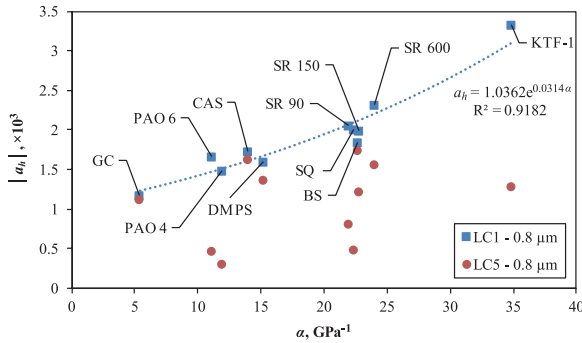


Fig. 9. Influence of PVC on slope of dimple side shape for each lubricant at  $w=110$  N.

the film profiles shape of most of other lubricants behaves in a similar manner as in the case of the SR 600 given above. By comparing of film profiles of SR 90, PAO 6, and KTF-1, for which both initial gaps were used, it is evident that the minimum film thicknesses of appropriate lubricants are again identical with respect to LCs and regardless of initial gap.

In terms of the rheological properties of lubricants listed in Table 2, the overall film thickness is particularly influenced by the ambient viscosity  $\eta_0$  (viscosity at ambient pressure), whereas the pressure-viscosity coefficient  $\alpha$  (PVC) is here less significant. The effect of ambient viscosity has been already pointed out for example by Kuwano et al. [5] and Larson and Lundberg [13]. The main importance of ambient viscosity is given during the initial approach stage of impact. Lubricants with lower viscosity can more easily escape from the decreasing gap between the contact surfaces due to less resistance of oil flow than those with high viscosity, and subsequently, the apex of dimple film shape is formed at lower residual film thickness.

In the second stage of impact, the PVC of lubricant can affect the slope of dimple side shape. Nevertheless, Fig. 9 shows that the influence of PVC on the slope is strongly predetermined by LCs used. For LCs with low rate of pressure increase due to low speeds, the influence of PVC is indistinct. When the approaching and loading speeds are sufficient, then the higher PVC of lubricant leads to a more concentrated dimple shape with the steeper sides of dimple. Conversely, the lubricants with low value of PVC produce a flattened dimple shape. The reason for this phenomenon of the dimple side shape formation in term of PVC is very similar to that for the loading speed. When the viscosity build-up is low due to low value of PVC then the flow of oil leaking out of the contact is more pronounced; this flow extends the shape of dimple during loading, thus the sides of dimple are more flattened and its slope is low, and vice versa for lubricants with high value of PVC. However, the increase in PVC does not result in significant enlargement of lubricant entrapment or overall film thickness unlike the increase in loading speed, which is associated with the initial approaching speed, or increase in ambient viscosity. Also, any

direct relationship has not been found between the slope at the side of dimple and the curvature at the top of dimple of corresponding film profile.

As can be seen in Fig. 7 and Fig. 8, the lubricants GC, DMPS and BS behave differently from the general trend of dimple formation described above. It is mainly given by their very specific rheology and molecular structure in comparison with other lubricants used. The common feature of GC, DMPS and BS is the high ambient viscosity about 1 Pa s. Despite the high viscosity, the GC and DMPS formed a thin film comparable to film thickness of the KTF-1 lubricant with significantly lower ambient viscosity. The GC is specific in very low value of both the PVC and the molecular weight of 92 g/mol, which caused a wide dimple with low thickness and flattened top due to oil leakage. On the other hand, the DMPS has high molecular weight, roughly of 32 000 g/mol, but it is strongly non-newtonian pseudoplastic fluid; this is probably the reason for the resulting low film thickness due to a drop in the apparent viscosity.

The behaviour of BS started to distinctly vary when a combination of low initial gap with high approaching speed was applied. For these conditions, the maximum film thickness occurred out of the centre of contact and deviated from the central film thickness, as is shown in Fig. 10. This specific local squeeze effect of BS lubricant was predicted and examined in previous papers [25–30]. The peripheral dimple was formed at the beginning of the loading stage of impact when the oil flow resistance in this region significantly increased. Based on the results of Ohno [51] and Kaneta [27], the BS can start being viscoelastic and get close to a solid-like state for present experimental conditions. However, almost all lubricants used seem to behave like a viscoelastic solid under present impact conditions and also a non-central dimple occurs usually rather for small initial impact gaps. Therefore, if the impact is applied under a zero impact gap, almost all oils used may show the non-central dimple. Since the BS gets easier close to a solid-like state compared to other lubricants used, the non-central dimple was formed and the minimum film thickness of BS started to vary for the same LCs and different initial gaps (see Fig. 7(b)) due to the formation of non-central dimple. This phenomenon has not been observed for the higher initial gap and LCs with low speeds where the maximum film thickness corresponds with the central film thickness. The dotted trend lines in Fig. 10(b) demonstrate that the dependence of central and maximum film thickness on the approaching speed can be approximated by power-law.

### 3.3. Development of central film thickness during impact

As was demonstrated above, the central film thickness is more affected by the change in approaching speed than by the change in initial gap over the range of test conditions used. The development of central film thickness during impact is shown in Fig. 11 for LC1 and LC5. At the beginning of impact, the central film thickness of most

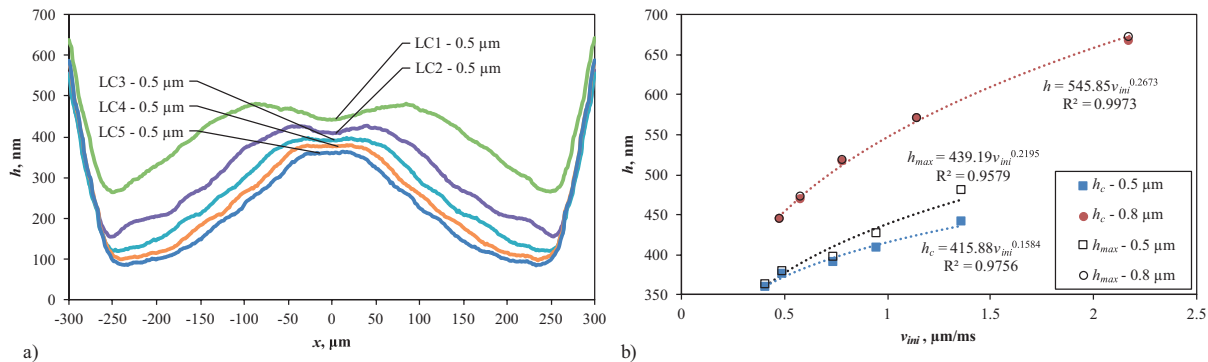


Fig. 10. (a) Effect of LCs on entrapped oil film thickness profile for BS lubricant at  $w=110$  N and  $h_{ini}=0.5$   $\mu\text{m}$ ; (b) effect of initial gaps and LCs on central  $h_c$  and maximum  $h_{max}$  film thickness of BS entrapped oil.

lubricants decreased rapidly. Then the dimple shape started to form and the central film thickness remained almost unchanged until the end of test. From the comparison of air gap  $h_{gap}$  decrease between the contact surfaces for dry contact (dashed curve) with drop in the thickness of lubricated contacts, it is clear that the squeezed films are strongly influenced by the speed of this approach. The initial time of dimple formation is very similar to the approach time  $t_{ini}$  of dry contact, especially for low-viscosity lubricants. The time required for central film thickness stabilization extends with the increase in viscosity. This observation can be explained by flow resistance which increases directly with apparent viscosity but it is reduced by the third power of film thickness ( $\eta/h^3$ ) [27]. High-viscosity lubricants produce a much thicker film in the periphery region of the contact (see the minimum film thicknesses in Fig. 7 and Fig. 8) and the reduction of this minimum film thickness during the impact also takes more time than in the case of lubricants with lower viscosity. Hence, the low-viscosity lubricants are entrapped within the central region of contact almost immediately and their central film thickness is stable, while the high-viscosity lubricants can leak out for some time after  $t_{ini}$  resulting in slow decrease in central film thickness during the impact loading. This observation agrees with the recent numerical solution [33] employing the Carreau shear-thinning viscosity model where low-viscosity lubricants exhibited rapidly collapsing EHL entrapment.

Furthermore, Fig. 12 illustrates that the initial speed of central film thickness reduction  $v_{hc}$  (determined in a similar manner as  $v_{ini}$  from Fig. 11) seems to be given by viscosity and independent of PVC for most of lubricants used (except for the GC, DMPS and BS whose behaviour is considerably different, as mentioned above). However, taking into account also the GC, DMPS and BS, the best fit of experimental data by power-law trend line is achieved for the product of lubricant viscosity and PVC where the quotient of index of viscosity and index of PVC is equal to 3 with average value of the coefficient of determination  $\overline{R^2}=0.889$ . This ratio of viscosity's and PVC's index demonstrates a general degree of influence of viscosity and PVC to  $v_{hc}$ .

### 3.4. Comparison with analytical results

The experimental results of central film thickness obtained at load of 110 N were compared with recent theoretical solution published by Venner et al. [38]. The common parameter for comparison of these two approaches was the impact time  $t_0$  which represents a combination of initial impact velocity, moving body mass, reduced radius of curvature and reduced elastic modulus. The impact time was obtained for dry contact via the analysis of progress of impact loading (see Table 1 and Fig. 2) in the current study and predicted by the Johnson dry impact analysis [52] in the case of Venner solution. The theoretical solution considers film thickness generated by a free impacting ball (excluding initial gap) and adopts the density-pressure relationship according to Dowson and Higginson [53] and the Roelands relations [54] as the viscosity-pressure relationship. The prediction of film thickness [38] is based on the Moes parameters (M, L) and it is intended for both

isoviscous and piezoviscous elastic lubrication.

The lubricants PAO 4, PAO 6 and GC reached the values of the L parameter below 1 for most conditions used in the experiments due to their low value of PVC. The low value of the L parameter suggests that the lubricant enters the piezoviscous regime later, which is reflected in a flattened top of dimple. This behaviour was observed only for the GC, whereas the dimple shape of polyalphaolefins was similar to the other low-viscosity lubricants, as is shown in Figs. 7 and 8. Fig. 13 shows that the theoretical solution (dashed/dotted lines) leads to an average of 32% thinner central film thickness in comparison with the measured data (symbols). It is probably caused by the absence of initial gap parameter in the analytical prediction and also by the results from Roleands viscosity-pressure relationship [55] used in the analysis which underestimates the increase in viscosity with pressure compared with Bair relationship [56], as was demonstrated in [29].

Besides the thicker film, the measured data also vary in the index  $n$  of power-law dependence of thickness on the impact time (corresponds to the slope of solid trend lines in log-log plot), while the index remains constant at  $-0.5125$  regardless of the lubricant for the theoretical solution. This disagreement in data trends apparently follows from the dry impact analysis [52] under which the impact time  $t_0$  is predicted because the impact times/speeds are also influenced by properties of lubricants and by their flow resistance, as was demonstrated in Fig. 11 and Fig. 12. The power index  $n$  derived from the measured data indicates how the central film thickness of particular lubricant is influenced by approaching or/and loading speed. In terms of this index, a good agreement between the measured and predicted data was obtained for the KTF-1 lubricant but, on the other hand, this lubricant differs in film thickness from the theoretical solution by more than 48% on average. For other lubricants, the index  $n$  ranged between  $-0.27$  for BS and  $-0.83$  for PAO 4 at  $h_{ini}=0.8\mu\text{m}$ .

Although Fig. 13 illustrates mainly how the index is obtained and contains only a few examples of the indices values for its better clarity, Fig. 14 is established on the values of indices of all lubricants and initial gaps used according to the adequate lubricant which is represented as

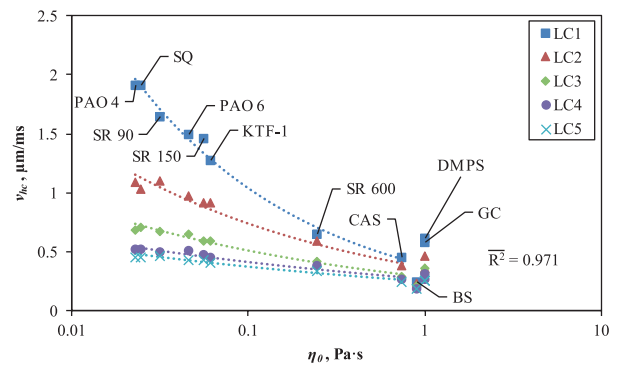


Fig. 12. Influence of lubricant viscosity and LCs on the initial speed of central film thickness reduction at  $h_{ini}=0.8\mu\text{m}$ .

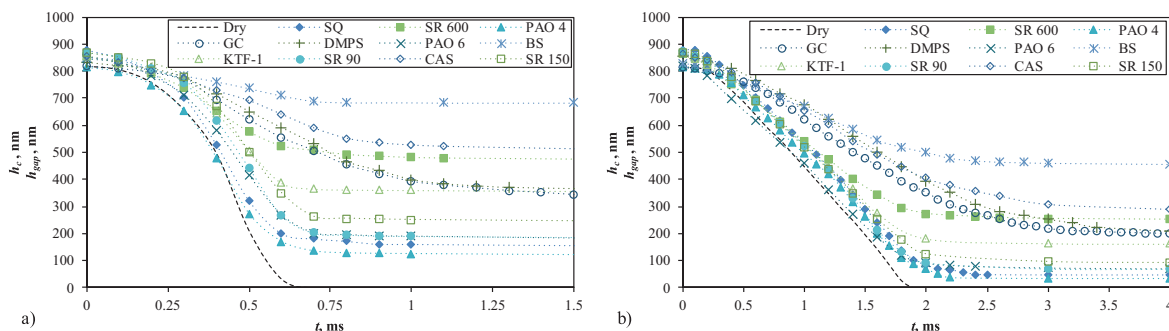


Fig. 11. Temporal evolution of central film thickness for lubricated contact (dotted line) and air gap between contact surfaces for dry contact (dashed line) at  $h_{ini}=0.8\mu\text{m}$  for the load curve (a) LC1 and (b) LC5.

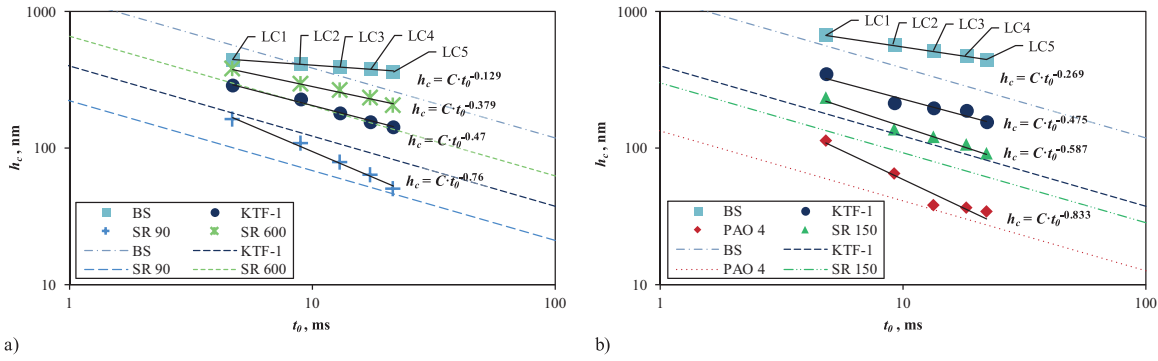


Fig. 13. Comparison of experimental (symbols) and analytical (dashed/dotted lines) results of central film thickness using solution by Venner et al. [38] obtained at  $w=110$  N and at (a)  $h_{im}=0.5 \mu\text{m}$  and (b)  $h_{im}=0.8 \mu\text{m}$ .

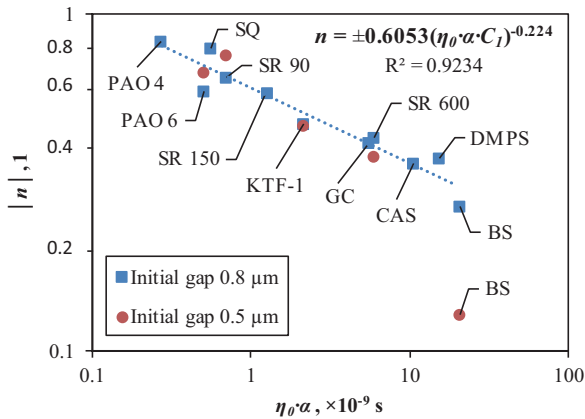


Fig. 14. Influence of rheological properties of lubricants on the index  $n$  in power-law relationship between central film thickness and impact time/speeds.

the product of its ambient viscosity multiplied by its PVC. Hence, it was found that the index itself can be estimated from basic rheological properties of lubricants, as is indicated in Fig. 14 by power-law trend line. This conclusion supports the findings of Ohno and Yamada [20] who showed that the entrapped film thickness at EHL halting motion is related to the product of the lubricant parameter  $\eta_0 \alpha$  and deceleration  $a$ . On the other hand, Martini and Bair [15] expressed their concern that the lubricant parameter  $\eta_0 \alpha$ , which is obtained at lower lubricant pressure/viscosity instead under pressure close to the glass transition, may result in predictions which contradict the actual behaviour of high-pressure applications. Nevertheless, it is often difficult to obtain high-pressure characteristics of lubricants and also the pressure used in the current measurements seems to be sufficient for this purpose.

Please note in Fig. 14 that the values of index  $n$  in the vertical axis are negative for thickness – impact time ( $h_c - t_0$ ) relationship and positive for both thickness – loading speed ( $h_c - v_f$ ) and thickness – initial approaching speed ( $h_c - v_{im}$ ) relationships. A unified expression of power-law index is given by the empirical formula  $n = \pm 0.6053 (\eta_0 \alpha C_1)^{-0.224}$ , where  $C_1 = 10^9 \text{s}^{-1}$  is used to obtain a dimensionless number in the formula. Also here is the effect of ambient viscosity more pronounced than in the case of PVC. If only the viscosity is used as a representing parameter of lubricants, the power-law index has the relation  $\pm 0.3361 (\eta_0 C_2)^{-0.201}$  with the value of the coefficient of determination  $R^2 = 0.835$ , whereas for PVC only as a representing parameter there was no clear trend found in the obtained data. The constant  $C_2 = 1 \text{Pa}^{-1} \text{s}^{-1}$  was used for the same purpose as  $C_1$ . It is obvious, based on the trend line in Fig. 14, that the resulting central film thickness of squeezed films is more affected by the change in both approaching and loading speeds for the lubricants with low value of the lubricant parameter  $\eta_0 \alpha$ , while the higher value of this parameter (typically for high-viscosity lubricants) leads to a greater stability of the

central film thickness relative to the impact speeds/times. Moreover, it seems that the index value is not significantly dependent on the initial gap, since the values of indices have been very similar for both initial gaps of appropriate lubricants used except for the BS at  $h_{im}=0.5 \mu\text{m}$ . This evident disagreement can be justified by formation of non-central dimple (see Fig. 10), which was discussed above.

#### 4. Conclusions

In this paper, the effects of initial impact gaps, initial approaching and loading speeds together with a wide variety of lubricants on EHL squeezed films have been examined experimentally by direct observations using the thin film colorimetric interferometry method. The main results obtained are summarized as follows:

1. The resulting central film thickness of squeezed films is mainly given by the approaching speed and lubricant viscosity at the end of the initial approach stage of impact process. At that moment, the central film thickness follows from instantaneous residual film thickness predetermined by initial impact gap and viscosity of lubricant, whereas the specific time of dimple film shape formation is given by initial approaching speed and is not affected by initial gap, loading speed, and PVC. This initial time of dimple formation is similar to the approach time of dry contact, especially for low-viscosity lubricants. During the initial stage of impact, the speed of central film thickness reduction seems to be given by viscosity and independent of PVC for most of lubricants used.
2. The dependences of central and maximum film thickness on the approaching speed can be approximated by power-law for both central and peripheral dimple film shape.
3. The minimum film thickness is dependent on the progress of loading over time and it is unaffected by the initial gap for particular lubricants over the range of test conditions. This foundation is not valid for the case of occurrence of non-central (peripheral) dimple.
4. A dimple film shape is formed during the loading stage of impact process. The slope of dimple sides directly depends on loading speed of loading progress and it is predetermined by the introductory stage of impact process. The slope is also influenced by PVC only if the approaching and loading speeds or the rate of viscosity build-up are sufficiently high. For linear loading, the film thickness decreases uniformly at the appropriate distance from the midpoint of circular contact up to the point where the film profile is influenced substantially by lubricant flow out of the contact due to low local viscosity.
5. The time required for stabilization of central film thickness extends with the increase in the ambient viscosity of lubricant in the course of the impact loading stage due to the lubricant flow resistance.
6. The experimental results showed a higher central film thickness and a different trend of thickness – impact time/speeds relationship in

comparison with recent theoretical solution published by Venner et al. [38].

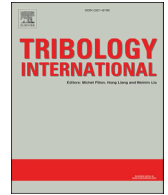
7. The influence of impact time/loading and initial approaching speeds on the resulting central film thickness can be estimated from basic rheological properties of the used lubricant via power-law dependence with the index expressed as  $\pm 0.6053(\eta_0\alpha)^{-0.224}$ . This estimation is only suitable for central dimple.
8. In general, for most of the results, an overall film thickness is particularly influenced by the ambient viscosity, whereas the PVC is less significant.

## Acknowledgement

This work was supported by the Czech Science Foundation (Project No. 14-31016S).

## References

- [1] H. Christensen, Oil film in a closing gap, *Proc R Soc Lond Ser-A* 266 (1962) 312–328.
- [2] D. Dowson, D.A. Jones, Lubricant entrapment between approaching elastic solids, *Nature* 214 (1967) 947–948.
- [3] H.D. Conway, Rate of change of film thickness in elastohydrodynamic squeeze film process, *J Lubric Tech-T Asme* 95 (1973) 391–393.
- [4] H.D. Conway, H.C. Lee, Impact of a lubricated surface by a sphere, *J Lubric Tech-T Asme* 97 (1975) 613–615.
- [5] N. Kuwano, N. Ohno, F. Hirano, Investigation on entrapment of mineral oils under impact, *J Jpn Soc Lubr Eng* 31 (1985) 477–484.
- [6] M.M.A. Safa, R. Gohar, Pressure distribution under a ball impacting a thin lubricant layer, *J Tribol-Trans Asme* 108 (1986) 372–376.
- [7] R. Larsson, E. Hoglund, Elastohydrodynamic lubrication at impact loading, *J Tribol-Trans Asme* 116 (1994) 770–776.
- [8] D. Dowson, D.C. Wang, An analysis of the normal bouncing of a solid elastic ball on an oily plate, *Wear* 179 (1994) 29–37.
- [9] R. Larsson, E. Hoglund, Numerical-simulation of a ball impacting and rebounding a lubricated surface, *J Tribol-Trans Asme* 117 (1995) 94–102.
- [10] H.M. Chu, W.L. Li, S.Y. Hu, Effects of couple stresses on pure squeeze EHL motion of circular contacts, *J Mech* 22 (2006) 77–84.
- [11] H.M. Chu, W.L. Li, M.D. Chen, Elastohydrodynamic lubrication of circular contacts at pure squeeze motion with non-Newtonian lubricants, *Tribol Int* 39 (2006) 897–905.
- [12] F. Guo, H. Nishikawa, P. Yang, M. Kaneta, EHL under cyclic squeeze motion, *Tribol Int* 40 (2007) 1–9.
- [13] R. Larsson, J. Lundberg, Study of lubricated impact using optical interferometry, *Wear* 190 (1995) 184–189.
- [14] H.-M. Chu, R.-T. Lee, Y.-C. Chiou, Study on pure squeeze elastohydrodynamic lubrication motion using optical interferometry and the inverse approach, *Proc Inst Mech Eng J: J Eng Tribol* 218 (2004) 503–512.
- [15] A. Martini, S. Bair, The role of fragility in EHL entrapment, *Tribol Int* 43 (2010) 277–282.
- [16] J. Sugimura, W.R. Jones, H.A. Spikes, EHD film thickness in non-steady state contacts, *J Tribol-Trans Asme* 120 (1998) 442–452.
- [17] R.P. Glovnea, H.A. Spikes, The influence of lubricant upon EHD film behavior during sudden halting of motion, *Tribol T* 43 (2000) 731–739.
- [18] R.P. Glovnea, H.A. Spikes, Elastohydrodynamic film collapse during rapid deceleration: part I – experimental results, *J Tribol-Trans Asme* 123 (2001) 254–261.
- [19] J. Sugimura, Elastohydrodynamic lubrication films in non-steady state conditions, *J Jpn Soc Tribol* 47 (2002) 752–757.
- [20] N. Ohno, S. Yamada, Effect of high-pressure rheology of lubricants upon entrapped oil film behaviour at halting elastohydrodynamic lubrication, *Proc Inst Mech Eng J-J Eng Tribology* 221 (2007) 279–285.
- [21] R.P. Glovnea, H.A. Spikes, Elastohydrodynamic film collapse during rapid deceleration: part II – theoretical analysis and comparison of theory and experiment, *J Tribol-Trans Asme* 123 (2001) 262–267.
- [22] M.J.A. Holmes, H.P. Evans, R.W. Snidle, Comparison of transient EHL calculations with shut-down experiments, *Tribol Res Des Eng Syst* 41 (2003) 91–99.
- [23] J.X. Zhao, F. Sadeghi, Analysis of EHL circular contact shut down, *J Tribol-Trans Asme* 125 (2003) 76–90.
- [24] H. Nishikawa, M. Kaneta, Traction in EHL under pure sliding reciprocation with cyclic impact loading, *JSME Int J Ser C-Dyn Control Robot Des Manuf* 38 (1995) 568–576.
- [25] M. Sakamoto, H. Nishikawa, M. Kaneta, Behaviour of point contact EHL films under pulsating loads, *Transient Process Tribol* 43 (2004) 391–399.
- [26] F. Guo, M. Kaneta, J. Wang, H. Nishikawa, P. Yang, Occurrence of a noncircular dimple in squeezing EHL contacts, *J Tribol-Trans Asme* 128 (2006) 632–640.
- [27] M. Kaneta, S. Ozaki, H. Nishikawa, F. Guo, Effects of impact loads on point contact elastohydrodynamic lubrication films, *Proc Inst Mech Eng J-J Eng Tribol* 221 (2007) 271–278.
- [28] H. Nishikawa, H. Miyazaki, M. Kaneta, F. Guo, Effects of two-stage impact load on point contact elastohydrodynamic lubrication films, *Proc Inst Mech Eng J-J Eng Tribol* 222 (2008) 807–814.
- [29] M. Kaneta, H. Nishikawa, M. Mizui, F. Guo, Impact elastohydrodynamics in point contacts, *Proc Inst Mech Eng J-J Eng Tribol* 225 (2011) 1–12.
- [30] M. Kaneta, J. Wang, F. Guo, I. Krupka, M. Hartl, Effects of loading process and contact shape on point impact elastohydrodynamics, *TribolTrans* 55 (2012) 772–781.
- [31] L.M. Chu, J.Y. Lai, C.H. Chien, W.L. Li, Effects of surface forces on pure squeeze thin film EHL motion of circular contacts, *Tribology Int* 43 (2010) 523–531.
- [32] L.M. Chu, J.R. Lin, Y.P. Chang, W.L. Li, Effects of surface forces and surface roughness on squeeze thin film of elastohydrodynamic lubricated spherical conjunction, *Lubr Sci* 25 (2013) 11–28.
- [33] P. Kumar, T.J. Kalita, Transient elastohydrodynamic lubrication film thickness during normal approach considering shear-thinning and linear piezoviscous oils, *J Tribol-Trans Asme* 137 (2015) 021504–021507.
- [34] L.M. Chu, Y.P. Chang, J.J. Sheu, Elastohydrodynamic lubrication of circular contacts at pure squeeze motion involving the mixture of two lubricants, *J Mar Sci Technol-Taiwan* 23 (2015) 516–522.
- [35] C.J. Hooke, G.E. Morales-Espejel, The effects of small sinusoidal load variations in elastohydrodynamic line contacts, *J Tribol-Trans Asme* 138 (2016) 031501–031509.
- [36] Y.Y. Zhang, H.J. Liu, C.C. Zhu, M.Y. Liu, C.S. Song, Oil film stiffness and damping in an elastohydrodynamic lubrication line contact-vibration, *J Mech Sci Technol* 30 (2016) 3031–3039.
- [37] J. Wang, C.H. Venner, A.A. Lubrecht, Central film thickness prediction for line contacts under pure impact, *Tribol Int* 66 (2013) 203–207.
- [38] C.H. Venner, J. Wang, A.A. Lubrecht, Central film thickness in EHL point contacts under pure impact revisited, *Tribol Int* 100 (2016) 1–6.
- [39] M. Hartl, I. Krupka, M. Liska, Elastohydrodynamic film thickness mapping by computer differential colorimetry, *Tribol T* 42 (1999) 361–368.
- [40] M. Hartl, I. Krupka, R. Poliscuk, M. Liska, J. Molimard, M. Querry, et al., Thin film colorimetric interferometry, *Tribol T* 44 (2001) 270–276.
- [41] N. Ohno, M. Rahman, H. Tsutsumi, High-pressure short time behavior of traction fluids, *Lubr Sci* 18 (2006) 25–36.
- [42] W. Habchi, D. Eyheramendy, S. Bair, P. Vergne, G. Morales-Espejel, Thermal elastohydrodynamic lubrication of point contacts using a Newtonian/generalized newtonian lubricant, *Tribol Lett* 30 (2008) 41–52.
- [43] S. Bair, F. Qureshi, The high pressure rheology of polymer-oil solutions, *Tribol Int* 36 (2003) 637–645.
- [44] S. Bair, F. Qureshi, Accurate measurements of pressure-viscosity behavior in lubricants, *Tribol T* 45 (2002) 390–396.
- [45] T. Hiemstra, S. Mia, P.B. Duhaut, B. Molleman, Natural and pyrogenic humic acids at goethite and natural oxide surfaces interacting with phosphate, *Environ Sci Technol* 47 (2013) 9182–9189.
- [46] T. Mawatari, R. Fukuda, H. Mori, S. Mia, N. Ohno, High pressure rheology of environmentally friendly vegetable oils, *Tribology Lett* 51 (2013) 273–280.
- [47] P.A. Kottke, S.S. Bair, W.O. Winer, The measurement of viscosity of liquids under tension, *J Tribol-Trans Asme* 125 (2003) 260–266.
- [48] T. Zolper, Z. Li, C. Chen, M. Jungk, T. Marks, Y.-W. Chung, et al., Lubrication properties of polyalphaolefin and polysiloxane lubricants: molecular structure-tribology relationships, *Tribol Lett* 48 (2012) 355–365.
- [49] N. Ohno, High-pressure behavior of toroidal CVT fluid for automobile, *Tribol Int* 40 (2007) 233–238.
- [50] S. Bair, J. Jarzynski, W.O. Winer, The temperature, pressure and time dependence of lubricant viscosity, *Tribol Int* 34 (2001) 461–468.
- [51] N. Ohno, N. Kuwano, F. Hirano, Diagrams for estimation of the solidified film thickness at high pressure EHD contacts, *Tribol Ser* 27 (1994) 507–518.
- [52] K.L. Johnson, *Contact mechanics*, Cambridge University Press, Cambridge, 1985.
- [53] D. Dowson, G.R. Higginson, *Elasto-hydrodynamic lubrication: the fundamentals of roller and gear lubrication*, Pergamon Press, 1966.
- [54] C.J.A. Roelands, Correlational aspects of the viscosity-temperature-pressure relationship of lubricating oils [Ph.D thesis], Technische Hogeschool Delft, Netherlands, 1966.
- [55] C.J.A. Roelands, J.C. Vlughter, H.I. Waterman, The viscosity-temperature-pressure relationship of lubricating oils and its correlation with chemical constitution, *J Basic Eng* 85 (1963) 601–607.
- [56] S. Bair, Measurements of real non-Newtonian response for liquid lubricants under moderate pressures, *Proc Inst Mech Eng J-J Eng Tribol* 215 (2001) 223–233.



## Effects of lateral harmonic vibrations on film thickness in EHL point contacts



Josef Fryza<sup>\*</sup>, Petr Sperka, Ivan Krupka, Martin Hartl

Faculty of Mechanical Engineering, Brno University of Technology, Technická 2896/2, 61669 Brno, Czech Republic

### ARTICLE INFO

#### Keywords:

Elastohydrodynamic lubrication  
Non-steady state film thickness  
Micro-oscillations  
Lubricants

### ABSTRACT

Vibrations are an integral part of machine operation and affect every elastohydrodynamically lubricated conjunctions. In the present experimental study, a rolling contact is subjected to lateral-sliding vibrations with short stroke length. Film thickness behaviour is investigated under diverse conditions including rolling speeds, stroke lengths, frequencies, loads, and variety of lubricants. The results obtained under vibrations are compared with the results for corresponding steady state conditions to determine the effects of vibrations. It is shown that the lubricant rheology and the ratio of main and lateral entrainment speed are crucial parameters where the influence of this ratio on relative film thickness and its deviations can be estimated by exponential functions uniformly for all lubricants. The thresholds for film failures were found.

### 1. Introduction

Since the elastohydrodynamic lubrication (EHL) theory was established in 1945 by Ertel (see Ref. [1]), there has been one common aim of all tribology researchers in this field of study; i.e. to advance the theory closer to actual operating conditions of machines. However, this issue is very complex consisting of subdivisions, which deal with rheology and traction, thermal phenomena, surface topography and wear, or non-steady state conditions and other factors affecting lubricated contacts in machines. To distinguish individual effects of various factors, it is appropriate to address these challenges separately. Nowadays, accurate predictions of film thickness, and even friction, are a matter of routine for EHL contacts under steady state conditions. Nevertheless, machine contacts do not work under time-independent conditions. Particularly, the speeds and loads of contact surfaces and, consequently, other related factors may vary over time if ubiquitous vibrations are taken into account. Thus, film thicknesses and frictions estimated in terms of these widely used and unmodified predictions can be very different from the reality depending on the rate of vibrations.

A typical machine element, which is subjected to vibrations, is a rolling bearing. Almost every machine contains it, but nearly half of failed bearings fail because of a breakdown in the lubrication film and another one-third of them fail as a result of an improper mounting. If the common size of bearing and the usual shaft speed are employed, a rolling element frequency over 200 Hz is obtained. This frequency and the internal clearance represent the possible vibratory motions excited by the operation of single bearing. The resulting sliding movements of the

rolling elements are additionally accompanied by vibrations at different frequencies, which are transferred from other parts of the machine into the element-raceway contact. Micro-oscillations are also characteristic for bearings, where the stroke ratio  $S/D$  is lower than one.  $S/D$  is the ratio between the stroke length of rolling element  $s$  due to vibrations and the axis length of contact ellipse (or the diameter of Hertzian contact area)  $d$  in the direction of vibrations. To provide real-time simulations of bearings performance, several papers have been focused on dynamic models of rolling bearings and their parts without [2–7] or with [8–11] considering the EHL theory.

An arrangement of locating (preloaded) and floating (end play) bearings is frequently used. When a movement of rolling elements is limited or prevented in tangential direction on account of axial preloading, these elements tend to move in normal direction in response to vibrations affecting the contact load together with lubricant squeezing/damping action. Nevertheless, a certain internal clearance is retained to ensure low heating and a minimum friction torque in most operations of rolling bearings. Consequently, a film of lubricant is exposed to both impacts of vibrations at the same time, the sliding movements of contact surfaces and the fast changes in load. On the other hand, these simultaneous effects are less pronounced compared to the occurrence of a single effect. This applies not only to bearings, but also to other EHL contacts of machine elements exposed to vibrations and operating in oscillatory or intermittent duty applications, such as gears or cam mechanisms. These non-steady state conditions could be one of the reasons for EHL film failure and they often lead to excessive wear (fretting, false brinelling) and a shorter lifetime of machine elements [12,13].

<sup>\*</sup> Corresponding author.

E-mail address: [fryza@fme.vutbr.cz](mailto:fryza@fme.vutbr.cz) (J. Fryza).

Nomenclature	
$a_e'$	time-dependent entrainment acceleration, $a_e' = \partial u_e' / \partial t$
$a_{ey}'$	time-dependent entrainment acceleration in the lateral-sliding direction, $a_{ey}' = \pi^2 s f^2 \cos(2\pi f t)$
$\overline{a_{ey}}$	mean value of time-dependent entrainment acceleration in the lateral-sliding direction over time step
$A, B, C$	general nonzero parameters
$d$	diameter of Hertzian contact area
$d_p$	diameter of path of contact on the disc
$f$	frequency
$h_c$	central film thickness
$h_{c,max}$	maximum value of film thickness from film profile within the central area of the contact
$h_{c,mean}$	mean value of film thickness from film profile within the central area of the contact
$h_{c,min}$	minimum value of film thickness from film profile within the central area of the contact
$h_{c,ref}$	reference (central) film thickness
$H_{dev}$	relative overall deviation of central film thickness, $H_{dev} = \Delta h_c / h_{c,mean}$
$H_{dev}^{(+)}$	relative positive deviation of central film thickness, $H_{dev}^{(+)} = \Delta h_c^{(+)} / h_{c,mean}$
$H_{dev}^{(-)}$	relative negative deviation of central film thickness, $H_{dev}^{(-)} = \Delta h_c^{(-)} / h_{c,mean}$
$H_{mean}$	relative mean value of central film thickness, $H_{mean} = h_{c,mean} / h_{c,ref}$
$p_{00}$	polynomial coefficient
$p_h$	maximum Hertzian pressure
$R^2$	coefficient of determination
$s$	stroke length
$S/D$	stroke ratio, $S/D = s/d$
$t$	time
$u_b$	surface velocity of ball at the point of EHL contact
$u_{bx}$	speed of ball in the main rolling direction
$u_{by}'$	time-dependent speed of ball in the lateral-sliding direction, $u_{by}' = \pi s f \sin(2\pi f t)$
$u_d$	surface velocity of disc at the point of EHL contact
$u_{dx}$	speed of disc in the main rolling direction, $u_{dx} \cong u_d$
$u_e'$	time-dependent entrainment speed, $u_e' =  u_{by}'/2  \sqrt{1 + (2u_{ex}/u_{by})^2}$
$u_e'_{max}$	maximum value of time-dependent entrainment speed over stroke
$u_e'_{mean}$	mean value of time-dependent entrainment speed over stroke
$u_{ex}$	entrainment speed in the main rolling direction, $u_{ex} = (u_{dx} + u_{bx})/2$
$u_{ey}'$	time-dependent entrainment speed in the lateral-sliding direction, $u_{ey}' = u_{by}'/2$
$\overline{u_{ey}}$	mean value of time-dependent entrainment speed in the lateral-sliding direction over time step
$u_{ey}'_{max}$	maximum value of time-dependent entrainment speed in the lateral-sliding direction over stroke
$ u_{ey}' _{max}$	maximum of absolute values of time-dependent lateral entrainment speed over one cycle of motion
$u_s'$	time-dependent sliding speed, $u_s' =  u_{by}'  \sqrt{1 + (u_{sx}/u_{by})^2}$
$u_{sx}$	sliding speed in the main rolling direction, $u_{sx} = u_{dx} - u_{bx}$
$U_{y/x}$	entrainment speeds ratio (rate of lateral vibrations), $U_{y/x} =  u_{ey}' _{mean} / u_{ex}$
$x$	position in the main rolling direction of contact
$\overline{x}$	position in the direction represented by the median of $\delta$ angle achieved during the half-stroke
$x_i, x_{(i-1)}$	estimated set of positions in the main rolling direction, $x_i = x_{(i-1)} - \overline{u_{ex}} \Delta t$
$y$	position in the lateral-sliding direction of contact
$y_i, y_{(i-1)}$	estimated set of positions in the lateral-sliding direction, $y_i = y_{(i-1)} - \overline{u_{ey}} \Delta t - 0.5 \overline{a_{ey}} \Delta t^2$
$\delta$	time-dependent angle (direction) of entrainment velocity, $\delta = \tan^{-1}  u_{by}' / (2u_{ex}) $
$\Delta h_c$	maximum (overall) fluctuation of central film thickness, $\Delta h_c = h_{c,max} - h_{c,min}$
$\Delta h_c^{(+)}$	positive deviation of central film thickness, $\Delta h_c^{(+)} = h_{c,max} - h_{c,mean}$
$\Delta h_c^{(-)}$	negative deviation of central film thickness, $\Delta h_c^{(-)} = h_{c,mean} - h_{c,min}$
$\Delta t$	time step
$\epsilon'$	time-dependent angle between entrainment and sliding velocity, $\epsilon' = \delta - \tan^{-1} (u_{sx} /  u_{by}' ) + 90^\circ$
$\Sigma$	slide-to-roll ratio, $\Sigma = u_{sx} / u_{ex}$
$\Sigma'$	time-dependent value of slide-to-roll ratio, $\Sigma' = (u_s' \cos \epsilon') / u_e'$
$\Sigma'_{max}$	maximum value of time-dependent slide-to-roll ratio over stroke
$\Sigma'_{mean}$	mean value of time-dependent slide-to-roll ratio over stroke
$\omega_b$	angular speed of ball
$\omega_d$	angular speed of disc

Scientists began to deal with influences of non-steady state operating conditions on the EHL film behaviour during 1960s. At that time, Christensen published his pioneer theoretical work [14] focused on the phenomena associated with the impact loading of lubricated contact. Many of the following authors [15–20] proved that the lubricant is entrapped between the surfaces under specific pressure distribution and the so-called dimple film shape is formed. Afterwards, the lubricant entrapment was also observed in experimental studies investigating sudden halting or rapid deceleration of motion [21,22], and reciprocation [23–25]. As Kaneta et al. [26] pointed out for applications of stepper motors, a crescent-shaped entrapped film can be formed in the case of sudden start-up of motion and a slip within EHL contact may occur at or very close to the lubricant-surface interface for thin films. This

phenomenon (referred to as a wall-slip or boundary-slip) is often associated with the hypotheses of limiting shear stress [27] and plug flow [28,29] of solid-like lubricant. These phenomena are still the subject of discussions and are conditioned by the presence of sliding motions, which are typical for non-steady state operating conditions. Results similar to [26] were likewise achieved under pure rolling and pure sliding reciprocation [30].

Sugimura and Spikes [31,32] demonstrated the deviations of central film thickness under accelerated/decelerated motion in comparison with a film thickness under relevant steady state conditions in terms of speeds. Interesting different phases of formation [33] and collapse [34,35] of EHL film were distinguished during the controlled start-up and halt of motion, respectively. The courses of these phases were predetermined

mainly by applied acceleration and lubricant rheology. Glovnea and Spikes further showed that the central film thickness can be considerably affected by a fluctuation of the entrainment speed depending also on the rheological properties of lubricants [36].

The experimental evidence of lubricant entrapment under reciprocation was given by direct observation in Ref. [37]. The entrapped lubricant ensured the load-carrying capacity of contact at the ends of stroke despite the zero entrainment speed at which the EHL film failure is predicted. However, the film thickness of entrapped oil was substantially affected by the stroke length and the frequency. For short strokes and high frequencies, the air bubbles, produced from the previous stroke, reduced the film formation at contact inlet causing film failure, especially in combination with surface irregularities enhancing a lubricant leakage [38]. However, the behaviour in the areas affected by air bubbles is very difficult to predict [39–42]. In addition, a certain minimum value of  $S/D$  ratio is necessary for the separation of contact surfaces by lubricant over the whole stroke of pure sliding reciprocation, as was published in Ref. [43]. Moreover, it was discussed in Ref. [44] that a high-pressure spike occurs in the contact with entrapped lubricant when the contact starts to move after a previous stop of motion.

The aforesaid publications have dealt mostly with dynamic motions acting in the main rolling/sliding or in the normal direction of contact and helped to bring an insight into phenomena under the non-steady state conditions. Unfortunately, only a very few studies considered the lateral vibrations as additional - secondary motions acting simultaneously with the main movement in tangential directions, similarly as in the case of rolling bearings and other EHL contacts. Both the replenishment and the degree of starvation of grease-lubricated contact were investigated under conditions of lateral harmonic vibrations [45]. When the film thickness in a starved contact was fully recovered because of the vibrations, it was concluded that the vibrations can be important for lubricant replenishment and can thus help to prevent starvation. On the other hand, an unrealistically large  $S/D$  ratio exceeding 1 and low frequency of vibrations were applied in Ref. [45]. The full recovery of film thickness was not acquired for  $S/D < 1$  [46], although a degree of starvation was not being increased over time. Moreover, crescent-shaped film thickness fluctuations were obtained for combination of low rolling speed and frequency of 100 Hz depending on the lubricant rheology.

It is obvious that knowledge in this field of research remains rather limited. Additionally, the occurrence of vibrations is unjustly neglected, even though they can have a significant impact on the performance of actual EHL contacts, and not only on these lubricated by greases. Substantial effects of lubricant rheology, acceleration, ratio of main rolling and lateral speed,  $S/D$  ratio, etc., have not been fully explained considering formation, distribution, and failure of EHL films under transient operating conditions, particularly in the case of lateral vibrations. For clarification of the phenomena occurring under such conditions, more extensive parametric studies are necessary. Accordingly, in this paper, the film thickness behaviour within a point EHL contact is investigated experimentally under diverse conditions including a variety of lubricants, loads, main rolling speeds, and lateral-sliding harmonic motions at low values of stroke ratio  $S/D < 1$  (relative stroke lengths) and frequencies up to 300 Hz. The results obtained under lateral vibrations are compared with the results for appropriate steady state conditions to determine the effect of lateral vibrations.

## 2. Materials and methods

### 2.1. Experimental set-up

The experimental apparatus, employed in this study for film thickness measurements, was a ball-on-disc optical tribometer. An EHL film was formed in the point contact between a smooth bearing steel (100Cr6) ball of 25.4 mm diameter and a flat glass (BK7) disc coated with a semi-reflective layer of chromium. Both the ball and the disc are driven separately by close-loop servo drives allowing to achieve various

combinations of rolling and sliding in the main direction of contact. Moreover, the ball can perform a pure sliding harmonic motion in the direction perpendicular to the main rolling/sliding direction of point EHL contact. These simulated lateral-sliding vibrations are excited by a high-speed DC motor via a simple cam mechanism. Frequency  $f$  and stroke length  $s$  of harmonic motion were measured each 0.1 ms by a capacitive displacement transducer with a resolution under 0.02  $\mu\text{m}$ . An observance of sinewave stroke was determined by mean value of the coefficient of determination (R-squared) of 0.9986. A lubricant temperature was controlled by means of PID loop where the temperature was measured by a thermocouple close to the contact inlet. A lubricant was tempered using heaters located in an oil cup. A schematic view of the experimental apparatus is shown in Fig. 1. A film thickness distribution was recorded through a microscope by a high-speed CMOS camera. A sampling rate of camera was fixed at 10 000 Hz and a 1 kW xenon lamp was used as a light source. This adjustment allows to apply an exposure time of 40  $\mu\text{s}$  for capturing of short-term transient phenomena in the EHL contact without significant motion blur regarding to used speeds. A thin film colorimetric interferometry technique (TFCI) [47,48] was employed for evaluation of the film thickness and the film shape of lubricant passing through the contact. The film thickness resolution of this technique is greater than 1 nm.

### 2.2. Kinematic analysis of contact conditions

Fig. 2 represents the movement of EHL contact and the contact kinematics in terms of surface velocities acting within the rolling/sliding contact considering a lateral-sliding motion. For common ball-on-disc simulators without the presence of lateral motions, a path of contact on the disc is circular of diameter  $d_p$  and all velocities are concentrated only in one direction of contact. In the present article, this direction is referred to as the main rolling direction of contact  $x$ . The velocities in the  $x$  direction are controlled by constant angular speeds of the ball  $\omega_b$  and the disc  $\omega_d$  relative to the radius of the ball and the radius of the circular path on the disc. The relationship and the ratio between the surface velocities of the ball  $u_b$  and the disc  $u_d$  determine the entrainment speed (also called the mean speed)  $u_{ex} = (u_{dx} + u_{bx})/2$ , the sliding speed  $u_{sx} = u_{dx} - u_{bx}$  and also the slide-to-roll ratio (SRR)  $\Sigma = u_{sx}/u_{ex}$ . The negative value of  $\Sigma$  indicates that the ball speed is greater than the disc speed and vice versa for the positive value of  $\Sigma$ . Along with the velocities applied in  $x$  direction, the contact was subjected to sliding harmonic reciprocation of the ball in the lateral direction of contact  $y$  changing the contact conditions from the steady state to the non-steady state. The lateral-sliding direction  $y$  coincides with the axis of ball rotation.

It should be noted that the surface speed of the disc  $u_{dx}$  varies at the point of the contact over reciprocation cycles as the contact moves towards or away from the centre of the disc rotation due to the lateral reciprocation of the ball. Nevertheless, these speed variations are negligible for the conditions applied in the current study, since only small stroke lengths (relative to the diameter of contact path) and constant angular speeds of disc  $\omega_d$  are used in the individual tests. For this reason, the surface speed of the disc, unlike the surface speed of the ball, is assumed to be in steady state, where  $u_{dx} \cong u_d$ . The instantaneous ball speed in  $y$  direction is defined by the equation  $u_{by}' = \pi s f \sin(2\pi f t)$ . All related time-dependent values (indicated by the apostrophe) of speeds, the angles between the vectors and SRR can be expressed as follows:

$$u_e' = \left| \frac{u_{by}'}{2} \right| \sqrt{1 + \left( \frac{2u_{ex}}{u_{by}'} \right)^2}, u_{by}' = 0 \Rightarrow u_e' = u_{ex} \quad (1)$$

$$u_s' = |u_{by}'| \sqrt{1 + \left( \frac{u_{sx}}{u_{by}'} \right)^2}, u_{by}' = 0 \Rightarrow u_s' = u_{sx} \quad (2)$$

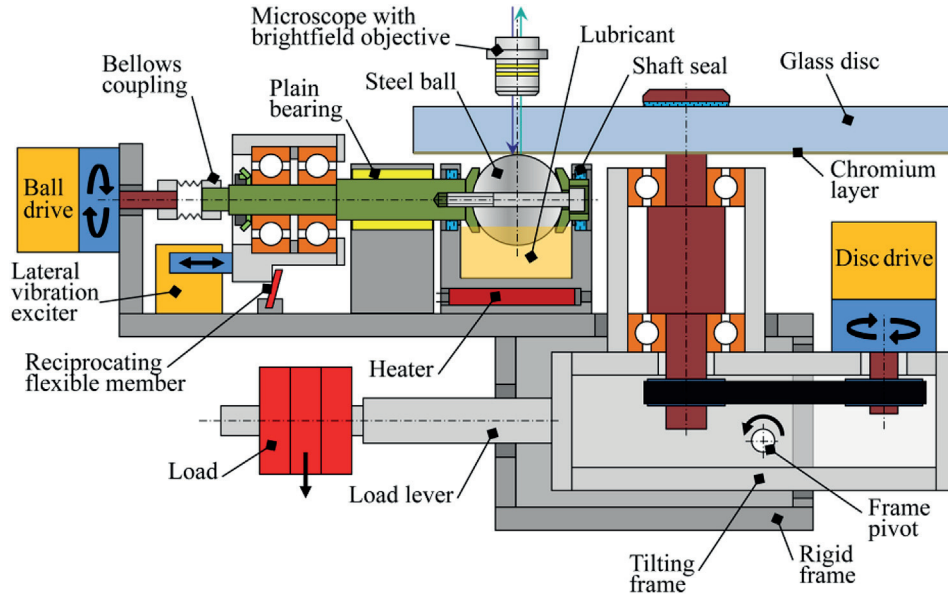


Fig. 1. Schematic representation of experimental apparatus.

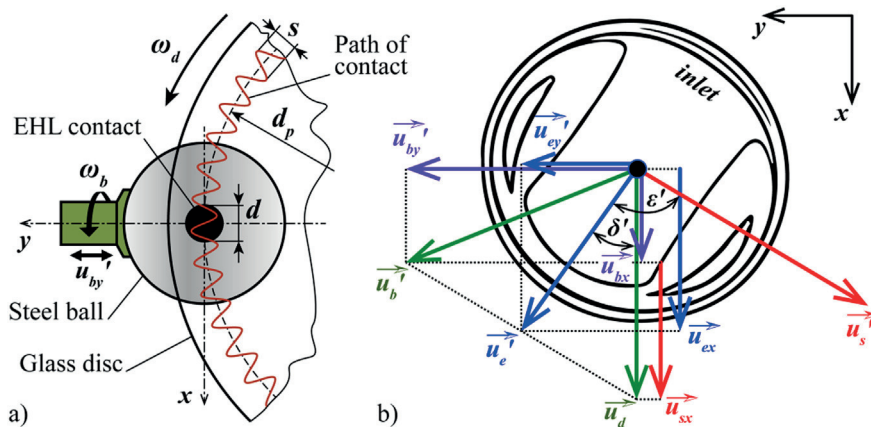


Fig. 2. Movement of EHL contact (a) and velocities within rolling/sliding EHL contact (b) under lateral-sliding motion.

$$\delta' = \tan^{-1} \left| \frac{u_{by'}}{2u_{ex}} \right|, u_{ex} = 0 \Rightarrow \delta' = 0 \quad (3)$$

$$\epsilon' = \delta' - \tan^{-1} \left( \frac{u_{sx}}{|u_{by'}|} \right) + 90^\circ, u_{by'} = 0 \Rightarrow \epsilon' = 0 \quad (4)$$

$$\Sigma' = \frac{u_s \cos \epsilon'}{u_e} \quad (5)$$

The instantaneous value of slide-to-roll ratio  $\Sigma'$  is assumed as a ratio of sliding speed  $u_s'$  and entrainment speed  $u_e'$  in the direction of entrainment speed. The relationships (1) to (5) are used for direct comparison of steady state and non-steady state conditions via the entrainment and sliding speeds.

### 2.3. Experimental liquids

Five liquid lubricants were employed in the experiments of this investigation. First, a mixture of mineral base oil SN650 and 15 wt% of polyisoprene (PIP) was used for the clarification of lubricant passage

through the contact and its film thickness distribution at the oil temperature of 30 °C. This solution represents gear and engine oils, where a film thickness should be affected by a shear thinning at the inlet of contact due to a high molecular weight of PIP [49]. The following four lubricants were used as the reference liquids for a quantitative evaluation of the central film thicknesses possessed by the lateral vibrations at a temperature of 40 °C: a castor oil (CAS) as a representative of engine biodegradable oils whose characteristics are largely similar to synthetic ester oils exhibiting Newtonian behaviour; a high-viscosity mineral base oil R560/88; a mixture of 15 wt% of PIP and paraffinic squalane (SQ; low-molecular-weight alkane) that represents multigrade oils; and finally, a high-molecular-weight polyglycol (PGLY). In the case of non-Newtonian PGLY, a sliding motion should have a considerable impact on the film thickness. For more detailed rheological description of the last two mentioned lubricants, see Ref. [49]. The basic properties of lubricants at the given temperatures are listed in Table 1.

### 2.4. Layout of the experiments

The first experiment of this study dealt with a passage of lubricant through the contact and a film thickness distribution within the contact under lateral vibrations. It was shown both experimentally and

**Table 1**  
Viscosity at ambient pressure, pressure-viscosity coefficient (PVC) and molecular weight of lubricants.

Lubricant	Temperature (°C)	Viscosity (Pa·s)	PVC (GPa <sup>-1</sup> )	Mol. wt. (g/mol)
SN650 + PIP	30	1.007	≈12	≈450/40 000
CAS	40	0.239	12.4	927
R560/88	40	0.406	≈30	≈500
SQ + PIP	40	0.071	20.9	423/40 000
PGLY	40	16.3	13.2	12 000

theoretically in Refs. [50–52] for steady state conditions that the film thickness and its distribution should be affected by long-time shear loading of lubricant according to the angle  $\epsilon'$  between the vectors of entrainment and sliding velocities. Under the current test conditions, the lubricant was subjected to short-term cyclical changes of the angle  $\epsilon'$ , speeds and shear loading. Besides the examination of the film thickness distribution, the film thickness measured at the contact inlet under specific kinematic conditions of vibrations was compared with the film thickness obtained under the corresponding steady state conditions in terms of the entrainment and sliding speeds. It is generally accepted that the lubricant passes through the EHL contact at the mean speed of contact surfaces. In accordance with this statement, the simple formulas (6) and (7) were used for the elementary estimation of the lubricant position when passing through the contact:

$$x_i = x_{(i-1)} - u_{ex}\Delta t \tag{6}$$

$$y_i = y_{(i-1)} - \overline{u_{ey}}\Delta t - \frac{1}{2}\overline{a_{ey}}\Delta t^2 \tag{7}$$

where  $x_i$ ,  $x_{(i-1)}$  and  $y_i$ ,  $y_{(i-1)}$  is a set of positions of the tracked element of lubricant from an initial position,  $\Delta t$  is time step,  $\overline{u_{ey}}$  and  $\overline{a_{ey}}$  are the mean values of entrainment speed and entrainment acceleration in the lateral direction over the time step, respectively. These formulas are based on the assumption that the passage is driven only by the vector of entrainment velocity regardless of the sliding velocity vector (see Fig. 2). The estimation of the lubricant passage from the chosen initial position for the given input parameters is illustrated in Fig. 3.

Before the main experiment for conditions of lateral vibrations was carried out, the central film thicknesses for four reference liquids were measured by means of TFCI under steady state conditions at the corresponding temperature and loads. However, the steady state conditions exceeded the ranges of entrainment speeds  $u_e'$  and slide-to-roll ratios  $\Sigma'$  used in the main experiment. Thereafter, the dependencies of these

central film thicknesses on the operating parameters were determined empirically (see Appendix) by the fitting of cubic surface polynomial models to the acquired thickness data. All the coefficients of determination of the fitted models were over the value of 0.9985. The central film thickness gained on the basis of these models is referred to as the reference film thickness  $h_{c,ref}$ .

The main experiment was focused on the film thickness deviations due to the lateral vibrations. The deviations were evaluated via a systematic comparison of the film thickness profiles obtained under non-steady state conditions (vibrations) with the reference film thicknesses originating from the relevant steady state conditions. Tests were carried out for EHL contact subjected to a pure rolling in the main direction simultaneously with a sliding harmonic motion in the lateral direction of contact. Each test lasted approximately 5 s and was performed for different combinations of lubricant, load, entrainment speed in the main direction  $u_{ex}$ , and frequency  $f$  and stroke length  $s$  of lateral harmonic motion. After each test, at least a minute break was maintained to ensure the same and stable initial temperature of lubricant before starting the next test. Relatively low speeds were applied during the experiment to minimize shear heating effects, as is listed in Table 2 together with the other operating parameters. The EHL contact was recorded during the operating time. Each record was checked to see whether the film thickness distribution was periodically repeated without any undesirable effect on the thickness due to a potential variation in the lubricant temperature during the test. The test was repeated, if the changes in film thickness during ten consecutive strokes exceeded 15 nm. A representative interferogram image was captured from the record at the end of the stroke and the corresponding film thickness profile was evaluated in the plane oriented at the median of  $\delta'$  angle acquired in the course of the half-stroke. Subsequently, for each test conditions, the reference film thickness  $h_{c,ref}$  was calculated based on the relevant empirical relationship (see Appendix) using the mean values of entrainment speed  $u_{e,mean}'$  and SRR  $\Sigma'_{mean}$  achieved during the stroke as the input parameters. The values  $u_{e,mean}'$  and  $\Sigma'_{mean}$  were used to include both simultaneously occurring effects of the hydrodynamic (entraining) action and the shear loading of lubricant (sliding) on film thickness to the reference film thickness  $h_{c,ref}$ . Finally, the reference film thicknesses were compared with the film thickness profiles acquired under the lateral vibrations to evaluate the film thickness deviations within the central area of the contact.

The example of the evaluation of central film thickness deviations for a single film profile (solid line) is illustrated in Fig. 4 where the reference film thickness  $h_{c,ref}$  corresponds to a central thickness of the reference film profile (dotted line). The film thickness maximum  $h_{c,max}$ , minimum  $h_{c,min}$  and its mean value  $h_{c,mean}$  within the central area of the contact are gained from the film profile obtained under the conditions of lateral vibrations. The parameter  $h_{c,mean}$  is taken into consideration for its com-

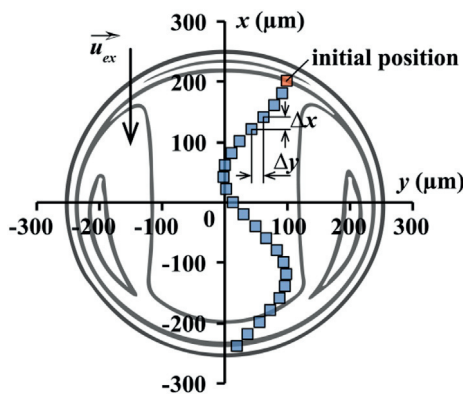


**Fig. 3.** Estimation of lubricant passage through EHL contact under lateral vibrations for  $u_{ex} = 0.1 \text{ m/s}$ ,  $f = 300 \text{ Hz}$ ,  $s = 200 \text{ μm}$ ,  $S/D = 0.4$  and  $\Delta t = 0.2 \text{ ms}$ .

**Table 2**  
Ranges of operating parameters used in tests.

Operating parameter	Minimum value of parameter	Maximum value of parameter
Entrainment speed $u_e'$ (m/s)	0.006	0.55
SRR $\Sigma'$ (1)	0	-1.99
Frequency $f$ (Hz)	0	300
Stroke length $s$ (μm)	80	400
Lateral entrainment acceleration $a_{ey}'$ (m/s <sup>2</sup> )	0	335
Entrainment acceleration $a_e'$ (m/s <sup>2</sup> )	0	250
S/D ratio (1)	0.1	0.9
Contact pressure $p_h$ (GPa)	0.45	0.88

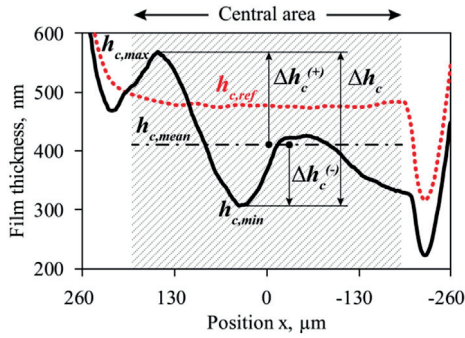


Fig. 4. Illustration of evaluation of central film thickness deviations; solid line - evaluated film profile, dotted line - reference film profile.

parison with  $h_{c,ref}$ . To determine how the central film thickness is affected by the lateral vibrations, the following four relative dimensionless numbers (ratios) are used:

$$H_{mean} = h_{c,mean} / h_{c,ref} \tag{8}$$

$$H_{dev} = \Delta h_c / h_{c,mean} = (h_{c,max} - h_{c,min}) / h_{c,mean} \tag{9}$$

$$H_{dev}^{(+)} = \Delta h_c^{(+)} / h_{c,mean} = (h_{c,max} - h_{c,mean}) / h_{c,mean} \tag{10}$$

$$H_{dev}^{(-)} = \Delta h_c^{(-)} / h_{c,mean} = (h_{c,mean} - h_{c,min}) / h_{c,mean} \tag{11}$$

where  $\Delta h_c$  is maximum fluctuation of central film thickness,  $\Delta h_c^{(+)}$  and  $\Delta h_c^{(-)}$  is the positive and negative film deviation related to  $h_{c,mean}$ , respectively.

### 3. Results and discussion

#### 3.1. Lubricant passage and film thickness distribution

Fig. 5 illustrates the courses of entrainment speed, sliding speed, and

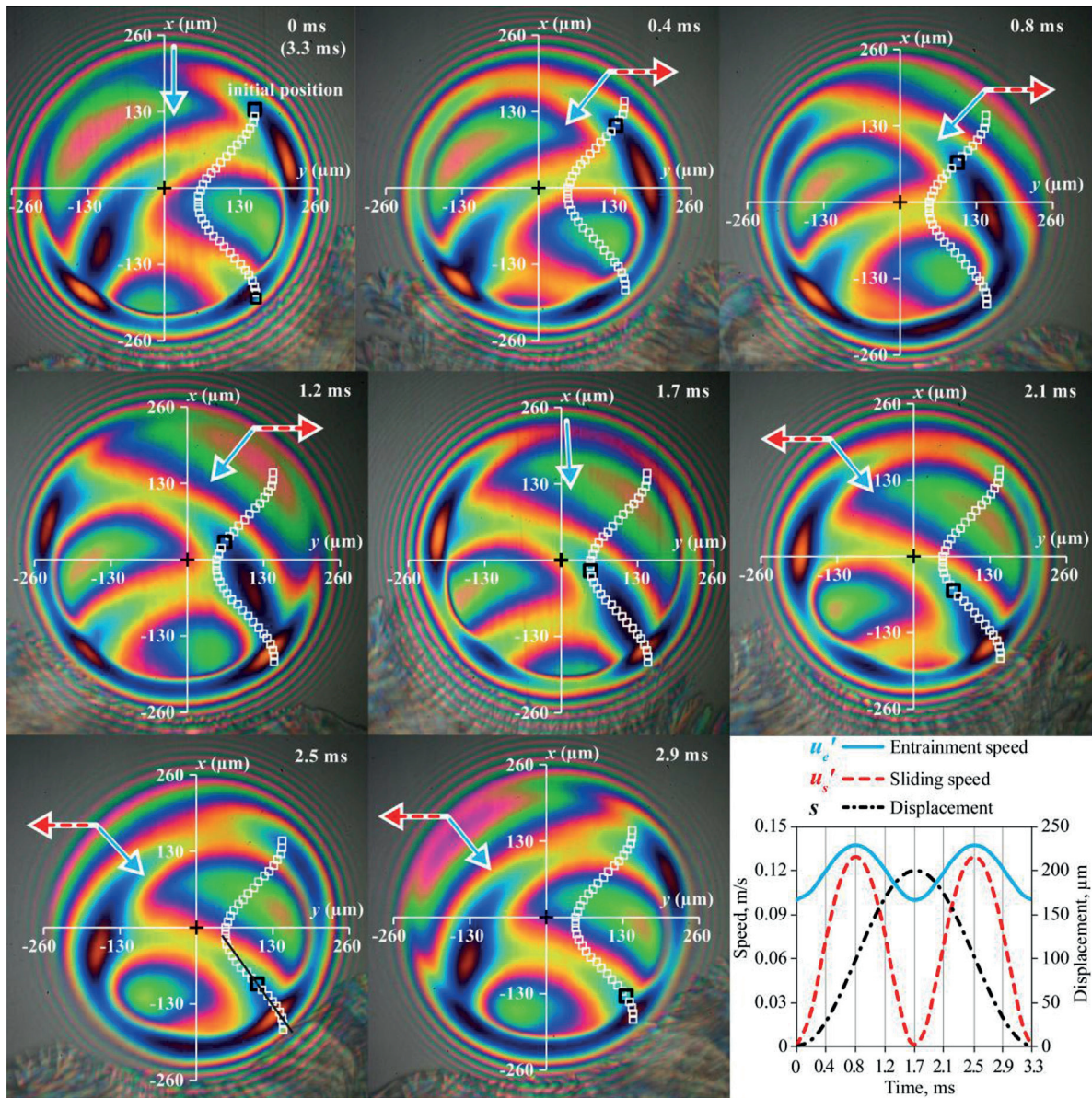


Fig. 5. Comparison of the estimation of lubricant passage through EHL contact with the actual passage of SN650 + PIP lubricant.

lateral displacement over time together with the comparison of the estimated and actual passage of SN650 + PIP lubricant through the contact at specific moments of stroke. During the stroke, the entrainment speed  $u_e'$  and the slide-to-roll ratio  $\Sigma'$  reach their maxima and minima at the moments of half-stroke and end-stroke positions of lateral motion, respectively. The instantaneous vectors of entrainment and sliding velocities are indicated by the blue and red arrows in Fig. 5. The used operating conditions were  $u_{ex} = 0.1 \text{ m/s}$ ,  $f = 300 \text{ Hz}$ ,  $s = 200 \text{ }\mu\text{m}$ ,  $S/D = 0.4$  and  $p_h = 0.7 \text{ GPa}$ . The time step  $\Delta t = 0.1 \text{ ms}$  was set equally to the time lag between two images captured by a camera to facilitate a direct comparison of these two approaches. In the view of the fact that the centre of the contact changes its position in the images over time and the contact diameter fluctuates, the origin of coordinate system (marked by the plus symbol) of the estimation was fitted to the centre of contact for each interferogram with respect to the centre of interference pattern (concentric Newton's rings). Since the end of the horseshoe-shaped constriction of EHL film passes through the contact area for most of the movement cycle and is easily recognizable in the interferograms, its position at 0 ms was chosen as the initial position for the estimation of lubricant passage. The individual estimated positions are indicated by the symbol of the minor white square regarding to the time step  $\Delta t$ . To enable the direct comparison of the estimated position and the actual position, the instantaneous estimated position of the lubricant is highlighted by the symbol of the bold black square in the interferogram obtained at the corresponding time.

It can be seen from the sequence of images that the tracked part of the horseshoe-shaped constriction is drawn into the central area of the contact and passes through it along the sinusoidal trajectory. Moreover, this sinusoidal passage seems to be common for overall central film thickness distribution. Furthermore, the interferograms captured at time of 0 and 3.3 ms were practically identical, since the film thickness distribution was cyclically repeated for each cycle of the lateral motion. Consequently, the new end of horseshoe-shaped constriction was formed in the location of the initial position at time of 3.3 ms while the tracked part of the constriction left the central area of the contact. It is clear from the comparison in Fig. 5 that the estimation is in good agreement with the actual passage of the lubricant. Therefore, the lubricant passage through the central area of the contact is controlled exclusively by the entrainment velocity vector regardless of the sliding velocity vector which had a negligible effect on the actual lubricant passage. It means that the passage of lubricant through the EHL conjunction can be simply estimated considering only a vector of entrainment velocity from the kinematics of the contact surfaces. However, this statement is valid only for the conditions where rapid changes of entrainment and sliding

velocity vectors occur, not for steady-shear cases as used in Refs. [50–52].

The origin of the film thickness distribution is further examined under the same transient conditions in relation to the film thicknesses obtained at the corresponding entraining and sliding speeds but under steady state conditions. Fig. 6 shows the interferogram (a) captured at the end of the stroke and the appropriate film thickness profile (a) along the illustrated axis  $\vec{x}$ . The time data on the axis  $\vec{x}$  refer to the times at which the film of lubricant was entrained into the inlet of contact, and thus they determine the speeds at the moments of film thickness formation (see the courses of speeds in Fig. 5). The axis  $\vec{x}$  is almost in line with the axis of symmetry of EHL contact with respect to its horseshoe-shaped constriction, and it is inclined at the median of  $\delta$  angle achieved during the half-stroke within the interval from 1.7 to 3.3 ms. Over this interval, the direction of entrainment velocity  $\delta$  or the direction of lubricant passage are roughly identical, especially near the central part of this interval, as it is illustrated by a solid black line in the interferogram at 2.5 ms in Fig. 5. Consequently, the straight axis  $\vec{x}$ , instead of a sine axis, is used for the investigation of time-dependent film thickness distribution without any significant distortion. Accordingly, the film profile (a) contains most of the thicknesses originating from the contact inlet under transient conditions and passing through the central area of the contact. The film profiles (b) to (e) were acquired under steady state conditions.

It is apparent from the comparison of film profiles in Fig. 6 that the film thickness in profile (a), which was formed at the contact inlet at the time of 1.7 ms (the end of the stroke), is in good agreement at the given time with the central thickness in film profile (b). The compliance is reached because of these thicknesses were formed at the same magnitudes of speeds  $u_e' = u_{ex}$  and SRRs  $\Sigma' = \Sigma$ . In addition, the instantaneous vector of  $u_e'$  at the end of the stroke is also the same as the vectors of  $u_{ex}$  under steady state conditions, since the lateral speed of the ball  $u_{by}'$  is equal to zero. So, it seems that the effect of this transient conditions on the film thickness is negligible at the end of the stroke. When the speed  $u_e'$  increases at the contact inlet over the stroke, the film thickness should also increase as the result of the enhancement of oil flow followed by the pressure build-up in this area. However, on the contrary, the film thickness in profile (a) is significantly reduced at the time of 1.9 ms because of the presence of the part of horseshoe-shaped constriction passing through the contact, as was explained above. If the profile (c) is compared with the film thickness in the profile (a) at time of 2.5 ms, at which the maximum speeds over stroke are achieved, there is again a good agreement in the film thicknesses. Nevertheless, when the speed  $u_e'$  consequently starts to decrease, the film thickness still increases up to the time of 2.9 ms. This excessive increase in the thickness cannot be

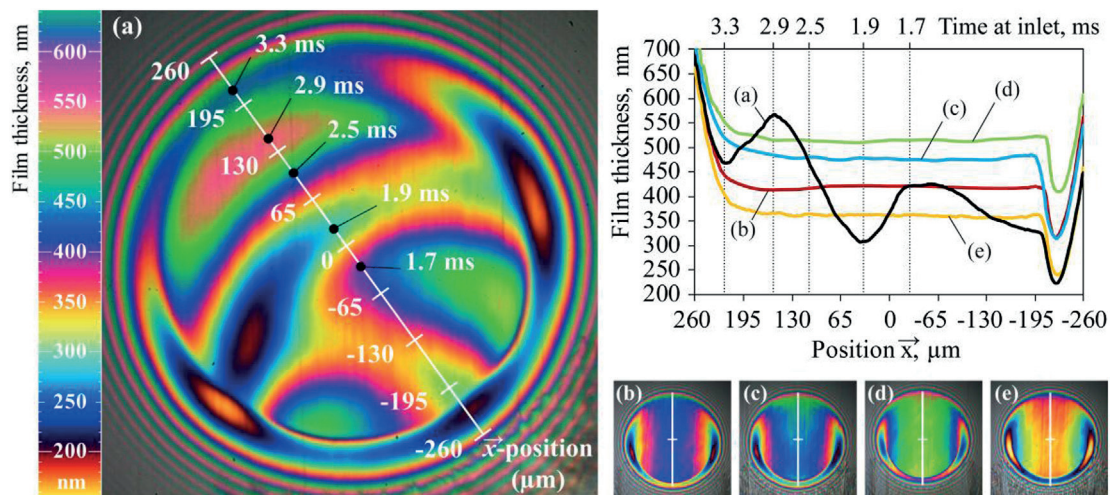


Fig. 6. Interferograms and film thickness profiles of SN650 + PIP lubricant obtained under non-steady state conditions at (a)  $u_{e' \max} = 0.137 \text{ m/s}$ ,  $\Sigma'_{\max} = -0.94$  and under steady state conditions at (b)  $u_{ex} = 0.1 \text{ m/s}$ ,  $\Sigma = 0$ ; (c)  $u_{ex} = 0.137 \text{ m/s}$ ,  $\Sigma = -0.94$ ; (d)  $u_{ex} = 0.137 \text{ m/s}$ ,  $\Sigma = 0$ ; (e)  $u_{ex} = 0.1 \text{ m/s}$ ,  $\Sigma = -0.94$ .

explained by the speed  $u_e'$  and SRR  $\Sigma'$ , but it is attributed to the influence of entrainment deceleration  $a_e' = \partial u_e' / \partial t$  and subsequent squeeze of the lubricant.

During the decrease in the entrainment speed  $u_e'$  at deceleration  $a_e'$ , the contact surfaces of the ball and the disc began to approach each other because of sudden reduction in the entrainment of lubricant at contact inlet. Since the film of lubricant has a high viscosity within the central area of the contact and its shape is relatively flat, a viscous damping of lubricant prevented the mutual approach of the contact surfaces in this area. On the other hand, a steeper shape of film and low viscosity of lubricant enabled some approach at the contact periphery due to initially low viscous damping of such film, as can be recognized from the small changes in the size of the contact area in Fig. 5. At the very beginning of the approach, the local increase in pressure and viscosity of lubricant took place at the contact boundary, which caused the lubricant to barely flow. This lubricant was squeezed/entrapped between the contact surfaces, when its leakage was suppressed from the outside of the contact (contact periphery) by the closing gap of contact surfaces and from the inside of the contact (the contact area) by the presence of the high-viscous lubricant. The entrapped film was gradually entrained into the contact inlet forming a shape of a crescent, oriented symmetrically with respect to the instantaneous vector of  $u_e'$ , during the deceleration  $a_e'$  (2.5–3.3 ms and 0.8–1.7 ms; see Fig. 5). Moreover, the film thickness of the entrapped film increased from 2.5 to 2.9 ms (see Fig. 6), because the value of deceleration  $a_e'$ , and thus the squeeze effect, increased as well. Accordingly, the entrapped film diminished during the second half of the speed  $u_e'$  reduction (2.9–3.3 ms), when the deceleration and squeeze effect disappeared. In the final consequence, the reduction in the entrainment speed did not lead to the expected drop in film thickness as in the case of steady state conditions. Instead, the thick crescent-shaped film passed through the contact without a change in its shape or rotation. A similar behaviour of entrapped films was observed previously in rolling/sliding conjunctions subjected to sudden changes in load [23,53].

The profile (d) was acquired for the maximum entrainment speed ( $u_{ex} = u_{e' max}$ ) and the minimum SRR ( $\Sigma = 0$ ) reached during the stroke. These conditions led to the formation of a thick film. For the opposite conditions, i.e. the minimum entrainment speed and the maximum SRR reached during the stroke, a thin film was formed, as illustrated by the profile (e). Although such extreme kinematic conditions did not occur at the same time under the conditions of lateral vibrations, the extremes of the central film thickness in the profile (a) at times of 1.9 and 2.9 ms were beyond the thicknesses in the profiles (d) and (e). This points out that

even the extreme steady state conditions are not able to cover the film thickness fluctuations caused by the lateral vibrations. This leads to the conclusion that the fluctuations of central film thickness due to lateral vibrations cannot be currently estimated from the commonly applied Hamrock-Dowson film thickness predictions or on the basis of kinematics in the contact, as in the case of the passage of lubricant. On the contrary, Kalogiannis deduced a rather different conclusion in his PhD thesis [46], where the predicted and measured thicknesses were comparable. However, a good agreement was achieved only for a very few cases under mild lateral vibrations, when frequencies  $f$  were low and  $S/D$  ratios were considerably higher than one. From the limited ranges of parameters used in Ref. [46], it is difficult to reliably distinguish the effects of individual parameters, or even establish a trend describing the influence of vibrations on film thickness. To clarify this task, it should be necessary to obtain a sufficient amount of experimental data under various combinations of comprehensive operating parameters and lubricants.

### 3.2. Effects of lubricant rheology and main and lateral speeds

Figs. 7–9, respectively, show the effect of lateral entrainment speed  $u_{ey}'$  (resulting from frequency  $f$ ), main entrainment speed  $u_{ex}$  and lubricant rheology on film thickness distribution, its fluctuations and/or relative deviations. To determine the effects of these operating parameters individually, a film of CAS lubricant was first measured at various frequencies of lateral motion from 50 up to 300 Hz while other operating parameters were fixed. Only minor fluctuations of film thickness  $\Delta h_c$  were observed at the frequencies of 50 and 100 Hz, as it is shown by means of the film profiles (a) and (b) in Fig. 7. The evaluated relative film deviations  $H_{dev}$  are below the value of 0.15 for these conditions. Such small film deviations are fairly common in practical applications of lubricated contacts not only due to vibrations but also as a result of other factors, e.g. surface roughness, defects of surfaces, impurities or solid components in lubricants. Similarly, neither the mean value of film thickness  $h_{c,mean}$  nor the ratio  $H_{mean}$  are significantly affected by the vibrations with respect to the film thicknesses  $h_{c,ref}$  obtained under steady state conditions, when the values of  $H_{mean}$  are above 0.95.

At higher frequencies of 200 and 300 Hz, the central thickness begins to suffer from film fluctuations  $\Delta h_c$  due to the entrainment of the minimum thicknesses and thick squeezed films. Besides this, the thickness  $h_{c,mean}$  should be enhanced as the entrainment speed  $u_e'$  increases along with the frequency  $f$ . The diagram in Fig. 7 shows the exponential dependencies of the ratios  $H_{dev}$  and  $H_{mean}$  on the frequency. The trends of

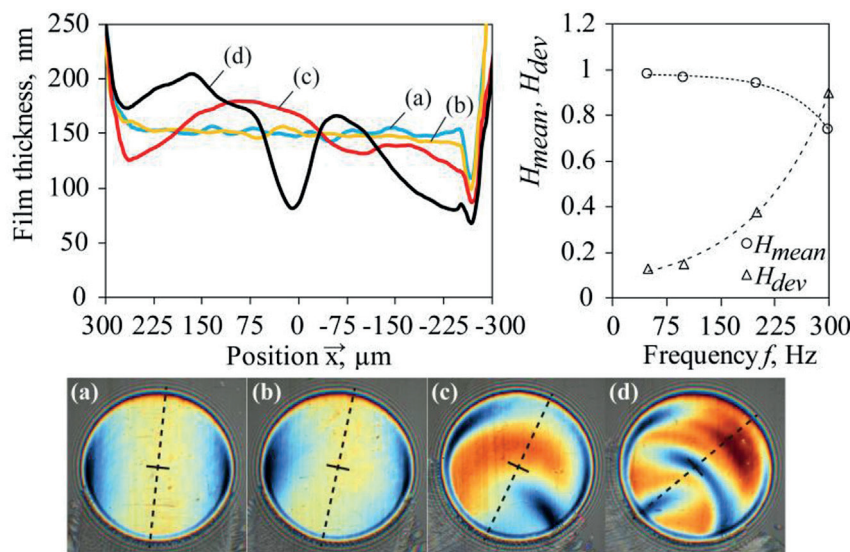


Fig. 7. Effect of frequencies (a) 50 Hz, (b) 100 Hz, (c) 200 Hz and (d) 300 Hz on film thickness distribution and deviations of CAS lubricant at  $u_{ex} = 0.1 \text{ m/s}$ ,  $s \cong 310 \mu\text{m}$ ,  $S/D \cong 0.55$  and  $p_h = 0.88 \text{ GPa}$ .

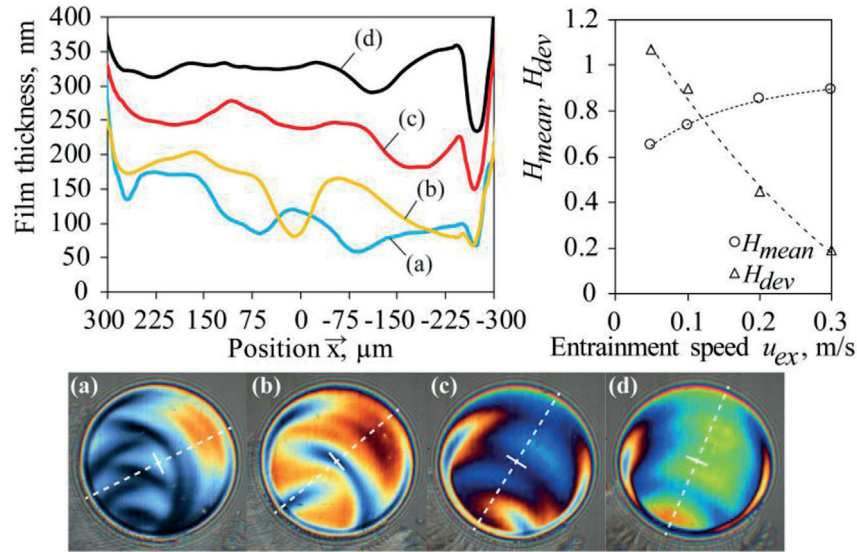


Fig. 8. Effect of entrainment speeds (a) 0.05 m/s, (b) 0.1 m/s, (c) 0.2 m/s and (d) 0.3 m/s on film thickness distribution and deviations of CAS lubricant at  $f = 300$  Hz,  $s \cong 310 \mu\text{m}$ ,  $S/D \cong 0.55$  and  $p_h = 0.88$  GPa.

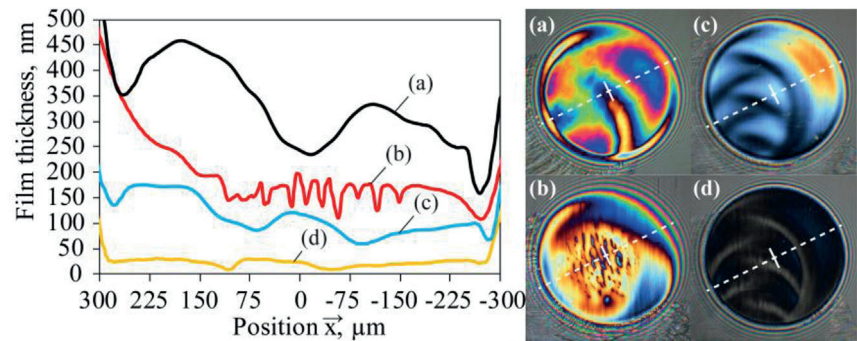


Fig. 9. Comparison of film thickness distributions of (a) R560/88, (b) PGLY, (c) CAS and (d) SQ + PIP lubricants obtained under identical non-steady state conditions of  $u_{ex} = 0.05$  m/s,  $f = 300$  Hz,  $s \cong 310 \mu\text{m}$ ,  $S/D \cong 0.55$  and  $p_h = 0.88$  GPa.

the experimental data can be described/fitted by the formula  $y = A \exp(Bx) + C$  with the adjusted R-squared above the value of 0.998, where  $A$ ,  $B$  and  $C$  are nonzero parameters. For current conditions, there is an exponential growth in relative film deviations  $H_{dev}$  with increase in frequency, and at the same time, an exponential decline in ratio  $H_{mean}$ . Please note that at the highest frequency of 300 Hz, the mean thickness  $h_{c,mean}$  was reduced by only 30%, but the maximum fluctuations  $\Delta h_c$  nearly reached the magnitude of  $h_{c,mean}$ . Since the entrainment speed, rather than the sliding speed, is the important parameter for both the passage of lubricant and the distribution of film thickness within the contact, the frequency  $f$  can be adequately represented by the lateral entrainment speed  $u_{ey}$  even though the lateral motion was performed as pure sliding.

In contrast to the experiment conducted at different frequencies/lateral entrainment speeds  $u_{ey}$  with a fixed value of  $u_{ex}$ , the next experiment was performed at various main entrainment speeds  $u_{ex}$  with a fixed value of frequency  $f$  and other operating parameters. When the speed  $u_{ex}$  increased from 0.05 to 0.3 m/s, the overall film thickness also increased (see Fig. 8) due to the hydrodynamic action at the contact inlet. However, the film fluctuations  $\Delta h_c$  exhibit the opposite trend. The film in the central area of the contact is greatly affected if the overall film of lubricant is thin, brought about by low speed  $u_{ex}$  or low viscosity of lubricant, and the speed  $u_{ey}$  is high because of lateral vibrations. This influence stems from the passage of the minimum film thicknesses of EHL horseshoe-shaped constriction and thick crescent-shaped film through

the central area of the contact at the same time. This can be seen from the interferograms and film profiles (a) and (b) in Fig. 8. The parts of entrained horseshoe-shaped constrictions cease to encroach upon the central area of the contact with the increase in the speed  $u_{ex}$  while the film formed by the squeeze action persists. Consequently, the maximum film fluctuations  $\Delta h_c$  are reduced by  $u_{ex}$ , thus, they do not correspond to the increase in the mean film thicknesses  $h_{c,mean}$  which reaches to the values of  $h_{c,ref}$  for high main speed  $u_{ex}$ . Again, the evident exponential dependencies (see the dashed lines in Fig. 8) of the ratios  $H_{dev}$  and  $H_{mean}$  were obtained, this time with respect to the speed  $u_{ex}$ .

The four lubricants were employed in the main quantitative study. Fig. 9 shows that their rheological differences led to very diverse film thickness distributions under identical non-steady state conditions. Despite this, the value of  $H_{mean}$  is close to 0.57 for all lubricants, because the reference thickness of the individual lubricants  $h_{c,ref}$  suppresses their differences in terms of the entrainment and shear impacts on the central film thickness. It is obvious from Fig. 9 that the film fluctuations of PGLY differ from the other lubricants. The film of PGLY is disrupted by stripes of low thickness in the central area of the contact. It is noteworthy that these low-thickness stripes are not formed at the contact inlet, but they are produced within the central area of the contact approximately at the moment of the maximum lateral speed. Moreover, the stripes disappear before reaching the contact outlet. According to the authors' knowledge, the observed behaviour has not been described in literature yet. Moreover, it is apparently not caused by the temperature-viscosity wedge

effect [54–57], which is often discussed for conditions of sliding, because this effect leads to a thicker film in the central area of the contact (dimple formation), not to its reduction. This unusual phenomenon is very likely caused by a combination of rapid shear loadings that acts in different directions and a high-molecular weight of PGLY. The film thickness of PGLY is first possessed by a shear thinning at the contact inlet, and then it is additionally affected by shear stress within the central area of the contact. These sharp fluctuations of the central film thickness can have a substantial impact on friction and on contact fatigue as a consequence of associated rapid changes in the pressure distribution. The same argument can be also valid for other lubricants, not only for PGLY. Nevertheless, a smaller impact on pressure distribution can be expected for other lubricants due to smoother changes in film thickness than it was found in the case of PGLY.

It is worth noting that the squeeze effect, as a result of which the lubricant is entrapped in the crescent-shaped bulge, is more pronounced for lubricants forming a thicker film under the same kinematic conditions. This observation is in good agreement with the findings of the recent experimental study [58] involving conditions of pure squeeze action. However, along with rheology of lubricants, the tangential speeds and accelerations of contact surfaces are essential parameters influencing the squeeze action, and subsequently its impact on the film thickness of the particular lubricant, as demonstrated in this paper.

If the results in Figs. 7 and 8 are compared, it is easy to infer that the effects of the speeds  $u_{ex}$  or  $u_{ey}$  are inverse, and both relationships of ratios  $H_{dev}$  and  $H_{mean}$  lead to exponential dependencies according to these speeds. Moreover, the exponential functions  $y = A \exp(Bx) + C$  are convex (the parameter  $A$  is positive) in the case of the dependence of relative deviations  $H_{dev}$  on both speeds  $u_{ex}$  and  $u_{ey}$ , where these deviations increase with the lateral speed  $u_{ey}$  (the parameter  $B$  is positive) and decrease with the mean speed  $u_{ex}$  (the parameter  $B$  is negative). Conversely, the concave functions (the parameter  $A$  is negative) were obtained for the dependence of relative mean thickness  $H_{mean}$  on these speeds, where their trend is also reversed. These facts suggest that there is a similar exponential function that can summarize the effects of both speeds  $u_{ex}$  and  $u_{ey}$  on  $H_{mean}$  or  $H_{dev}$ .

From another point of view, when the main speed  $u_{ex}$  increases and the lateral speed  $u_{ey}$  remains the same, a range of angle  $\delta'$ , which represents the direction of overall entrainment velocity  $u_e'$ , is reduced and vice versa. Let us recall that the axis  $\vec{x}$  depicted in the interferograms is inclined at the median of  $\delta'$  angle achieved in the course of the half-stroke. It can be seen in Figs. 7 and 8 how the inclination of axis  $\vec{x}$  varies according to the speeds  $u_{ex}$  and  $u_{ey}$  or frequency  $f$ . Based on equation (3) defining the angle  $\delta'$ , the mean, median or maximum value of this angle are capable to describe a rate of lateral vibrations considering both simultaneous effects of the main and lateral speeds on film thickness behaviour in general applications. Nevertheless, a more suitable and straightforward way to express the rate of lateral vibrations is to use a dimensionless number defined as the ratio of lateral entrainment speed  $u_{ey}$  and main entrainment speed  $u_{ex}$ . In the case of simple harmonic vibrations, the rate of lateral vibrations can be defined by the dimensionless numbers  $U_{y,max/x} = |u_{ey}|_{max}/u_{ex}$  and  $U_{y/x} = |u_{ey}|_{mean}/u_{ex}$ , where  $|u_{ey}|_{max}$  and  $|u_{ey}|_{mean}$  is the maximum and the mean of absolute values of lateral entrainment speed  $u_{ey}$  over one cycle of motion. It comes from the harmonic course of speed  $u_{ey}$  that  $U_{y,max/x}/U_{y/x} = \pi/2$ . The number  $U_{y,max/x}$  is convenient for assessing the relative film deviations  $H_{dev}$ ,  $H_{dev}^{(+)}$  and  $H_{dev}^{(-)}$ , because the extremes observed in the central film thickness are directly associated with the maximum value of the parameter that caused them. Similarly,  $U_{y/x}$  is more appropriate for the evaluation of the relative mean thickness  $H_{mean}$ . Unfortunately, in practical applications, where the operation of machine contacts under vibrations is investigated, it is often difficult to determine the exact period of maxima movement speeds together with their magnitudes. This is because the vibrations are often excited in a broad range of frequencies and a signal is almost always

filtered during its processing for frequency analysis. For these reasons, only  $U_{y/x}$  is used in the present paper as the rate of lateral vibrations based on  $|u_{ey}|_{mean}$ , which is easier to derive from technical diagnostics of machines than  $|u_{ey}|_{max}$ .

### 3.3. Effect of lateral vibrations (quantitative description of film variations)

The following main results of this study were obtained for a wide range of operating parameters (see Tables 1 and 2). The results show how the mean value of central film thickness differs from the reference film thickness and also the relative film thickness deviations according to the rate of vibrations represented by the entrainment speeds ratio  $U_{y/x}$ , as discussed above. It should be noted that there are many approaches how to express the rate of vibrations. One of them is the stroke ratio  $S/D$  representing a relative degree of displacement. This approach has been used by other authors for evaluation of film formation under reciprocating motions [43] or track replenishment [45] due to lateral vibrations with  $S/D > 1$ . However, if the  $S/D$  approach is employed for assessment of current experimental data, there is no clear trend at all. Therefore, the stroke ratio is not a suitable parameter for this purpose, since the  $S/D$  is not able to include all the kinematic variables influencing the behaviour of the film thickness used in this study.

The effect of lateral vibrations (represented by  $U_{y/x}$ ) on the relative mean thickness  $H_{mean}$  was found to be comparable for all four reference liquids used in the experiments, as can be seen in Fig. 10. The trend of  $H_{mean}$  reduction with the increase in  $U_{y/x}$  was fitted by the depicted trendline of exponential function  $H_{mean} = \exp(-0.29U_{y/x})$  with the value of coefficient of determination  $R^2 = 0.9545$ . Certain changes in film thickness behaviour can be distinguished with respect to  $U_{y/x}$ . In the first part of the diagram, the central film thicknesses of lubricated contacts are stable without significant consequences of lateral vibrations. This is because these conditions of low value of  $U_{y/x}$  are very close to the steady state conditions of pure rolling. It can be seen that some data points are below the trendline. This mismatch is attributed to the way of evaluation in particular. Since the representative interferograms and their corresponding film profiles were evaluated at the end positions of the strokes, substantial variations of central film thickness could not be captured at these positions for some cases of conditions involving high main rolling speeds  $u_{ex}$  and low frequencies  $f$  (low value of  $U_{y/x}$ ). In these cases, the film thickness affected by the vibrations passed through the contact before the end of the stroke was reached, although the reference film thickness  $h_{c,ref}$  was calculated from the mean value of entrainment speed  $u_e'$  achieved during the whole stroke. Such a combination consequently led to the evaluation of slightly lower  $H_{mean}$  at low  $U_{y/x}$ .

If the rate of vibrations  $U_{y/x}$  exceeds 0.6, the central film thickness starts to be distinctly affected. A continuous layer of lubricant is increasingly disrupted; initially, due to a thick crescent-shaped film resulting from the squeeze action at the contact inlet, and subsequently, also by a thin film of EHL horseshoe-shaped constriction entrained into the central area of the contact. The lateral-sliding vibrations take a major role in the formation of film over the rolling motion for  $U_{y/x} > 1$ . This change in the control of film thickness causes a film reduction due to decrease in hydrodynamic pressure at the contact inlet. The hydrodynamic pressure build-up and film formation are suppressed by the presence of air streamers and bubbles interspersed in the lubricant close to the contact (so-called EHL cavitation zone). This zone was originally created at the outlet of the contact during the previous stroke. However, as a consequence of small stroke lengths and high frequencies of lateral motion, the cavitation zone reaches at the contact inlet when the lateral motion is reversed. This observation and explanation support the previous experimental findings given by Nishikawa and Kaneta [37,38] considering the conditions of reciprocating motions.

The film thickness reduction, caused by the presence of cavitation zone at the contact inlet, together with fluctuations of central film

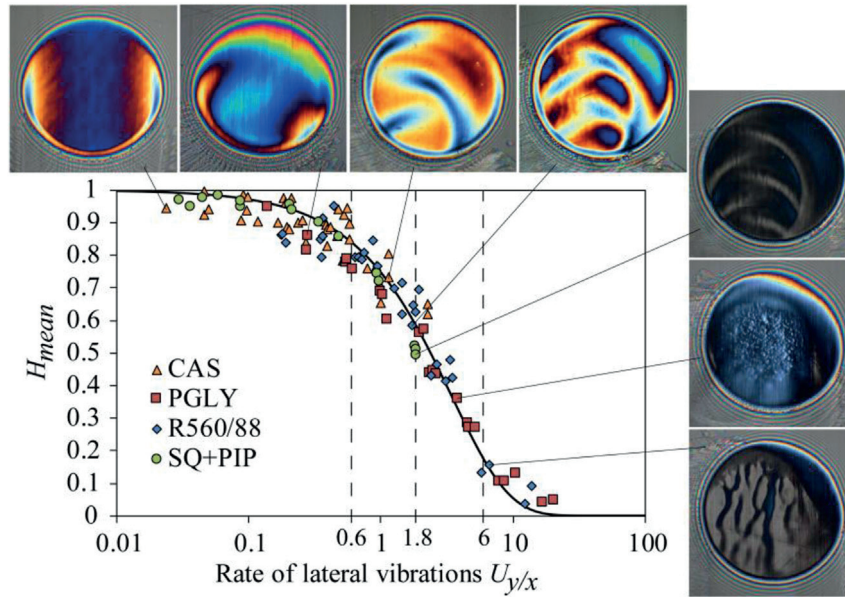


Fig. 10. Effect of lateral vibrations on relative mean value of central film thickness.

thickness can lead to a film failure, especially for low-viscosity lubricants and surfaces with defects or high roughness. The local film breakdown was observed for  $U_{y/x} \geq 1.8$  (see the light grey areas in the interferograms on the right in Fig. 10). The film breakdown occurs at  $U_{y/x} = 1.8$  even though the mean film thickness  $h_{c,mean}$  corresponds to seemingly sufficient 60% of the thickness obtained under appropriate steady state conditions. In the last part of the diagram, where the mean lateral speed  $|u_{ey}|_{mean}$  is 6 and more times higher than the main rolling speed  $u_{ex}$ , the

film almost completely collapsed even for the high-viscosity lubricants. This is because the film formation at the contact inlet is no longer sufficient for full film lubrication. Under these operating conditions, air streamers and bubbles interspersed in lubricant at the contact inlet are quickly renewed due to the high-frequency and short-stroke length nature of movement, when this cavitation zone is not carried away from the contact inlet by the main rolling speed  $u_{ex}$ .

From the general point of view, the fitted trendline in Fig. 10 for

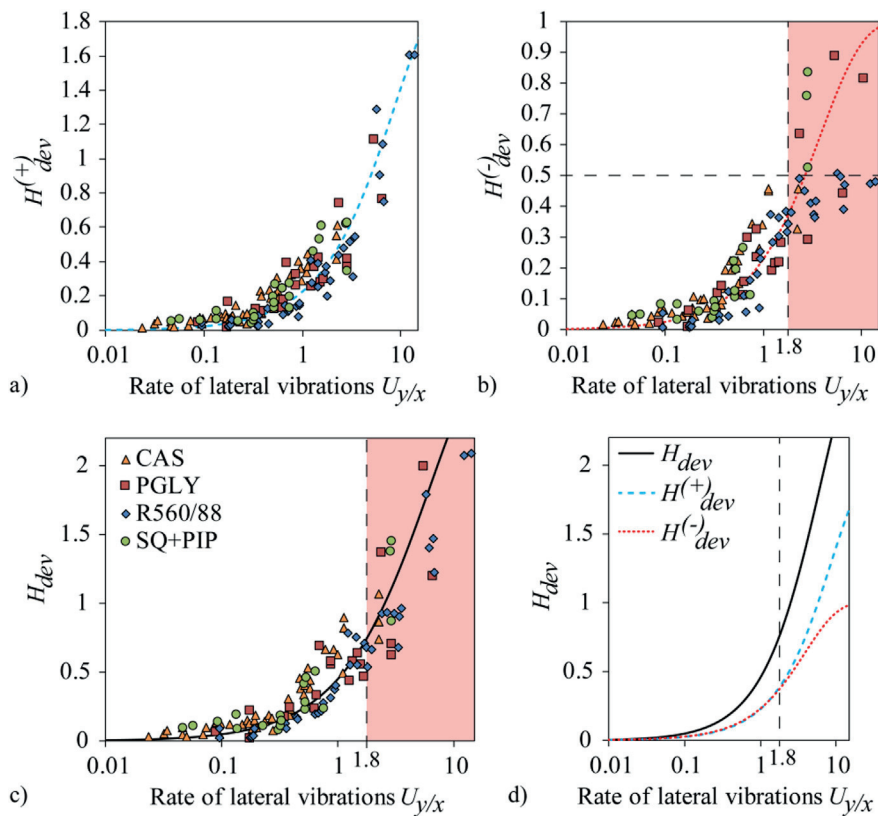


Fig. 11. Effect of lateral vibrations on relative film thickness deviations (a)  $H_{dev}^{(+)}$ , (b)  $H_{dev}^{(-)}$ , (c)  $H_{dev}$  and their comparison (d).

$S/D < 1$  is the transition between the steady state conditions of pure rolling on the one side ( $U_{y/x} \rightarrow 0$ ) and the non-steady state conditions in the form of pure sliding reciprocating motions on the other side ( $U_{y/x} \rightarrow \infty$ ). The trendline should be valid for much higher speeds and frequencies as well; nevertheless, thermal effects should be taken into account for such conditions. In addition, the results can be influenced by the geometry of the contact; however, the general trend will most likely remain the same for other curvatures and materials of contact bodies.

Fig. 11 shows that the comparable results for all reference liquids were also obtained in the case of relative film deviations depending on  $U_{y/x}$ . The overall (maximum) deviation  $H_{dev}$ , and likewise its positive  $H_{dev}^{(+)}$  and negative  $H_{dev}^{(-)}$  parts, exhibit the exponential growth with the increase in the rate of vibrations  $U_{y/x}$ . This good correlation of experimental data was achieved even though the film thickness fluctuations of PGLY can be additionally produced by a different mechanism compared with the other used lubricants, as explained above.

Interestingly, the relative positive  $H_{dev}^{(+)}$  and negative  $H_{dev}^{(-)}$  deviations are exactly the same, i.e. the deviations  $\Delta h_c^{(+)}$  and  $\Delta h_c^{(-)}$  are symmetrical with respect to  $h_{c,mean}$ , when  $U_{y/x} < 1.8$  (see the comparison of trendlines in Fig. 11(d)). The symmetry of the deviations probably stems from the effort of mechanisms within the contact to maintain a stable load-carrying capacity of EHL film. Accordingly, there is a force balance across the film of lubricant despite a variety of pressure distribution. This variety can be expected under non-steady state conditions. The effort seems to be successful up to the point where the film failure (local breakdown) was observed ( $U_{y/x} = 1.8$ ).

Beyond this threshold, with  $U_{y/x} \geq 1.8$ , it should be taken into consideration that a certain scatter of data points can occur. This can be seen in Fig. 11(b) at high values of  $U_{y/x}$ , where some data points are close to  $H_{dev}^{(-)} = 0.5$  and substantially distant from the dotted trendline. The trendline was fitted excluding these data points, and it naturally leads towards  $H_{dev}^{(-)} = 1$ , because there is no possibility to obtain the film thickness lower than zero (situation when  $h_{c,min} > h_{c,mean}$ ). The scatter of the data arose when  $h_{c,mean}$  or overall film thickness were very low due to the suppression of film formation at high  $U_{y/x}$ , and consequently the ratios  $h_{c,min}/h_{c,mean}$  were high despite the low values of  $h_{c,min}$ . In these cases, the minimum film thickness  $h_{c,min}$  is close to the height of surface asperities and a residual film no longer fulfils the conditions of full-film lubrication. Therefore, the scatter affects primarily the data points of  $H_{dev}^{(-)}$  and secondarily those of  $H_{dev}$  for  $U_{y/x} \geq 1.8$ , since  $H_{dev} = H_{dev}^{(+)} + H_{dev}^{(-)}$ , while  $H_{dev}^{(+)}$  is not influenced by this scatter.

Based on these results, for similar operating conditions, it can be assumed that the positive film deviations  $H_{dev}^{(+)}$ , caused mainly by the squeeze action, and overall deviations  $H_{dev}$  can reach the maximum values slightly exceeding 2 and 3, respectively. The relative film deviations can be estimated by means of equations:  $H_{dev}^{(+)} = 2.041[1 - \exp(-0.117U_{y/x})]$  and  $H_{dev}^{(-)} = 1 - \exp(-0.259U_{y/x})$ . These relationships correspond to the fitted trendlines depicted in Fig. 11(a) and (b). The trendline of  $H_{dev}$  can be obtained as the sum of  $H_{dev}^{(+)}$  and  $H_{dev}^{(-)}$  or it is possible to use the relationship  $H_{dev} = 3.041[1 - \exp(-0.147U_{y/x})]$  with the coefficient of determination  $R^2 = 0.805$ . Both approaches lead to almost the same estimated values.

#### 4. Conclusions

A modified ball-on-disc apparatus together with the thin film

#### Appendix

The central film thickness  $h_c$  obtained under steady state conditions or the reference film thickness  $h_{c,ref}$  can be estimated by the following polynomial relationship:

colorimetric interferometry technique were employed in the present study for examination of film thickness behaviour and revelation of phenomena occurring in EHL contacts under lateral vibrations. A variety of lubricants, loads, main rolling speeds, lateral-sliding harmonic motions, and low values of stroke ratio  $S/D < 1$  were used in experiments. The effects of lateral vibrations on film thickness were deduced from a comparison of film thicknesses under vibrations and film thicknesses under the corresponding steady state conditions. The main results are summarized as follows:

- A lubricant passage through the EHL conjunction is driven mainly by the entrainment vector despite the sliding vector. This conclusion is valid for rapid changes of entrainment and sliding velocity vectors occurring during vibrations; it is invalid in the case of steady shear loading at angle  $\epsilon$ , as used in Refs. [50–52].
- Thicknesses of film disturbed by fluctuations due to lateral vibrations differ from the thicknesses acquired under the corresponding steady state conditions. Hence, the thicknesses affected by the vibrations cannot be directly estimated from the usual film thickness predictions.
- Rheological differences of lubricants can cause very diverse distributions of film thickness under identical conditions of lateral vibrations. Numerous sharp slumps can take place in the central film thickness for high-molecular weight lubricants.
- The relative central film deviations  $H_{dev}$  grow with the increase in the lateral component of entrainment speed  $u_{ey'}$  or frequency of vibrations. This is caused by combinations of entrained thin films of horseshoe-shaped EHL constrictions, low-thickness stripes formed within the central area of the contact, and thick crescent-shaped films generated at the contact inlet due to the squeeze action. These effects, and thus  $H_{dev}$ , are reduced by the increase in the main rolling (entrainment) speed  $u_{ex}$ .
- The impacts of entrainment speeds  $u_{ex}$  and  $u_{ey'}$  on the relative mean thickness  $H_{mean}$  and film deviations  $H_{dev}$  are inverse. Dependencies of  $H_{dev}$  and  $H_{mean}$  with respect to these speeds are exponential.
- The rate of vibrations expressed by means of the entrainment speeds ratio  $U_{y/x}$  is a suitable parameter for the evaluation of the effects of lateral vibrations with combined kinematics on EHL films. This approach leads to comparable results for different lubricants considering the reference thicknesses  $h_{c,ref}$ . On the contrary, the stroke ratio  $S/D$ , which represents a relative degree of displacement, is appropriate only for the assessment of EHL films under reciprocating movement with less complex kinematics.
- The reduction in the relative mean thickness  $H_{mean}$  along with the increase in  $U_{y/x}$  is in accordance with the relationship  $H_{mean} = \exp(-0.29U_{y/x})$  representing the transition between EHL under pure rolling steady state conditions ( $U_{y/x} \rightarrow 0$ ) and EHL under pure sliding reciprocating motion ( $U_{y/x} \rightarrow \infty$ ). The thresholds for a local film breakdown and film collapse were found.
- To maintain a stable load-carrying capacity of EHL film, the relative positive  $H_{dev}^{(+)}$  and negative  $H_{dev}^{(-)}$  film deviations, which grow exponentially with the increase in  $U_{y/x}$ , are equal up to the point of film failure.

#### Acknowledgement

This work was supported by the Czech Science Foundation (Project No. 17-23235S).

$$h_c = p_{00} + p_{10}\Sigma + p_{01}u_e + p_{20}\Sigma^2 + p_{11}\Sigma u_e + p_{02}u_e^2 + p_{30}\Sigma^3 + p_{21}\Sigma^2 u_e + p_{12}\Sigma u_e^2 + p_{03}u_e^3, \tag{A.1}$$

where the polynomial coefficients  $p$  are defined in Tab. A1 for the relevant conditions in the range of  $\Sigma$  0 to  $-2$ .

Each set of the polynomial coefficients was determined by fitting 50 measured values of film thickness evenly distributed over a given range of conditions using the cubic surface model. To calculate the reference film thickness  $h_{c,ref}$  for non-steady state conditions, the mean values of slide-to-roll ratio  $\Sigma_{mean}$  and entrainment speed  $u_{e,mean}$  achieved over one stroke are used in the formula (A.1) instead of  $\Sigma$  and  $u_e$ , respectively.

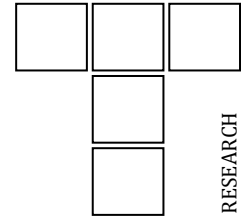
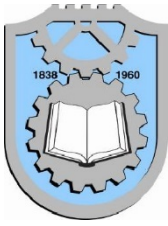
**Table A.1**  
Values of polynomial coefficients in formula (A.1) at lubricant temperature of 40 °C.

Lubricant	CAS			R560/88				SQ + PIP			PGLY	
	Range of $u_e$ (m/s)			0.005 to 0.1				0.05 to 0.6			0.005 to 0.1	
Load (N)	20	45	144	58	75	130	144	45	75	144	75	144
$p_{00}$	45.433	40.907	36.706	44.069	29.696	43.529	29.382	18.978	12.157	12.52	180.37	173.84
$p_{10}$	7.9617	0.4343	8.351	20.915	13.886	10.635	14.278	5.9866	-4.458	9.4994	39.123	43.494
$p_{01}$	1890.3	1772.3	1318.5	9161.3	10 163	7767.3	8659.2	472.38	512.86	470.81	14 664	11 390
$p_{20}$	8.7884	2.2880	0.3147	29.045	21.541	14.033	21.015	-6.019	-12.57	-0.332	-53.26	-43.55
$p_{11}$	29.127	81.334	-88.77	1675.2	1901.6	732.14	1392.6	-91.22	-23.55	-56.09	4080.1	2566.3
$p_{02}$	-3333	-2651	-1776	-47499	-69095	-40571	-50015	-464.4	-473.7	-649.9	-157 120	-118 984
$p_{30}$	2.3696	0.9252	-0.854	13.297	10.522	8.2660	9.7807	-2.887	-4.164	-0.42	-18.63	-16.57
$p_{21}$	-28.72	-24.01	-51.33	-92.62	-170.5	-268.5	-292.9	-28.16	-9.8	-12.86	329.39	-184.6
$p_{12}$	92.156	-82.22	353.63	-1806	-2761	5249.1	-2411	203.79	149.30	175.3	-15588	-15141
$p_{03}$	4121	2080.2	2787.7	199 261	328 186	237 007	219 992	480.31	323.07	685.13	708 834	522 176

**References**

[1] Cameron A. Righting a 40-year-old wrong. *Tribol Int* 1985;18:92.  
 [2] Walters CT. Dynamics of ball bearings. *J Lubr Technol* 1971;93:1–10.  
 [3] Gupta PK. Dynamics of rolling-element bearings .3. Ball-bearing analysis. *J Lubric Tech-T Asme* 1979;101:312–8.  
 [4] Meeks CR, Ng KO. The dynamics of ball separators in ball-bearings .1. *Anal Asle Trans* 1985;28:277–87.  
 [5] Stacke LE, Fritzon D. Dynamic behaviour of rolling bearings: simulations and experiments. *Proc Inst Mech Eng Part J-J Eng Tribol* 2001;215:499–508.  
 [6] Xi H, Wang HY, Han W, Le Y, Xu H, Chen W, et al. Contact trajectory of angular contact ball bearings under dynamic operating condition. *Tribol Int* 2016;104: 247–62.  
 [7] Gomez JL, Bourdon A, Andre H, Remond D. Modelling deep groove ball bearing localized defects inducing instantaneous angular speed variations. *Tribol Int* 2016; 98:270–81.  
 [8] Houpert L. CAGEDYN: a contribution to roller bearing dynamic calculations Part I: basic tribology concepts. *Tribol T* 2010;53:1–9.  
 [9] Houpert L. CAGEDYN: a contribution to roller bearing dynamic calculations Part II: description of the numerical tool and its outputs. *Tribol T* 2010;53:10–21.  
 [10] Houpert L. CAGEDYN: a contribution to roller bearing dynamic calculations. Part III: experimental validation. *Tribol T* 2010;53:848–59.  
 [11] Dong GH, Liu Y, Jing MQ, Wang FT, Liu H. Effect of elastohydrodynamic lubrication on the dynamic analysis of ball bearing. *Proc Inst Mech Eng Part K-J Multi-Body Dyn* 2016;230:134–46.  
 [12] Komba EH, Massi F, Bouscharain N, Le Jeune G, Berthier Y, Maheo Y. Experimental damage analysis in high loaded oscillating bearings. *Tribol Int* 2016;102:507–15.  
 [13] Haviez L, Fouvry S, Yantio G. Investigation of grease behavior under simple and complex displacement amplitudes conditions. *Tribol Int* 2016;100:186–94.  
 [14] Christensen H. Oil film in a closing gap. *Proc R Soc Lon Ser-A* 1962;266:312–28.  
 [15] Dowson D, Jones DA. Lubricant entrapment between approaching elastic solids. *Nature* 1967;214:947–8.  
 [16] Conway HD, Lee HC. Impact of a lubricated surface by a sphere. *J Lubric Tech-T Asme* 1975;97:613–5.  
 [17] Safa MMA, Gohar R. Pressure distribution under a ball impacting a thin lubricant layer. *J Tribol-Trans Asme* 1986;108:372–6.  
 [18] Dowson D, Wang DC. An analysis of the normal bouncing of a solid elastic ball on an oily plate. *Wear* 1994;179:29–37.  
 [19] Larsson R, Hoglund E. Elastohydrodynamic lubrication at impact loading. *J Tribol-Trans Asme* 1994;116:770–6.  
 [20] Larsson R, Hoglund E. Numerical-simulation of a ball impacting and rebounding a lubricated surface. *J Tribol-Trans Asme* 1995;117:94–102.  
 [21] Kaneta M. For the establishment of a new EHL theory. *Lubr A. T Front* 1999;36: 25–36.  
 [22] Glovnea RP, Spikes HA. The influence of lubricant upon EHD film behavior during sudden halting of motion. *Tribol T* 2000;43:731–9.  
 [23] Nishikawa H, Kaneta M. Traction in Ehl under pure sliding reciprocation with cyclic impact loading. *Jsm Int J Ser C-Dyn Contr Robot Des Manuf* 1995;38:568–76.  
 [24] Glovnea RP, Spikes HA. Behavior of EHD films during reversal of entrainment in cyclically accelerated/decelerated motion. *Tribol T* 2002;45:177–84.  
 [25] Wang J, Meng XH, Wang SS, Zou Q. Grease film variation in reciprocating sliding motion. *Tribol Int* 2017;114:373–88.  
 [26] Kaneta M, Nishikawa H, Kameishi K. Observation of wall slip in elastohydrodynamic lubrication. *J Tribol-Trans Asme* 1990;112:447–52.  
 [27] Plint MA. Third paper: traction in elastohydrodynamic contacts. *Proc Inst Mech Eng* 1967;182:300–6.  
 [28] Ehret P, Dowson D, Taylor CM. On lubricant transport conditions in elastohydrodynamic conjunctions. *P Roy Soc a-Math Phy* 1998;454:763–87.  
 [29] Ehret P, Dowson D, Taylor CN. Transient EHL solutions with interfacial slip. *J Tribol-Trans Asme* 1999;121:703–10.  
 [30] Li G, Zhang CH, Xu HY, Luo JB, Liu SH. The film behaviors of grease in point contact during microoscillation. *Tribol Lett* 2010;38:259–66.  
 [31] Sugimura J, Jones WR, Spikes HA. EHD film thickness in non-steady state contacts. *J Tribol-Trans Asme* 1998;120:442–52.  
 [32] Sugimura J. Elastohydrodynamic lubrication films in non-steady state conditions. *J Jpn Soc Tribol* 2002;47:752–7.  
 [33] Glovnea RP, Spikes HA. Elastohydrodynamic film formation at the start-up of the motion. *Proc Inst Mech Eng Part J-J Eng Tribol* 2001;215:125–38.  
 [34] Glovnea RP, Spikes HA. Elastohydrodynamic film collapse during rapid deceleration: Part I - experimental results. *J Tribol-Trans Asme* 2001;123:254–61.  
 [35] Glovnea RP, Spikes HA. Elastohydrodynamic film collapse during rapid deceleration: Part II - theoretical analysis and comparison of theory and experiment. *J Tribol-Trans Asme* 2001;123:262–7.  
 [36] Glovnea RP, Spikes HA. The influence of lubricant properties on EHD film thickness in variable speed conditions. *Transient Process Tribol* 2004;43:401–8.  
 [37] Nishikawa H, Handa K, Kaneta M. Behavior of Ehl films in reciprocating motion. *Jsm Int J Ser C-Dyn Contr Robot Des Manuf* 1995;38:558–67.  
 [38] Kaneta M, Nishikawa H. Experimental study on microelastohydrodynamic lubrication. *Proc Inst Mech Eng Part J-J Eng Tribol* 1999;213:371–81.  
 [39] Wang J, Hashimoto T, Nishikawa H, Kaneta M. Pure rolling elastohydrodynamic lubrication of short stroke reciprocating motion. *Tribol Int* 2005;38:1013–21.  
 [40] Stadler K, Izumi N, Morita T, Sugimura J, Piccigallo B. Estimation of cavity length in EHL rolling point contact. *J Tribol-Trans Asme* 2008:130.  
 [41] van Emden E, Venner CH, Morales-Espejel GE. Aspects of flow and cavitation around an EHL contact. *Tribol Int* 2016;95:435–48.  
 [42] van Emden E, Venner CH, Morales-Espejel GE. A challenge to cavitation modeling in the outlet flow of an EHL contact. *Tribol Int* 2016;102:275–86.  
 [43] Maruyama T, Saitoh T. Oil film behavior under minute vibrating conditions in EHL point contacts. *Tribol Int* 2010;43:1279–86.  
 [44] Sperka P, Wang J, Krupka I, Hartl M, Kaneta M. Occurrence of high pressure spike in unidirectional start-stop-start point contacts. *J Tribol-Trans Asme* 2014:136.  
 [45] Nagata Y, Kalogiannis K, Glovnea R. Track replenishment by lateral vibrations in grease-lubricated EHD contacts. *Tribol T* 2012;55:91–8.  
 [46] Kalogiannis K. Behaviour of elastohydrodynamic films subjected to oscillatory motion. Doctoral thesis. Brighton: University of Sussex; 2013.  
 [47] Hartl M, Krupka I, Liska M. Differential colorimetry: tool for evaluation of chromatic interference patterns. *Optice* 1997;36:2384–91.  
 [48] Hartl M, Krupka I, Poliscuk R, Liska M, Molimard J, Querry M, et al. Thin film colorimetric interferometry. *Tribol T* 2001;44:270–6.  
 [49] Bair S. Reference liquids for quantitative elastohydrodynamics: selection and rheological characterization. *Tribol Lett* 2006;22:197–206.  
 [50] Omasta M, Krupka I, Hartl M. Effect of surface velocity directions on elastohydrodynamic film shape. *Tribol T* 2013;56:301–9.  
 [51] Stahl K, Michaelis K, Mayer J, Weigl A, Lohner T, Omasta M, et al. Theoretical and experimental investigations on EHL point contacts with different entrainment velocity directions. *Tribol T* 2013;56:728–38.  
 [52] Omasta M, Krupka I, Hartl M. Effect of sliding direction on EHL film shape under high sliding conditions. *Tribol T* 2017;60:87–94.

- [53] Sakamoto M, Nishikawa H, Kaneta M. Behaviour of point contact EHL films under pulsating loads. *Transient Process Tribol* 2004;43:391–9.
- [54] Qu SY, Yang PR, Guo F. Theoretical investigation on the dimple occurrence in the thermal EHL of simple sliding steel-glass circular contacts. *Tribol Int* 2000;33: 59–65.
- [55] Yang P, Qu S, Kaneta M, Nishikawa H. Formation of steady dimples in point TEHL contacts. *J Tribol-Trans Asme* 2001;123:42–9.
- [56] Yang PR, Kaneta M. Multi-dimple phenomena in TEHL point contacts. *Sci China Ser B* 2002;45:127–34.
- [57] Zhang JJ, Yang PR, Wang J, Guo F. The effect of an oscillatory entrainment velocity on the film thickness in thermal EHL point contact. *Tribol Int* 2015;90:519–32.
- [58] Fryza J, Sperka P, Kaneta M, Krupka I, Hartl M. Effects of lubricant rheology and impact speed on EHL film thickness at pure squeeze action. *Tribol Int* 2017;106: 1–9.



# Frictional Response of Lubricant in EHL Contact under Transient Bi-directional Shear Loading

J. Fryza<sup>a</sup>, P. Sperka<sup>a</sup>, I. Krupka<sup>a</sup>, M. Hartl<sup>a</sup>

<sup>a</sup>Brno University of Technology, Technická 2896/2 Brno, Czech Republic.

## Keywords:

Elastohydrodynamic lubrication  
Friction  
Shear flow  
Non-steady state  
Limiting shear stress

## ABSTRACT

Consideration of performance, efficiency and energy consumption is nowadays an inherent part of the design of every modern machine. These factors are mainly determined by mechanisms taking place within the lubricated contacts. Unfortunately, the physical origins of these mechanisms have been investigated exclusively for steady conditions that do not occur in actual contacts of machines affected by vibrations. This study presents novel experimental data describing friction in the elastohydrodynamically lubricated contact exposed to the main steady sliding motion along with lateral-sliding micro-oscillations. Friction forces were measured simultaneously in two perpendicular directions of point contact. It is shown that the lubricant response in the main direction of motion suffers from shear-thinning and thermal effects whereas its lateral response is isothermal Newtonian. Moreover, the lateral friction affects the friction in the main direction, but not vice versa, when the majority of shear flow is maintained in this main direction. These findings are attributed to the perturbation of structural arrangement of lubricant. The results also suggest that a response of mineral oils to shearing is anisotropic. A limiting shear stress is discussed since the total friction was not able to exceed a certain value.

## Corresponding author:

Josef Fryza  
Brno University of Technology,  
Technická 2896/2 Brno,  
Czech Republic.  
E-mail: fryza@fme.vutbr.cz

© 2017 Published by Faculty of Engineering

## 1. INTRODUCTION

Since many of the elastohydrodynamically lubricated (EHL) contacts work under transient conditions or are subjected to vibrations, there is presently a need to consider more realistic operating conditions in theoretical/numerical and experimental studies dealing with the lubrication mechanisms. These counterformal contacts can be found in the applications of rolling element bearings, gears, cams and

followers, constant velocity joints, traction drives, continuously variable transmissions, ball screws, etc. The presence of sliding motions and subsequently the unsteady shear loading of lubricant is typical for such EHL conjunctions. Unfortunately, even today, the overwhelming majority of studies continue to focus on steady state conditions despite the fact that, during the last few years, there has been a sufficient progress in the predictions of both the EHL film thickness and the friction/traction. In certain

limits, the steady state solutions are sensible approximations. On the other hand, the investigation of transient conditions can be a way to build on these frequently used and often nearly exhausted approaches and to introduce a new and more realistic perspective on the behaviour of EHL interfaces. This should be done mainly via an experimental approach, as this is the manner how to ultimately prove or refute phenomena and hypotheses, while the theoretical/numerical solutions should serve primarily to explain and generalize these findings.

The efficiency, energy consumption, and performance of machines are directly associated with their contact frictional responses. The changes in EHL friction depending on a sliding speed were shown in 1960s via disc machine measurements [1] where the first traction curves were obtained. The limit of shear stress in lubricant (limiting shear stress  $\tau_{lim}$ ) was speculated by Smith [2] and confirmed by Plint [3] and other followers. Then, several entire decades have been devoted to investigation and clarification of the effects impacting friction, viscosity and other rheological parameters of lubricants, such as the effects of surface roughness, thermo-physical properties, temperature, pressure, density, shear stress, shear strain, strain rate, molecular structure, etc. The knowledge of these effects has been used to establish more general and physics-based models of rheological flow curve (rheological models) for EHL predictions.

It is well known from the previous studies that the four regimes of traction curves can be obtained and distinguished regarding to the contact conditions: linear viscous, non-linear viscous, plateau, and thermal. An excellent quantitative description of these friction regimes for mineral oil can be found by the interested reader in the numerical results [4] based on measured rheological data [5].

The experimental studies referring to the non-steady state conditions began to emerge mostly during the 1990s. However, a majority of these studies deal with the film thickness rather than friction. Some exceptions are listed below. The relation of the transient sliding speed to friction was studied by Hess and Soom [6] on a disc machine, where the speed of the disc was varied at constant acceleration and deceleration

for different frequencies of oscillations. These authors pointed out that the size of obtained friction loops increases with the increase in the frequency or viscosity of oil with respect to speed. Moreover, the constant time delay was observed between the minimum speed and the maximum friction. This time delay was independent of speed and was influenced by load and viscosity. The transient frictional response described above was attributed to combined entraining and squeeze film action. This experimental study has been a basis for several theoretical friction models [7-10]. Unfortunately, a large part of these results was obtained for the boundary and mixed regimes of lubrication, rather than for the EHL regime.

Nishikawa and Kaneta [11] showed that the effect of EHL squeeze action can reduce the friction and surface damage during the short-stroke sliding reciprocation as the oil is entrapped by the cyclic impact loads, when the contact suffers from starvation [12] without these impact loadings; especially at short stroke lengths. The effect of impact speed on the film shape and thickness of the entrapped lubricant has recently been described in [13]. For sliding oscillations, the oil did not behave like a viscous fluid as friction was almost the same regardless of the differences in sliding speed [14]. A reduction in friction due to the transversely oriented bump, which probably introduced a small amount of oil during its entry into the point contact, was reported in [15] for the similar conditions.

A significant effect of heating by shearing of the lubricant film was demonstrated via the ball-on-disc simulator during a variation in the slip ratio [16]. The resulting calculations were focused on the design of traction drives. Later, series of experiments on the ball-on-disc apparatus were carried out by Bassani and Ciulli et al. [17]. First, an evaluation methodology was developed and the previously published results by Hess and Soom [6] were confirmed. After that, the effect of both the thermal properties of the contact bodies and the slide-to-roll ratio (sliding speed divided by mean speed of contact surfaces; SRR in short) on the friction was investigated [18]. It was shown that the temperature-viscosity wedge phenomenon (caused by variation of viscosity and temperature through the film thickness [19])

together with the squeeze action can significantly affect the friction according to SRR and the differences in the thermal properties. Also, the squeeze effect was more pronounced at high frequencies and was possibly reduced by the value of SRR. Accordingly, friction decreased faster when the body with a lower thermal conductivity (glass disc) was running faster than the body with a higher thermal conductivity (steel ball) [20,21].

A free sliding oscillating motion was used in [22] to establish a friction law in relation to the operating conditions and rheology of pressurized lubricants. A friction force was not measured directly at the contact interface, but it was estimated from the energy dissipation. The overall dissipation was attributed to viscous damping at the area around the EHL contact, as the pin was passing through the layer of lubricant during reciprocation, and to the friction within the EHL contact. It was admitted that the friction characteristic should be significantly affected by a periodic variation of the lubricant film distribution within the contact and a lubricant piezoviscosity should be taken into account under such conditions. A corresponding numerical model [23] has been developed for the frictional responses obtained on the relaxation tribometer used in [22]. A good agreement between the experimental and numerical data was achieved. Moreover, it was pointed out that thanks to this oscillatory approach it is possible to measure very low values of friction with the "unsurpassed" accuracy of the coefficient of friction of  $\pm 0.0002$ . Friction was recently measured simultaneously with the film thickness of the lubricant at transient kinematics from the boundary up to the full-film lubrication regimes [24]. The total friction was given by the contributions of sub-contact areas of different film thicknesses. Also, the formation of friction loops and the squeeze action were observed for high frequencies and long stroke lengths [25].

From the foregoing outline of unsteady friction studies, it is evident that these studies bring new insights into the behaviour of EHL interfaces. On the other hand, the conditions used in the above-mentioned experiments, albeit transient, are still very distant from the real ones. Often, low pressures are used, and the transient movement is always performed in only one direction of contact.

The influence of vibrations that are present in every EHL contact during any machine operation is thus completely omitted. It is still far from clear what the frictional response of high-pressurized lubricant in the actual EHL contacts is, and where the omnidirectional vibrations occur. Being aware of various limitations and deviations from the actual conditions, this work can be a starting point for future investigations of such EHL contacts. For this reason, the present study should not be seen as a completed analysis, but rather as its introductory part. In this study, a sliding EHL contact is subjected to lateral-sliding micro-oscillations in order to examine the frictional response simultaneously in both the main and lateral directions of contact and to evaluate these increments with respect to the total friction of the contact and to the friction under corresponding steady state conditions. The lubricant rheology is considered.

## **2. MATERIALS AND METHODS**

### **2.1 Experimental apparatus**

The experimental apparatus used in this study for friction measurements is a modified ball-on-disc apparatus. The original ball-on-disc apparatus was designed primarily for direct observation and measurement of film thickness in the EHL contacts via the thin film colorimetric interferometry technique (TFCI) [26,27]. The accuracy of film thickness measurement by TFCI is higher than 1 nm. In the related study [28], the apparatus was used to reveal the influence of lateral vibrations on film thickness.

Figure 1a illustrates a schematic view of the modified mechanical part of the apparatus, where a relative motion between the rolling element (ball) and the flat transparent window allows a formation of the EHL film separating the contact surfaces. The point contact was loaded through the window employing a lever mechanism with a dead weight (see [28] for more details). The ball of 25.4 mm diameter was made of bearing steel (100Cr6) and polished to the average surface roughness  $R_a$  of less than 7 nm. A transparent 3 mm thick window was coated with 10 nm thick semi-reflective layer of chromium with the aim to apply the TFCI technique for measurement of film thickness and determination of the normal load. The

contact surface of the chromium layer is considered to be optically smooth. Normal loads  $F_N$  and contact pressures  $p_h$  were quantified by the static contacts from the comparison of the deformed shapes of contact bodies obtained by TFCI and calculated from the Hertz theory.

The window was fixed in the compliant mechanism with flexure hinges and a rotational motion of the ball was controlled by a close-loop servo drive. It means that a pure sliding motion was applied in the main direction of contact  $x$  (see Fig. 1b). At the same time, a cam mechanism moved harmonically the ball in the lateral direction of contact  $y$ , which resulted in transient bi-directional shearing of lubricant. A lateral position of the ball was measured with a non-contact displacement transducer with dynamic resolution of 20 nm and the sampling frequency of 10 kHz. The same sampling frequency was used for measuring of friction forces  $F_{Tx}$  and  $F_{Ty}$  acting in the main  $x$  and the lateral  $y$  direction of contact, respectively. All quantitative data were simultaneously recorded at the time intervals of one second. Friction forces were transferred from the contact through the flexible structure and the connecting rods to the precise load sensors. This design enables the friction forces to be measured simultaneously in both directions of the lubricated contact.

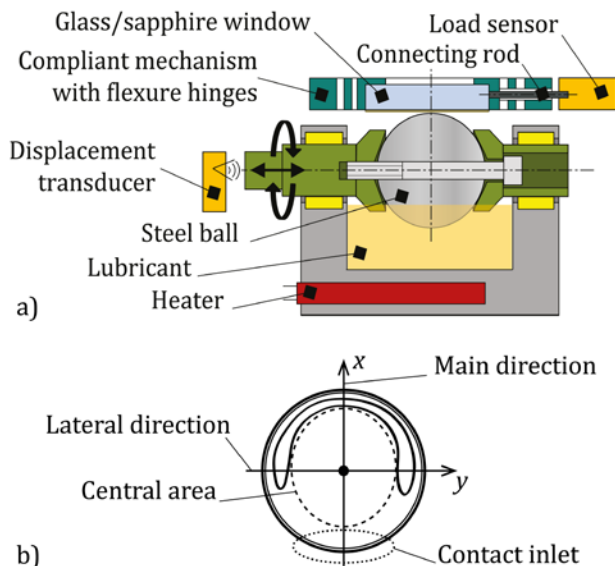


**Fig. 1.** (a) Schematic representation of experimental apparatus and (b) EHL point contact.

The forces are subsequently used to calculate the coefficient of friction (CoF) according to the following formulas:

$$\mu_x = F_{Tx}/F_N, \mu_y = F_{Ty}/F_N \quad (1)$$

Similar expressions can be used for the estimation of mean shear stress  $\bar{\tau}$  acting over the contact area at mean contact pressure  $\bar{p}$ :

$$\bar{\tau}_x = \mu_x \bar{p}, \bar{\tau}_y = \mu_y \bar{p} \quad (2)$$

A measurable range of CoF in both directions is from  $\mu = 0.005$  to  $\mu = 0.2$  with uncertainty of CoF under 0.0005. The photograph of the above described system is shown in Fig. 2.

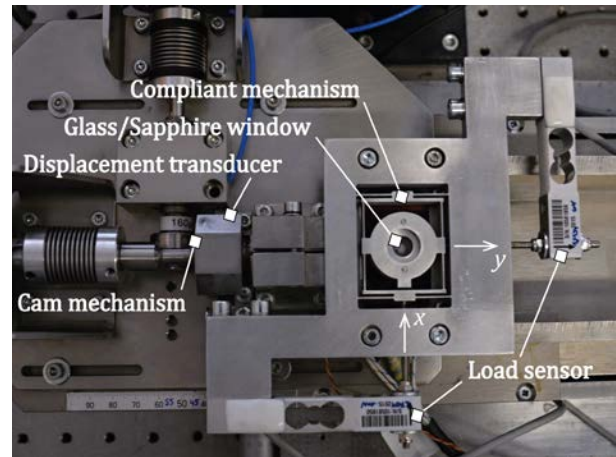


**Fig. 2.** Mechanical part of experimental apparatus with indicated directions  $x$  and  $y$ .

## 2.2 Experimental conditions

Combinations of two loads  $F_N$  and two material configurations were employed to achieve various maximum contact pressures  $p_h$  and Hertzian contact diameters  $d$ . A contact was created between the 100Cr6 steel ball and the N-BK7 glass or sapphire window. The resulting values of  $p_h$  and  $d$  are listed in Table 1. Please note that almost the same contact diameter (area) is achieved for the highest and the lowest pressure.

**Table 1.** Hertz contact conditions.

Material of window	$F_N$ (N)	$p_h$ (GPa)	$d$ ( $\mu\text{m}$ )
N-BK7 glass	35	0.53	357
N-BK7 glass	89	0.72	487
Al <sub>2</sub> O <sub>3</sub> (sapphire)	89	1.32	358

In the course of measurements, the sliding speed in the main direction of contact  $u_x$  was kept fixed at 0.1 m/s. This relatively low speed was applied to reduce the impacts of inlet shear heating, bulk heating and other associated thermal effects on the EHL contact, which are significant at high sliding

speeds. A lateral sliding motion was performed for different combinations of frequencies and stroke lengths. The frequency  $f$  ranged from 30 to 100 Hz and the stroke length  $s$  was in the range from 30 to 220  $\mu\text{m}$ . If these stroke lengths are compared with the contact diameters given in Table 1, then it is clear that the stroke ratio  $S/D$  is lower than one. It means that only micro-oscillations were used in this study. The  $S/D$  ratio varies from 0.06 to 0.62. A total of 96 measurements were performed under individual contact / kinematic conditions. These conditions allow to apply short-stroke oscillations with  $S/D < 1$ , but at the same time they prevent the starvation observed in [11,14,15] under sliding reciprocation.

All experiments were carried out at a lubricant temperature of  $40\text{ }^\circ\text{C} \pm 0.5\text{ }^\circ\text{C}$ . The temperature of lubricant was measured close to the contact inlet with a thermocouple and maintained by a single loop temperature controller. The lubricant was heated through an oil cup via cartridge heaters. Considering low speeds used in the experiments, a bright stock (BS) mineral oil was chosen as the lubricant. This oil is usually employed in low-speed applications such as marine engine oils, cylinder lubes, and gear oils, where a high viscosity is desired. The ambient viscosity and the pressure-viscosity coefficient of BS at  $40\text{ }^\circ\text{C}$  are  $0.329\text{ Pa}\cdot\text{s}$  and  $19.03\text{ GPa}$ , respectively. The same BS oil has been frequently used by Kaneta and Nishikawa in their studies on dynamic motions [11,14,15].

### 2.3 Determination of variables

Since the frictional response of lubricant is assessed in relation to the kinematic variables such as position or speed, it should be mentioned how the values of these variables were obtained. Figure 3 shows a relative displacement between the surfaces of the ball and the window in the lateral direction of contact  $s_y$ . This displacement is defined as the distance of instantaneous position of the ball  $s_{by}$  relative to the instantaneous position of the window  $s_{wy}$ ; accordingly:

$$s_y = s_{by} - s_{wy} \quad (3)$$

The lateral position of the ball  $s_{by}$  is driven by the cam mechanism and is measured with a displacement transducer, as mentioned above. Due to the friction forces acting on the compliant mechanism, to which the window is

attached, the window changes its relative position  $s_{wy}$ . The instantaneous position  $s_{wy}$  is determined considering the force  $F_{Ty}$  and the stiffness of the measuring system  $k$ , which includes a flexible structure, connecting rods, and force sensors, as follows:

$$s_{wy} = F_{Ty}/k \quad (4)$$

The stiffness  $k$  of  $0.165\text{ N}/\mu\text{m}$  was estimated during the system design using the finite element analysis (FEA) and subsequently confirmed on the experimental apparatus by direct observations of changes in the position of the window. In the final consequence, the change in the relative position  $s_y$  over time is not only determined by the excitation mechanism of vibrations, but it is also dependent on the frictional response of the lubricant. The central (mean) point, around which the resulting relative motion oscillates, was chosen as the reference point for the position  $s_y$ .

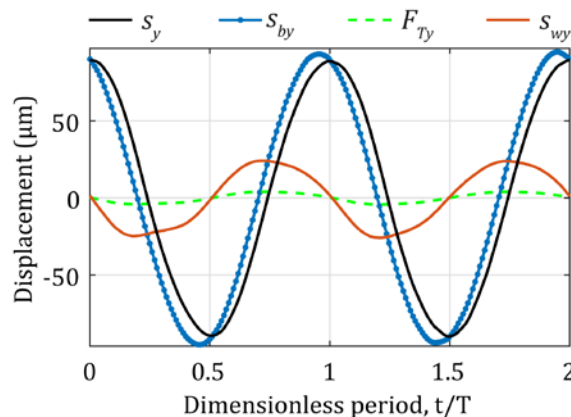


Fig. 3. Relative displacement between contact surfaces.

The lateral sliding speed  $u_y$  is then estimated based on the numerical derivation of  $s_y$  with respect to the sampling time. The results of the derivation are further filtered via the fast Fourier transform (FFT) and its inverse (IFFT) algorithms to eliminate numerical errors. The data in the frequency domain, the frequency of which is close to the number of data points, are removed from  $u_y$ .

## 3. RESULTS AND DISCUSION

### 3.1 Uni-directional shear loading

The BS lubricant was first subjected to shearing only in the main direction of contact. The sliding

speeds from 0.01 m/s to 0.5 m/s were used together with different contact pressures and material configurations. The central film thickness  $h_c$  was measured to ensure that EHL conditions were attained. The film thickness ranged from 25 up to 375 nm for given sliding speeds and contact pressures, as it is illustrated in Fig. 4. The EHL regime was confirmed by means of the minimum value of the lambda ratio  $\lambda$  exceeding 3.5 (full-film lubrication corresponds to  $\lambda > 3$ ) according to the composite surface roughness of the contacting surfaces  $R_{1,2}$ :

$$\lambda = h_c / \sqrt{R_1^2 + R_2^2} \quad (5)$$

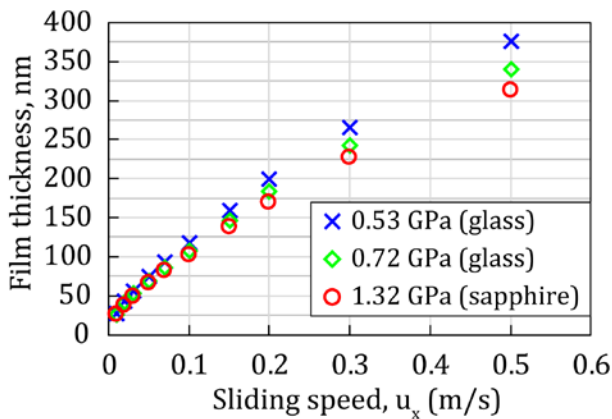


Fig. 4. Central film thickness of BS oil under pure sliding conditions.

Corresponding CoF in the main direction  $\mu_x$  is illustrated in Fig. 5. CoF in the lateral direction of contact  $\mu_y$  was at the level of signal noise under these conditions. Therefore, CoF  $\mu_x$  can be considered as the overall frictional response  $\mu$ . These values of CoF are used below for the comparison with CoF obtained under bi-directional shearing of lubricant. From Fig. 5 it can be seen that CoF decreases with the increase in the sliding speed for all pressures. However, an opposite trend could be expected with respect to a general trend of Stribeck-Hersey curve, as the full-film lubrication is considered where friction (traction) increases with the increase in the relative speed of contact surfaces due to viscous shearing of lubricant. These results indicate the influences of shear thinning and/or in-contact shear heating of lubricant. The obtained traction curves in Fig. 5 then belong to the thermal regime of EHL traction where the thermal effects on lubricant take place.

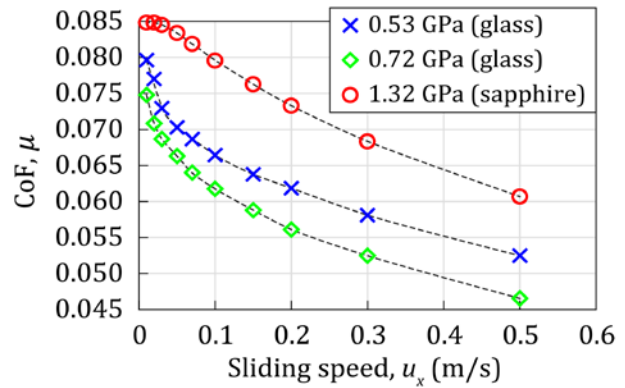


Fig. 5. Frictional response of BS to pure sliding in the main direction of contact.

Just like in the case of speed, friction should be higher for higher contact pressures due to the increase in lubricant viscosity. This did not occur at material configuration of steel ball - glass window probably due to more pronounced thermal effects at higher pressure of 0.72 GPa than at 0.53 GPa. To be true, the effects of heating and shear thinning of BS oil on the reduction of its viscosity and film thickness would have to be greater than the effect of pressure on the increase in BS viscosity.

When the sapphire window is used instead of glass, a significantly higher friction is obtained. This is due to a considerable higher viscosity of lubricant resulting from the contact pressure. It should be noted that the thermal properties of sapphire are closer to the properties of steel than in the case of glass properties. Heat can thus accumulate more at the surface of glass than at the surface of sapphire window, thereby raising the temperature and affecting the viscosity of the lubricant.

### 3.2 Bi-directional shear loading - friction in the lateral direction of contact

Consequently, the sliding EHL contact at  $u_x = 0.1$  m/s was exposed to the lateral-sliding oscillations of different stroke lengths and frequencies introducing the bi-directional shearing of BS lubricant. Fig. 6a shows the mechanical excitation of lubricant as a shear strain to which BS is experienced for four different stroke lengths at frequency of 60 Hz and pressure of 1.32 GPa. Accordingly, Fig. 6b represents CoF in the lateral direction of contact as the stress response to the excitation under such conditions.

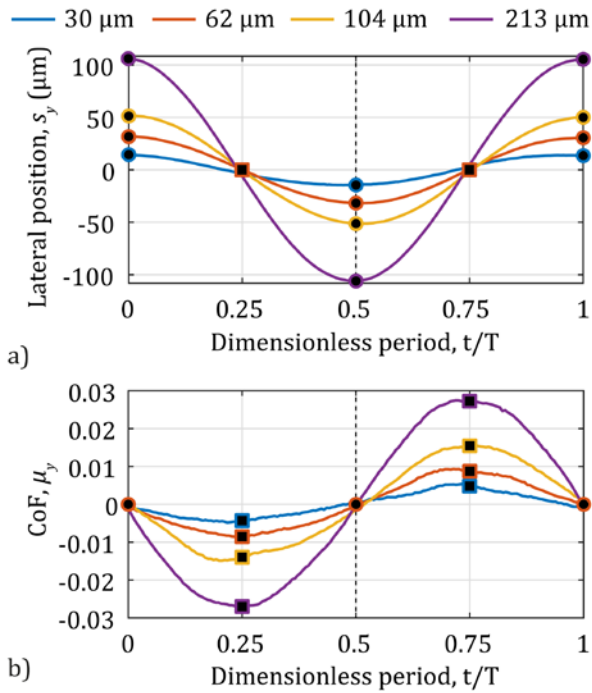


**Fig. 6.** a) Changes in lateral position, and b) CoF in lateral direction of contact during the cycle of oscillatory motions at  $f = 60$  Hz, and  $p_h = 1.32$  GPa for different stroke lengths.

If the corresponding excitations and responses of BS are compared at the ends of strokes (highlighted by circles in Fig. 6), then it can be seen that the friction is close to zero for different maximum positions at the ends of strokes. Similarly, various values of CoF were measured for the zero positions at the half-strokes (symbols of squares). This means that there is no significant dependence between CoF (stress) and the lateral position (strain). Therefore, a substantial viscoelastic behaviour of BS lubricant cannot be expected under these circumstances. The charts for other pressures, frequencies and stroke lengths are not listed in this article for better clarity, since these results were found to be very similar to those presented above.

The level of viscoelasticity can be quantified from the experimental data by evaluation of the phase shift  $\varphi$  between the excitation and the response of lubricant. The algorithm of Hilbert transform was applied to the data sequence in Matlab in order to obtain the phase information on the measured signals. The resulting phase shift  $\varphi$  for measurements under different combinations of kinematic and contact conditions is shown in Fig. 7. The error bars represent the standard deviation of the phase shift determination between the signals. The maximum lateral speed

$u_{y,max}$  achieved over the stroke is used on the horizontal axis of the graph to distinguish the individual kinematic conditions.

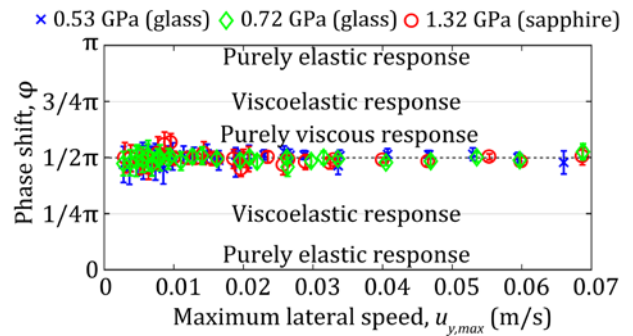


**Fig. 7.** Phase shift between the excitation and the response of BS lubricant to oscillatory shear stress in the lateral direction of contact.

Based on the phase shifts in Fig. 6 and 7, it is evident that the frictional response of BS is out of phase by  $\varphi \approx \pi/2$  from the strain for all tested conditions. These results point out to a nearly purely viscous behaviour without the influence of elasticity in the lateral direction of contact even at the highest pressure, when a purely elastic response would occur at  $\varphi = 0$  or  $\varphi = \pi$ .

When the cyclic variations of CoF and the lateral position are plotted against each other with respect to their phase shift, the Lissajous plots are obtained (see Fig. 8). Since the phase shift between these two variables is close to  $\pi/2$ , the curves (the Lissajous patterns) are in the shape of concentric ellipses for various stroke lengths and frequencies. Three successive cycles are shown for each condition. The Lissajous patterns are quite stable and they do not differ significantly for the individual oscillatory cycles over time. It is rather obvious that the frictional response in the lateral direction is then time-independent of the rheological point of view and without the consequence of thermal effects developed during the measurements. Moreover, the Lissajous patterns are symmetrical according to both axes, where the horizontal axis corresponds to the ends of strokes and the vertical axis to the maximum speeds over the cycle. Therefore, finally, the applied frequency or stroke length are not important; the only important parameter (in the context of these conditions for the frictional response in this direction of contact) is the resulting lateral speed.

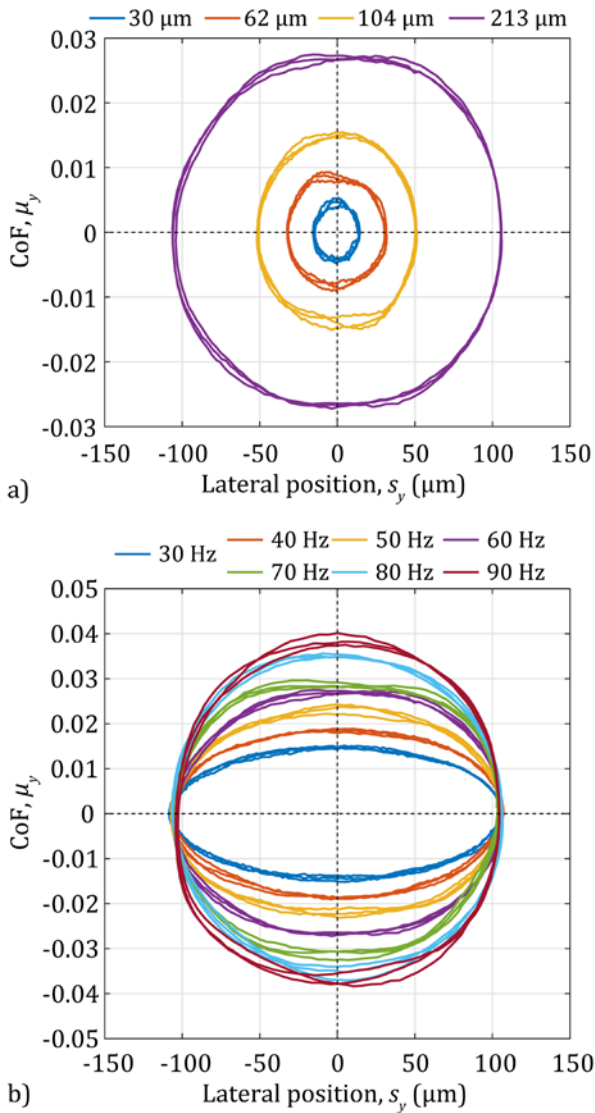


**Fig. 8.** Lissajous plots showing viscous behaviour of BS at  $p_h = 1.32$  GPa; a) for different stroke lengths and  $f = 60$  Hz; b) for  $s = 213$   $\mu\text{m}$  and different frequencies.

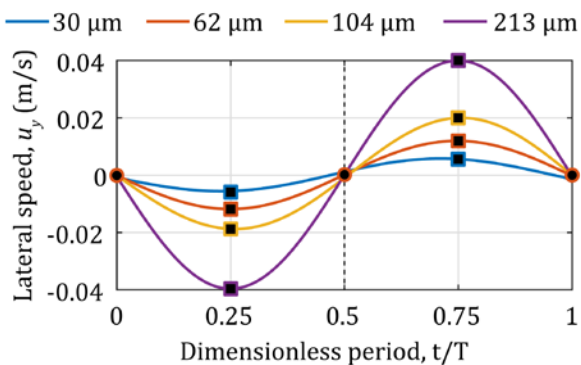


**Fig. 9.** Courses of lateral sliding speed during the cycle of oscillatory motions at  $f = 60$  Hz and  $p_h = 1.32$  GPa for different stroke lengths.

Subsequently, the lateral speed  $u_y$  can be considered as the excitation representing the rate of shear strain (shear strain rate) of BS

instead of the position  $s_y$ . Let us recall that the lateral sliding speed  $u_y$ , the course of which during the oscillation cycle is shown in Fig. 9, is given by the numerical derivation of position  $s_y$ . Due to derivation, the phase shift of  $\pi/2$  between  $s_y$  and  $u_y$  is obtained. Then, speed  $u_y$  and CoF  $\mu_y$  are in the phase, as is apparent from the comparison of Fig. 6b and Fig. 9.

To evaluate the influence of speed  $u_y$  on CoF  $\mu_y$ , the absolute values of their extrema (maximum and minimum) reached over the individual stroke periods (see the square symbols in Fig. 6b and Fig. 9) were taken into account from the record lasting 1 second. The mean values of these data points of  $u_y$  and  $\mu_y$  were assigned to each other with respect to the experimental conditions. The result is illustrated in Fig. 10, where the linear frictional response of BS can be seen in dependence on the sliding speed.

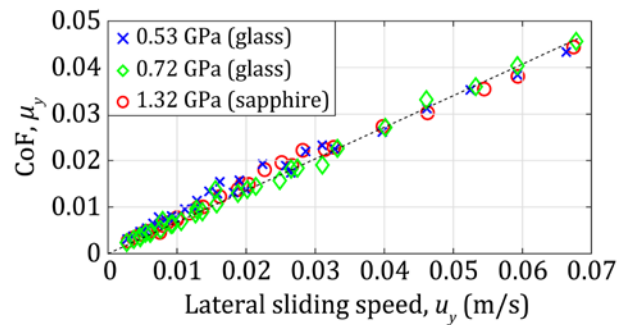


**Fig. 10.** Frictional response of BS lubricant in the lateral direction of contact under transient bi-directional shearing.

It is noteworthy that this frictional response is the very same for all contact pressures and even for all material configurations used in the experiments. A linear response is clearly not caused by elastic creep of contact bodies explained in [29], which may be mistakenly substituted for a viscous response at low values of SRR. For the current data, the shear stress is linearly proportional to the contact pressure; this proportionality is given by the value of CoF as in formula (2). In the light of these findings, the frictional response in the lateral direction of contact is very likely isothermal and Newtonian viscous, which is highly desirable for investigation of the rheological properties of lubricants under high pressure (mainly pressure-temperature-viscosity relationship usually analysed via high pressure viscometers). Both the isothermal and Newtonian behaviour is

very difficult to achieve for actual EHL contacts, especially for those exposed to high pressure and sliding conditions.

### 3.3 Comparison of uni- and bi-directional shear loading responses and total friction

The two different cases of frictional responses are compared to bring insight into the behaviour of CoF in the lateral direction of contact. The first case is the friction under pure sliding without vibrations, which is shown in Fig. 5, and the second one is the lateral friction under vibrations, as in the case of Fig. 10. As was explained above, if pure sliding is applied only in one direction of contact, the frictional response of lubricant naturally depends on the contact pressure and is reduced with the increase in the sliding speed because of shear thinning and shear heating. On the contrary, none of these effects was observed for  $\mu_y$  under vibrations, where the friction uniformly increased with the sliding speed.

An explanation for these substantial differences is as follows: when the lubricant is shear loaded only in the main direction of contact and this shearing is of sufficient magnitude and takes a sufficient time, then the structural arrangement of lubricant is changed with respect to the direction of shearing (flow). Since the BS lubricant is a mixture of different hydrocarbon chains with structures of various complexity, the shear stress about 1 to 5 MPa is needed to perturb or disrupt (align, stretch, deform, disintegrate) its chains and structures. The shear stress  $\bar{\tau}$  applied to the BS was significantly higher approximately of 20 up to 70 MPa at  $u_x = 0.1$  m/s for different pressures (see formula (2)), when the shear strain rate was about  $9 \cdot 10^5 \text{ s}^{-1}$  at the measured film thickness of  $110 \text{ nm} \pm 10 \text{ nm}$  (assuming that the velocity of lubricant flow is distributed linearly through the film thickness). Consequently, the non-Newtonian behaviour (shear-thinning) as the response to the applied stress, along with the thermal and pressure effects on the lubricant viscosity, was obtained in the main direction of contact.

However, when the BS lubricant affected by shearing in the main direction is additionally exposed to short-term shearing oscillations in the lateral direction, then it seems that only the isothermal Newtonian response can be observed in the lateral direction, because the other effects

are included in the response in the main direction. This linear response is probably given only by the perturbation of current structural arrangement of lubricant in the perpendicular direction to its main flow. The structure may be re-arranged after its unloading during oscillation cycles at the ends of stroke; therefore, this phenomenon can be repeated in subsequent cycles over and over again, as is evident from Fig. 8.

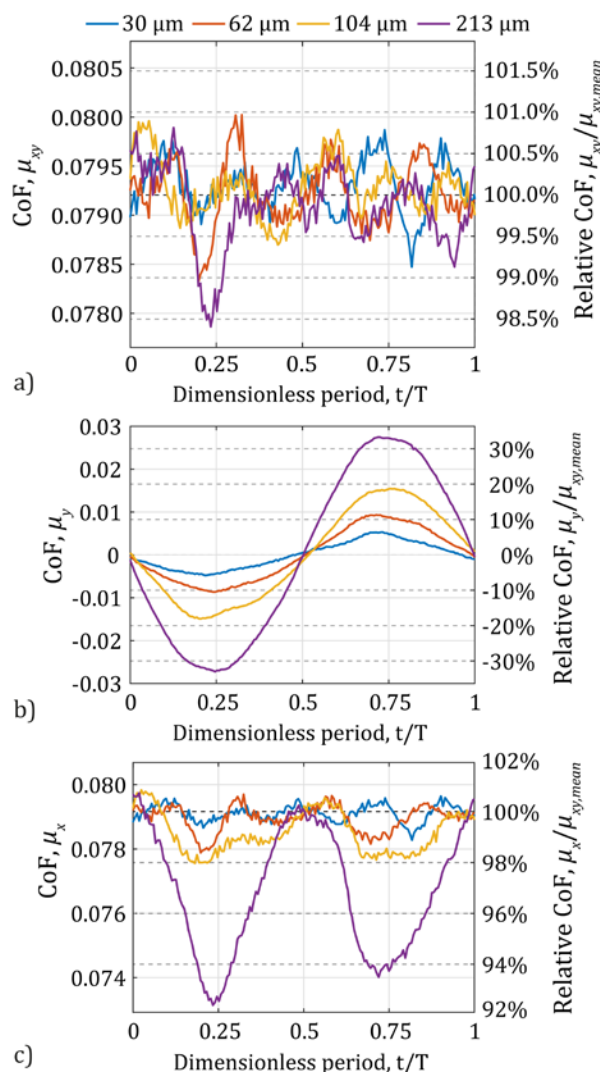


**Fig. 11.** Frictional response of BS lubricant in the direction of overall sliding speed (a), and in the lateral (b) and the main direction (c) of contact under transient bi-directional shearing at  $f=60$  Hz and  $p_h=1.32$  GPa for different stroke lengths.

It would be interesting to compare these experimental results with the results of molecular dynamic simulations [30] involving similar conditions. For the sake of clarity, this can be imagined as a tension-loaded rod, which is additionally cyclically loaded by a radial force in the middle of its length. If this assumption is

correct, then the friction (stress) in the lateral direction  $\mu_y$  should affect the friction in the main direction of contact  $\mu_x$  under vibrations, but not vice versa at the same main sliding speed.

It should be noted that there is an interrelation between the steady and oscillatory shearing flow of lubricant known as the Cox-Merz rule [31]. This rule is mainly applied to the data from vibrational viscometers (often employing cut quartz crystal or shear impedance spectrometer) to characterize the rheological parameters and complex responses of lubricants (low-shear viscosity, shear thinning, time-dependence, linear or non-linear viscoelastic behaviour, etc.). However, it turned out that this rule is applicable only in a very limited range of operating conditions with respect to EHL [32].

Figure 11a shows the total CoF  $\mu_{xy}$  expressed in the direction of instantaneous sliding velocity over the dimensionless period  $t/T$  of motion. It is noteworthy that the mean values of total CoF  $\mu_{xy,mean}$  for different stroke lengths are very similar ( $\mu_{xy,mean} = 0.0793$ ) regardless of different lateral sliding speeds. The exhibited disturbance of total friction is given, in particular, by the signal noise which determines the uncertainty of CoF measurements of 0.0005. This disturbance of friction corresponds to approximately  $\pm 0.5\%$  of the mean value of total friction  $\mu_{xy,mean}$  under these conditions, as it is illustrated by the second vertical axis of relative CoF. The fluctuations in CoF higher than 0.5 % of  $\mu_{xy,mean}$  were observed near the quarter of the oscillation cycle for the two conditions of stroke lengths. Since these fluctuations of 1.5 % of  $\mu_{xy,mean}$  did not recur during the reciprocation of motion, their origin is attributed to the dynamic response of the measuring system (not to the response of lubricant) to excited vibrations. Moreover, the occurrence of these fluctuations was rather random, not being identical from cycle to cycle.

The total CoF  $\mu_{xy}$  is the result of vector sum of the friction components  $\mu_y$  and  $\mu_x$  showed in Fig. 11b and Fig. 11c, respectively. It can be seen that the friction in the lateral direction  $\mu_y$  reaches almost  $\pm 30\%$  of  $\mu_{xy,mean}$  for certain conditions, whereas the friction in the main direction  $\mu_x$  varies in the range of at most 8 % of  $\mu_{xy,mean}$  under the same conditions. It is

important to note that when both the positive or the negative friction force  $F_{Ty}$  is obtained in the lateral direction, then the friction force in the main direction  $F_{Tx}$  is reduced. In other words, the friction in the main direction  $\mu_x$  is influenced by the friction in the lateral direction  $\mu_y$ , but not vice versa, because there is no other reason for such fluctuations in  $\mu_x$  than the changes in  $\mu_y$ , when the main shearing of lubricant is maintained by the constant value of sliding speed  $u_x$ . Above that, the friction in lateral direction  $\mu_y$  was not affected by  $\mu_x$ , since  $\mu_x$  varied with contact pressure; however, this change in  $\mu_x$  had no impact on  $\mu_y$ , as can be seen in Fig. 10. This observation justifies the above discussed reasons for the differences in the uni- and the bi- directional shear loading responses of the BS lubricant regarding the perturbation of its structural arrangement and the pressure and thermal effects. Moreover, these results suggest that a response of mineral oils to shearing should not be treated as isotropic.

Moreover, achieving of limiting shear stress  $\tau_{lim}$  is often reported in experiments for similar conditions. There are two indicators of this phenomenon. First, the vector sum of CoFs  $\mu_x$  and  $\mu_y$  is not able to significantly exceed a certain value of friction (stress) when this value is represented by  $\mu_{xy,mean}$ , or by the value of CoF  $\mu$  under the corresponding steady state conditions (according to contact conditions and speeds). Secondly, the increase in the vector sum of sliding velocities  $u_x$  and  $u_y$  is not reflected in the change of total CoF  $\mu_{xy}$  in the direction of this overall velocity. Then also the assumption that the velocity of lubricant flow is distributed linearly through the film thickness (Couette flow) is unlikely to be correct [33,34]. Nevertheless, reaching of  $\tau_{lim}$  cannot be attributed only to the applied vibrations, but it is a consequence of a combination of contact conditions (pressure, temperature, shear stress) and a complex lubricant rheology.

In the final consequence, the mean values of total CoF  $\mu_{xy,mean}$  achieved under vibrations (bi-directional shearing) are very close to the values of CoF  $\mu$  obtained under steady state conditions at  $u_x = 0.1$  m/s (unidirectional shearing) with respect to the contact pressures, as is illustrated in Fig. 12.

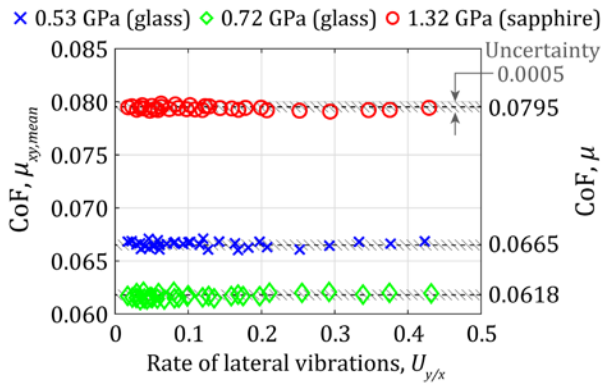


**Fig. 12.** Comparison of the mean values of total CoF under vibrations with CoF under steady state conditions at  $u_x = 0.1$  m/s.

The rate of lateral vibrations  $U_{y/x}$  on the horizontal axis is represented by the ratio of speeds acting in the lateral and main directions. More specifically, it is the ratio of the mean of absolute values of these speeds achieved during one cycle of motion:

$$U_{y/x} = |u_y|_{mean} / |u_x|_{mean} \quad (6)$$

Steady state conditions occur for  $U_{y/x} = 0$ , whereas a pure sliding reciprocation is assumed at  $U_{y/x} = \infty$ . Since  $U_{y/x}$  was lower than 0.5 for all experimental conditions used in this study, the contact was exposed only to mild micro-oscillations. It can be assumed that the symptoms of the non-Newtonian response of lubricant on its shear loading and the thermal or pressure effects in the specific directions of contact are influenced by the ratio of sliding speeds  $U_{y/x}$ . If the speed in the lateral direction of contact exceeds the speed in its main direction over most of the cycle (situation when  $U_{y/x} > 1$ ), and thus the direction of the majority of shear flow is changed, then the effects of shear-thinning, heating and pressure on the frictional response of lubricant would probably also be observable in the lateral direction of contact. In addition, the frictional response is predetermined by the behaviour of film thickness in the central area of contact under such conditions. The entrapment of thick film of lubricant due to the squeeze action, the film dimple due to the thermal wedge action, the film thickness fluctuations as the result of dynamic motions, the reduction in the film thickness due to starvation, and the film failure may occur under severe vibrations and affect substantially (positively or negatively) friction. None of these phenomena, except for slight fluctuations in the thickness due to the changes in the entrainment

speed and because of a surface roughness, was observed in the film thickness under conditions of the current study; therefore, they did not affect the resulting frictional response. In further studies, it would be advisable to experimentally investigate likewise the frictional response in the both directions of contact under kinematic conditions for  $U_{y/x} > 1$  and analyse the behaviour of lubricant through numerical simulations.

#### 4. CONCLUSION

In the present experimental study, the frictional response of lubricant in the point EHL contact was investigated under transient conditions of bi-directional shear loading. A modified ball-on-disc apparatus was employed, where the contact was exposed to a steady sliding motion in the main direction of contact simultaneously with the sliding oscillations in the lateral direction of contact. Friction forces were measured using the compliant mechanism with flexure hinges by the precise load sensors in both directions of contact at the same time. Different materials of contact body, contact loads, and frequencies and stroke lengths of lateral motion were applied during the experiments, where the stroke lengths were shorter than the contact diameter.

In regard to the results of the friction measured in the lateral direction of contact, a nearly purely viscous behaviour of BS lubricant was obtained. The influence of lubricant elasticity was negligible even at the highest contact pressure of 1.3 GPa and for different stroke lengths. The course of friction was stable with respect to the oscillatory cycles and regardless of stroke lengths and frequencies of lateral motion. The lateral sliding speed was detected as the only crucial parameter affecting the friction in the lateral direction. It is remarkable that no impacts of shear-thinning, shear-heating, and likewise no influence of contact pressure on the frictional response of lubricant were found in the lateral direction in contrast with the frictional response in the main direction of contact. The absence of these effects is explained via the comparison of frictions under uni- and bi- directional shearing of lubricant. It is deduced that the source of the frictional response in the lateral direction is the perturbation of structural arrangement of lubricant in the perpendicular direction to its main flow. The results suggest that a response of mineral oils to

shearing should not be treated as isotropic. This may be useful for investigating the rheological properties of lubricants under severe in-contact conditions of EHL conjunctions.

For conditions where the main shear flow of lubricant was maintained in the main direction of contact, it was shown that the friction in the lateral direction affects the frictional response in the main direction, but not vice versa. The total values of the frictional responses under vibrations were similar to each other in spite of different lateral sliding speeds and considering the contact pressures. These values were also comparable with the values of friction obtained under steady state conditions at the same main sliding speed. The last-mentioned results indicate the occurrence of the limiting shear stress phenomenon, which was discussed for these specific conditions. Finally, the investigation of frictional responses for EHL contact under more severe vibrational conditions is proposed.

## Acknowledgement

This work was supported by the Czech Science Foundation (Project No. 17-23235S).

## REFERENCES

- [1] A. Crook, 'The lubrication of rollers IV. Measurements of friction and effective viscosity', *Philosophical Transactions of the Royal Society of London A: Mathematical, Physical and Engineering Sciences*, vol. 255, no. 1056, pp. 281-312, 1963.
- [2] F. Smith, 'Lubricant behavior in concentrated contact—some rheological problems', *ASLE Transactions*, vol. 3, no. 1, pp. 18-25, 1960.
- [3] M.A. Plint, 'Third Paper: Traction in Elastohydrodynamic Contacts', *Proceedings of the Institution of Mechanical Engineers*, vol. 182, no. 1, pp. 300-306, 1967.
- [4] W. Habchi, S. Bair and P. Vergne, 'On friction regimes in quantitative elastohydrodynamics', *Tribology International*, vol. 58, pp. 107-117, 2013.
- [5] W. Habchi, P. Vergne, S. Bair, O. Andersson, D. Eyheramendy and G.E. Morales-Espejel, 'Influence of pressure and temperature dependence of thermal properties of a lubricant on the behaviour of circular TEHD contacts', *Tribology International*, vol. 43, no. 10, pp. 1842-1850, 2010.
- [6] D.P. Hess and A. Soom, 'Friction at a Lubricated Line Contact Operating at Oscillating Sliding Velocities', *Journal of Tribology-Transactions of the Asme*, vol. 112, no. 1, pp. 147-152, 1990.
- [7] A. Harnoy and B. Friedland, 'Dynamic friction model of lubricated surfaces for precise motion control', *Tribology transactions*, vol. 37, no. 3, pp. 608-614, 1994.
- [8] H. Rachoor and A. Harnoy, 'Modeling of dynamic friction in lubricated line contacts for precise motion control', *Tribology transactions*, vol. 39, no. 2, pp. 476-482, 1996.
- [9] X.J. Zhai, G. Needham and L. Chang, 'On the mechanism of multi-valued friction in unsteady sliding line contacts operating in the regime of mixed-film lubrication', *Journal of Tribology-Transactions of the Asme*, vol. 119, no. 1, pp. 149-155, 1997.
- [10] H. Sojoudi and M. M. Khonsari, 'On the Modeling of Quasi-Steady and Unsteady Dynamic Friction in Sliding Lubricated Line Contact', *Journal of Tribology-Transactions of the Asme*, vol. 132, no. 1, 2010.
- [11] H. Nishikawa and M. Kaneta, 'Traction in Ehl under Pure Sliding Reciprocation with Cyclic Impact Loading', *Jsmc International Journal Series C-Dynamics Control Robotics Design and Manufacturing*, vol. 38, no. 3, pp. 568-576, 1995.
- [12] D. Kostal, P. Sperka, I. Krupka and M. Hartl, 'Experimental Comparison of the Behavior between Base Oil and Grease Starvation Based on Inlet Film Thickness', *Tribology in Industry*, vol. 39, no. 1, pp. 110-119, 2017.
- [13] J. Fryza, P. Sperka, M. Kaneta, I. Krupka and M. Hartl, 'Effects of lubricant rheology and impact speed on EHL film thickness at pure squeeze action', *Tribology International*, vol. 106, pp. 1-9, 2017.
- [14] H. Nishikawa, K. Handa and M. Kaneta, 'Behavior of Ehl Films in Reciprocating Motion', *Jsmc International Journal Series C-Dynamics Control Robotics Design and Manufacturing*, vol. 38, no. 3, pp. 558-567, 1995.
- [15] M. Kaneta and H. Nishikawa, 'The Effects of a Transversely Oriented Bump on Point Contact EHL Films in Reciprocating Motion with a Short Length of Stroke', *Tribology Series*, vol. 36, pp. 185-192, 1999.
- [16] Y. Tozaki, N. Hayashi and S. Matsumoto, 'The study on tribological characteristics of traction drives in non-steady condition (Optical interferometric observations of transient oil film)', *Jsmc International Journal Series C-Mechanical Systems Machine Elements and Manufacturing*, vol. 44, no. 1, pp. 223-229, 2001.
- [17] R. Bassani and E. Ciulli, 'Friction investigation under constant and variable speed conditions', *Tribology Series*, vol. 43, pp. 783-794, 2003.

- [18] R. Bassani, E. Ciulli, M. Carli and K. Stadler, 'Experimental investigation of transient and thermal effects on lubricated non-conformal contacts', *Tribotest*, vol. 13, no. 4, pp. 183-194, 2007.
- [19] S.Y. Qu, P.R. Yang and F. Guo, 'Theoretical investigation on the dimple occurrence in the thermal EHL of simple sliding steel-glass circular contacts', *Tribology International*, vol. 33, no. 1, pp. 59-65, 2000.
- [20] E. Ciulli, K. Stadler and T. Draexl, 'The influence of the slide-to-roll ratio on the friction coefficient and film thickness of EHD point contacts under steady state and transient conditions', *Tribology International*, vol. 42, no. 4, pp. 526-534, 2009.
- [21] E. Ciulli, 'Non-steady state non-conformal contacts: friction and film thickness studies', *Meccanica*, vol. 44, no. 4, pp. 409-425, 2009.
- [22] E. Rigaud, D. Mazuyer and J. Cayer-Barrioz, 'An Interfacial Friction Law for a Circular EHL Contact Under Free Sliding Oscillating Motion', *Tribology Letters*, vol. 51, no. 3, pp. 419-430, 2013.
- [23] F. Majdoub, J. Perret-Liaudet, M. Belin and J. Martin, 'Decaying law for the free oscillating response with a pseudo-polynomial friction law: Analysis of a superlow lubricated friction test', *Journal of Sound and Vibration*, vol. 348, pp. 263-281, 2015.
- [24] A. Ernesto, D. Mazuyer and J. Cayer-Barrioz, 'From Full-Film Lubrication to Boundary Regime in Transient Kinematics', *Tribology Letters*, vol. 59, no. 1, 2015.
- [25] M. Yahiaoui, E. Rigaud, D. Mazuyer and J. Cayer-Barrioz, 'Forced oscillations dynamic tribometer with real-time insights of lubricated interfaces', *Rev Sci Instrum*, vol. 88, no. 3, p. 035101, 2017.
- [26] M. Hartl, I. Krupka and M. Liska, 'Differential colorimetry: Tool for evaluation of chromatic interference patterns', *Optical Engineering*, vol. 36, no. 9, pp. 2384-2391, 1997.
- [27] M. Hartl, I. Krupka, R. Poliscuk, M. Liska, J. Molimard, M. Querry, *et al.*, 'Thin film colorimetric interferometry', *Tribology Transactions*, vol. 44, no. 2, pp. 270-276, 2001.
- [28] J. Fryza, P. Sperka, I. Krupka and M. Hartl, 'Effects of lateral harmonic vibrations on film thickness in EHL point contacts', *Tribology International*, vol. 117, pp. 236-249, 2018.
- [29] S. Bair and M. Kotzalas, 'The contribution of roller compliance to elastohydrodynamic traction', *Tribology Transactions*, vol. 49, no. 2, pp. 218-224, 2006.
- [30] B.D. Todd and P.J. Davis, 'Homogeneous non-equilibrium molecular dynamics simulations of viscous flow: techniques and applications', *Molecular Simulation*, vol. 33, no. 3, pp. 189-229, 2007.
- [31] W. Cox and E. Merz, 'Rheology of Polymer Melts—A Correlation of Dynamic and Steady Flow Measurements', in *International Symposium on Plastics Testing and Standardization*, 1959.
- [32] S. Bair, T. Yamaguchi, L. Brouwer, H. Schwarze, P. Vergne and G. Poll, 'Oscillatory and steady shear viscosity: The Cox-Merz rule, superposition, and application to EHL friction', *Tribology International*, vol. 79, pp. 126-131, 2014.
- [33] P. Šperka, I. Křupka and M. Hartl, 'Evidence of plug flow in rolling-sliding elastohydrodynamic contact', *Tribology Letters*, vol. 2, no. 54, pp. 151-160, 2014.
- [34] P. Sperka, I. Krupka and M. Hartl, 'Transition from plug-flow to linear speed profile near a dent in a rolling-sliding EHL contact', *Tribology International*, vol. 100, pp. 344-350, 2016.

## Nomenclature

$d$	diameter of Hertzian contact area (m)
$f$	frequency (Hz)
$F_N$	normal load (N)
$F_T$	friction force (N)
$h_c$	central film thickness (m)
$k$	stiffness of the measuring system (N/m)
$\bar{p}$	mean contact pressure (Pa)
$p_h$	maximum Hertzian contact pressure (Pa)
$R_{1,2}$	roughness of contact surface (m)
$s$	stroke length (m)
$s_{by}$	lateral position of the ball (m)
$s_{wy}$	lateral position of the window (m)
$s_y$	relative displacement between contact surfaces (m)
$t$	time (s)
$T$	period of motion (s)
$u$	sliding speed (m/s)
$U_{y/x}$	rate of lateral vibrations; speeds ratio
$\lambda$	lambda ratio
$\mu$	coefficient of friction; CoF
$\bar{\tau}$	mean shear stress (Pa)
$\tau_{lim}$	limiting shear stress (Pa)
$\varphi$	phase shift

## Subscripts:

$max$	maximum value over a given period
$mean$	mean value over a given period
$x$	in the main direction of contact
$xy$	vector sum of variable components in the directions $x$ and $y$
$y$	in the lateral direction of contact

## 7 CONCLUSIONS

The current thesis is devoted to the study of the behaviour of elastohydrodynamic lubricating films and their frictional response under transient operating conditions. The elastohydrodynamic lubrication (EHL) is the most beneficial regime of lubrication considering no wear and low friction and is frequently employed in the contacts working under severe non-steady state conditions. In spite of that the main attention of researchers is still paid to EHL under steady state conditions contradicting the actual operations of machines. Due to the lack of knowledge about the effects of transient conditions on the EHL mechanisms and consequent absence of adequate predictions for estimation of EHL film thickness and friction, components of machines are often designed by means of unmodified predictions for steady state conditions. This simplistic approach may not provide the desired efficiency, reliability, and service life of these machines.

Scientific investigations pointed out that the transient operating conditions can not only negatively but also positively influence the behaviour of EHL film and friction. For instance, the entrapped EHL film ensuring separation of the contact surfaces even at zero speeds can be produced because of the squeeze action resulting from sudden loading of the contact or rapid deceleration of the motion. Moreover, lateral vibrations can be one of the mechanisms causing a track replenishment and reduction of starvation in rolling bearings. In contrary, lateral vibrations can cause as well a film failure in the dependence on the operating conditions. Previous numerical studies revealed the importance of the approaching speed for the formation of entrapped films, and the analytical prediction of the entrapped film thickness was recently established. However, the validity of the prediction has not been experimentally verified yet. Furthermore, only the loading speed was analysed in experimental studies instead of the approaching speed. The real role of these simultaneously acting essential parameters is thus far from clear. Although vibrations are inseparably linked to the operation of every machine, their impact on EHL film thickness was examined only sporadically lacking any quantitative description. Besides that, there has not been an experimental or numerical study considering the effect of lateral vibrations on EHL friction.

The above-mentioned facts were extracted from the first part of this thesis providing a summary of the literature review in the field. Subsequently, the aim of the thesis was defined based on the critical analysis of the current state of the art. The main goal of the thesis was to experimentally determine the effects of operating parameters on the EHL film behaviour in the point contact under impact load and lateral vibrations when the emphasis was placed on the film thickness. For this purpose, laboratory test rigs have been developed for measurement of film thickness and friction of EHL films under controlled non-steady state conditions. Since the thesis was conceived as a set of scientific articles, the original results of this study are presented in three related papers.

The first paper dealt with the film thickness behaviour under conditions of pure squeeze action (linear impact loading). The purpose of the paper was to clarify the mechanism of entrapped film formation and determine the effects of individual

operating parameters including lubricant rheology. New rules of dimple film shape formation and film entrapment were established with respect to operating conditions. Experimental results were compared with a recent theoretical solution by other authors pointing to its shortcomings. The appropriate improvements of this solution were proposed in the form of empirical relationships to provide a realistic and yet simple to apply estimate of film thickness considering lubricant rheology and operating conditions.

The following paper was devoted to the behaviour of film thickness distribution under lateral vibrations taking into account the actual ratio between the stroke length of lateral motion and the diameter of the contact. The effects of vibrations on film thickness were identified for a wide range of operating conditions, both qualitatively and quantitatively. The origins of the film behaviour were detected together with the thresholds of local and overall film breakdowns. Exponential functions were derived, describing the effect of lateral vibrations on the central film thickness and its deviations uniformly for all lubricants.

The simultaneous frictional responses in the main and lateral directions of the contact under mild lateral vibrations were examined in the last paper. Although the impact of lateral vibrations on the total EHL friction was found to be negligible because of the limiting shear stress phenomenon, where the impact on the film thickness was likewise unimportant for given conditions, the used innovative approach gives a new insight into lubricant rheology. The important conclusion was that the effective viscosity and frictional response of lubricant should not be assumed as isotropic.

The original results of the current thesis, which were confronted with the previous scientific studies, extended the knowledge in the field of EHL lubrication under transient conditions. The main contribution of the thesis can be summarized into the following points:

- For the first time, the influence of approaching speed on entrapped films was investigated experimentally.
- The role of approaching and loading speed on dimple film shape formation and resulting film thickness was revealed.
- Empirical relationships for prediction of EHL film thickness were established for conditions of both impact loading and lateral vibrations.
- For the first time, the effect of lateral vibrations on EHL friction was studied as well as the simultaneous frictional responses of lubricant were analysed in two directions of EHL contact.

Regarding the scientific question, the obtained knowledge can be summarized in the following concluding remarks:

- Although the approaching speed and the loading speed were often considered as interchangeable as they have seemingly the same effect on the dimple film thickness, it was revealed that their role during dimple

formation is crucially different. The approaching speed, viscosity of lubricant, and initial gap determine the resulting central film thickness of the central dimple at the end of the approach stage of the impact process. Subsequently, the progress of the loading speed determines the shape of dimple sides during the loading stage of the impact (**hypothesis H1 was FALSIFIED**).

- In general, an overall film thickness of entrapped film is particularly influenced by the viscosity at ambient pressure, whereas the pressure-viscosity coefficient (PVC) is less important; even though PVC determines the rate of the increase in viscosity, which is an essential parameter for film entrapment. The reason is that the top of the dimple begins to be formed at the end of the approach stage of the impact process predetermining overall resulting thickness. During this stage, the pressure build-up is negligible and thus PVC has a negligible impact on dimple film thickness. The influence of PVC was proved only in the course of the loading stage of the impact affecting a slope of dimple sides, but only when the pressure build-up was sufficiently high (**hypothesis H2 was FALSIFIED**).
- The experiments confirmed that the passage of lubricant through an EHL contact is driven mainly by entrainment velocity regardless of the sliding velocity even if rapid changes in the vectors and magnitudes of these velocities took place due to lateral vibrations (**hypothesis H3 was CONFIRMED under given conditions**).
- The central film thickness is affected by a film formed at the contact inlet as a result of the squeeze action and variation in the entrainment and sliding speed occurring during lateral vibrations. However, it is also affected by thin films in EHL horseshoe-shaped constriction, which are entrained into the central area of the contact because of rapid changes in the entrainment velocity vector. Moreover, the central film thickness can be disrupted directly by low-thickness sharp stripes originating from lubricant reaction on shear loading (**hypothesis H4 was FALSIFIED**).
- Due to perturbation of the structural arrangement of lubricant according to the majority of shear flow, the thermal, pressure, and other effects on lubricant viscosity were recognized only in the main direction of the contact, whereas the response of lubricant to short-term shear loading in the lateral direction was the isothermal Newtonian. Additionally, since the frictional responses and thus effective viscosities at the same shear rate were found to be affected by measurement direction, they cannot be considered as isotropic (**hypothesis H5 was FALSIFIED**).
- When the majority of shear flow was maintained in the main direction of the contact, the frictional response in this direction was influenced by the changes in friction in the lateral direction of the contact, but not vice versa. This “one-way interaction” is attributed to the molecular nature of lubricant and re-arrangement of its structure during lateral vibrations with respect to shear flow (**hypothesis H6 was FALSIFIED**).

Regardless of the progress made in this thesis, further research in the field of transient EHL is necessary. It is suggested to focus the further research on the influence of contact geometry (elliptical contacts) and surface roughness (artificial asperities and realistic roughness profiles) on EHL film behaviour, its frictional response, and in-contact temperature. Moreover, greases should also be employed in experimental investigations together with non-linear progresses of impact loadings; and frictional response should be examined for more severe kinematic conditions of lateral vibrations and a broad spectrum of lubricants.

---

## LIST OF AUTHOR'S PUBLICATIONS

### Papers published in journals with impact factor

FRYZA, J., P. SPERKA, I. KRUPKA and M. HARTL. Effects of lateral harmonic vibrations on film thickness in EHL point contacts. *Tribology International*. 2018, vol. 117, p. 236-249. DOI: 10.1016/j.triboint.2017.08.022.

FRYZA, J., P. SPERKA, M. KANETA, I. KRUPKA, et al. Effects of lubricant rheology and impact speed on EHL film thickness at pure squeeze action. *Tribology International*. 2017, vol. 106, p. 1-9. DOI: 10.1016/j.triboint.2016.10.023.

### Papers published in peer-reviewed journals

FRYZA, J., P. SPERKA, I. KRUPKA and M. HARTL. Frictional response of lubricant in EHL contact under transient bi-directional shear loading. *Tribology in Industry*. 2017, vol. 39, no. 4, p. 506-518. DOI: 10.24874/ti.2017.39.04.10.

### Papers in conference proceedings

FRYZA, J. and M. OMASTA. The Experimental Determination of the Grease Amount to Effective Wear Reduction in the Wheel-Rail Contact. In *The Latest Methods of Construction Design*. Cham: Springer International Publishing, 2016, p. 127-132. ISBN: 978-3-319-22761-0. DOI: 10.1007/978-3-319-22762-7\_20.

FRYZA, J.; SPERKA, P.; KRUPKA, I.; HARTL, M. Behaviour of EHL Films under Lateral Vibrations. In *Book of Proceedings of 56th International Conference of Machine Design Departments*. Nitra: Slovak University of Agriculture in Nitra, 2015. p. 349-352. ISBN: 978-80-552-1377-4.

OMASTA, M.; FRYZA, J.; HARTL, M.; KRUPKA, I. Study of Effects of Wheel Flange/Rail Gauge Contact Lubrication. In *Proceedings of World Tribology Congress 2013*. Torino: Politecnico di Torino (DIMEAS), 2013. p. 3007-3009. ISBN: 9781634393522.

OMASTA, M.; FRYZA, J.; HARTL, M.; KRUPKA, I. An experimental approach to the study of rail wheel/flange lubrication. In *STLE Annual Meeting & Exhibition 2013 / Proceedings of a meeting held 5-9 May 2013*. Detroit, Michigan, USA: Society of Tribologists and Lubrication Engineers, 2013. p. 1-3. ISBN: 978-1-62993-289-7.

### Conference abstracts

FRYZA, J.; SPERKA, P.; KRUPKA, I.; HARTL, M. Viscoelastic response of lubricant in an EHL contact under transient bi-directional shear loading. *STLE 72nd Annual Meeting & Exhibition*. 2017. Atlanta, Georgia, USA.

FRYZA, J.; SPERKA, P.; KRUPKA, I.; HARTL, M. Effects of lateral vibrations on film thickness distribution in a point EHL contact. *The 17th Nordic Symposium on Tribology - NORDTRIB 2016*. 2016. Hämeenlinna, Finland.

FRYZA, J.; SPERKA, P.; KRUPKA, I.; HARTL, M. Roughness Effects in Impact EHL of Elliptical Contacts. *International Tribology Conference*. 2015. Tokyo, Japan.

**REFERENCES**

- [1] HUTCHINGS, I. M. Leonardo da Vinci's studies of friction. *Wear*. 2016, vol. 360, p. 51-66. DOI: 10.1016/j.wear.2016.04.019.
- [2] HERTZ, H. On the contact of elastic solids. *J. Reine Angew Math*. 1881, vol. 92, p. 156-171.
- [3] TOWER, B. First report on friction experiments. *Proceedings of the institution of mechanical engineers*. 1883, vol. 34, no. 1, p. 632-659.
- [4] PETROV, N. Friction in Machines and the Effect of the Lubricant. *Inzhenerno Zhurnal St. Petersburg*. 1883, vol. 1, p. 71-140.
- [5] REYNOLDS, O. On the Theory of Lubrication and Its Application to Mr. Beauchamp Tower's Experiments, Including an Experimental Determination of the Viscosity of Olive Oil. *Proceedings of the Royal Society of London*. 1886, vol. 40, no. 242-245, p. 191-203.
- [6] MARTIN, H. Lubrication of gear teeth. *Engineering*. 1916, vol. 102, p. 119.
- [7] GÜMBEL, L. Über geschmierte arbeitsräder (On the lubrication of gears). *Zeitschrift für das gesamte Turbinenwesen*. 1916, vol. 24, p. 245-248.
- [8] PEPPLER, W. Untersuchungen über die Druckübertragung bei Belasteten und Geschmierten Umlaufenden Achsparallelen Zylindern. *Maschinenelemente—Tagung Aachen*. 1935.
- [9] MELDAHL, A. Contribution to the Theory of the Lubrication of Gears and of the Stressing of the Lubricated Flanks of Gear Teeth. *Brown Boveri Rev*. 1941, vol. 28, no. 11, p. 374-382.
- [10] GATCOMBE, E. K. *Lubrication characteristics of involute spur gears*. Edition ed.: Cornell University, 1945.
- [11] ERTEL, A. Hydrodynamic lubrication based on new principles. *Akad. Nauk. SSSR, Prikladnaya Matematika i Mekhanika*. 1939, vol. 3, no. 2, p. 41-52.
- [12] GRUBIN, A. Fundamentals of the hydrodynamic theory of lubrication of heavily loaded cylindrical surfaces. *Investigation of the Contact Machine Components*. 1949, vol. 2.
- [13] CAMERON, A. Righting a 40-Year-Old Wrong. *Tribology International*. 1985, vol. 18, no. 2, p. 92-92. DOI: 10.1016/0301-679x(85)90038-6.
- [14] MACCONOCHIE, I. O. and A. CAMERON. The Measurement of Oil-Film Thickness in Gear Teeth. *Journal of Basic Engineering*. 1960, vol. 82, no. 1, p. 29-34. DOI: 10.1115/1.3662549.
- [15] LANE, T. and J. HUGHES. A study of the oil-film formation in gears by electrical resistance measurements. *British Journal of Applied Physics*. 1952, vol. 3, no. 10, p. 315.
- [16] CROOK, A. W. The Lubrication of Rollers. *Philosophical Transactions of the Royal Society of London. Series A, Mathematical and Physical Sciences*. 1958, vol. 250, no. 981, p. 387-409. DOI: 10.1098/rsta.1958.0001.
- [17] SIBLEY, L. and F. ORCUTT. Elasto-hydrodynamic lubrication of rolling-contact surfaces. *ASLE TRANSACTIONS*. 1961, vol. 4, no. 2, p. 234-249.
- [18] ARCHARD, J. and M. KIRK. Lubrication at point contacts. In *Proceedings of the Royal Society of London A: Mathematical, Physical and Engineering Sciences*. The Royal Society, 1961, vol. 261, p. 532-550.

- 
- [19] GOHAR, R. and A. CAMERON. Optical measurement of oil film thickness under elasto-hydrodynamic lubrication. *Nature*. 1963, vol. 200, no. 4905, p. 458-459.
- [20] CAMERON, A. and R. GOHAR. Theoretical and Experimental Studies of the Oil Film in Lubricated Point Contact. *Proceedings of the Royal Society of London. Series A. Mathematical and Physical Sciences*. 1966, vol. 291, no. 1427, p. 520-536. DOI: 10.1098/rspa.1966.0112.
- [21] GOHAR, R. Report 1: A Ball-and-Plate Machine for Measuring Elastohydrodynamic Oil Films. *Proceedings of the Institution of Mechanical Engineers, Conference Proceedings*. 1967, vol. 182, no. 7, p. 43-45. DOI: 10.1243/pime\_conf\_1967\_182\_176\_02.
- [22] HAMROCK, B. J. and D. DOWSON. Isothermal Elastohydrodynamic Lubrication of Point Contacts .1. Theoretical Formulation. *Journal of Lubrication Technology-Transactions of the Asme*. 1976, vol. 98, no. 2, p. 223-229.
- [23] HAMROCK, B. J. and D. DOWSON. Isothermal Elastohydrodynamic Lubrication of Point Contacts .2. Ellipticity Parameter Results. *Journal of Lubrication Technology-Transactions of the Asme*. 1976, vol. 98, no. 3, p. 375-383.
- [24] HAMROCK, B. J. and D. DOWSON. Isothermal Elastohydrodynamic Lubrication of Point Contacts .3. Fully Flooded Results. *Journal of Lubrication Technology-Transactions of the Asme*. 1977, vol. 99, no. 2, p. 264-276.
- [25] CHENG, H. S. Calculation of Elastohydrodynamic Film Thickness in High Speed Rolling and Sliding Contacts. 1967.
- [26] BAIR, S. and F. QURESHI. The high pressure rheology of polymer-oil solutions. *Tribology international*. 2003, vol. 36, no. 8, p. 637-645.
- [27] LARSSON, R. EHL Film Thickness Behavior. In *Encyclopedia of Tribology*. Springer, 2013, p. 817-827.
- [28] BAIR, S. and W. O. WINER. Shear-Strength Measurements of Lubricants at High-Pressure. *Journal of Lubrication Technology-Transactions of the Asme*. 1979, vol. 101, no. 3, p. 251-257.
- [29] DOWSON, D. Elastohydrodynamic and micro-elastohydrodynamic lubrication. *Wear*. 1995, vol. 190, no. 2, p. 125-138. DOI: 10.1016/0043-1648(95)06660-8.
- [30] SPIKES, H. and Z. JIE. History, Origins and Prediction of Elastohydrodynamic Friction. *Tribology Letters*. 2014, vol. 56, no. 1, p. 1-25. DOI: 10.1007/s11249-014-0396-y.
- [31] BAIR, S., P. VERGNE, P. KUMAR, G. POLL, et al. Comment on "History, Origins and Prediction of Elastohydrodynamic Friction" by Spikes and Jie. *Tribology Letters*. 2015, vol. 58, no. 1. DOI: 10.1007/s11249-015-0481-x.
- [32] SPIKES, H. and J. ZHANG. Reply to the Comment by Scott Bair, Philippe Vergne, Punit Kumar, Gerhard Poll, Ivan Krupka, Martin Hartl, Wassim Habchi, Roland Larson on "History, Origins and Prediction of Elastohydrodynamic Friction" by Spikes and Jie in *Tribology Letters*. *Tribology Letters*. 2015, vol. 58, no. 1. DOI: 10.1007/s11249-015-0483-8.
- [33] TODD, B. D. and P. J. DAIVIS. Homogeneous non-equilibrium molecular dynamics simulations of viscous flow: techniques and applications. *Molecular Simulation*. 2007, vol. 33, no. 3, p. 189-229. DOI: 10.1080/08927020601026629.

- [34] PETRUSEVICH, A. I. Fundamental Conclusions from the Contact-Hydro-Dynamic Theory of Lubrication. *Izv. Akad. Nauk SSSR. (OTN)*. 1951, vol. 2, p. 209-233.
- [35] VAN EMDEN, E., C. H. VENNER and G. E. MORALES-ESPEJEL. Aspects of flow and cavitation around an EHL contact. *Tribology International*. 2016, vol. 95, p. 435-448. DOI: 10.1016/j.triboint.2015.11.042.
- [36] HABCHI, W., S. BAIR and P. VERGNE. On friction regimes in quantitative elastohydrodynamics. *Tribology International*. 2013, vol. 58, p. 107-117. DOI: 10.1016/j.triboint.2012.10.005.
- [37] SMITH, F. Lubricant behavior in concentrated contact—some rheological problems. *ASLE Transactions*. 1960, vol. 3, no. 1, p. 18-25.
- [38] PLINT, M. A. Traction in elastohydrodynamic contacts. *ARCHIVE: Proceedings of the Institution of Mechanical Engineers 1847-1982 (vols 1-196)*. 1967, vol. 182, no. 1967, p. 300-306. DOI: 10.1243/pime\_proc\_1967\_182\_028\_02.
- [39] BAIR, S., W. O. WINER and K. W. DISTIN. Experimental Investigations into Shear Localization in an Operating Ehd Contact. *Thin Films in Tribology*. 1993, vol. 25, p. 383-388.
- [40] KANETA, M., H. NISHIKAWA and K. KAMEISHI. Observation of Wall Slip in Elastohydrodynamic Lubrication. *Journal of Tribology-Transactions of the Asme*. 1990, vol. 112, no. 3, p. 447-452. DOI: Doi 10.1115/1.2920280.
- [41] EHRET, P., D. DOWSON and C. M. TAYLOR. On lubricant transport conditions in elastohydrodynamic conjunctions. *Proceedings of the Royal Society a-Mathematical Physical and Engineering Sciences*. 1998, vol. 454, no. 1971, p. 763-787.
- [42] CIULLI, E. and R. BASSANI. Influence of vibrations and noise on experimental results of lubricated non-conformal contacts. *Proceedings of the Institution of Mechanical Engineers Part J-Journal of Engineering Tribology*. 2006, vol. 220, no. J3, p. 319-331. DOI: 10.1243/13506501jet138.
- [43] BOWDEN, F. and D. TABOR. Friction and Lubrication of Solids, vol. I. Clarendon. In.: Oxford, 1950.
- [44] CIULLI, E. Non-steady state non-conformal contacts: friction and film thickness studies. *Meccanica*. 2009, vol. 44, no. 4, p. 409-425. DOI: 10.1007/s11012-008-9178-7.
- [45] CHRISTENSEN, H. Oil Film in a Closing Gap. *Proceedings of the Royal Society of London Series a-Mathematical and Physical Sciences*. 1962, vol. 266, no. 1326, p. 312-328. DOI: 10.1098/rspa.1962.0064.
- [46] DOWSON, D. and D. A. JONES. Lubricant Entrapment between Approaching Elastic Solids. *Nature*. 1967, vol. 214, no. 5091, p. 947-948. DOI: 10.1038/214947b0.
- [47] CONWAY, H. D. Rate of Change of Film Thickness in Elastohydrodynamic Squeeze Film Process. *Journal of Lubrication Technology-Transactions of the Asme*. 1973, vol. 95, no. 3, p. 391-393.
- [48] CONWAY, H. D. and H. C. LEE. Impact of a Lubricated Surface by a Sphere. *Journal of Lubrication Technology-Transactions of the Asme*. 1975, vol. 97, no. 4, p. 613-615.

- [49] KUWANO, N., N. OHNO and F. HIRANO. Investigation on entrapment of mineral oils under impact. *Journal of Japan Society of Lubrication Engineers*. 1985, vol. 31, no. 7, p. 477-484.
- [50] SAFA, M. M. A. and R. GOHAR. Pressure Distribution under a Ball Impacting a Thin Lubricant Layer. *Journal of Tribology-Transactions of the Asme*. 1986, vol. 108, no. 3, p. 372-376.
- [51] DOWSON, D. and D. C. WANG. An Analysis of the Normal Bouncing of a Solid Elastic Ball on an Oily Plate. *Wear*. 1994, vol. 179, no. 1-2, p. 29-37. DOI: 10.1016/0043-1648(94)90215-1.
- [52] LARSSON, R. and E. HOGLUND. Elastohydrodynamic Lubrication at Impact Loading. *Journal of Tribology-Transactions of the Asme*. 1994, vol. 116, no. 4, p. 770-776. DOI: 10.1115/1.2927331.
- [53] LARSSON, R. and E. HOGLUND. Numerical-Simulation of a Ball Impacting and Rebounding a Lubricated Surface. *Journal of Tribology-Transactions of the Asme*. 1995, vol. 117, no. 1, p. 94-102. DOI: 10.1115/1.2830614.
- [54] LARSSON, R. and J. LUNDBERG. Study of lubricated impact using optical interferometry. *Wear*. 1995, vol. 190, no. 2, p. 184-189. DOI: 10.1016/0043-1648(96)80016-0.
- [55] CHU, H.-M., R.-T. LEE and Y.-C. CHIOU. Study on pure squeeze elastohydrodynamic lubrication motion using optical interferometry and the inverse approach. *Proceedings of the Institution of Mechanical Engineers, Part J: Journal of Engineering Tribology*. 2004, vol. 218, no. 6, p. 503-512. DOI: 10.1243/1350650042794725.
- [56] NISHIKAWA, H., K. HANDA, K. TESHIMA, K. MATSUDA, et al. Behavior of EHL Films in Cyclic Squeeze Motion. *Jsm International Journal Series C-Dynamics Control Robotics Design and Manufacturing*. 1995, vol. 38, no. 3, p. 577-585.
- [57] GUO, F., H. NISHIKAWA, P. YANG and M. KANETA. EHL under cyclic squeeze motion. *Tribology International*. 2007, vol. 40, no. 1, p. 1-9. DOI: 10.1016/j.triboint.2005.10.006.
- [58] SAKAMOTO, M., H. NISHIKAWA and M. KANETA. Behaviour of point contact EHL films under pulsating loads. *Transient Processes in Tribology*. 2004, vol. 43, p. 391-399.
- [59] GUO, F., M. KANETA, J. WANG, H. NISHIKAWA, et al. Occurrence of a noncentral dimple in squeezing EHL contacts. *Journal of Tribology-Transactions of the Asme*. 2006, vol. 128, no. 3, p. 632-640. DOI: 10.1115/1.2194919.
- [60] ROELANDS, C. J. A., J. C. VLUGTER and H. I. WATERMAN. The Viscosity-Temperature-Pressure Relationship of Lubricating Oils and Its Correlation With Chemical Constitution. *Journal of Basic Engineering*. 1963, vol. 85, no. 4, p. 601-607. DOI: 10.1115/1.3656919.
- [61] KANETA, M., S. OZAKI, H. NISHIKAWA and F. GUO. Effects of impact loads on point contact elastohydrodynamic lubrication films. *Proceedings of the Institution of Mechanical Engineers Part J-Journal of Engineering Tribology*. 2007, vol. 221, no. J3, p. 271-278. DOI: 10.1243/13506501jet236.

- [62] OHNO, N., N. KUWANO and F. HIRANO. Diagrams for estimation of the solidified film thickness at high pressure EHD contacts. *Tribology Series*. 1994, vol. 27, p. 507-518.
- [63] NISHIKAWA, H., H. MIYAZAKI, M. KANETA and F. GUO. Effects of two-stage impact load on point contact elastohydrodynamic lubrication films. *Proceedings of the Institution of Mechanical Engineers Part J-Journal of Engineering Tribology*. 2008, vol. 222, no. J7, p. 807-814. DOI: 10.1243/13506501jet389.
- [64] KANETA, M., H. NISHIKAWA, M. MIZUI and F. GUO. Impact elastohydrodynamics in point contacts. *Proceedings of the Institution of Mechanical Engineers Part J-Journal of Engineering Tribology*. 2011, vol. 225, no. J1, p. 1-12. DOI: 10.1177/13506501jet838.
- [65] BAIR, S. Measurements of real non-Newtonian response for liquid lubricants under moderate pressures. *Proceedings of the Institution of Mechanical Engineers Part J-Journal of Engineering Tribology*. 2001, vol. 215, no. J3, p. 223-233. DOI: 10.1243/1350650011543493.
- [66] MARTINI, A. and S. BAIR. The role of fragility in EHL entrapment. *Tribology International*. 2010, vol. 43, no. 1-2, p. 277-282. DOI: 10.1016/j.triboint.2009.06.006.
- [67] KANETA, M., J. WANG, F. GUO, I. KRUPKA, et al. Effects of Loading Process and Contact Shape on Point Impact Elastohydrodynamics. *Tribology Transactions*. 2012, vol. 55, no. 6, p. 772-781. DOI: 10.1080/10402004.2012.709920.
- [68] KANETA, M., F. GUO and J. WANG. Impact Micro-Elastohydrodynamics in Point Contacts. *Journal of Tribology-Transactions of the Asme*. 2011, vol. 133, no. 3. DOI: 10.1115/1.4004312.
- [69] KANETA, M., F. GUO, J. WANG, I. KRUPKA, et al. Formation of micro-grooves under impact loading in elliptical contacts with surface ridges. *Tribology International*. 2013, vol. 65, p. 336-345. DOI: 10.1016/j.triboint.2013.02.004.
- [70] KANETA, M., F. GUO, J. WANG, I. KRUPKA, et al. Pressure Increase in Elliptical Impact Elastohydrodynamic Lubrication Contacts With Longitudinal Asperities. *Journal of Tribology-Transactions of the Asme*. 2013, vol. 135, no. 1. DOI: 10.1115/1.4007808.
- [71] KANETA, M., F. GUO, J. WANG, I. KRUPKA, et al. Microgroove formation in surface ridges in impact elliptical EHL contacts. *Lubrication Science*. 2014, vol. 26, no. 5, p. 283-299. DOI: 10.1002/lc.1250.
- [72] WANG, J., N. WANG, P. R. YANG, M. KANETA, et al. A theoretical simulation of thermal elastohydrodynamic lubrication for a Newtonian fluid in impact motion. *Tribology International*. 2013, vol. 67, p. 116-123. DOI: 10.1016/j.triboint.2013.07.008.
- [73] CHU, L. M., J. Y. LAI, C. H. CHIEN and W. L. LI. Effects of surface forces on pure squeeze thin film EHL motion of circular contacts. *Tribology International*. 2010, vol. 43, no. 3, p. 523-531. DOI: 10.1016/j.triboint.2009.09.001.

- [74] CHU, L. M., J. R. LIN, Y. P. CHANG and W. L. LI. Effects of surface forces and surface roughness on squeeze thin film of elastohydrodynamic lubricated spherical conjunction. *Lubrication Science*. 2013, vol. 25, no. 1, p. 11-28. DOI: 10.1002/lis.1200.
- [75] CHU, L. M. Thin film elastohydrodynamic lubrication of circular contacts at pure squeeze motion. *Industrial Lubrication and Tribology*. 2010, vol. 62, no. 4, p. 238-244. DOI: 10.1108/00368791011051107.
- [76] WANG, J., C. H. VENNER and A. A. LUBRECHT. Central film thickness prediction for line contacts under pure impact. *Tribology International*. 2013, vol. 66, p. 203-207. DOI: 10.1016/j.triboint.2013.05.011.
- [77] JOHNSON, K. L. *Contact mechanics*. Edition ed. Cambridge: Cambridge University Press, 1985. ISBN 0521255767.
- [78] VENNER, C. H., J. WANG and A. A. LUBRECHT. Central film thickness in EHL point contacts under pure impact revisited. *Tribology International*. 2016, vol. 100, p. 1-6. DOI: 10.1016/j.triboint.2015.08.029.
- [79] VICHARD, J. P. Transient Effects in Lubrication of Hertzian Contacts. *Journal of Mechanical Engineering Science*. 1971, vol. 13, no. 3, p. 173-&.
- [80] REN, N., D. ZHU and S. Z. WEN. Experimental-Method for Quantitative-Analysis of Transient Ehl. *Tribology International*. 1991, vol. 24, no. 4, p. 225-230. DOI: 10.1016/0301-679x(91)90047-D.
- [81] SCALES, L., J. RYCROFT, N. HORSWILL and B. WILLIAMSON. Simulation and observation of transient effects in elastohydrodynamic lubrication. 1996. 0148-7191.
- [82] WIJNANT, Y. H., C. H. VENNER, R. LARSSON and P. ERIKSSON. Effects of structural vibrations on the film thickness in an EHL circular contact. *Journal of Tribology-Transactions of the Asme*. 1999, vol. 121, no. 2, p. 259-264. DOI: 10.1115/1.2833929.
- [83] WEDEVEN, L. D. and C. CUSANO. Elastohydrodynamic Film Thickness Measurements of Artificially Produced Surface Dents and Grooves. *Asle Transactions*. 1979, vol. 22, no. 4, p. 369-381.
- [84] KANETA, M. Effects of Surface-Roughness in Elastohydrodynamic Lubrication. *Jsm International Journal Series Iii-Vibration Control Engineering Engineering for Industry*. 1992, vol. 35, no. 4, p. 535-546.
- [85] WIJNANT, Y. H. and C. H. VENNER *Contact dynamics in starved elastohydrodynamic lubrication*. edited by D. Dowson, M. Priest, C. M. Taylor, P. Ehret, T. H. C. Childs, G. Dalmaz, Y. Berthier, L. Flamand, J. M. Georges and A. A. Lubrecht. Edition ed., 1999. 705-716 p. ISBN 0-444-50267-X.
- [86] YANG, P., J. CUI, Z. M. JIN and D. DOWSON. A theoretical study on the response of a point elasto-hydrodynamic lubrication contact to a normal harmonic vibration under thermal and non-Newtonian conditions. *Proceedings of the Institution of Mechanical Engineers Part C-Journal of Mechanical Engineering Science*. 2007, vol. 221, no. 9, p. 1089-1102. DOI: 10.1243/09544062jmes539.

- [87] KALOGIANNIS, K., C. MARES, R. P. GLOVNEA and S. IOANNIDES *Elastohydrodynamic film thickness response to harmonic vibrations*. edited by H. W. Chu, M. Savoie, J. Ferrer, P. Franco and M. Estrems. Edition ed., 2008. 44-49 p. ISBN 978-1-934272-43-5.
- [88] MORALES-ESPEJEL, G. E. Central film thickness in time-varying normal approach of rolling elastohydrodynamically lubricated contacts. *Proceedings of the Institution of Mechanical Engineers Part C-Journal of Mechanical Engineering Science*. 2008, vol. 222, no. 7, p. 1271-1280. DOI: 10.1243/09544062jmes1017.
- [89] HESS, D. P. and A. SOOM. Friction at a Lubricated Line Contact Operating at Oscillating Sliding Velocities. *Journal of Tribology-Transactions of the Asme*. 1990, vol. 112, no. 1, p. 147-152. DOI: 10.1115/1.2920220.
- [90] HARNOY, A. and B. FRIEDLAND. Dynamic friction model of lubricated surfaces for precise motion control. *Tribology transactions*. 1994, vol. 37, no. 3, p. 608-614.
- [91] RACHOOR, H. and A. HARNOY. Modeling of dynamic friction in lubricated line contacts for precise motion control. *Tribology transactions*. 1996, vol. 39, no. 2, p. 476-482.
- [92] ZHAI, X. J., G. NEEDHAM and L. CHANG. On the mechanism of multi-valued friction in unsteady sliding line contacts operating in the regime of mixed-film lubrication. *Journal of Tribology-Transactions of the Asme*. 1997, vol. 119, no. 1, p. 149-155. DOI: 10.1115/1.2832451.
- [93] SOJOURI, H. and M. M. KHONSARI. On the Modeling of Quasi-Steady and Unsteady Dynamic Friction in Sliding Lubricated Line Contact. *Journal of Tribology-Transactions of the Asme*. 2010, vol. 132, no. 1. DOI: 10.1115/1.4000272.
- [94] GLOVNEA, R., E. DIACONESCU and L. FLAMAND. EHD film thickness under transient speed conditions. *Acta Tribol*. 1995, vol. 3, p. 31-36.
- [95] SUGIMURA, J., W. R. JONES and H. A. SPIKES. EHD film thickness in non-steady state contacts. *Journal of Tribology-Transactions of the Asme*. 1998, vol. 120, no. 3, p. 442-452. DOI: 10.1115/1.2834569.
- [96] SUGIMURA, J. Elastohydrodynamic lubrication films in non-steady state conditions. *Journal of Japanese Society of Tribologists*. 2002, vol. 47, no. 10, p. 752-757.
- [97] SUGIMURA, J., T. OKUMURA, Y. YAMAMOTO and H. A. SPIKES. Simple equation for elastohydrodynamic film thickness under acceleration. *Tribology International*. 1999, vol. 32, no. 2, p. 117-123. DOI: 10.1016/s0301-679x(99)00022-5.
- [98] AL-SAMIEH, M. and H. RAHNEJAT. Ultra-thin lubricating films under transient conditions. *Journal of Physics D-Applied Physics*. 2001, vol. 34, no. 17, p. 2610-2621. DOI: 10.1088/0022-3727/34/17/307.

- [99] TOZAKI, Y., N. HAYASHI and S. MATSUMOTO. The study on tribological characteristics of traction drives in non-steady condition (Optical interferometric observations of transient oil film). *Jsmc International Journal Series C-Mechanical Systems Machine Elements and Manufacturing*. 2001, vol. 44, no. 1, p. 223-229. DOI: 10.1299/jsmec.44.223.
- [100] GLOVNEA, R. P. and H. A. SPIKES. The influence of lubricant properties on EHD film thickness in variable speed conditions. *Transient Processes in Tribology*. 2004, vol. 43, p. 401-408.
- [101] VENNER, C. H. and R. HAGMEIJER. Film thickness variations in elasto-hydrodynamically lubricated circular contacts induced by oscillatory entrainment speed conditions. *Proceedings of the Institution of Mechanical Engineers Part J-Journal of Engineering Tribology*. 2008, vol. 222, no. J4, p. 533-547. DOI: 10.1243/13506501jet306.
- [102] BASSANI, R. and E. CIULLI. Friction investigation under constant and variable speed conditions. *Tribology Series*. 2003, vol. 43, p. 783-794. DOI: 10.1016/s0167-8922(03)80106-2.
- [103] BASSANI, R., E. CIULLI, M. CARLI and K. STADLER. Experimental investigation of transient and thermal effects on lubricated non-conformal contacts. *Tribotest*. 2007, vol. 13, no. 4, p. 183-194. DOI: 10.1002/tt.43.
- [104] QU, S. Y., P. R. YANG and F. GUO. Theoretical investigation on the dimple occurrence in the thermal EHL of simple sliding steel-glass circular contacts. *Tribology International*. 2000, vol. 33, no. 1, p. 59-65. DOI: 10.1016/S0301-679x(00)00031-1.
- [105] YANG, P., S. QU, M. KANETA and H. NISHIKAWA. Formation of steady dimples in point TEHL contacts. *Journal of Tribology-Transactions of the Asme*. 2001, vol. 123, no. 1, p. 42-49. DOI: 10.1115/1.1332399.
- [106] KANETA, M. and P. YANG. Effects of thermal conductivity of contacting surfaces on point EHL contacts. *Journal of Tribology-Transactions of the Asme*. 2003, vol. 125, no. 4, p. 731-738. DOI: 10.1115/1.1540121.
- [107] GUO, F. and P. L. WONG. An anomalous elastohydrodynamic lubrication film. Inlet dimple. *Journal of Tribology-Transactions of the Asme*. 2005, vol. 127, no. 2, p. 425-434. DOI: 10.1115/1.1866165.
- [108] CIULLI, E., K. STADLER and T. DRAEXL. The influence of the slide-to-roll ratio on the friction coefficient and film thickness of EHD point contacts under steady state and transient conditions. *Tribology International*. 2009, vol. 42, no. 4, p. 526-534. DOI: 10.1016/j.triboint.2008.04.005.
- [109] ERNESTO, A., D. MAZUYER and J. CAYER-BARRIOZ. From Full-Film Lubrication to Boundary Regime in Transient Kinematics. *Tribology Letters*. 2015, vol. 59, no. 1. DOI: 10.1007/s11249-015-0551-0.
- [110] GLOVNEA, R. P. and H. A. SPIKES. The influence of lubricant upon EHD film behavior during sudden halting of motion. *Tribology Transactions*. 2000, vol. 43, no. 4, p. 731-739. DOI: 10.1080/10402000008982402.

- [111] GLOVNEA, R. P. and H. A. SPIKES. Elastohydrodynamic film collapse during rapid deceleration: Part I - Experimental results. *Journal of Tribology-Transactions of the Asme*. 2001, vol. 123, no. 2, p. 254-261. DOI: 10.1115/1.1308011.
- [112] GLOVNEA, R. P. and H. A. SPIKES. Elastohydrodynamic film collapse during rapid deceleration: Part II - Theoretical analysis and comparison of theory and experiment. *Journal of Tribology-Transactions of the Asme*. 2001, vol. 123, no. 2, p. 262-267. DOI: 10.1115/1.1308012.
- [113] NELIAS, D. and A. T. JIMENEZ. A simplified model to study EHL film collapse during rapid halting motion. *Tribology Transactions*. 2002, vol. 45, no. 4, p. 512-520. DOI: 10.1080/10402000208982582.
- [114] GLOVNEA, R. P. and H. A. SPIKES. Elastohydrodynamic film formation at the start-up of the motion. *Proceedings of the Institution of Mechanical Engineers Part J-Journal of Engineering Tribology*. 2001, vol. 215, no. J2, p. 125-138. DOI: 10.1243/1350650011541774.
- [115] POPOVICI, G., C. H. VENNER and P. M. LUGT. Effects of load system dynamics on the film thickness in EHL contacts during start up. *Journal of Tribology-Transactions of the Asme*. 2004, vol. 126, no. 2, p. 258-266. DOI: 10.1115/1.1645296.
- [116] KANETA, M. For the establishment of a new EHL theory. *Lubrication at the Frontier*. 1999, vol. 36, p. 25-36.
- [117] HOLMES, M. J. A., H. P. EVANS and R. W. SNIDLE. Comparison of transient EHL calculations with start-up experiments. *Tribological Research and Design for Engineering Systems*. 2003, p. 79-89.
- [118] USOV, P. P. Effects of lubricant viscoelasticity on film thickness in elastohydrodynamic line contacts during start-up. *Proceedings of the Institution of Mechanical Engineers Part J-Journal of Engineering Tribology*. 2016, vol. 230, no. 7, p. 769-782. DOI: 10.1177/1350650115618924.
- [119] OHNO, N. and S. YAMADA. Effect of high-pressure rheology of lubricants upon entrapped oil film behaviour at halting elastohydrodynamic lubrication. *Proceedings of the Institution of Mechanical Engineers Part J-Journal of Engineering Tribology*. 2007, vol. 221, no. J3, p. 279-285. DOI: 10.1243/13506501JET215.
- [120] KUMAR, P. and T. J. KALITA. Transient Elastohydrodynamic Lubrication Film Thickness During Normal Approach Considering Shear-Thinning and Linear Piezoviscous Oils. *Journal of Tribology-Transactions of the Asme*. 2015, vol. 137, no. 2, p. 021504-7. DOI: 10.1115/1.4029673.
- [121] PETROUSEVITCH, A. I., D. L. BAKASHVILI, V. S. SCHWARZMAN, R. G. SALUKVADZE, et al. Investigation of Oil Film Thickness in Lubricated Ball-Race Rolling Contact. *Wear*. 1972, vol. 19, no. 4, p. 369-+. DOI: 10.1016/0043-1648(72)90312-2.
- [122] NISHIKAWA, H., K. HANDA and M. KANETA. Behavior of Ehl Films in Reciprocating Motion. *Jsm International Journal Series C-Dynamics Control Robotics Design and Manufacturing*. 1995, vol. 38, no. 3, p. 558-567.

- [123] NISHIKAWA, H. and M. KANETA. Traction in Ehl under Pure Sliding Reciprocation with Cyclic Impact Loading. *Jsm International Journal Series C-Dynamics Control Robotics Design and Manufacturing*. 1995, vol. 38, no. 3, p. 568-576.
- [124] KANETA, M. and H. NISHIKAWA *The effects of a transversely oriented bump on point contact EHL films in reciprocating motion with a short length of stroke*. edited by D. Dowson, M. Priest, C. M. Taylor, P. Ehret, T. H. C. Childs, G. Dalmaz, Y. Berthier, L. Flamand, J. M. Georges and A. A. Lubrecht. Edtion ed. Amsterdam: Elsevier Science Bv, 1999. 185-192 p. ISBN 0-444-50267-X.
- [125] KANETA, M. and H. NISHIKAWA. Experimental study on microelastohydrodynamic lubrication. *Proceedings of the Institution of Mechanical Engineers Part J-Journal of Engineering Tribology*. 1999, vol. 213, no. J5, p. 371-381. DOI: 10.1243/1350650991542749.
- [126] JALALI-VAHID, D., H. RAHNEJAT, Z. M. JIN and D. DOWSON. Transient analysis of isothermal elastohydrodynamic circular point contacts. *Proceedings of the Institution of Mechanical Engineers Part C-Journal of Mechanical Engineering Science*. 2001, vol. 215, no. 10, p. 1159-1173. DOI: 10.1243/0954406011524586.
- [127] GLOVNEA, R. P. and H. A. SPIKES. Behavior of EHD films during reversal of entrainment in cyclically accelerated/decelerated motion. *Tribology Transactions*. 2002, vol. 45, no. 2, p. 177-184. DOI: 10.1080/10402000208982537.
- [128] LI, G., C. ZHANG, J. LUO, S. LIU, et al. Film-forming Characteristics of Grease in Point Contact under Swaying Motions. *Tribology Letters*. 2009, vol. 35, no. 1, p. 57-65. DOI: 10.1007/s11249-009-9433-7.
- [129] WANG, J., A. KANETA and P. YANG. Numerical analysis of TEHL line contact problem under reciprocating motion. *Tribology International*. 2005, vol. 38, no. 2, p. 165-178. DOI: 10.1016/j.triboint.2004.07.025.
- [130] WANG, J., T. HASHIMOTO, H. NISHIKAWA and M. KANETA. Pure rolling elastohydrodynamic lubrication of short stroke reciprocating motion. *Tribology International*. 2005, vol. 38, no. 11-12, p. 1013-1021. DOI: 10.1016/j.triboint.2005.07.022.
- [131] STADLER, K., N. IZUMI, T. MORITA, J. SUGIMURA, et al. Estimation of cavity length in EHL rolling point contact. *Journal of Tribology-Transactions of the Asme*. 2008, vol. 130, no. 3. DOI: 10.1115/1.2919780.
- [132] MARUYAMA, T. and T. SAITOH. Oil film behavior under minute vibrating conditions in EHL point contacts. *Tribology International*. 2010, vol. 43, no. 8, p. 1279-1286. DOI: 10.1016/j.triboint.2009.11.004.
- [133] LI, G., C. H. ZHANG, H. Y. XU, J. B. LUO, et al. The Film Behaviors of Grease in Point Contact During Microoscillation. *Tribology Letters*. 2010, vol. 38, no. 3, p. 259-266. DOI: 10.1007/s11249-010-9602-8.
- [134] RIGAUD, E., D. MAZUYER and J. CAYER-BARRIOZ. An Interfacial Friction Law for a Circular EHL Contact Under Free Sliding Oscillating Motion. *Tribology Letters*. 2013, vol. 51, no. 3, p. 419-430. DOI: 10.1007/s11249-013-0177-z.

- [135] MAJDOUB, F., J. PERRET-LIAUDET, M. BELIN and J. MARTIN. Decaying law for the free oscillating response with a pseudo-polynomial friction law: Analysis of a superlow lubricated friction test. *Journal of Sound and Vibration*. 2015, vol. 348, p. 263-281.
- [136] YAHIAOUI, M., E. RIGAUD, D. MAZUYER and J. CAYER-BARRIOZ. Forced oscillations dynamic tribometer with real-time insights of lubricated interfaces. *Rev Sci Instrum*. 2017, vol. 88, no. 3, p. 035101. DOI: 10.1063/1.4977234.
- [137] GLOVNEA, R. P. and H. A. SPIKES. EHD Contacts in Low-Amplitude Oscillatory Motion. In *World Tribology Congress III*. Washington DC: American Society of Mechanical Engineers, 2005, p. 455-456.
- [138] KALOGIANNIS, K., R. P. GLOVNEA and S. IOANNIDES. The Response of EHD Films to Lateral Oscillations. In *World Tribology Congress IV*. Kyoto, Japan: Japanese Society of Tribologists, 2009, p. 223.
- [139] KALOGIANNIS, K., R. GLOVNEA, G. MORALES and E. IOANNIDES. Behaviour of EHD films subjected to lateral oscillations. *Bulletin of the Polytechnic Institute of IASI*. 2011, vol. 57, no. 2, p. 27-36.
- [140] NAGATA, Y., K. KALOGIANNIS and R. GLOVNEA. Track Replenishment by Lateral Vibrations in Grease-Lubricated EHD Contacts. *Tribology Transactions*. 2012, vol. 55, no. 1, p. 91-98. DOI: 10.1080/10402004.2011.629404.
- [141] NAGATA, Y. EHD phenomena in grease lubricated contacts. Doctoral thesis University of Sussex, 2011.
- [142] KALOGIANNIS, K. Behaviour of elastohydrodynamic films subjected to oscillatory motion. Doctoral thesis University of Sussex, 2013.
- [143] FRYZA, J., P. SPERKA, M. KANETA, I. KRUPKA, et al. Effects of lubricant rheology and impact speed on EHL film thickness at pure squeeze action. *Tribology International*. 2017, vol. 106, p. 1-9. DOI: 10.1016/j.triboint.2016.10.023.
- [144] FRYZA, J., P. SPERKA, I. KRUPKA and M. HARTL. Effects of lateral harmonic vibrations on film thickness in EHL point contacts. *Tribology International*. 2018, vol. 117, p. 236-249. DOI: 10.1016/j.triboint.2017.08.022.
- [145] FRYZA, J., P. SPERKA, I. KRUPKA and M. HARTL. Frictional response of lubricant in EHL contact under transient bi-directional shear loading. *Tribology in Industry*. 2017, vol. 39, no. 4, p. 506-518. DOI: 10.24874/ti.2017.39.04.10.
- [146] HARTL, M., I. KRUPKA and M. LISKA. Differential colorimetry: Tool for evaluation of chromatic interference patterns. *Optical Engineering*. 1997, vol. 36, no. 9, p. 2384-2391. DOI: 10.1117/1.601415.
- [147] HARTL, M., I. KRUPKA and M. LISKA. Elastohydrodynamic film thickness mapping by computer differential colorimetry. *Tribology Transactions*. 1999, vol. 42, no. 2, p. 361-368. DOI: 10.1080/10402009908982229.
- [148] HARTL, M., I. KRUPKA, R. POLISCUK and M. LISKA. An automatic system for real-time evaluation of EHD film thickness and shape based on the colorimetric interferometry. *Tribology Transactions*. 1999, vol. 42, no. 2, p. 303-309. DOI: 10.1080/10402009908982221.

- [149] HARTL, M., I. KRUPKA, R. POLISCUK, M. LISKA, et al. Thin film colorimetric interferometry. *Tribology Transactions*. 2001, vol. 44, no. 2, p. 270-276. DOI: 10.1080/10402000108982458.
- [150] OHNO, N., M. RAHMAN and H. TSUTSUMI. High-pressure short time behavior of traction fluids. *Lubrication Science*. 2006, vol. 18, no. 1, p. 25-36.
- [151] HABCHI, W., D. EYHERAMENDY, S. BAIR, P. VERGNE, et al. Thermal elastohydrodynamic lubrication of point contacts using a Newtonian/generalized newtonian lubricant. *Tribology Letters*. 2008, vol. 30, no. 1, p. 41-52. DOI: 10.1007/s11249-008-9310-9.
- [152] BAIR, S. and F. QURESHI. Accurate measurements of pressure-viscosity behavior in lubricants. *Tribology Transactions*. 2002, vol. 45, no. 3, p. 390-396. DOI: 10.1080/10402000208982564.
- [153] HIEMSTRA, T., S. MIA, P. B. DUHAUT and B. MOLLEMAN. Natural and pyrogenic humic acids at goethite and natural oxide surfaces interacting with phosphate. *Environ Sci Technol*. 2013, vol. 47, no. 16, p. 9182-9. DOI: 10.1021/es400997n.
- [154] MAWATARI, T., R. FUKUDA, H. MORI, S. MIA, et al. High Pressure Rheology of Environmentally Friendly Vegetable Oils. *Tribology Letters*. 2013, vol. 51, no. 2, p. 273-280. DOI: 10.1007/s11249-013-0180-4.
- [155] KOTTKE, P. A., S. S. BAIR and W. O. WINER. The measurement of viscosity of liquids under tension. *Journal of Tribology-Transactions of the Asme*. 2003, vol. 125, no. 2, p. 260-266. DOI: 10.1115/1.1537270.
- [156] ZOLPER, T., Z. LI, C. CHEN, M. JUNGK, et al. Lubrication Properties of Polyalphaolefin and Polysiloxane Lubricants: Molecular Structure–Tribology Relationships. *Tribology Letters*. 2012, vol. 48, no. 3, p. 355-365. DOI: 10.1007/s11249-012-0030-9.
- [157] BAIR, S., J. JARZYNSKI and W. O. WINER. The temperature, pressure and time dependence of lubricant viscosity. *Tribology International*. 2001, vol. 34, no. 7, p. 461-468. DOI: 10.1016/S0301-679x(01)00042-1.
- [158] OHNO, N. High-pressure behavior of toroidal CVT fluid for automobile. *Tribology International*. 2007, vol. 40, no. 2, p. 233-238. DOI: 10.1016/j.triboint.2005.09.015.
- [159] BAIR, S. Reference liquids for quantitative elastohydrodynamics: selection and rheological characterization. *Tribology Letters*. 2006, vol. 22, no. 2, p. 197-206. DOI: 10.1007/s11249-006-9083-y.

## LIST OF FIGURES AND TABLES

### List of figures:

Fig. 1. Stribeck-Hersey (Gümbel) curve, film thickness, and lubrication regimes (the values of lambda ratio are only roughly indicative).....	12
Fig. 2. Left: pressure distribution and film thickness profile in mid-plane of EHL contact (modified from [27]); right: interferogram of point contact with indication of movements/flows directions in tangential plane of contact. ....	16
Fig. 3. Traction curve at various contact pressures (black) and asymptotes of some rheological models of viscoelastic fluids (blue). ....	18
Fig. 4. Non-steady state motions (modified from [44]). ....	21
Fig. 5. (a) Load as function of film thickness at various pressures; (b) Pressure distribution and film shape; (c) Deformation of flat surface [45]. ....	22
Fig. 6. The interferograms and film thickness distribution of entrapped lubricant 1.6 s and 60 s after the impact loading [46]. ....	23
Fig. 7. (a) Changes in entrapment of low-viscosity P 60 and high-viscosity bright stock (BS) oil over time; (b) Film shape and pressure distribution of P 500 oil [49]. ....	24
Fig. 8. The pressure-time trace and effects of drop height and ball weight [50]. ....	24
Fig. 9. The influence of lubricant viscosity on dimple depth (a) and the influence of impact velocity on dimple diameter (b) [54]. ....	25
Fig. 10. A dimple film shape during cyclic loading and unloading (left; [56]) and relation between the dimple film thickness and the frequency of squeeze cycles (right; [57]). ....	26
Fig. 11. Interferograms and mid-plane film profiles demonstrating the film entrapment at the contact periphery and the corresponding load curve [58]. ....	27
Fig. 12. The effect of initial impact gap (top) and initial impact speed (bottom) on the pressure (left) and film thickness (right) distributions [59]. ....	28
Fig. 13. The experimental results of the influence of initial impact gap (a) and average loading speed (b) on the film thickness [61]. ....	29
Fig. 14. The two-stage impact results: the impact at preloaded contact (left) or including initial gap (right) and corresponding effects of average loading speed and initial impact gap on the film thickness [63]. ....	30
Fig. 15. Left: Comparison of experimental (symbols) and numerical (lines) results for various initial gaps; Right: Time trace of central film thickness and pressure representing the effect of impact body mass [64]. ....	31
Fig. 16. The interferograms of PAO and POE entrapment and predicted film thickness and pressure distributions [66]. ....	32
Fig. 17. Linear, progressive, and degressive loading curves and corresponding distributions of film thickness (solid line) and pressure (dotted line) [67]. ...	33
Fig. 18. Comparison of thermal and isothermal solutions (left), corresponding temperature rise (top-right), and the effect of initial impact gap on temperature rise (bottom-right) [72]. ....	34

---

Fig. 19. Simulation of film thickness at different times during impact (left) and estimated central film thickness (Moes) as a function of M and L parameters (right) [78].	35
Fig. 20. Film shape variations under sinusoidal load [80].	36
Fig. 21. Mutual approach, and corresponding central and minimum film thickness under structural vibrations [82].	37
Fig. 22. Effect of entrainment and impact speed on film entrapment (left; [58]) and the passage of crescent-shaped entrapped lubricant through a point contact (right; [61]).	38
Fig. 23. Cyclic variation in coefficient of friction, central and minimum film thickness (top to bottom) predicted by isothermal or thermal and Newtonian (dotted lines) or non-Newtonian (solid lines) solutions [86].	39
Fig. 24. Effect of frequency on friction loops and time delay between the points of the minimum sliding speed and the maximum friction force [89].	40
Fig. 25. Changes in central film thickness with speed at frequency of 2 Hz (left) and dependence of normalized film thickness on acceleration [95].	41
Fig. 26. Variation of normalised film thickness deviation with speed and acceleration [97].	42
Fig. 27. Traction coefficient and minimum film thickness obtained experimentally and numerically with respect to the slip ratio [99].	43
Fig. 28. Film thickness ratio for PAO (left) and 5P4E (right) at 50 Hz and 1 GPa [100].	43
Fig. 29. Effect of SRR on friction loops [102].	44
Fig. 30. Effect of thermal properties and SRR on friction and central film thickness [103].	45
Fig. 31. Typical contact sub-areas during transition of lubrication regimes (left) and comparison of experimental and theoretical shear stresses (right) [109].	46
Fig. 32. Speed variation of glass disc (top-left), mid-plane film profile at different sliding speeds (top-right), and interferograms of crescent-shaped film at start/stop sliding motion (bottom) [40].	48
Fig. 33. The effect of viscosity on central film thickness during sudden halting (left) and film profiles at different time intervals after halting (right) [110].	49
Fig. 34. The effect of deceleration on film thickness during rapid halting of motion (left) and comparison of experimental data with predicted steady state thickness [111].	50
Fig. 35. Film thickness profiles (left) with interferograms (bottom) at acceleration of 5 m/s <sup>2</sup> and central film thickness at different accelerations (right) [114].	51
Fig. 36. Results of numerical analysis [117] to describe experimental start-up results in [114].	52
Fig. 37. Effect of deceleration on entrapped film thickness (left) and relation between film thickness and product of deceleration and lubricant parameter [119].	53

Fig. 38. Comparison of friction for contact with and without entrapped film at the beginning of motion [66].....	54
Fig. 39. Film profiles of cylinder oil at (a-b) left to right motion, (c) interruption of motion, (d-f) right to left motion [121]. .....	55
Fig. 40. Effect of stroke length on film profile at the end of stroke for rolling (left) and sliding (right) reciprocation [122]. .....	56
Fig. 41. Variation of friction over the reciprocation cycle (left) and comparison of frictional response at short-stroke reciprocation with and without cyclic impact loads (right) [123].....	57
Fig. 42. Comparison of experimental results [122] (top) with the results of numerical simulation [126] (bottom). .....	58
Fig. 43. Central film thickness of PAO for reciprocation frequency of 50 Hz under pure sliding conditions (left; [127]) and central film thickness of lithium grease over the reciprocation cycle for frequency of 2 Hz under pure rolling conditions (right; [128]). .....	58
Fig. 44. Temperature rise (left), and comparison of isothermal and thermal results of film thickness (middle) and friction (right) over the reciprocation cycle [129]. .....	59
Fig. 45. Comparison of experimental and theoretical results (left) and variation of predicted central film thickness with frequency over reciprocation cycle (right) [130]. .....	60
Fig. 46. Numerical simulation of cavity zone (left) and comparison of measured and predicted cavity length (right) [131]. .....	61
Fig. 47. Effect of maximum sliding speeds (left) and used oil (right) on minimum film thickness over reciprocation cycle [132]. .....	62
Fig. 48. Frictional response versus viscosity at contact pressure (left) and friction versus dimensionless parameter involving the characteristic time [134].....	63
Fig. 49. Friction loops from 48 Hz (purple-blue) to 7 Hz (red) and average friction values (left); sliding speed, friction, and central film thickness over the reciprocation cycles (right) [136]. .....	64
Fig. 50. Average central film thickness in the course of experiment (left) and the central film thickness with respect to lateral position and time of experiment [140]. .....	66
Fig. 51. Central film thickness in the middle of stroke for rolling speed of 0.5 m/s and S/D ratio of 0.185 (left) and 1.3 (right) [142]. .....	67
Fig. 52. Comparison of film thickness of PAO with and without additive for rolling speed of 0.05 m/s and frequency of 50 Hz (left) and 100 Hz (right) [142]. .....	68
Fig. 53. Optical tribometer. ....	76
Fig. 54. Scheme of the test rig for impact loading [A]. .....	77
Fig. 55. Scheme of the modified ball-on-disc simulator for excitation of lateral vibrations [B]. .....	79
Fig. 56. Photo and scheme of the test rig enabling friction measurement under lateral vibrations [C]. .....	79
Fig. 57. Optical interference by reflection (left) and TFCI method (right). .....	81

Fig. 58. Impact load curves (left) and initial approach of contact surfaces (right) for dry contact [A].....83

Fig. 59. Movement of EHL contact (left) and velocities within rolling/sliding EHL contact (right) under lateral vibrations [B].....85

**List of tables:**

Table 1 Mechanical and physical properties of contact bodies.....82

Table 2 Summary of experimental conditions for impact loading [A].....84

Table 3 Viscosity at ambient pressure, pressure-viscosity coefficient (PVC) and molecular weight of lubricants at 25 °C used in paper [A].....84

Table 4 Ranges of operating parameters used in paper [B]. .....86

Table 5 Viscosity at ambient pressure, pressure-viscosity coefficient (PVC) and molecular weight of lubricants at given temperature used in paper [B].....86

Table 6 Experimental conditions of measurements under lateral vibrations employed in paper [C]. .....88

## LIST OF SYMBOLS, PHYSICAL CONSTANTS AND ABBREVIATIONS

---

$\alpha$	Pa <sup>-1</sup>	Pressure-viscosity coefficient
$\eta$	Pa·s	Dynamic viscosity
$\xi$	1	Dimensionless location of film formation
$a$	m·s <sup>-2</sup>	Acceleration
$b$	m	Hertzian contact radius
$E$	Pa	Modulus of elasticity
$h$	m	Film thickness
$h_e$	m	Entrapped film thickness
$h_s$	m	Film thickness under steady state conditions
$H_c$	1	Dimensionless central film thickness
$L$	1	Dimensionless load parameter (Moes)
$M$	1	Dimensionless material parameter (Moes)
$p$	Pa	Pressure
$p_m$	Pa	Mean Hertzian pressure
$t_c$	s	Characteristic time
$u$	m	Entrainment speed
BS		Bright stock
CoF		Coefficient of friction
CMOS		Complementary Metal-Oxide-Semiconductor
EHL		Elastohydrodynamic lubrication/lubricated
LC		Loading curve
LSS		Limiting shear stress
PAO		Poly-alfa-olefin
POE		Polyol ester
PVC		Pressure-viscosity coefficient
S/D		Ratio of stroke length and contact diameter
SRR		Slide-to-roll ratio
TFCI		Thin film colorimetric interferometry

